

Université de Montréal

# **Quantitative functional neuroimaging of cerebral physiology in healthy aging**

par

Claudine Gauthier

Département de Physiologie

Faculté de Médecine

Thèse présentée à la Faculté de Médecine  
en vue de l'obtention du grade de Doctorat  
en Sciences neurologiques

Août 2012

© Claudine Gauthier, 2012

Université de Montréal  
Faculté des études supérieures et postdoctorales

Cette thèse intitulée :  
Quantitative functional neuroimaging of cerebral physiology in healthy aging

Présentée par :  
Claudine Gauthier

a été évaluée par un jury composé des personnes suivantes :

Paul Cisek, président-rapporteur  
Richard D. Hoge, directeur de recherche  
Sylvie Belleville, membre du jury  
Beau Ances, examinateur externe  
Florin Amzica, représentant du doyen de la FES

## Résumé

Les études d'imagerie par résonance magnétique fonctionnelle (IRMf) ont pour prémisse générale l'idée que le signal BOLD peut être utilisé comme un succédané direct de l'activation neurale. Les études portant sur le vieillissement cognitif souvent comparent directement l'amplitude et l'étendue du signal BOLD entre des groupes de personnes jeunes et âgés. Ces études comportent donc un *a priori* additionnel selon lequel la relation entre l'activité neurale et la réponse hémodynamique à laquelle cette activité donne lieu restent inchangée par le vieillissement. Cependant, le signal BOLD provient d'une combinaison ambiguë de changements de métabolisme oxydatif, de flux et de volume sanguin. De plus, certaines études ont démontré que plusieurs des facteurs influençant les propriétés du signal BOLD subissent des changements lors du vieillissement. L'acquisition d'information physiologiquement spécifique comme le flux sanguin cérébral et le métabolisme oxydatif permettrait de mieux comprendre les changements qui sous-tendent le contraste BOLD, ainsi que les altérations physiologiques et cognitives propres au vieillissement. Le travail présenté ici démontre l'application de nouvelles techniques permettant de mesurer le métabolisme oxydatif au repos, ainsi que pendant l'exécution d'une tâche. Ces techniques représentent des extensions de méthodes d'IRMf calibrée existantes. La première méthode présentée est une généralisation des modèles existants pour l'estimation du métabolisme oxydatif évoqué par une tâche, permettant de prendre en compte tant des changements arbitraires en flux sanguin que des changements en concentrations sanguine d'O<sub>2</sub>. Des améliorations en terme de robustesse et de précisions sont démontrées dans la matière grise et le cortex visuel lorsque cette méthode est combinée à une manipulation respiratoire incluant une composante d'hypercapnie et d'hyperoxie. La seconde technique présentée ici est une extension de la première et utilise une combinaison de manipulations respiratoires incluant l'hypercapnie, l'hyperoxie et l'administration simultanée des deux afin d'obtenir des valeurs expérimentales de la fraction d'extraction d'oxygène et du métabolisme oxydatif au repos. Dans la deuxième partie de cette thèse, les changements vasculaires et métaboliques liés à l'âge sont explorés dans un

groupe de jeunes et âgés, grâce au cadre conceptuel de l'IRMf calibrée, combiné à une manipulation respiratoire d'hypercapnie et une tâche modifiée de Stroop. Des changements de flux sanguin au repos, de réactivité vasculaire au CO<sub>2</sub> et de paramètre de calibration *M* ont été identifiés chez les âgés. Les biais affectant les mesures de signal BOLD obtenues chez les participants âgés découlant de ces changements physiologiques sont de plus discutés. Finalement, la relation entre ces changements cérébraux et la performance dans la tâche de Stroop, la santé vasculaire centrale et la condition cardiovasculaire est explorée. Les résultats présentés ici sont en accord avec l'hypothèse selon laquelle une meilleure condition cardiovasculaire est associée à une meilleure fonction vasculaire centrale, contribuant ainsi à l'amélioration de la santé vasculaire cérébrale et cognitive.

mots-clés:

IRMf calibré, métabolisme oxydatif, vieillissement, santé vasculaire, flux sanguin cérébral, condition cardiovasculaire, cognition

## Abstract

Functional MRI (fMRI) studies using the BOLD signal are done under the general assumption that the BOLD signal can be used as a direct index of neuronal activation. Studies of cognitive aging often compare BOLD signal amplitude and extent directly between younger and older groups, with the additional assumption that the relationship between neuronal activity and the hemodynamic response is unchanged across the lifespan. However, BOLD signal arises from an ambiguous mixture of changes in oxidative metabolism, blood flow and blood volume. Furthermore, previous studies have shown that several BOLD signal components may be changed during aging. More physiologically-specific information on blood flow and oxidative metabolism would allow a better understanding of these signal changes and of the physiological and cognitive changes seen with aging. The work presented here demonstrates techniques to estimate oxidative metabolism at rest and during performance of a task. These techniques are extensions of previous calibrated fMRI methods and the first method presented is based on a generalization of previous models to take into account both arbitrary changes in blood flow and blood O<sub>2</sub> content. The improved robustness and accuracy of this method, when used with a combined hypercapnia and hyperoxia breathing manipulation, is demonstrated in visual cortex and grey matter. The second technique presented builds on the generalization of the model and uses a combination of breathing manipulations including hypercapnia, hyperoxia and both simultaneously, to obtain experimentally-determined values of resting oxygen extraction fraction and oxidative metabolism. In the second part of this thesis, age-related vascular and metabolic changes are explored in a group of younger and older adults using a calibrated fMRI framework with a hypercapnia breathing manipulation and a modified Stroop task. Changes in baseline blood flow, vascular reactivity to the CO<sub>2</sub> challenge and calibration parameter  $M$  were identified in the older participants. Potential biases in BOLD signal measurements in older adults arising from these physiological changes are discussed. Finally, the relationship between these cerebral changes and performance on the modified Stroop task, central vascular health and cardiovascular fitness are explored. The results of this

thesis support the hypothesis that greater cardiovascular fitness is associated with improvements in central vascular function, contributing in turn to improved brain vascular health and cognition.

Keywords: calibrated fMRI, oxidative metabolism, aging, vascular health, cerebral blood flow, cardiovascular fitness, cognition.

# **Table of contents**

## **List of tables**

**16**

## **List of figures**

**17**

## **Acknowledgments**

**20**

## **Abbreviations and acronyms**

**22**

## **Preface**

**25**

## **1.Introduction 28**

### **1.1. Vascular and metabolic changes with aging 28**

**1.1.1. Vascular aging in the brain 31**

**1.1.2. Mitochondrial theory of aging 32**

### **1.2. Aging and physical fitness 34**

### **1.3. Aging and cognition 37**

**1.3.1. Mechanisms leading to changes in activation patterns 40**

**1.3.2. Cognitive theories 41**

### **1.4. The BOLD contrast mechanism 44**

**1.4.1. Underlying neuronal activity 45**

**1.4.2. Oxidative metabolism 47**

**1.4.3. Neurovascular coupling 49**

1.4.4.	Blood flow response	53
1.4.5.	Blood volume	56
1.4.6.	Limitations of the BOLD signal	57
	<i>1.4.6.1. Confounds in aging studies</i>	<i>57</i>
1.5.	Calibrated fMRI techniques	59
1.5.1.	Hypercapnia calibration method	59
1.5.2.	Hyperoxia calibration method	63
1.5.3.	R2' method	65
1.6.	Baseline CMRO2	65
1.7.	Quantitative studies of brain aging	70
<b>2.A generalized procedure for calibrated MRI incorporating hyperoxia and hypercapnia</b>		
<b>77</b>		
2.1.	Preface	77
2.2.	Abstract	78
2.3.	Introduction	79
2.3.1.	Theory	81
2.4.	Methods	84
2.4.1.	Image acquisition	84
2.4.2.	Manipulations	85
	<i>2.4.2.1. Visual stimulus</i>	<i>85</i>
	<i>2.4.2.2. Gas manipulations</i>	<i>85</i>
2.4.3.	Data analysis	86
	<i>2.4.3.1. Visual</i>	<i>88</i>
	<i>2.4.3.2. Grey matter</i>	<i>88</i>
	<i>2.4.3.3. Analysis of sensitivity to errors in CBF</i>	<i>88</i>
2.5.	Results	89
2.6.	Discussion	98
2.6.1.	Estimation of M parameter	98

- 2.6.1.1.ROI analysis 99*
- 2.6.1.2.Susceptibility-weighted venograms 99*
- 2.6.1.3.M mapping 100*
- 2.6.1.4.Spatial heterogeneity of M values 100*
- 2.6.1.5.Robustness of M estimates 101*

**2.6.2. CMRO2 103**

**2.6.3. Limitations of the study 103**

- 2.6.3.1.M value confounds 104*

**2.7. Conclusion 106**

**2.8. Acknowledgements 106**

**2.9. Appendix 107**

**2.9.1. Davis model with hypercapnia manipulation 108**

**2.9.2. Chiarelli model with hyperoxia manipulation 108**

**2.9.3. Generalized calibration model (GCM) with hyperoxia and hypercapnia 109**

**2.9.4. Stability of the models during hypercapnic manipulations 110**

**2.9.5. Stability of the models during hyperoxia manipulations 111**

**3.Magnetic resonance imaging of resting OEF and CMRO2 using a generalized calibration model for hypercapnia and hyperoxia**

**113**

**3.1. Preface 113**

**3.2. Abstract 114**

**3.2.1. Keywords 115**

**3.3. Introduction 115**

**3.3.1. Theory 117**

- 3.3.1.1.Determination of resting BOLD signal M and OEF 118*

- 3.3.1.2.Determination of resting CMRO2 120*

**3.4. Methods 121**

**3.4.1. Image acquisition 121**

3.4.2.	<b>Gas manipulations</b>	<b>122</b>
3.4.3.	<b>Data analysis</b>	<b>123</b>
3.5.	<b>Results</b>	<b>128</b>
3.5.1.	<b>Gas manipulations</b>	<b>128</b>
3.5.2.	<b>ROI analyses</b>	<b>129</b>
	<i>3.5.2.1. MRI responses</i>	<i>129</i>
	<i>3.5.2.2. Group average M vs. OEF0 curves</i>	<i>129</i>
	<i>3.5.2.3. Individual grey matter ROI values of OEF0, M, and CMRO2</i>	<i>130</i>
3.5.3.	<b>Parametric maps</b>	<b>132</b>
	<i>3.5.3.1. Resting BOLD signal M</i>	<i>132</i>
	<i>3.5.3.2. Resting oxygen extraction fraction OEF0</i>	<i>132</i>
	<i>3.5.3.3. Resting oxygen metabolism CMRO2</i>	<i>134</i>
	<i>3.5.3.4. Group average maps</i>	<i>134</i>
	<i>3.5.3.5. Sensitivity to model parameters, possible CMRO2 changes during hypercapnia</i>	<i>134</i>
3.6.	<b>Discussion</b>	<b>136</b>
3.6.1.	<b>Accuracy</b>	<b>136</b>
3.6.2.	<b>Stability</b>	<b>143</b>
3.6.3.	<b>Similar methods</b>	<b>144</b>
3.6.4.	<b>Applications</b>	<b>144</b>
3.7.	<b>Conclusion</b>	<b>146</b>
3.8.	<b>Acknowledgements</b>	<b>146</b>
<b>4. Age-dependence of hemodynamic response characteristics in human fMRI</b>		
<b>148</b>		
4.1.	<b>Preface</b>	<b>148</b>
4.2.	<b>Abstract</b>	<b>149</b>
4.3.	<b>Introduction</b>	<b>150</b>
4.4.	<b>Methods</b>	<b>153</b>

- 4.4.1. **Participants 153**
- 4.4.2. **MR Image acquisition 155**
- 4.4.3. **Hypercapnic manipulation 156**
- 4.4.4. **Stroop task 156**
- 4.4.5. **Data analysis 158**
- 4.4.6. **Regions-of-interest definition 161**
- 4.4.7. **Statistical analysis 162**
- 4.5. **Results 164**
  - 4.5.1. **Modified Stroop task behavioral results 164**
  - 4.5.2. **Modified Stroop activation maps 165**
  - 4.5.3. **Stroop evoked responses 169**
  - 4.5.4. **Respiratory manipulation 170**
  - 4.5.5. **Vascular parameters 171**
  - 4.5.6. **Calibrated fMRI estimates 175**
  - 4.5.7. **Temporal SNR 176**
- 4.6. **Discussion 179**
  - 4.6.1. **BOLD measurement of the cognitive task 179**
  - 4.6.2. **Blood flow measurements during the cognitive task 181**
  - 4.6.3. **Hypercapnic responses 181**
  - 4.6.4. **Calibrated fMRI measurements 182**
  - 4.6.5. **Potential confounds 183**
  - 4.6.6. **Limitations 186**
  - 4.6.7. **Future directions 187**
- 4.7. **Conclusion 188**
- 4.8. **Acknowledgments 188**

## **5. Relationship between cardiovascular health, cerebral physiology and cognition in healthy aging**

**189**

**5.1. Preface 189**

**5.2. Abstract 190**

**5.3. Introduction 191**

**5.3.1. Effects of cardiorespiratory fitness 192**

**5.4. Methods 193**

**5.4.1. Participants 193**

**5.4.2. Maximal continuous graded exercise test 193**

**5.4.3. Modified Stroop task 194**

**5.4.4. MR Image acquisition 194**

*5.4.4.1. Brain exam 194*

*5.4.4.2. Aortic exam 195*

**5.4.5. Tonometry 195**

**5.4.6. Hypercapnic manipulation 195**

**5.4.7. Data analysis 196**

*5.4.7.1. Brain data 196*

*5.4.7.2. Aortic data 196*

**5.4.8. Statistical analysis 196**

**5.5. Results 197**

**5.5.1. Central vascular health and fitness 197**

**5.5.2. Cerebral measures 198**

**5.5.3. Correlations between parameters 201**

**5.6. Discussion 202**

**5.6.1. Differences between age groups 202**

**5.6.2. Correlations within older participants 203**

**5.7. Conclusion 205**

**5.8. Acknowledgments 206**

**6.General Discussion 207**

**6.1. Calibrated fMRI method comparisons 208**

**6.2. Accuracy of measurement 209**

**6.3. Baseline metabolism 211**

**6.3.1. QUO2 technique 212**

**6.3.2. Future improvements 214**

**6.4. Calibrated fMRI of aging 215**

**6.4.1. Calibrated fMRI of aging literature 216**

**6.4.2. Future improvements 217**

**6.5. Vascular changes with aging 219**

**6.5.1. Future improvements 221**

**6.6. Future studies 222**

**Conclusion**

**224**

**G.Appendix - Elimination of visually evoked BOLD responses during carbogen inhalation: implications for calibrated MRI 225**

**G.1. Abstract 225**

**G.2. Introduction 226**

**G.3. Methods 229**

**G.3.1. Gas manipulations 232**

**G.3.2. Data analysis 233**

**G.4. Results 235**

**G.4.1. Additional tests 239**

**G.4.2. Subjective discomfort rating 241**

**G.5. Discussion 241**

- G.5.1. Arterial spin-labeling 242**
- G.5.2. Susceptibility-weighted imaging 243**
- G.5.3. Implications for calibrated MRI 243**

*G.5.3.1. Pitfalls and future directions 246*

- G.6. Conclusion 248**
- G.7. Acknowledgments 249**
- G.8. Appendix 249**

## **H.Appendix - Absolute quantification of resting oxygen metabolism and metabolic reactivity during functional activation using QUO2 MRI 253**

- H.1. Abstract 253**
- H.2. Introduction 254**
- H.3. Methods 256**
  - H.3.1. Image acquisition 256**
  - H.3.2. Gas manipulations 257**
  - H.3.3. Visual stimulus 258**
  - H.3.4. Stroop task 258**
  - H.3.5. Data analysis 259**
  - H.3.6. Visual ROI 262**
  - H.3.7. Stroop ROIs definition 262**
- H.4. Results 265**
  - H.4.1. Gas manipulations 265**
  - H.4.2. M, OEF0 and resting CMRO2 266**
  - H.4.3. Task-evoked CMRO2 268**
  - H.4.4. Vascular and metabolic profile 269**
- H.5. Discussion 270**
  - H.5.1. Accuracy of estimates 271**

*H.5.1.1. Visual 271*

*H.5.1.2. Stroop 273*

**H.5.2. Implementation biases and confounds 276**

**H.6. Conclusion 280**

**H.7. Acknowledgments 280**

**Bibliography**

**281**

# List of tables

<b>Chapter 2</b>	<b>A generalized procedure for calibrated MRI incorporating hyperoxia and hypercapnia</b>	
Table 1	End-tidal values for each breathing manipulation	89
Table 2	Calibrated fMRI results	98
<b>Chapter 3</b>	<b>Magnetic resonance imaging of resting OEF and CMRO<sub>2</sub> using a generalized calibration model for hypercapnia and hyperoxia</b>	
Table 1		128
Table 2		131
<b>Chapter 4</b>	<b>Age-dependence of hemodynamic response characteristics in human fMRI</b>	
Table 1	Neuropsychological battery results	164
Table 2	ROI quantification results	178
<b>Chapter 5</b>	<b>Relationship between cardiovascular health, cerebral physiology and cognition in healthy aging</b>	
Table 1	Partial correlations between health indices in the older subjects	201
<b>Appendix A</b>	<b>Elimination of visually evoked BOLD responses during carbogen inhalation: implications for calibrated MRI</b>	
Table 1	Gas mixture compositions	231
Table 2	Literature <i>M</i> values at 3 Tesla	245
<b>Appendix B</b>	<b>Absolute quantification of resting oxygen metabolism and metabolic reactivity during functional activation using QUO2 MRI</b>	
Table 1	Respiratory parameters	265
Table 2	Vascular and metabolic profile	270

# List of figures

<b>Chapter 1 Introduction</b>		
Figure 1	Near-infrared multiphoton LSM	30
Figure 2	Mitochondrial energy production	33
Figure 3	Exercise and cognition	37
Figure 4	Reliable patterns of brain activity across studies of aging	39
Figure 5	A conceptual model of the scaffolding theory of aging and cognition (STAC)	44
Figure 6	Electrical underpinnings of the BOLD signal	46
Figure 7	Neurovascular unit	50
Figure 8	Neurovascular coupling response	52
Figure 9	Tag delivery in ASL during normocapnia and hypercapnia	55
Figure 10	Example case of BOLD comparisons across lifespan	58
Figure 11	BOLD attenuation from metabolism	60
Figure 12	Deoxyhemoglobin dilution model	61
Figure 13	QUIXOTIC	68
Figure 14	Calibrated fMRI of visual activation in aging	71
Figure 15	Calibrated fMRI of Stroop activation in aging	72
Figure 16	The association between age and regional CBF as well as cortical thickness	73
Figure 17	Whole brain hemodynamic age-related changes	74
Figure 18	Decade-by-decade alterations in prefrontal CVR and CBF	75
<b>Chapter 2 A generalized procedure for calibrated MRI incorporating hyperoxia and hypercapnia</b>		
Figure 1	Group average percent CBF and BOLD for each breathing manipulation	90
Figure 2	Individual and average $M$ values over the visual and grey-matter ROI's for each breathing manipulation	91
Figure 3	Individual $M$ maps for each breathing manipulation	93

Figure 4	Spatial heterogeneity of $M$ maps	94
Figure 5	Susceptibility-weighted venograms during each breathing manipulation	95
Figure 6	Effect of CBF errors on $M$ estimates from different models and breathing manipulations	96
Figure 7	Individual and average $CMRO_2$ estimates over the visual ROI	97
<hr/>		
<b>Chapter 3</b>	<b>Magnetic resonance imaging of resting OEF and <math>CMRO_2</math> using a generalized calibration model for hypercapnia and hyperoxia</b>	
<hr/>		
Figure 1		130
Figure 2		131
Figure 3		133
Figure 4		134
Figure 5		135
Figure 6		136
<hr/>		
<b>Chapter 4</b>	<b>Age-dependence of hemodynamic response characteristics in human fMRI</b>	
<hr/>		
Figure 1	Modified Stroop task paradigm	158
Figure 2	Modified Stroop behavioral response	165
Figure 3	Modified Stroop Z-score maps	167
Figure 4	Modified Stroop task ROIs	168
Figure 5	Percent BOLD and CBF responses to the modified Stroop task	170
Figure 6	BOLD hypercapnia time courses	172
Figure 7	CBF hypercapnia time courses	173
Figure 8	Baseline CBF and CVR	174
Figure 9	$M$ and $CMRO_2$ values	175
Figure 10	Temporal SNR of CBF and BOLD measurements	177
<hr/>		
<b>Chapter 5</b>	<b>Relationship between cardiovascular health, cerebral physiology and cognition in healthy aging</b>	
<hr/>		
Figure 1	Central vascular health and cardiorespiratory fitness	197

Figure 2	Stroop task performance	198
Figure 3	Cerebral hemodynamic properties	200

---

**Appendix A Elimination of visually evoked BOLD responses during carbogen inhalation: implications for calibrated MRI**

---

Figure 1	Visual cortex regions of interest for each subject	234
Figure 2	Percent BOLD response maps from example subject	236
Figure 3	BOLD Time course for carbogen inhalation and carbogen + visual stimulation	237
Figure 4	Individual BOLD percent changes in visual ROI	238
Figure 5	Group-average BOLD response amplitudes	239
Figure 6	Susceptibility-weighted venogram	240
Figure 7	BOLD and ASL time courses for visual stimulation during carbogen-10 breathing	240
Figure 8	Maps of percent BOLD increase during carbogen-10 breathing	246

---

**Appendix B Absolute quantification of resting oxygen metabolism and metabolic reactivity during functional activation using QUO2 MRI**

---

Figure 1	ROI for Stroop task	264
Figure 2	Percent CBF and BOLD changes during breathing manipulations	266
Figure 3	Intersection plots for all ROIs	267
Figure 4	$M$ , $OEF_0$ and resting $CMRO_2$ values over all ROIs	268
Figure 5	Task-evoked percent CBF and BOLD changes	269
Figure 6	Task-evoked percent $CMRO_2$ change	269

# Acknowledgments

First and foremost, I want to thank my supervisor, Rick, for his mentorship, his unwavering support throughout the six years I spent in his lab and all the confidence he placed in me. Being a PI's first PhD student is something of a special position: both parties come with the enthusiasm and idealism of ignorance and learn together both the harsh reality of their obligations and the enjoyment of their new scientific freedom. I come away with much gratitude for all the freedom, knowledge and extra attention I received. I am looking forward to working again together in the future as collaborators.

En seconde part dans cette liste de remerciement doit venir l'amie, la collègue, la coloc de bureau, la personne qui a partagé tous les hauts et les bas de ce grand défi que fût ce doctorat: Cécile. Sans son support, son travail acharné, sa générosité, son imagination, ses talents de programmation, son écoute et sans son amitié, je n'aurais pas accompli la moitié de ce que j'ai fait. Elle mérite ce doctorat autant que moi et je la remercie du fond du coeur pour l'opportunité fantastique d'avoir pu travailler avec elle. J'aimerais aussi remercier les membres passés et actuels de mon labo. Merci à Paul-Olivier pour son aide sur mon projet et sa personnalité adorable, merci à mes petits frères Brice et Sébastien pour leur enthousiasme et leur écoute, merci à Felipe pour son support affectueux et à Isabelle pour avoir adouci le départ de Cécile. Finalement merci à Louis, Tarik, Lorenzo et Élodie pour leur aide toujours souriante et merci à Anne-Marie pour avoir pourfendu avec vaillance et joie de vivre tous les défis organisationnels de ma soumission et ma défense.

J'ai eu la chance de travailler sur un projet fascinant qui m'aura permis de connaître des personnes généreuses et sympathiques dans d'autres labos. Merci à Louis et aux membres de son équipe d'avoir contribué avec tant d'enthousiasme à mon projet. Un merci particulier à Laurence dont la générosité constante et tranquille a grandement contribué au succès de cette épopée, à Saïd pour avoir de son entrain sans faille rendu un test d'effort agréable à tous mes participants, et merci à Mélanie pour les prouesses organisationnelles dont elle a fait preuve. Merci à Frédéric et à son équipe pour leur aide pour tous les aspects d'imagerie optique. Un merci particulier à Michelle et Nicolas pour leur aide constante et toujours enthousiaste. Un grand merci aussi aux gens de l'INSERM de m'avoir accueillie et aidée. Merci à Frédérique et Muriel surtout, qui ont contribué une diligence et un enthousiasme sans faille à mon projet. Merci à Pierre, qui est à la fois un collègue, un ami et une source d'inspiration dans sa ferveur scientifique inépuisable. Un immense merci aux employés de l'UNF qui m'ont fourni un support constant. Merci à

Carolyn et André pour tous les sacrifices de lunch et toute l'aide qu'ils m'ont apportée dans mon doctorat. Merci à Francine d'avoir toléré pendant toutes ces années mon manque d'organisation et d'avoir de si bonne grâce remédié à mes oublis.

On ne peut survivre avec succès les années de doctorat sans le support des amis. Donc un immense merci à mes amies-soeurs: Christine, Hélène, Sigrid et Olivia. Qu'aurais-je fait sans les heures incalculables de conversations, les rires et tout ce que nous avons partagé? Elles sont une partie de moi et je les remercie du fond du coeur d'être les filles fantastiques qu'elles sont. Merci à leurs conjoints et bébés, Vincent, Sebastian, Yannick et Jon qui sont aussi devenus des amis chers. Merci à Clarisse et Jean pour m'avoir adoptée quand j'étais seule aux conférences et pour m'avoir ensuite donné une amitié précieuse. Merci aussi à Jenny, Gab, Catherine, 'la gang' et Charlotte, pour une petite baignade rafraîchissante chez les gens qui vivent dans le vrai monde et en font une place qui en vaut la peine. Thanks to Dimo and Henrik for their conference-started friendship and warm welcome on my post-doc tour. Merci à Anne-Julie pour les matinées d'écriture et l'amitié renouvelée. Merci aux nouveaux amis qui ont ensoleillé ma dernière année: Josh, Dom, Eric, Desirée, Gonzalo, Anita et Mark. Merci à Tarek pour toutes les discussions uniques qui ont permis l'envol de mon imagination. Merci à Patrick pour son support et pour avoir stimulé ma fibre lyrique. Et finalement merci à Marie-Claude, Aaron, Zoë et James pour ces visites de la dernière année qui m'ont tant aidée à garder les pieds sur terre et à profiter de la vie.

Je tiens à dire deux mercis vraiment très spéciaux pour moi: merci à Nicolas et Julien qui ont été pendant cette aventure une source de support vraiment précieux. Merci à Nicolas qui m'a donné le support dont j'avais besoin pour entreprendre la grande traversée. Nos discussions m'ont fait grandir et son amitié a fait de moi une personne mille fois plus forte et belle. Merci à sa famille aussi, qui m'a adoptée comme une des leur et dont le support m'a touchée énormément. Merci à Julien qui a été un grand-frère scientifique incomparable, mais surtout un ami sincère et constant. Merci pour son humour qui fait scintiller la vie et pour son écoute dans tous les moments difficiles.

Merci à ma famille, qui a cru plus que tous à ma capacité à me dépasser, peu importe le but que je m'étais fixé. Merci à ma mère, mon père, Laurent, Mathilde, Aline et Diane pour leur fierté, leur confiance et leur patience. And finally, I want to thank Chris who allowed me by his constant support and affection to get to the end of this last demanding year with all the grace and happiness possible. I am looking forward to the next step of this adventure together.

## Abbreviations and acronyms

AD	Alzheimer's disease
AI	Augmentation index
AMPA	2-amino-3-(5-methyl-3-oxo-1,2-oxazol-4-yl)propanoic acid
ASL/PASL/ pCASL	Arterial spin labeling/Pulsed ASL/Pseudo-continuous ASL
ATP	Adenosine triphosphate
BDNF	Brain-derived neurotrophic factor
BOLD	Blood oxygen level-dependent
CaO <sub>2</sub>	Arterial content of O <sub>2</sub>
CBF	Cerebral blood flow
CBV	Cerebral blood volume
CMRO <sub>2</sub>	Cerebral metabolic rate of O <sub>2</sub>
CPMG	Carr Purcell Meiboom Gill
CRP	C-reactive protein
CRUNCH	Compensation-Related Utilization of Neural Circuits
CvO <sub>2</sub>	Venous content of O <sub>2</sub>
CVR	Cerebrovascular reactivity
ETO <sub>2</sub> /ETCO <sub>2</sub>	End-tidal O <sub>2</sub> /CO <sub>2</sub> concentration
FDG	Fluoro-D-glucose
FLAIR	Fluid attenuated inversion recovery
fMRI	Functional magnetic resonance imaging
FWHM	Full width at half maximum
GABA	gamma-Aminobutyric acid
GCM	Generalized calibration model
GESSE	Gradient echo sampling of the spin echo
GLM	General linear model
GM	Grey matter

GRAPPA	Generalized autocalibrating partially parallel acquisition
HAROLD	Hemispheric asymmetry reduction in older adults
Hb/dHb	Hemoglobin/Deoxyhemoglobin
HO/HC	Hyperoxia/Hypercapnia
HRF	Hemodynamic response function
LFP	Local field potentials
<i>M</i>	Maximal possible BOLD signal change
MPRAGE	Magnetization prepared rapid gradient echo
MRI	Magnetic resonance imaging
mtDNA	Mitochondrial DNA
MUA	Multi-unit activity
<i>n</i>	Flow-metabolic coupling constant
NADH	Nicotinamide adenine dinucleotide
NMDA	N-Methyl-D-aspartic acid
NO	Nitric oxide
OEF	Oxygen extraction fraction
PaO <sub>2</sub>	Arterial partial pressure of O <sub>2</sub>
PASA	Posterior anterior shift in aging
PET	Positron emission tomography
PGE2	Prostaglandin E2
PWV	Pulse wave velocity
qBOLD	Quantitative BOLD
QUIPSS II	Quantitative imaging of perfusion using a single subtraction
QUIXOTIC	Quantitative imaging of extraction of oxygen and tissue
QUO2	Quantitative O <sub>2</sub>
ROI	Region-of-interest
ROS	Reactive oxygen species
RT	Reaction time

SaO <sub>2</sub>	Arterial O <sub>2</sub> saturation
SNR	Signal-to-noise ratio
STAC	Scaffolding theory of aging and cognition
SvO <sub>2</sub>	Venous O <sub>2</sub> saturation
T	Tesla
T1	Longitudinal relaxation time
T2/T2*	Transverse relaxation time
TE	Echo time
TR	Repetition time
TRUST	T2 relaxation under spin tagging
TSE	Turbo spin echo
tSNR	Temporal signal-to-noise ratio
VASO	Vascular space occupancy
VERVE	Venous refocussing for volume estimation
VO <sub>2</sub> max	Maximal volume of O <sub>2</sub> consumed during exercise

## Preface

*Longevity is a vascular question. A man is only as old as his arteries.*

-- Dr William Osler

Aging is associated with a variety of cognitive and behavioral changes. In order to understand the cognitive changes associated with normal and pathological aging, we need to investigate the anatomical and physiological correlates of these changes. While cortical atrophy and white matter lesions are known to occur at the later stages in life even in healthy older adults, functional changes that go beyond the straight-forward effects of the loss of grey-matter can also be observed. However, while the study of the anatomical changes associated with aging is becoming well established, the investigation of dynamic changes in the brain still remains a technical challenge. The technique of choice to study brain function non-invasively is functional magnetic resonance imaging (fMRI) using the blood oxygen level-dependent (BOLD) contrast. This technique's popularity can be attributed to the fact that it is fairly simple to implement on any modern MRI scanner and is sensitive to the local activity of brain regions at the millimeter scale. Thanks to these characteristics, it can yield robust results with adequate spatial and temporal resolution that allow inferences to be made about local brain function.

The effect of aging on BOLD signal changes evoked by a variety of tasks has been the subject of intense research in recent years. However, while BOLD contrast is a useful measure of local brain activity, the information that can be derived from it is intrinsically ambiguous in nature. This is because the BOLD signal arises from an ambiguous combination of changes in oxidative metabolism, blood flow and blood volume. Furthermore, the BOLD signal is measured as a relative change from an unknown baseline. These characteristics call for caution when comparing BOLD signal changes between groups, especially when either the baseline or the dynamic range of any of its component is suspected to differ between them. Aging is known to be associated with vascular and metabolic changes that can potentially influence all components of the BOLD signal. Therefore, while BOLD studies of aging can be helpful in identifying potential loci of task-related differences between

young and old, more physiologically-specific information is needed to understand the underlying differences in neuronal usage.

The work presented in this thesis was motivated by the need to both characterize the vascular and metabolic changes associated with aging and provide a more physiologically-specific context in which to discuss the functional changes we observe in BOLD studies of cognitive aging. The body of this thesis will be comprised of four manuscripts. Two of these will present the technical and modeling development work done in the course of my project. These techniques were developed in parallel with the aging study forming Chapter 4 of this thesis and therefore represent separate novel findings. The first manuscript, entitled “A generalized procedure for calibrated MRI incorporating hyperoxia and hypercapnia” presents a new generalized model based on the hypercapnia and hyperoxia calibration models that can be used with breathing manipulations causing any arbitrary change in cerebral blood flow and arterial oxygen content. This model will be used to perform calibrated fMRI in the aging manuscripts. The second manuscript is entitled “Magnetic resonance imaging of resting OEF and CMRO<sub>2</sub> using a generalized calibration model for hypercapnia and hyperoxia” and demonstrates the use of the generalized model in combination with at least two breathing manipulations to estimate baseline oxygen extraction fraction and oxidative metabolism. The third and fourth manuscripts will focus on quantitative studies of aging. In the third manuscript entitled “Age-dependence of hemodynamic response characteristics in human fMRI”, the changes in hemodynamic components with aging will be explored. This manuscript explores the potential confounds associated with hemodynamic imaging in aging. The fourth manuscript entitled “Relationship between cardiovascular health, cerebral physiology and cognition in healthy aging” will discuss changes in vascular physiology in the brain and at the level of the aorta, and their link to hemodynamic signal changes will be discussed. Finally, two additional manuscripts will be presented as appendices to this thesis, since they provide additional support for the studies shown here. The first appendix will comprise a manuscript entitled “Elimination of visually evoked BOLD responses during carbogen inhalation: implications for calibrated MRI”, which presents a direct measurement through a breathing manipulation of the

calibration parameter we seek to determine through modeling in standard calibrated fMRI experiments. The second appendix is a manuscript entitled “Absolute quantification of resting oxygen metabolism and metabolic reactivity during functional activation using QUO2 MRI”. This manuscript demonstrates the comprehensive set of measurements that can be obtained using a combination of all the techniques presented in Chapters 2 and 3. While these were not all applied in our studies of aging, future studies will include them to provide an improved quantification of BOLD signal sub-components.

# 1. Introduction

Neurological components of aging can be detected by decreased accuracy and speed of cognitive and sensory responses, as well as structural and functional changes. These include atrophy and decreased cerebral perfusion and metabolism. While cortical thinning and decreases in white matter integrity can be found throughout the brain during old age, frontal and parietal cortex and the hippocampus, may be more vulnerable to the effects of age (Salat et al. 2004; Raz et al. 2010; Chen et al. 2011; Salat et al. 2012). The rate and severity of cortical thinning and white matter lesions is furthermore highly variable between individuals (Raz et al. 2010; Salat et al. 2012). The underlying causes of these anatomical changes are still unclear, but it may be that some of these changes have a vascular origin or contribution.

## 1.1. Vascular and metabolic changes with aging

Vascular changes may be an inevitable fact of aging, but the severity and rapidity of the progression of these changes show great heterogeneity within the population of older adults. The arterial network has two main functions: to deliver blood to all tissues in the body and dampen heart pulsations so that when blood reaches the capillaries, flow is continuous rather than pulsatile. As blood flow reaches the high resistance small diameter vessels (arterioles and capillaries) after going through the more elastic larger vessels, the remainder of the pressure wave is reflected back up the arterial tree so that flow in these small vessels becomes continuous. In young individuals, the arterial system can perform both of its functions very well and flow is continuous at the level of arterioles in all organs, except those with higher baseline blood flow such as the kidneys and the brain (O'Rourke et al. 2007).

The dampening of pulsatile flow is achieved by laminae of the protein elastin in blood vessel walls. This protein acts like rubber to allow vessel walls to be distended during the systolic phase of the cardiac cycle and return to their original shape during the diastolic phase (O'Rourke et al. 2007). This protein is the most inert in the body and has a half-life of decades. However, like all material, elastin

undergoes fatigue. Over an entire lifetime of being stretched at every heart beat, the laminae fracture and become less efficient. Laminae become thinner and since elastin is not replenished readily, the space created between laminae is filled with collagen (Figure 1). Collagen filling with age is thought to prevent overly large deformations of blood vessel walls. However, because collagen is not elastic, the decreased elastin to collagen ratio results in stiffer blood vessels with a larger diameter (Fritze et al. 2012). As this process unfolds, the vessels become partially distended and undergo little change in diameter to absorb the heart pulse and the added pressure of the reflection wave. As vessels harden, there is more and more mechanical stress on the already weakened elastin laminae and these processes of thinning and collagen filling accelerate. Larger vessels become more hardened and ever smaller arteries are affected by this phenomenon. Furthermore, lifestyle choices may also have a strong impact on this hardening mechanism through mitochondrial oxidative stress (Davenport et al. 2012; Zhou et al. 2012) and plaque deposition which further harden vessels (O'Rourke et al. 2007). High calorie intake and low exercise may lead to increased production of reactive oxygen species (ROS), which may contribute to elastin protein damage. ROS are highly reactive molecules since they have an unpaired valence shell electron. To fill their valence shell, ROS steal electrons from larger molecules such as DNA, proteins and lipids, thereby degrading them (Wallace 2005). Furthermore, ROS may cause decreased nitric oxide (NO) bioavailability, thereby reducing overall vascular tone and reserve (Pialoux et al. 2009). The mitochondrial theory of aging, which includes these phenomena, will be further discussed in the next section.

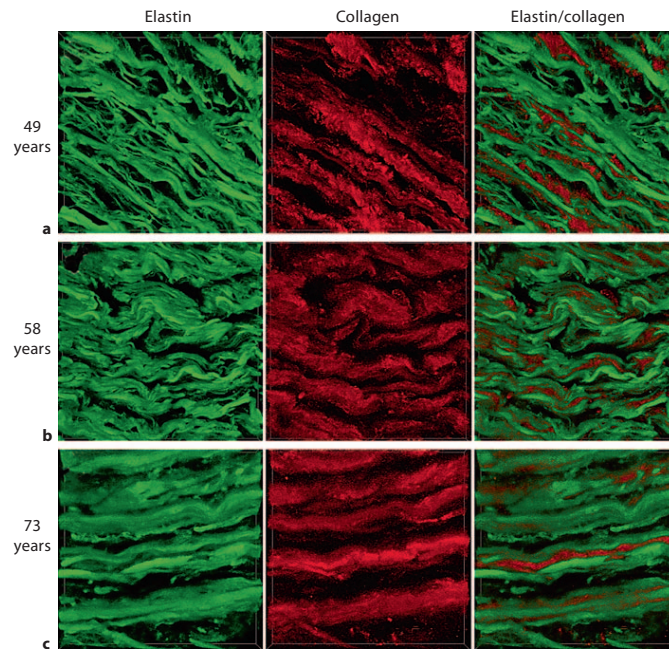


**Figure 1. Near-infrared multiphoton LSM.**

Elastin autofluorescence signals (green) and SHG signals of collagen (red) are depicted for aortic cross sections (circumferential view) of 49- (a), 58- (b) and 73- (c) year-old patients. This figure illustrates changes in elastin and collagen ratio and structure with age. This figure and its caption were reproduced from (Fritze et al. 2012).

Arterial hypertension is both the cause and effect of even greater vessel wall stiffening. As vessels harden, the pulse pressure wave from the heart increases in velocity. This leads to an increased amplitude and velocity of the reflection wave, as blood flow with higher pressure reaches high resistance vessels and is reflected back. This positive feedback loop accelerates, leading to increasing blood pressure and ever more damage to progressively smaller blood vessels (O'Rourke et al. 2007; Redheuil et al. 2010). Arterial hypertension is therefore an indication that damage has already started to occur. Though decreases in arterial elasticity are general and affect the whole body, the aorta may be the most representative of the state of other arteries. This is because the aorta may be the first to be affected since much of the pulsatile flow absorption and therefore the mechanical damage to elastin laminae occurs at this level (Laurent et al. 2006; Redheuil et al. 2010). The relationship between aortic hardening and measures of cerebral health will be discussed in Chapter 5 of this thesis.

Inflammation may be an important contributing factor to vascular stiffening. Arterial hypertension has been found to be associated with the presence of inflammatory markers such as interleukin-6, tumor necrosis factor-alpha and C-reactive protein (CRP) (Amar et al. 2005; Laurent et al. 2007). Though the mechanisms leading to this association are not well known, molecules released as a consequence of endothelial dysfunction are thought to lead to this chronic elevation of inflammatory markers (Devaraj et al. 2011). Furthermore, CRP level was found to be predictive of pulse pressure and treatment to lower CRP levels has been shown to have a positive effect on pulse pressure (Amar et al. 2005; Devaraj et al. 2011).

### **1.1.1. Vascular aging in the brain**

Arterial hypertension has long been known as a risk factor for stroke and is now recognized as playing a role in cognitive decline (Robbins et al. 2005; Waldstein et al. 2008; Elias et al. 2009; Brown et al. 2011; Gorelick et al. 2011). The brain may be particularly vulnerable to the effects of arterial hardening and it is thought that there is a link between arterial stiffening and cognitive decline (Waldstein et al. 2008; Elias et al. 2009; Brown et al. 2011). Several mechanisms have been proposed to contribute to this relationship. First, the brain is one of the only organs without protection against the pulsatile nature of blood flow. With age, cerebral arteries suffer from the loss of elastin (O'Rourke et al. 2007) and a decrease in microvascular density (Sonntag et al. 1997). The increased pulsatility associated with less elastic arteries may lead to distal cerebral lesions and impaired distal microcirculation (O'Rourke et al. 2007). Secondly, the severity of white matter hyperintensities is increased with hypertension and these have been shown to be associated with cognitive decline and dementia (Sierra et al. 2004; Au et al. 2006). Finally, impaired endothelial function leading to circulation of cellular debris (Wang et al. 2007; Wang et al. 2009) has also been proposed to lead to microvascular lesions (O'Rourke et al. 2007) and hence cognitive deficits. This may also be reflected in the fact that elevated CRP levels, indicative of endothelial dysfunction, are an independent risk factor for age-associated cognitive decline (Yaffe et al. 2003).

### 1.1.2. Mitochondrial theory of aging

While aging cannot be reduced to a single phenomenon, one of the most enduring theories of the cellular mechanisms of aging relates accumulating damage in the cellular environment to progressive breakdown of membrane integrity and of the electron transport chain of the mitochondria. Mitochondrial damage leads to an increased formation of reactive oxygen species (ROS). The progression of mitochondrial damage in normal aging, leading eventually to disease, is presumed to progress as described in the remainder of this section and summarized in Figure 2. Though mitochondrial aging occurs throughout the body, it is here discussed in the context of the brain.

The electron transport chain, which is used for oxidative phosphorylation and production of extra ATP molecules from glycolysis end-products, is the main source of ROS. These are created at all times even in the best of cases, but their production can be increased by several factors including a high-calorie diet and low exercise (Wallace 2005; Pialoux et al. 2009). Because electrons from fat and carbohydrate oxidation are produced even when there is no ADP to be phosphorylated (because, for example, of lack of exercise), excess protons from metabolism of fats and carbohydrates cause hyperpolarization of the mitochondrial membrane. Excess electrons fill all binding sites on electron carriers within the membrane and these electrons can then be added to O<sub>2</sub> to form ROS. These ROS diffuse and degrade DNA, proteins and lipids. Because ROS are mainly created in mitochondria and are very reactive, these organelles are the first and worst affected (Wallace 2005).

Since mitochondria are continually produced and destroyed in post-mitotic cells, mutations in mitochondrial DNA (mtDNA) can affect the function of cells even when they have stopped replicating. Throughout a lifetime, ROS will create somatic mutations in mtDNA and affect the functioning of proteins encoded by this mtDNA. Complexes I, III and IV of the electron transport chain (ETC) are especially prone to the effects of ROS-mediated damage, since they reside within mitochondria and some of their components are encoded by mtDNA (Aleari et al. 2005; Coskun et al. 2011). Mitochondria become more and more inefficient as electron transport

becomes progressively uncoupled from proton pumping due to damage to these protein complexes (Wallace 2005). As the process to produce ATP loses efficiency, more and more protons are required to make ATP.

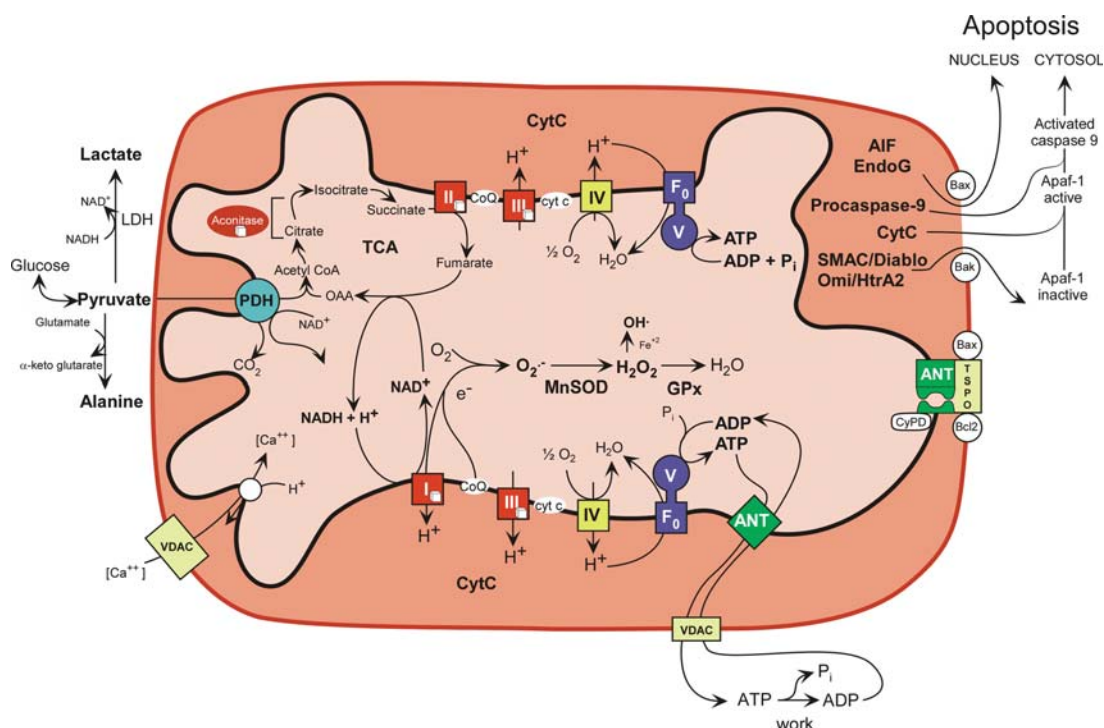


**Figure 2. Mitochondrial energy production**

This figure and its caption were reproduced from (Wallace 2011).

Eventually, mitochondria become so inefficient that energy production falls below the so-called bioenergetic threshold. At this point, the cell reduces its functions to adapt to its own inefficient energy production and enters a steady-state that enables only a basic operational level of functioning. This is the stage where damage and progression to disease start to occur. For example, the symptoms that form the hallmark of Alzheimer’s disease (AD) (including amyloid- $\beta$  production and deposition) develop at this point (Wallace 2005; Bonda et al. 2010; Coskun et al. 2011).

As oxidative stress damages the cell, a variety of protective mechanisms are put in place. One of these is the cleavage of the amyloid precursor protein into amyloid- $\beta_{1-42}$  by presenilin 1 and 2. amyloid- $\beta_{1-42}$  has been found to have antioxidant properties and is produced as a defensive mechanism against the effects of excess ROS (Kontush et al. 2001; Bonda et al. 2010; Coskun et al. 2011; Bartley et

al. 2012). However, as it accumulates, amyloid- $\beta$  becomes toxic and leads to a decrease in the activity of complexes I, III and IV (cytochrome c oxidase) (Canevari et al. 1999; Aleari et al. 2005), the inhibition of Mn superoxide dismutase (Aleari et al. 2005; Anantharaman et al. 2006) and perturbation in the functioning of the mitochondrial permeability transition pore (Bartley et al. 2012). These lead to decreased O<sub>2</sub> consumption and ATP synthesis and to an increase in ROS production (Aleari et al. 2005). Leakage through the permeability transition pore leads to the last stages of cell life as it triggers the induction of apoptosis cascades (Wallace 2005; Coskun et al. 2011; Bartley et al. 2012). This leads to the loss of neurons and brain atrophy. Though markers of these mechanisms are present in normal aging brains, these effects are more pronounced in the case of diseases such as AD. It may be, however, that these effects contribute to the atrophy and cognitive decline observed even in healthy aging (Wallace 2005), especially in individuals that adopt a less healthy lifestyle. However, the specific effects of these mechanisms on cognitive processes is largely unknown. Atrophy and vascular changes are known to occur at different rates in different brain regions (Salat et al. 2004; Chen et al. 2011) and the link between mitochondrial health and regional deficits still remains to be determined.

## **1.2. Aging and physical fitness**

The effects of aging often result in a significantly poorer quality of life and much research effort has been dedicated to alleviating the effects of aging. Lifestyle has a very substantial impact on health and quality of life. A healthy diet and regular exercise are, by far, the best recognized means to aging gracefully (Wallace 2005). However, the exact impact of regular exercise on cerebrovascular and cognitive aging remains in part unknown.

Studies on the effects of exercise can take two forms. In the first, participants with a history of regular exercise and sedentary participants are compared (Rogers et al. 1990; Yaffe et al. 2001; Churchill et al. 2002; Podewils et al. 2005; Etnier et al. 2006; Kramer et al. 2006; Larson et al. 2006; Brown et al. 2010; Brown et al. 2011). While these studies have the advantage of taking into account the long-term effects of exercise, they are subject to various confounds because the people who

exercise regularly may also be more likely to have a healthy lifestyle in other respects (Churchill et al. 2002; Kramer et al. 2006). People that engage in regular exercise may also be more likely to have a healthy diet, refrain from smoking and excessive drinking for example. The other type of study follows individuals with a similar background through a regular exercise training intervention and, typically, some other form of activity such as cognitive training in a control group of matched participants (Colcombe et al. 2006; Voss et al. 2010; Erickson et al. 2011; Prakash et al. 2011; Hopkins et al. 2012). While this type of study avoids the potential confounds of unmatched lifestyle choices, it does not address the question of long-term effects of regular exercise. However, with the combined information of these two types of studies, a cohesive picture of the effects of physical fitness on vascular and cognitive health is starting to emerge.

Retrospective population studies of questionnaire-based self-reported physical activity and cross-sectional studies including a cardiorespiratory fitness test have suggested that regular exercise may be partly protective for dementia (Podewils et al. 2005; Larson et al. 2006) and cognitive decline (Rogers et al. 1990; Yaffe et al. 2001; Churchill et al. 2002; Etnier et al. 2006; Kramer et al. 2006; Brown et al. 2010; Brown et al. 2011). Typically, recent studies quantify VO<sub>2</sub>max, to estimate cardiorespiratory fitness by measuring the amount of O<sub>2</sub> used for metabolism during maximal effort.

Despite the potential confounds of cross-sectional studies, a lifetime of regular exercise seems to have a beneficial effect on cognitive health. The effects of a physical training regimen on cognitive health are, however, more subtle (Churchill et al. 2002; Kramer et al. 2006) and may depend on many factors including the amount of exercise done on the day of the experiment and genetic polymorphisms (Hopkins et al. 2012). A meta-analysis of fitness training studies showed that fitness training results in improved cognitive scores, especially for tasks requiring executive control processes (Colcombe et al. 2003). Older adults's performance on executive function tasks may be improved by an aerobic physical training regimen. Furthermore, this type of intervention may also lead to patterns of functional connectivity more similar to those seen in younger adults (Voss et al. 2010; Prakash et al. 2011). Furthermore, grey matter atrophy associated with aging may

be reduced by a similar physical training program (Colcombe et al. 2006; Erickson et al. 2011).

Cardiorespiratory fitness also has a positive effect on vascular health. Physically fit older women were found to have lower blood pressures and higher cerebrovascular reserve (Brown et al. 2010). Results in animals have also shown that regular exercise leads to increased cerebrovascular reserve, possibly through angiogenesis (Swain et al. 2003). The positive effects of regular exercise on cognition and cerebral blood flow (CBF) in aging may be due in part to increased antioxidant activity leading to increased NO bioavailability and improvements in vascular tone (Pialoux et al. 2009; Davenport et al. 2012) (Figure 3). In a study of post-menopausal women, Pialoux and colleagues (Pialoux et al. 2009) found an inverse relationship between VO<sub>2</sub>max and oxidative stress markers, but a positive relationship between antioxidant activity and VO<sub>2</sub>max, indicating better mitochondrial function in more active older women. A similar relationship was seen between cerebrovascular conductance and oxidative stress markers, indicating that part of these effects may be due to changes in the regulation of vascular tone.

Animal studies suggest that exercise may result in increased serotonin and brain-derived neurotrophic factor (BDNF) levels in the brain, which may in turn lead to neurogenesis and cognitive improvement (Churchill et al. 2002; Vaynman et al. 2004; Hopkins et al. 2010; Spoelgen et al. 2011; Davenport et al. 2012). Though difficult to establish non-invasively, some of the same mechanisms may be involved in cognitive improvements following regular exercise regimen that have been detected in adult human populations (Hopkins et al. 2012). IGF-1, VEGF and BDNF, by their role in initiating both the angiogenesis and neurogenesis cascades, are thought to be the main effectors in regulating the effects of regular exercise on cerebrovascular function (Cotman et al. 2007; Davenport et al. 2012) (Figure 3).

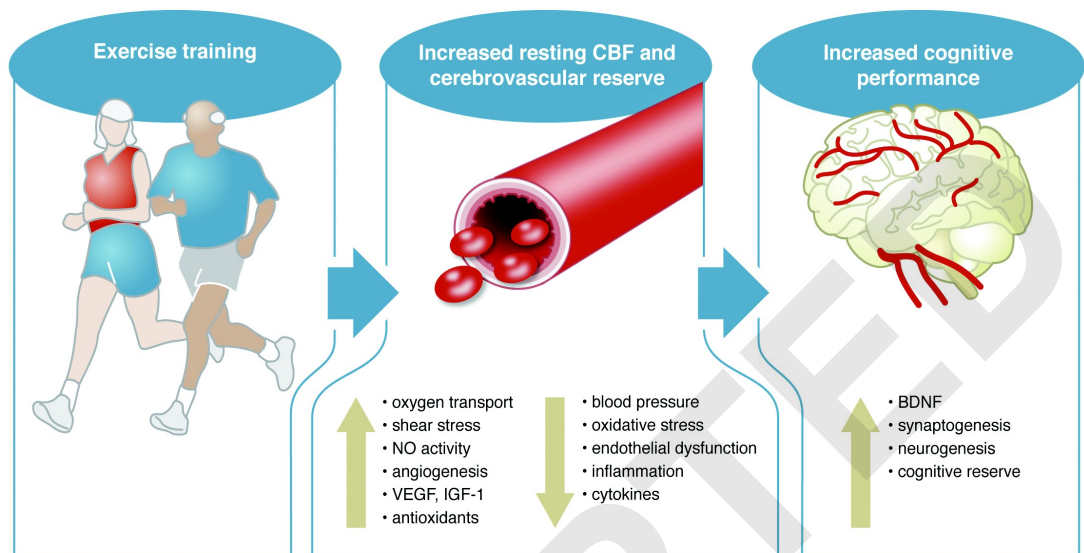


**Figure 3. Exercise and cognition**

Proposed vascular mechanisms in the association between exercise training and increased cognitive plasticity. This figure and its caption were reproduced from (Davenport et al. 2012).

Though the link between vascular health, fitness and cognition is becoming more established, some of the difficulties in pinning down the relationship between vascular health and cognition may arise from the fact that the exact impact of aging on cognition is still a much debated subject.

### 1.3. Aging and cognition

Aging is associated with changes in cognitive processing. While decreases in processing speed have been observed across the majority of cognitive tasks studied in older adults, there is some debate as to their specificity and source.

One of the most obvious confounds to take into account is that all sensory systems degrade with age. Within the visual system, for example, aging leads to hardening and increased density of the crystalline lens, a decrease in resting pupil diameter, increased opacity of the lens and retinal cell loss. All these factors combine to greatly reduce the light that enters the eye as we age. By 60 years of age, it is estimated that two thirds of retinal luminance has been lost (Cabeza et al. 2005). Because less information reaches the brain, this means that older brains must process information with a lower starting signal-to-noise ratio (SNR). This is true of other sensory systems as well, and must be kept in mind when assessing the effects of aging in cognitive tasks that include a significant sensory component.

Some of the decreased performance, both in terms of errors and reaction time, may therefore be attributed to the effects of decreased sensory system performance (Cabeza et al. 2005). However, certain tasks seem to be specifically impacted by age over and beyond these general sensory slowing effects. Furthermore, though decreased hemodynamic responses are expected in a system showing the effects of wear, it is the presence of specific and reproducible patterns of increased functional signals in specific types of task which has most intrigued the cognitive neuroscience community and will be a focus of the following discussion.

The functions thought to be most affected by the physiological changes associated with age fall under the category of 'executive functions'. This term is used to describe a range of functions such as planning, working memory, inhibition, problem-solving and monitoring. These functions generally involve a network of structures that includes some frontal component (Petrides 2005). This, combined with the ubiquitous observation of an increased frontal component in functional imaging studies of cognitive aging and the known plasticity of the brain even in later life, has led to the formulation of several theories of neuronal processing changes in healthy cognitive aging.

Recently, Spreng and colleagues published a meta-analysis of age-related differences reported across many cognitive domains in BOLD and positron emission tomography (PET) studies (Spreng et al. 2010). This study shows that it is possible to generalize across cognitive domains to find reliable age-related differences in activation foci (Figure 4). Most of these foci fell within the task positive network, which is known to be activated across many tasks and is one of the most reliable networks found in functional connectivity analyses (Fox et al. 2005; Toro et al. 2008). This study compared maps of various cognitive tasks acquired in high-performing and more poorly performing older adults. While left frontal areas showed consistently higher signals in older adults when age groups were matched for performance, frontal areas on the right hemisphere showed higher signal changes when older adults' performance was poorer than their younger counterparts'. When looking more specifically at studies of executive function, a bilateral increase in functional signal was seen over frontal areas, likely

because performance was not used to distinguish groups of older adults. There may therefore be a selective advantage to greater involvement of the left prefrontal areas, and older adults showing enhanced left frontal recruitment may be better able to maintain their performance at the level achieved by young subjects. Increased right prefrontal signal changes on the other hand, may reflect degrading of specialized neural constructs and therefore recruitment of brain areas not specific for the task.

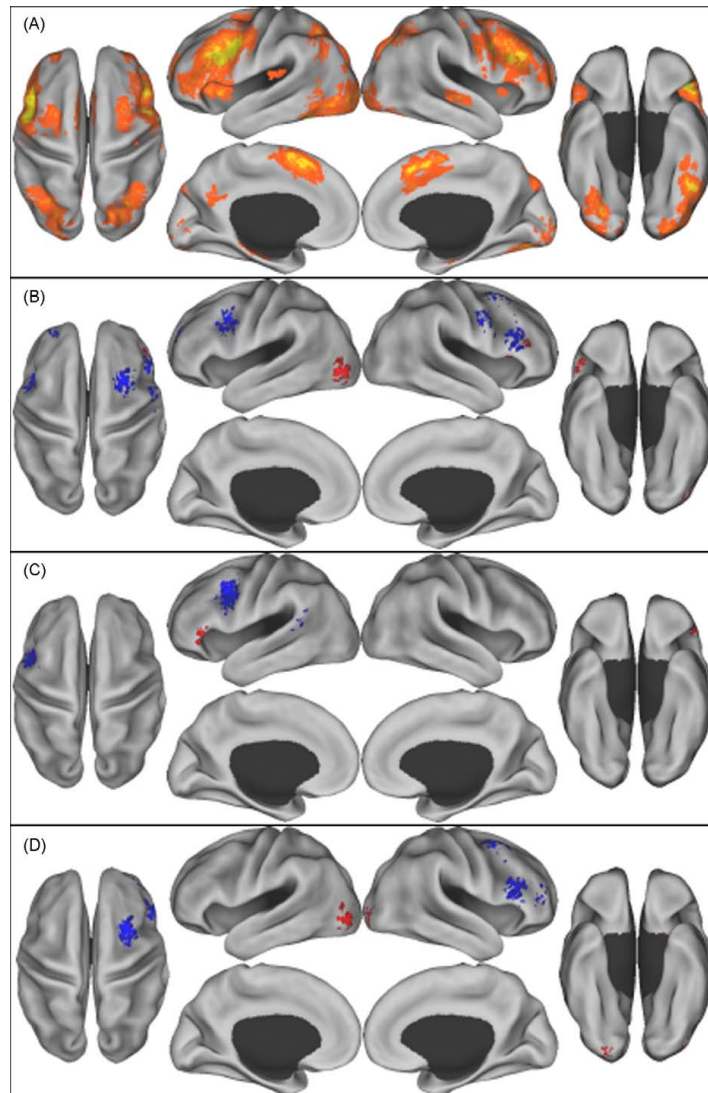


**Figure 4. Reliable patterns of brain activity across studies of aging**

A: Activation likelihood clusters across all studies and age groups. B: Age differences from all studies. C: Age differences from those studies where old and young adults had equivalent performance. D: Age differences from those studies where old adults had poorer performance relative to young adults. Red = young adults > old adults, Blue = old adults > young adults. Figure reproduced from (Spreng et al. 2010).

The theories addressing the hemodynamic signal changes observed across cognitive studies seek to address two aspects: the localization of signal changes (with particular attention being given to signal increases) and the underlying cause of these changes. While both aspects inform each other to some extent, the most difficult to address is no doubt the underlying cause of these changes. Two main ideas are proposed to explain these phenomena. One is the idea of compensation and the other is the idea of dedifferentiation.

### **1.3.1. Mechanisms leading to changes in activation patterns**

Compensation hypotheses express the idea that as the brain ages, there is an accumulation of damage that will eventually lead to deficits, and that deficits can be alleviated at least partially by recruiting additional neural resources. These can be in the same area, so that a given area normally used for a given task is now more active than previously, or by recruiting additional brain regions that are not normally involved in the task in younger individuals (Cabeza 2002; Reuter-Lorez et al. 2008; Reuter-Lorenz et al. 2010). This type of theory implies that additional recruitment will provide a processing advantage that is usually observed as lower error rates or faster reaction times.

Dedifferentiation hypotheses state that as we age, the specialization of brain regions acquired during development breaks down, so that tasks which in early adulthood gave rise to very localized hemodynamic signal increases, now give rise to more loosely localized networks (Baltes et al. 1997; Park et al. 2009; Cappell et al. 2010; Reuter-Lorenz et al. 2010). Thus, aging leads to similar or the same functional responses to different tasks. In other words, there is an increased correlation amongst the activation patterns and observed performance on a variety of tasks.

Evidence for dedifferentiation was identified in a study by Baltes and colleagues (Baltes et al. 1997), showing that as participants age the intercorrelation between different cognitive scores, perceptual speed and sensory information all increase. While visual and auditory performance can explain a large proportion of cognitive score variability during aging, the authors privilege a general dedifferentiation process to explain their results. According to this view, the degradation of sensory

and cognitive constructs are both the results of a third factor that reflects the 'true' effects of aging.

The effects of aging that lead to dedifferentiation could arise from several phenomena. Even in health aging, decreases in anatomical and vascular integrity may lead to decreased specificity of neuronal signals (Park et al. 2009). It may also be that neuromodulators such as the monoamines (especially dopamine) play a role in reducing the SNR of neural information. Aging is associated with a decrease in the density of dopamine receptors and it is thought that decreased efficiency in this, and possibly other neuromodulatory systems, could lead to what would be equivalent to a reduced gain of neural systems. This in turn may cause neural representations to become less distinct and lead to a more uniform pattern of neuronal responses than in younger participants (Li et al. 2002).

### **1.3.2. Cognitive theories**

Theories of cognitive aging have progressed from descriptions of changes in localization (with little information on the underlying causes) towards more integrated theories with testable predictions. One of the earliest reported patterns of change with aging is decreased lateralization of prefrontal BOLD activation patterns in a variety of cognitive tasks (Cabeza et al. 1997; Reuter-Lorenz et al. 2000; Cabeza 2002). This led to the Hemispheric asymmetry reduction in older adults (HAROLD) hypothesis (Cabeza 2002). In the original proposal of the HAROLD model, it was also hypothesized that decreased lateralization could arise from compensation or dedifferentiation. On the compensation side, recruitment of the hemisphere not normally recruited in younger adults serves to provide the additional neuronal units necessary for efficient performance of the task when neuronal units in the specialized hemisphere have been lost. Implied by this theory is that performance on the task can be improved by bilateral frontal recruitment. There is some evidence that this is the case in older adults (Reuter-Lorenz et al. 2000; Cabeza 2002) and young adult may also recruit bilateral frontal areas in more demanding tasks (Nolde et al. 1998). There is some ambiguity, however, as to the benefit to be derived from right prefrontal activation; a meta-analysis from Spreng et al. showed that right frontal recruitment mainly seen in poorer performing

groups of older adults (Spreng et al. 2010). In the dedifferentiation view, the brains of older adults show a gradual decrease in regional specialization so that tasks associated with recruitment of highly specialized areas in younger participants are now associated with the recruitment of a more diffuse network of less-specialized brain regions.

The Posterior anterior shift in aging (PASA) hypothesis was devised to explain a pattern observed in a variety of tasks whereby older adults showed higher frontal - but lower parieto-occipital signal increases - than their younger counterparts (Grady et al. 1994; Davis et al. 2008). When younger and older adults are matched according to performance on both an episodic memory and perceptual task, older adults show a negative correlation between occipital and prefrontal cortex activity. Older individuals with higher prefrontal BOLD signal change have the lowest signal changes in occipital areas and are the best performers on these tasks (Davis et al. 2008). This theory is most compatible with a compensation explanation, since frontal areas are here thought to compensate for degraded perceptual representations in more posterior areas (Grady et al. 1994; Davis et al. 2008).

Another compensation-based theory is called CRUNCH or Compensation-Related Utilization of Neural Circuits (Reuter-Lorenz et al. 2008; Reuter-Lorenz et al. 2010). In this model, the increases in hemodynamic signals in older adults reflect neuronal activation used to compensate for functional loss in areas normally sufficient for younger adults to perform a given task. Older adults are hypothesized to recruit additional neural units to meet the task demands. One of the tenets of this hypothesis is that the additional units recruited by older adults are units that would also be recruited in younger adults if demands of the task were increased beyond their capacity to perform it with the neural constructs specific for it (Mattay et al. 2006; Cappell et al. 2010; Schneider-Garces et al. 2010). In other words, there is some hierarchy of regions that could be used to perform a given task and, as the initial choices are found lacking, reinforcements are brought in and the brain brings in more and more units as they become required to perform the task. However, in the context of finite time, attention, motivation and neuronal resources, these strategies eventually fail and lead to decreases in activation and performance when task demands are very high (Reuter-Lorenz et al. 2008; Schneider-Garces et

al. 2010). Because older adults need to engage this compensatory recruitment mechanism for lower task loads, this also means that they do not have the additional resources to meet even greater task demands. Therefore, as task difficulty increases, a pattern becomes apparent whereby younger adults engage these compensatory regions, while these mechanisms now fail in the elderly. The failure to engage additional resources in the elderly to meet task demands results in a decreased hemodynamic signal pattern (Cappell et al. 2010; Schneider-Garces et al. 2010).

An extension the CRUNCH model to take into account dedifferentiation was subsequently proposed (Park et al. 2009). This theory is called the Scaffolding theory of aging and cognition (STAC) (Park et al. 2009; Reuter-Lorenz et al. 2010) (Figure 5). If the brain of older adults works under tighter SNR constraints than that of younger adults, more or different neural resources may be necessary to achieve equivalent levels of performance. The authors posit that throughout life, the brain must update its connections and structures in the context of challenging situations. In the STAC theory, some brain structures may be recruited when a new ability is learned at any point during one's lifetime. These structures serve to create the neural scaffolds that will be increasingly used as a task becomes familiar. Once the task is well honed, the areas initially recruited may not be used in normal contexts. However, when more difficult circumstances arise, such as increased task difficulty, sleep deprivation or in the presence of large amounts of conflicting information, the brain may fall back on the structures initially used to learn the task to help it meet these new challenges. In older adults, because of anatomical, vascular or neuromodulatory declines (Li et al. 2002; Salat et al. 2004; Chen et al. 2011), the brain is less able to meet task demands. As ever more trivial demands become challenging the brain relies more on those units initially used to learn the task (Cappell et al. 2010; Schneider-Garces et al. 2010). Changes in fMRI activation loci therefore reflect a compensation for age-related losses, as well as the effects of dedifferentiation (Park et al. 2009; Reuter-Lorenz et al. 2010). Prefrontal areas are involved in a variety of tasks and these areas may be recruited in cases of high task demands even in younger adults. Therefore, the increased reliance on a series of common frontal structures to perform various task may be a hallmark of

dedifferentiation. This theory is attractive in that it integrates the complexity of the different sources of age-related differences seen in many other studies, and provides a framework of testable hypotheses with good explanatory power. However, as will be seen later, much of the work used to generate these hypotheses has been based on assumptions about the meaning of BOLD signal changes that may be severely weakened by more careful consideration.

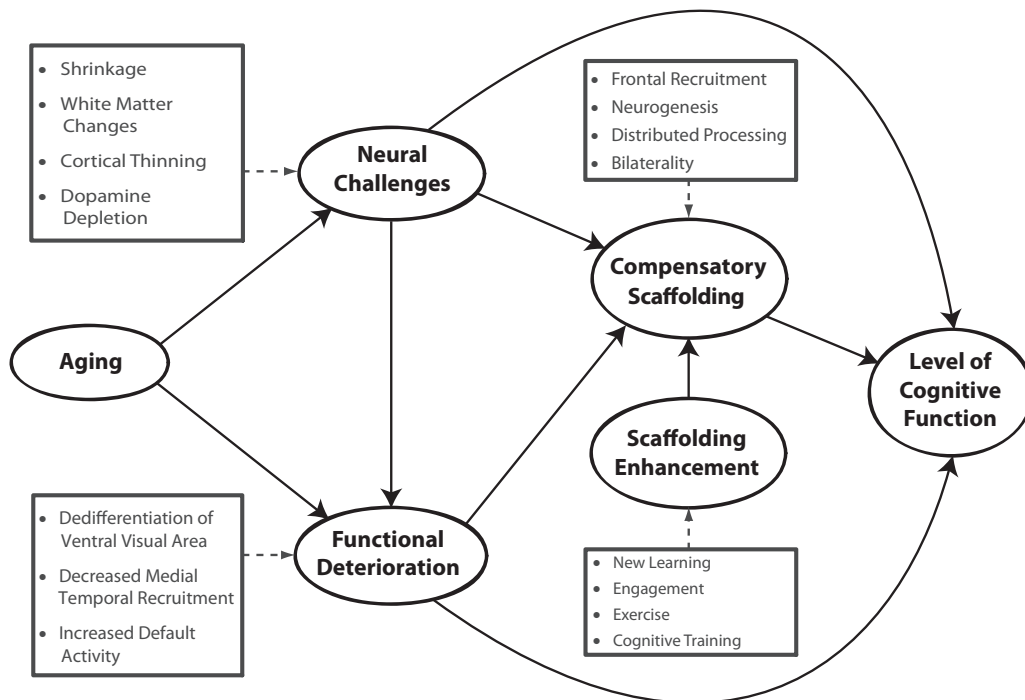


**Figure 5. A conceptual model of the scaffolding theory of aging and cognition (STAC).**

This figure and its caption were reproduced from (Park et al. 2009).

## 1.4. The BOLD contrast mechanism

BOLD contrast phenomenon arises from the fact that oxygenated and deoxygenated hemoglobin have different magnetic properties: oxyhemoglobin is diamagnetic while deoxyhemoglobin is paramagnetic. The paramagnetic nature of deoxyhemoglobin means that blood that is not fully oxygenated causes an attenuation of the  $T_2^*$ -weighted signal from increased dephasing of nearby water spins. Since arterial blood is almost fully oxygenated in healthy humans, there is specific attenuation of the  $T_2^*$  signal from venous blood and tissue containing parenchymal deoxyhemoglobin (Ogawa et al. 1990a; Ogawa et al. 1990b). During performance of a task, active brain regions consume oxygen to function, causing a

local increase in deoxyhemoglobin. It is debatable whether the local increase in deoxyhemoglobin is actually detectable using MRI scanners, especially at 1.5 or 3 Tesla (Kim et al. 2012). However, concomitant with this increased deoxyhemoglobin production comes a local vasodilation of blood vessels, which in turn causes an increase in local blood flow. This fractional increase in blood flow is much larger than the fractional increase in deoxyhemoglobin that it accompanies. This is thought to reflect the need for the  $O_2$  gradient from arterial blood to metabolizing tissue to be steep for effective diffusion of blood  $O_2$  into active tissue more distal to vessels (Buxton et al. 1997; Buxton et al. 1998b; Buxton 2010; Devor et al. 2011). One of the corollaries of this larger fractional blood flow change is that for a given increase in deoxyhemoglobin concentration through local metabolism, there is a corresponding larger increase in blood flow to the same area. Because the inflowing blood is fully oxygenated, this causes an increase in BOLD signal from a local reduction in the deoxyhemoglobin concentration. This vascular response is called the hemodynamic response. Functional MRI techniques measure it to make inferences about the underlying neuronal activity that triggers it. The exact characteristics of this hemodynamic response function, both in terms of shape and underlying physiology, have been and still are the subject of much debate (Glover 1999; Buxton 2010; Kim et al. 2012).

#### **1.4.1. Underlying neuronal activity**

Functional imaging using hemodynamic methods such as BOLD are based on the assumption that the signal changes observed are strongly correlated with underlying neuronal activity. Convincing evidence that this is the case comes from simultaneous electrophysiological and fMRI recordings in monkeys (Logothetis et al. 2001; Shmuel et al. 2002; Logothetis et al. 2004). In these studies, electrodes are implanted in monkey visual cortex and simultaneous recordings during spontaneous or visual task-elicited activity of neuronal currents and fMRI signal are made. Electrophysiological recordings can capture three types of neuronal electrical activity. The first and most obvious is the spiking activity. In this type of recording, a high impedance electrode is inserted in the cortex and action potentials of nearby neurons can be recorded. This method predominantly measures the action potentials coming from the largest neurons within 50–100  $\mu\text{m}$

of the electrode. A second type of recording involves the insertion of a lower impedance electrode (larger tip). Two sources of information are present within this signal: the high frequencies are isolated using a high-pass filter with a cutoff frequency of 300-400 Hz and the lower frequencies using a low-pass filter with a cutoff at 200 Hz. The high frequency component is called multi-unit activity (MUA) and is thought to represent spiking activity from more distant neurons. The low frequency component, called local field potentials (LFP) is thought to reflect predominantly sub-threshold somato-dendritic currents, with some contributions from voltage-gated membrane oscillations and membrane after-potentials (Logothetis et al. 2004).

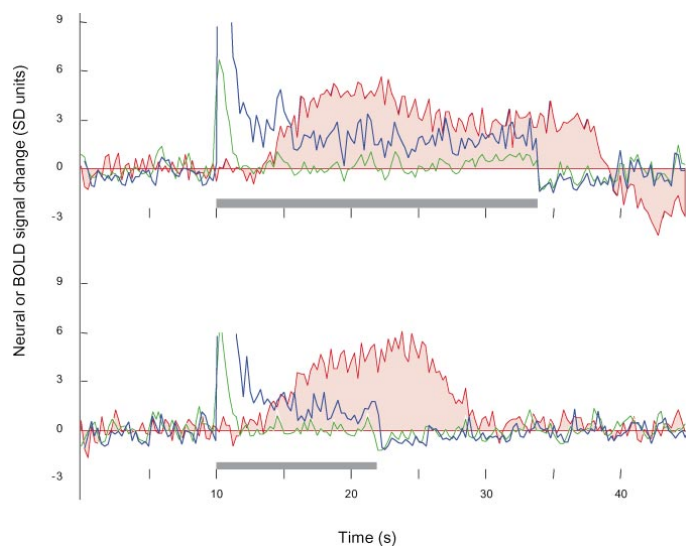


**Figure 6. Electrical underpinnings of the BOLD signal**

A cortical site in which the LFP and MUA predictions of the BOLD response differ significantly. Responses to a 24-s (upper) and 12-s (lower) stimulation are shown. The blue trace measures the LFP, the green trace measures the MUA, and the red-shaded trace measures the BOLD response. The MUA signal is brief and approximately the same in both experiments. The LFP and BOLD responses covary with the stimulus duration. This figure and its caption were reproduced from (Logothetis et al. 2004).

Early studies of this type have established that while BOLD signal amplitude is correlated with all aspects of neuronal firing, it is most closely linked with local field potentials (LFPs) than with other electrical activity such as spikes from action potential firing (Logothetis et al. 2001) (Figure 6). LFPs are thought to reflect a variety of neural processes including synaptic potentials, somato-dendritic spikes and voltage-gated membrane oscillations (Logothetis et al. 2004; Magri et al.

2012). More recent research has investigated the link between BOLD signal response components and frequency bands within the LFP signal. Magri and colleagues (Magri et al. 2012) have shown that the gamma band, including the higher frequencies within the LFP signal, is the most closely related component to the BOLD response. This band was found to contribute the most information in determining the overall shape of the hemodynamic response function (HRF). It was correlated with both amplitude and lag of the response and was found to be stimulus-dependent. The beta band of the spectrum, containing intermediate frequencies, also contained some information determining the shape of the HRF. It was found to be correlated with the time of the initial rising phase of the HRF. The alpha band, consisting of the lower frequencies within the LFP spectrum, was found to contain little information beyond what the other bands could contribute. However, the relative power distribution across all bands contributed to the shape of the HRF measured (Magri et al. 2012). In agreement with a heuristic theory of the relationship between frequency distribution of neural signals and BOLD signal amplitude (Kilner et al. 2005), a relative shift in frequency distribution towards higher frequencies was found to correlate with BOLD signal activation. In other words, while alpha band power did not add much information on its own, a relative decrease in power in this band as compared to the gamma band (containing higher frequencies) was an independent source of information about BOLD signal increases. All these relationships were found to be true also for BOLD signal decreases, with shifts towards lower frequencies indicative of a deactivation. Taken together, these results argue strongly for a neuronal activity contribution to the BOLD signal. However, the quantification of this underlying contribution may not be straightforward in the context of non-invasive human studies. Furthermore, the relationship between electrical signaling and downstream metabolic effects that lead in turn to the vascular response, present their own quantification challenges.

#### **1.4.2. Oxidative metabolism**

While little doubt now remains that the bulk of metabolism in the brain is oxidative, there was heated debate on this topic in the early days of functional neuroimaging. This debate was triggered by early PET results showing an unexpected

discrepancy between changes in glucose metabolism and oxygen consumption during activation (Fox et al. 1986).

The main energy expenditure of neurons is to maintain membrane potential to be ready to fire and integrate synaptic information when the need arises. To do so, the brain uses energy in the form of ATP, which is derived from the metabolism of glucose. Two forms of glucose metabolism exist: anaerobic, which does not use oxygen, and aerobic, which uses oxygen in the mitochondrial electron transport chain. Aerobic glycolysis is highly efficient, as it can lead to the formation of as many as 38 ATP molecules from a single glucose molecule. Anaerobic glycolysis is, on the other hand, faster but only produces 2 ATP molecules per glucose. The first steps of both pathways are the same, with the formation of two pyruvate molecules and two NADH molecules. In anaerobic glycolysis the pyruvate is then simply converted to lactate in the cytoplasm and not used for further energy production, while pyruvate goes to the mitochondria to generate more ATP molecules by going through the Krebs cycle and oxidative phosphorylation during aerobic metabolism. Because aerobic glycolysis is much more efficient at energy production and because the brain is known to be an avid user of oxygen, it was expected that oxidative metabolism would be the main form of metabolism used in the brain. Indeed, interruption of the brain's oxygen supply leads to unconsciousness within seconds and irreversible tissue damage within minutes (Levy et al. 1975).

The most likely interpretation of the early PET results (Fox et al. 1986) showing a coupling ratio between glucose and oxygen consumption more compatible with anaerobic glycolysis is that there were important quantification difficulties involved in the techniques used and possible biases that lead to underestimation of the O<sub>2</sub> consumption (Hattori et al. 2004; Buxton 2010). Glucose metabolism and O<sub>2</sub> consumption are both not trivial to quantify using MRI or PET techniques, and require a substantial modeling component that is difficult to validate. However, more recent experiments have yielded results much more compatible with the predicted predominant role of oxidative metabolism (Ishii et al. 1996; Mintun et al. 2002; Yamauchi et al. 2002; Hattori et al. 2004; Ito et al. 2005; Ibaraki et al. 2008; Ibaraki et al. 2010).

In order to make inferences about neuronal activity from the BOLD response, questions pertaining to the relative contribution of oxidative and non-oxidative metabolism will have to be elucidated. However, researchers who use the BOLD signal alone make the implicit assumption that oxidative metabolism is the main energy production pathway and that the amplitude of the BOLD response is in some way, directly or indirectly, proportional to the amount of oxidative metabolism (and therefore total metabolism) evoked by neuronal activity.

### **1.4.3. Neurovascular coupling**

Because the brain has no stores of oxygen and glucose, increases in metabolic activity must be met with increases in metabolic substrate availability and waste removal. These increases are achieved through local blood flow increases. The signaling cascades that underlie this process of neurovascular coupling (flow increases following neuronal activity) are complex and may be regionally dependent. While research in this area has identified the main mediators and modulators of this pathway (Lauritzen et al. 2003; Girouard et al. 2006; Lecrux et al. 2011), their relative importance and the cellular environment variables that determine their function are still largely unknown.

The neurovascular unit is composed of different cells which work together to orchestrate the blood flow increase required by increased metabolic demand. The neurovascular unit includes neurons, glia and vascular cells, including vessel endothelium, smooth muscle cells, pericytes and adventitial cells (Girouard et al. 2006). The general structure of the neurovascular unit is shown in Figure 7.

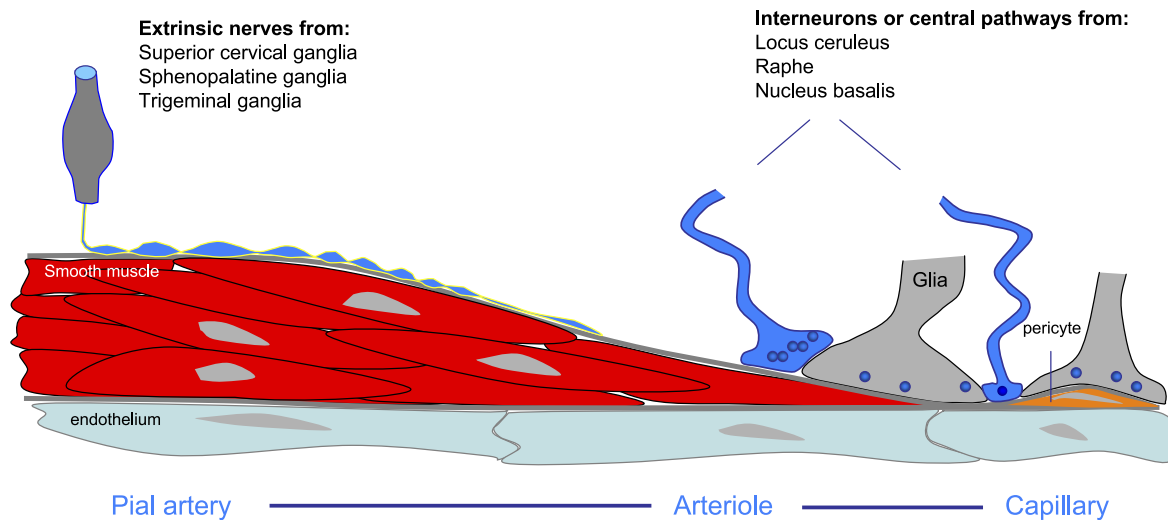


**Figure 7. Neurovascular unit**

Pial arteries and arterioles (on the surface of the brain) are innervated by nerve fibers arising from cranial autonomic ganglia. Smaller cerebral arterioles (<100  $\mu\text{m}$ ) come in contact with nerve terminals arising from local interneurons and from central pathways originating from distant sites in the brain stem or basal forebrain. These neurovascular associations often terminate on astrocytic end feet lining the abluminal vascular surface. Pericytes, contractile cells embedded in the capillary wall, are closely associated with astrocytic end feet and endothelial cells. The term “neurovascular unit” has been coined to define the close structural and functional relationships between brain cells and vascular cells. This figure and its caption are reproduced from (Girouard et al. 2006).

As arteries and arterioles branch out and penetrate deeper into the brain, the smooth muscle layer surrounding arteries becomes thinner and eventually disappears at the level of capillaries, where it is replaced by other contractile cells called pericytes. In the smaller arterioles and capillaries, there is direct contact between the vessel wall and astrocytic end-feet as well as neurons from a variety of sources (Girouard et al. 2006). Endothelial cells, perivascular astrocytes and neurons may all release molecules that lead to changes in arteriole diameter. Furthermore, there is some indications that pericytes may also contribute to changes in capillary diameter (Girouard et al. 2006; Lecrux et al. 2011).

One of the main contentious issue in the field of neurovascular coupling is the relative role of excitatory and inhibitory synaptic activity in triggering a CBF increase (Lecrux et al. 2011). The majority of research efforts have investigated excitatory transmission. Strong experimental evidence showed that glutamate, the main excitatory neurotransmitter in the brain, can trigger CBF increases through an indirect pathway involving both NMDA and AMPA glutamate receptor subtypes

(Gsell et al. 2006; Lecrux et al. 2011). The effects of glutamate may be mediated through the nitric oxide (NO) pathway, with neuronal NO release upon NMDA receptor activation (Yang et al. 1996; Bhardwaj et al. 2000; Lecrux et al. 2011). These effects may also be partially mediated through calcium waves in astrocytes, where glutamate-dependent increases in the concentration of  $Ca^{2+}$  ions in astrocytic end-feet may lead to changes in arteriolar diameter (Yang et al. 1996; Zonta et al. 2003; Girouard et al. 2006; Lecrux et al. 2011).

GABA interneurons may also play a role in mediating the CBF increases associated with LFPs. Immunocytochemistry studies of GABA interneurons have shown that subpopulations express a variety of vasoactive molecules including NO, neuropeptide Y, somatostatin, vasoactive intestinal polypeptide and acetylcholine (Valtschanoff et al. 1993; Kubota et al. 1994; Abounader et al. 1997; Lecrux et al. 2011). Through release of these mediators, GABAergic interneurons may contribute to the neurovascular coupling response (Kocharyan et al. 2008; Lecrux et al. 2011).

Beyond these indirect effects of neurotransmitter release, a variety of mediators of neurovascular coupling have been identified (Figure 8).

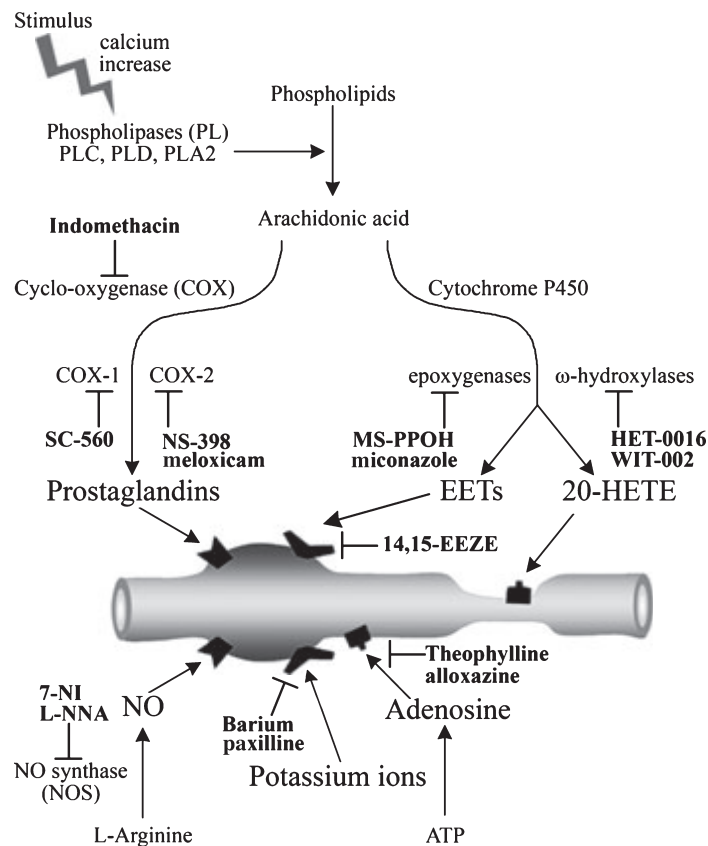


**Figure 8. Neurovascular coupling response**

Increased intracellular calcium levels following stimulation lead to the activation of phospholipases and production of arachidonic acid (AA). AA is processed by either COX-1 or COX-2 to release diverse prostaglandins or by the cytochrome P450: epoxygenases or x-hydroxylases to produce EETs and 20-HETE. Other key pathways in the haemodynamic response to sensory stimulation include nitric oxide, potassium and adenosine. This figure and its caption were reproduced from (Lecrux et al. 2011).

The most important signaling cascades include the NO pathway, present in smooth muscle cells, endothelial cells, astrocytes and neurons (Lecrux et al. 2011).

Inhibition of this pathway with NO synthase antagonists leads to less pronounced CBF increases in response to a variety of stimuli, including sensory stimulation (Dirnagl et al. 1993; Lindauer et al. 1999; Lecrux et al. 2011), direct cerebellar stimulation (Yang et al. 1996; Girouard et al. 2006) and hypercapnia (Yang et al. 1996).

Other frequently observed mediators include vasoactive ions such as potassium (K<sup>+</sup>) and hydrogen (H<sup>+</sup>). Both show increased extracellular concentration following action potential firing and synaptic transmission leading to vasodilation (Kuschinsky

et al. 1972; Girouard et al. 2006; Lecrux et al. 2011). Adenosine, also a product of metabolism through the catabolism of ATP, is also recognized as a potent vasodilator. Neurons, astrocytes and smooth muscle cells all express an adenosine receptor subtype and may mediate the neurovascular role of adenosine (Ngai et al. 2001; Lecrux et al. 2011).

Another group of mediators are derived from metabolism of arachidonic acid. Cyclo-oxygenase enzyme 2 breaks down arachidonic acid to form prostaglandin molecules. Prostaglandins may be produced in active neurons and act as vasodilator agents, but their role and locus of activity has not yet been fully elucidated (Stella et al. 1994; Niwa et al. 2000; Andreasson 2010; Lecrux et al. 2011). Other molecules have been shown to be vasoactive, but their role in activity-dependent CBF increases remains unclear (Lecrux et al. 2011).

From this branch of research it may be inferred that the regulation of blood flow in neurovascular coupling is complex and that the amplitude of the hemodynamic response may depend strongly on the specific cellular environment of brain regions. However, one encouraging conclusion to be drawn from these results is that in all cases, there is some relationship between aspects of neuronal signaling and the release of vasoactive molecules. Therefore, though the exact underpinning of this blood flow response may be difficult to untangle, the response itself can be taken as a surrogate for neuronal activity.

#### **1.4.4. Blood flow response**

The main component of the hemodynamic response resulting in BOLD signal changes during activation is the increase in blood flow. During performance of a task, the coupling ratio between the increase in blood flow to the increase in oxidative metabolism is thought to be around two under normal circumstances (Buxton 2010). In other words, during local brain activity in the absence of disease or pharmacological agents, the fractional blood flow change is thought to be about two times larger than the fractional change in oxidative metabolism. This measurement, however, remains somewhat speculative, given the low SNR of blood flow and oxidative metabolism measurement.

Cerebral blood flow can be directly measured non-invasively using MRI through techniques such as Arterial Spin Labeling (ASL). ASL measurements have the advantage over BOLD of yielding an absolute and unambiguous measure of a physiological quantity. However, widespread adoption of ASL as a functional contrast mechanism has been slowed by the fact that ASL is an intrinsically low SNR technique. This is because in all of its implementations it relies on image subtractions to provide functional contrast, thereby leading to addition of errors in measurements. Furthermore, the effect sizes are generally on the order of a fraction of a percent.

Though there exists a wide variety of ASL pulse sequences, all function under the same general principle. A magnetic tag is added to the inflowing blood in every other image of a time series and adjacent image pairs are subtracted to isolate the flow dependent component of the signal (Detre et al. 2012). There are two main families of ASL sequences in current use, pulsed and continuous ASL techniques. The terms 'pulsed' and 'continuous' refer to the tagging method used (Williams et al. 1992; Edelman et al. 1994; Wong et al. 1998). In modern ASL techniques, the blood is tagged at the level of the carotid arteries. More specifically, the spins in the blood of the main arteries flowing into the brain are inverted so that the signal of the tagged blood will not contribute to the image. Once the spins are inverted, there is a waiting period for inflowing blood to reach the volume we wish to image and, after the appropriate delay, an image of the brain is acquired. The blood that was tagged at the level of the neck is now darker (on a  $T_2^*$  acquisition) than the blood that was already in the volume imaged (the static signal). For the following image, the procedure is repeated, but this time the tagging is not performed, so that all the blood has the signal intensity provided by the image acquisition excitation pulse. By subtracting these two images, we can isolate the decreased signal component created by tagging the blood at the level of the neck. This is the flow dependent component, since only the inflowing blood has been labeled (Williams et al. 1992; Detre et al. 2012).

In pulsed ASL sequences (PASL), a large slab of blood is inverted by a single electromagnetic pulse at the level of the neck (Edelman et al. 1994; Wong et al. 1998). Continuous sequences label a thin slab for a longer period of time to

achieve an equivalent volume of labeled blood (Williams et al. 1992). True continuous sequences are technically challenging, but in recent years, techniques termed pseudo-continuous have been developed that provide several advantages over other techniques. Pseudo-continuous sequences (pCASL) use a train of short RF pulses to achieve a near continuous labeling. This provides a superior SNR and implicit control over label duration of continuous approaches, without the strain on scanner gradients that true continuous sequences represent (Wu et al. 2007; Dai et al. 2008; Detre et al. 2012).

With recent improvements in ASL techniques, local changes in CBF caused by task-induced oxidative metabolism are readily detectable. However, global flow changes such as those caused by blood gas changes provide a more difficult challenge to ASL techniques. In a paper recently published by our group (Tancredi et al. 2012), we have shown that pCASL sequences may provide improved accuracy and sensitivity to these changes as compared to PASL. This is likely due to the fact that, in the case of global flow increases, blood flow velocity increases in the carotid arteries results in tag compression effects in PASL sequences. Under certain conditions, uncontrolled shift in tag delivery dynamics can lead to systematic underestimation of CBF (Bolar et al. 2012).

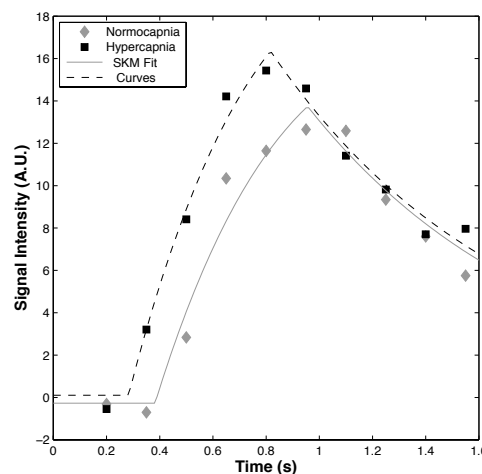


**Figure 9. Tag delivery in ASL during normocapnia and hypercapnia**

Kinetic modeling of tag delivery from multiple inversion time data during normocapnia and hypercapnia in a single subject. With standard parameters, ASL images are acquired during the outflow phase of this curve (around 1.4 seconds), where the two curves overlap. Using this set of parameters underestimates the effects of hypercapnia on flow. This figure was included with the permission of its authors (unpublished preliminary data).

Since measurement of the blood flow increase caused by hypercapnia is a crucial part of all studies presented in this thesis, a pseudo-continuous ASL approach has been used in all experiments.

#### **1.4.5. Blood volume**

Cerebral blood volume (CBV) changes with neuronal activity are strongly correlated with changes in CBF. This relationship was first estimated by Grubbs and colleagues from experiments in anesthetized rhesus monkeys during hypercapnia to be a power law relationship with an exponent value of 0.38 (Grubb et al. 1974). However, because this measurement was not done in awake humans, and because the exponent reflects total blood volume rather than venous blood volume, which is the quantity expected to affect BOLD signal changes, there have been recent attempts to revisit this exponent value.

Several MRI techniques exist to measure CBV changes. While some of these require the injection of a contrast agent such as MION, some non-invasive techniques using endogenous contrast mechanisms have also been developed. The most widely used of these techniques is called vascular space occupancy (VASO) and yields a measure of total blood volume (Lu et al. 2003). This technique uses a non-specific inversion recovery sequence to null the blood signal. The functional contrast arises from the fact that as blood volume increases during activation more spins move into the nulled compartment. While the VASO technique is not specific to the blood volume change that contributes to the BOLD signal change (i.e. venous blood), it is a measure of a physiological quantity and may be used as a functional contrast mechanism in its own right (Lu et al. 2003; Donahue et al. 2006; Lu et al. 2012a).

For a more specific depiction of the CBV changes that contribute to BOLD signal changes, a sequence called venous refocussing for volume estimation (VERVE) can be used to specifically measure venous blood volume changes (Stefanovic et al. 2005; Chen et al. 2009a; Chen et al. 2010c). This sequence uses the dependence of venous blood on  $T_2$  and refocussing interval in a Carr Purcell Meiboom Gill (CPMG) sequence to isolate CBV changes specific to the venous compartment. It has been used by Chen and colleagues to estimate the flow-

volume exponent. The exponent was found to be lower than previously thought, with values around 0.18-0.23 for activation in visual and motor task, as well as for a hypercapnic manipulation (Chen et al. 2009a; Chen et al. 2010c).

#### **1.4.6. Limitations of the BOLD signal**

While the BOLD contrast may be a sensitive measure of neuronal activity, it is limited in terms of physiological specificity since it arises from a mixture of oxidative metabolism, blood flow and blood volume. Its amplitude is dependent on neurovascular coupling, which may vary with age and vascular health status. Furthermore, because much of the complexity of the underlying molecular signaling pathways still remains to be elucidated, we cannot yet determine the degree of regional and pathway-specific heterogeneity to be expected even in healthy individuals.

##### *1.4.6.1. Confounds in aging studies*

Aging studies may be particularly vulnerable to the limitations of the BOLD contrast (Figure 10). Because older adults show altered vascular function and because their oxidative metabolism is also likely affected by life-long mitochondrial stress, all aspects of the BOLD signal may be affected by aging. This is likely the case both for the baseline and dynamic range of the signal. This renders interpretation of BOLD signal differences even more problematic since BOLD signals are relative changes from an unknown baseline.

Beyond the difficulties of interpretation of the BOLD signal itself, functional studies of aging suffer from a variety of other confounds. For example, aging studies suffer from an increased likelihood of partial volume effect biases. As grey matter density decreases with age, the signal within a given voxel contains a greater proportion of white matter and CSF. It should also be noted that the normalization procedure performed in group studies will inflate the grey matter, making it appear thicker than it really is and lead to an underestimation of atrophy. Another confound arises from the fact that most aging studies quantify the BOLD signal within a region-of-interest derived from group analyses. While some voxels are always expected to include some white matter and CSF when using this technique to draw ROIs, this

effect may be exacerbated in older cohorts with more heterogeneous degrees of grey matter atrophy (Samanez-Larkin et al. 2008).

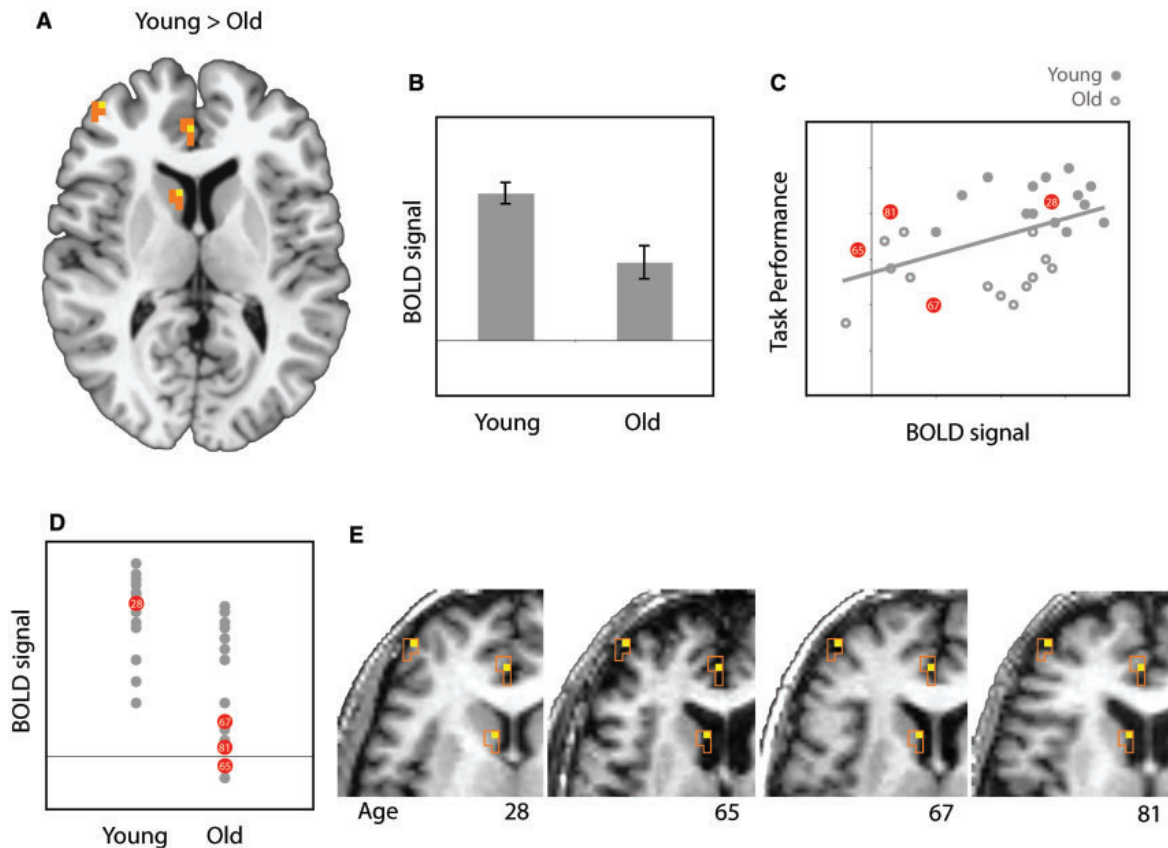


**Figure 10. Example case of BOLD comparisons across lifespan**

This figure displays hypothetical results from a cross-sectional study examining differences in brain activity between younger and older adults. Although, the results of this hypothetical study may seem to suggest that the poorer performance of older adults is due to their showing less brain activation than the younger adults in these regions, there are several reasons detailed in the text to be skeptical of these conclusions. (A) A whole brain analysis reveals a main effect of age (Young > Old) in three regions: lateral prefrontal cortex, anterior cingulate and medial caudate. (B) An example of BOLD signal change plotted from one of these regions reveals significantly greater activation in younger adults. (C) A scatter plot displays a significant simple correlation between neural signal (x-axis) and behavior (y-axis) across all participants (younger and older adults combined). (D) The individual data points (used in the previous bar graph and the x-axis in the scatter plot) plotted here by age group reveal a non-normal (bimodal) distribution of the data for the older adults. About half of the sample has BOLD signal change values near zero. (E) The data plotted in panels (B)–(D) were extracted using a single ROI mask shown here overlaid on a random sample of individual participants' T1 anatomy. The participant ages are listed below each image. It is clear in these images that this single mask does not align well with the individual participants' anatomy. The data points for each of these four sample participants have been highlighted with red dots and labeled with the participant ages in panels (C) and (D). This figure and its caption were reproduced from (Samanez-Larkin et al. 2008).

While all these sources of ambiguity limit the inferences that can be made about neuronal activity from the BOLD signal, the fact remains that its amplitude is correlated with synaptic activity and oxidative metabolism. Techniques have been developed that can isolate this metabolic component and thereby obtain a physiologically-specific quantity more closely related to neuronal activity. These techniques are called calibrated fMRI techniques and will be discussed in the next section.

## **1.5. Calibrated fMRI techniques**

Calibrated fMRI techniques have been developed to extract the oxidative metabolism component from the BOLD signal measured in response to a task. Oxidative metabolism is isolated by first estimating the vascular component of the BOLD response through a calibration manipulation. Once estimated, this vascular contribution can be used to estimate the signal attenuation from the metabolic increase in deoxyhemoglobin (dHb) during performance of a task. Such a determination requires expressing the activation-induced BOLD signal as a fraction of the total attenuation of  $T_2^*$ -weighted signal attributable to dHb at baseline. The calibration procedure is typically done by measuring the BOLD and CBF responses during a breathing manipulation. Using a biophysical model of the BOLD signal, we can extrapolate from these measurements to an estimate of the calibration parameter  $M$ , which corresponds to the maximal possible BOLD signal change that would occur upon removal of all dHb.

### **1.5.1. Hypercapnia calibration method**

The first calibrated fMRI method developed used a hypercapnia (increases in inhaled  $\text{CO}_2$  concentration) breathing manipulation (Davis et al. 1998; Hoge et al. 1999a). During this calibration procedure, the BOLD and ASL responses to a hypercapnia manipulation are measured.  $\text{CO}_2$  is a potent vasodilator and its inhalation causes large CBF increases all over grey matter without, presumably, causing any change in oxidative metabolism (McPherson et al. 1991; Hino et al. 2000; Chen et al. 2010a). Therefore, measurements acquired during this manipulation can, in the context of a biophysical model, yield the BOLD to CBF relationship in the absence of metabolism. The same measurements are then done

during a cognitive task and BOLD reduction for a given amount of CBF increase, as compared to the ideal relationship found for hypercapnia, can be directly attributed to an increased dHb concentration from oxidative metabolism (Hoge et al. 1999b). This concept is graphically depicted in Figure 11.

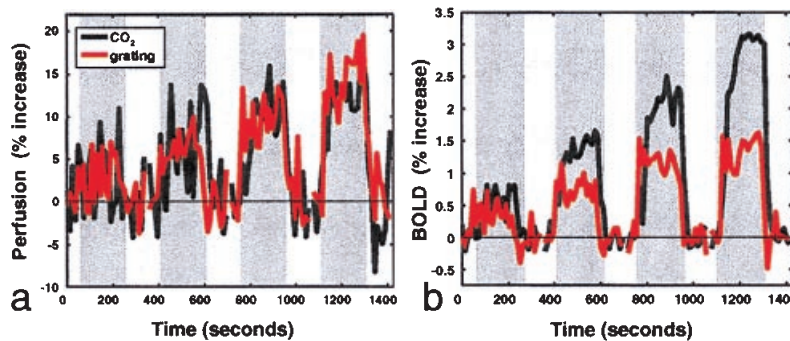


**Figure 11. BOLD attenuation from metabolism**

Perfusion and BOLD as a function of time during graded hypercapnia and visual stimulation ( $n = 12$ ; stimulation intervals indicated by grey background). (a) Relative perfusion as a function of time during graded hypercapnia (black curve) and graded visual stimulation (red curve) with contrasts adjusted to match hypercapnia-induced CBF increases. (b) BOLD signal as a function of time during perfusion increases shown in a. BOLD signals during visual stimulation are significantly lower than those observed during hypercapnia at matched perfusion levels, revealing graded increases in oxygen consumption. This figure and its caption were reproduced from (Hoge et al. 1999b).

In the hypercapnia method, small amounts of carbon dioxide (typically 5-10% CO<sub>2</sub> by volume) are added to the air breathed by subjects during acquisition of BOLD and CBF image series. The vasodilatory properties of CO<sub>2</sub> lead to increases in cerebral blood flow and tissue oxygen delivery, producing BOLD signal increases throughout grey matter as well as in large veins. The maximal BOLD signal  $M$  at a given location can then be extrapolated using the Davis model of BOLD as a function of CBF, assuming a constant arterial saturation of 100% and unchanged metabolism during hypercapnia (Figure 12a).

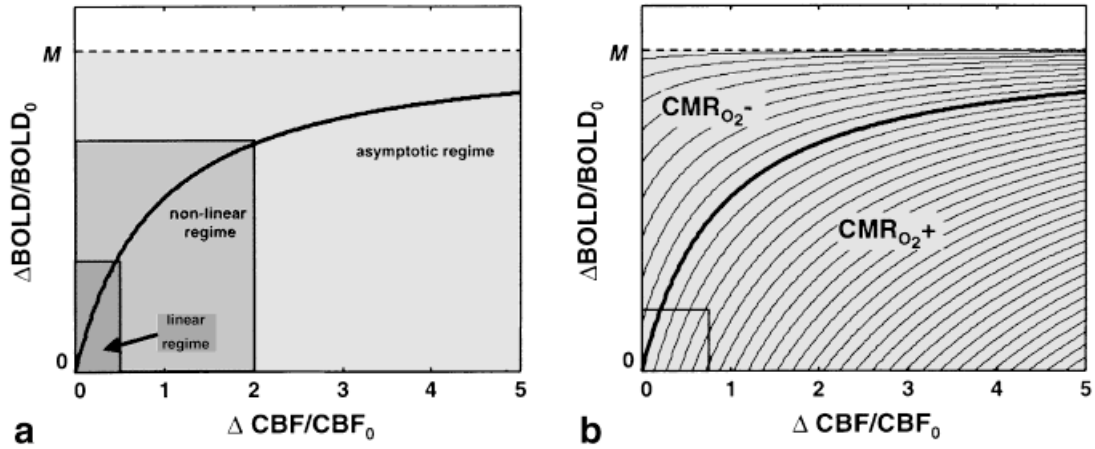


**Figure 12. Deoxyhemoglobin dilution model**

Relationships between BOLD MRI signal, CBF, and  $CMRO_2$  predicted by the dHb dilution model. a: Fractional BOLD signal change, plotted as a function of fractional CBF change, calculated using Eq. [11] with  $\alpha = 0.38$  and  $\beta = 1.5$ . The predicted function has a linear domain for perfusion increases up to approximately 50%, and becomes nonlinear at higher CBF levels. In the theoretical limit of very high perfusion rates, venous blood approaches complete oxygenation, leading to a sample-dependent asymptotic upper limit of  $M$  for BOLD signal increases. b: Iso- $CMRO_2$  contours predicted by the dHb dilution model at 10% intervals. Increases in  $CMRO_2$  lead to reductions in the BOLD signal observed at a given level of CBF, producing BOLD-CBF data in the zone labeled  $CMRO_2+$ . Every point along an iso- $CMRO_2$  contour corresponds to a different CBF: $CMRO_2$  coupling ratio. Iso- $CMRO_2$  contours are evenly spaced and approximately parallel over small patches of the BOLD-CBF plane, as indicated in the small box in the lower left corner of the plot. This figure and its caption were reproduced from (Hoge et al. 1999a).

The equation that relates  $M$  to the BOLD and CBF signal changes measured during the hypercapnia procedure in the original Davis model is as follows:

$$M = \frac{\frac{\Delta BOLD}{BOLD} - 1}{1 - \left(\frac{\Delta CBF}{CBF}\right)^{-(\beta-\alpha)}} \quad [1]$$

Where  $\alpha$  corresponds to the exponent in the power law relationship relating changes in CBF to changes in venous cerebral blood volume (CBV) during the manipulation. Though this value was originally measured by Grubb and colleagues to be 0.38 in anesthetized monkeys (Grubb et al. 1974), it is now understood to be much lower in adult humans. Chen and colleagues have measured it to be 0.18, using an MRI technique specific to changes in venous blood volume (Chen et al. 2009a; Chen et al. 2010c). This is the value used in the current literature and in the

manuscripts presented here. The  $\beta$  parameter corresponds to influence of deoxygenated hemoglobin on transverse relaxation (Boxerman et al. 1995). The value of this parameter  $\beta$  depends on field strength and was originally estimated to be 1.5. Recent studies have questioned the validity of this value as well as its interpretation and suggested that  $\beta$  should instead be viewed as a lumped parameter with a value closer to 0.91 (Griffeth et al. 2011). Throughout the manuscripts included in this thesis however, the original meaning of  $\beta$  was preserved and the value of 1.5 used.

Following estimation of the  $M$  parameter, percent changes in  $CMRO_2$  evoked by a task are estimated using the BOLD and CBF changes measured during the task and relating these parameters using the following expression:

$$CMRO_2 = \left( \frac{CBF}{CBF_0} \right)^{1-\alpha/\beta} \left( 1 - \frac{\frac{BOLD}{BOLD_0} - 1}{M} \right)^{1/\beta} \quad [2]$$

The BOLD to CBF relationship during a task can be conceptualized as a point on a curve parallel to the curve determined in the absence of metabolism (during hypercapnia) These curves are called iso- $CMRO_2$  contours (Figure 12b). By measuring the BOLD and CBF changes during a task, we can find which contour the measurement falls on, informing us on the BOLD attenuation attributable to the metabolic component. Equation 2 allows us to quantify this component in terms of percent change  $CMRO_2$ .

This method has been used in a number of studies (Davis et al. 1998; Hoge et al. 1999b; Stefanovic et al. 2006; Leontiev et al. 2007b; Ances et al. 2008; Lin et al. 2008; Perthen et al. 2008; Ances et al. 2009; Bulte et al. 2009; Chen et al. 2010a; Mark et al. 2011; Gauthier et al. 2012b), but has recently lost in popularity to the newer hyperoxia method (Chiarelli et al. 2007b; Goodwin et al. 2009; Mark et al. 2011; Mohtasib et al. 2012).

### 1.5.2. Hyperoxia calibration method

In the hyperoxia method, participants inhale high levels of oxygen (typically 50-100% O<sub>2</sub> with balance nitrogen where applicable) during acquisition of BOLD image series while expired oxygen concentration is recorded. The enriched O<sub>2</sub> raises the total oxygen content of the arterial blood, leading to increases in venous hemoglobin saturation Sv<sub>O<sub>2</sub></sub> and hence increases in BOLD signal. The maximal BOLD signal *M* can then be extrapolated using the hyperoxia calibration model of BOLD as a function of Sv<sub>O<sub>2</sub></sub>.

End-tidal concentrations are used in this model as a surrogate for arterial O<sub>2</sub> partial pressure (Pa<sub>O<sub>2</sub></sub>). From this measurement, arterial O<sub>2</sub> saturation (Sa<sub>O<sub>2</sub></sub>) can be estimated using the Severinghaus equation:

$$Sa_{O_2} = \frac{1}{\left( \frac{23400}{(Pa_{O_2})^3 + 150(Pa_{O_2})} + 1 \right)} \quad [3]$$

Arterial O<sub>2</sub> content (Ca<sub>O<sub>2</sub></sub>) can then be estimated as follows:

$$Ca_{O_2} = (\phi \cdot [Hb] \cdot Sa_{O_2}) + (Pa_{O_2} \cdot \varepsilon) \quad [4]$$

where  $\phi$  represents the O<sub>2</sub>-carrying capacity of hemoglobin, which corresponds to 1.34 ml O<sub>2</sub>/g Hb for humans, and  $\varepsilon$  is the solubility coefficient of oxygen in blood with a value of 0.0031 ml O<sub>2</sub>/(dlblood \* mm Hg). [Hb] corresponds to the hemoglobin concentration. In the original demonstration of this method, the value for this parameter was assumed to be 15 gHb/dl blood. However, hemoglobin can readily be determined individually using a blood test.

From the arterial content of O<sub>2</sub>, venous content of O<sub>2</sub> (Cv<sub>O<sub>2</sub></sub>) can be estimated using an assumed value for oxygen extraction fraction (OEF):

$$Cv_{O_2} = Ca_{O_2} - (Ca_{O_2}|_0 \cdot OEF) \quad [5]$$

In all expressions, a subscript of 0 is used to denote the baseline state measure. From this expression, a value for venous O<sub>2</sub> saturation (Sv<sub>O<sub>2</sub></sub>) can be estimated using the following expression

$$Sv_{O_2} = \frac{Cv_{O_2} - (Pv_{O_2} \cdot \varepsilon)}{\varphi \cdot [Hb]} \quad [6]$$

where Pv<sub>O<sub>2</sub></sub> represents an estimate of oxygen dissolved in venous plasma. This is expected to be a negligible fraction (<1%) of the total O<sub>2</sub> content in venous blood, due to the high affinity of Hb for O<sub>2</sub> in the partially saturated state expected in venous blood even at high inspired O<sub>2</sub> fractions. Therefore, this term is assumed to have a value of zero and is dropped from the expression.

All previous expressions are solved twice, once using the end-tidal O<sub>2</sub> values measured during baseline and once using the end-tidal O<sub>2</sub> values measured during the hyperoxia breathing manipulation. This allows the calculation of the fractional change in dHb concentration, which corresponds to:

$$\frac{[dHb]_v}{[dHb]_{v_0}} = \frac{(1 - Sv_{O_2})}{(1 - Sv_{O_2}|_0)} \quad [7]$$

In this model, the expression that relates the *M* parameter to BOLD and CBF changes during the manipulation is as follows:

$$\frac{\Delta BOLD}{BOLD_0} = M \left( 1 - \left( \frac{CBF}{CBF_0} \right)^\alpha \left( \frac{[dHb]_v}{[dHb]_{v_0}} + \frac{CBF_0}{CBF} - 1 \right)^\beta \right) \quad [8]$$

In all implementation of this method, an approximated correction for the small decreases in CBF known to occur during hyperoxia is used (Chiarelli et al. 2007b; Goodwin et al. 2009; Mark et al. 2011). Because these small CBF changes are difficult to measure with the somewhat noisy ASL method, a fixed value for the hyperoxia-induced CBF decrease is generally assumed.

Once *M* has been estimated, percent change CMRO<sub>2</sub> is estimated using the expression first proposed by Davis and colleagues (Equation 2) (Davis et al. 1998).

The hyperoxia model (Chiarelli et al. 2007b) can be generalized for arbitrary changes in cerebral blood flow during hyperoxia (Gauthier et al. 2011, included as Appendix A), rendering it valid for conditions such as simultaneous hyperoxia and hypercapnia (as would be produced during breathing of carbogen, a mixture composed largely of  $O_2$  with a balance of 5-10%  $CO_2$ ). The manuscript detailing this technique is included as Chapter 2 of this thesis.

### **1.5.3. $R_2'$ method**

Recently, an alternative method has been proposed that does not require the use of a breathing manipulation for calibration (Blockley et al. 2011b). This method uses the information in a spin echo and a gradient echo sequence to estimate  $R_2'$  and thereby obtain the  $M$  parameter.  $R_2'$ , also called the reversible transverse relaxation rate, is a component of the  $R_2^*$  signal used to obtain the BOLD contrast and is thought to be dependent on venous blood volume and dHb concentration (Yablonskiy et al. 1994; Blockley et al. 2011b). Though this approach was shown to be fairly robust to differences in underlying physiology, it was found by Blockley et al. to be less robust than the original hypercapnia calibration model (Davis et al. 1998), but more than the hyperoxia calibration model (Chiarelli et al. 2007b). The lower robustness to the effects of physiological variations of the hyperoxia model may arise from the fact that both OEF and hematocrit must be assumed in the hyperoxia model, rendering it more sensitive to variations of these parameters. Even though the  $R_2'$  may not perform quite as well as the hypercapnia calibration method in the context of physiological variability, it does provide the advantages of not requiring a breathing manipulation and a reduced dependence on various modeling parameters such as OEF,  $\alpha$  and  $\beta$  to determine the calibration constant  $M$ . Implicit within this technique is however another set of assumptions about tissue compartment contributions to  $R_2'$ .

## **1.6. Baseline $CMRO_2$**

Calibrated fMRI techniques allow the estimation of a valuable physiologically-specific quantity from the BOLD signal. However, the fractional change in  $CMRO_2$  estimated using these techniques preserves the ambiguity of an unknown baseline state. Therefore, though the measured changes can be directly compared between

groups with different vascular function, the meaning of these changes is weakened by the fact that we are ignorant of the baseline value from which this fractional change arises. The case could therefore arise where a seemingly higher percent  $CMRO_2$  change in one group may actually reflect a similar absolute increase in metabolism in terms of  $\mu\text{mol O}_2/100\text{g tissue}/\text{min}$ , but from a lower absolute baseline value. Therefore, there is great interest in developing MRI-based techniques to measure absolute resting  $CMRO_2$ . One such technique was developed during the course of this thesis and the manuscript detailing this method is included as Chapter 3. Other techniques have also recently been developed to estimate this value and will be discussed here.

While  $CMRO_2$  can be measured by MRI using  $^{17}\text{O}_2$  labeling methods (Fiat et al. 1992; Fiat et al. 1993; Fiat et al. 2004), these techniques are impractical due to the limited availability and high cost of  $^{17}\text{O}$ . More accessible alternatives are being developed using proton MRI. Some of these recently-proposed techniques yield whole-brain or single vessel estimates (An et al. 2000; Xu et al. 2009; Jain et al. 2010; Fan et al. 2011), but more recent efforts have focussed on mapping of these parameters (He et al. 2007; He et al. 2008; Bolar et al. 2011b; Bulte et al. 2011).

The  $T_2$  relaxation under spin tagging (TRUST) (Lu et al. 2008) technique can be used to obtain a whole brain estimate of oxidative metabolism by measuring  $T_2$  values in the sagittal sinus (Xu et al. 2009; Xu et al. 2011c; Liu et al. 2012; Lu et al. 2012b). This sequence uses a scheme reminiscent of ASL to isolate the venous signal, by tagging a large slab in one out of every two images and subtracting adjacent images. A  $T_2$  preparation is added to quantify  $T_2$  at various echo times. An exponential decay curve is then fit to the value obtained at each echo to estimate  $T_2$  values within selected voxels in the sagittal sinus. These  $T_2$  estimates can be converted to venous saturation using literature values from in vitro studies. Since arterial oxygen saturation can be measured using pulse oximetry and CBF in the sagittal sinus can be determined using ASL or phase contrast sequences, baseline  $CMRO_2$  can be estimated using the following expression:

$$CMRO_2 = (Sv_{O_2} - Sa_{O_2}) \cdot CBF \cdot \varphi \quad [9]$$

where  $\phi$  is the  $O_2$  carrying capacity of Hb,  $Sa_{O_2}$  represents arterial  $O_2$  saturation and  $Sv_{O_2}$  venous  $O_2$  saturation. The fact that this technique yields a single sagittal sinus estimate means that its use is limited to cases where a global effect is expected. In the case of more subtle local changes in baseline metabolism, dilution by venous blood from the rest of the brain may lead to underestimation or even disappearance of the effect.

Another recently proposed method uses values obtained through BOLD signal modeling in different tissue compartments to estimate baseline OEF and  $CMRO_2$ . The technique described by An and colleagues is an early, simplified version of the technique presented by He and colleagues termed quantitative BOLD (qBOLD) (An et al. 2000; He et al. 2007; He et al. 2008). This technique uses the MR signal modeling of the static dephasing regime to determine baseline hemodynamic parameters from a gradient echo sampling of the spin echo (GESSE) signal (He et al. 2007; He et al. 2008). This technique is based on a similar principle as the  $R_2'$  calibrated technique discussed above. It uses a multi-compartment model to determine the venous oxygen saturation in extravascular tissue and obtain maps of OEF. Though promising, the qBOLD method is limited because it depends on a fitting procedure involving a large number of parameters, some of which are simultaneously optimized as part of the model fit, and others which must be assumed based on previously determined values. The uniqueness of parameter combinations yielding convergent fits can be difficult to guarantee, and the remaining fixed parameters reflect fundamental magnetic properties of tissue which are difficult to measure directly on an individual basis.

The alternate approach proposed by Bolar et al., a sequence called quantitative imaging of extraction of oxygen and tissue (QUIXOTIC), uses velocity-sensitive ASL with a  $T_2$  preparation module to directly target the oxygenation signal from small venules (Bolar et al. 2011b). This two-step ASL-type sequence works as follows (Figure 13 for visual depiction). The first part of the sequence removes signal from all blood outside of capillaries using velocity encoding. Capillary spins are isolated by subtracting an image where only spins going at a speed below 2 cm/s (which all presumably reside in capillaries) from an image where no flowing spins are selected. A second module allows isolation of spins which, after being

selected in capillaries, have now progressed towards venules. During the second module applied a short time (725ms) after the first module to allow spins to flow into the venous system, velocity gradients are used to select spins going now faster than 2 cm/s. These are the spins which are now speeding up after leaving the capillaries, reflecting a selective venular component. A  $T_2$  preparation module is integrated in the second velocity-selective module, allowing the quantification of  $T_2$  within this venular compartment. By specifically measuring the signal from venules, a localized measure of oxygen extraction and metabolism can be obtained.

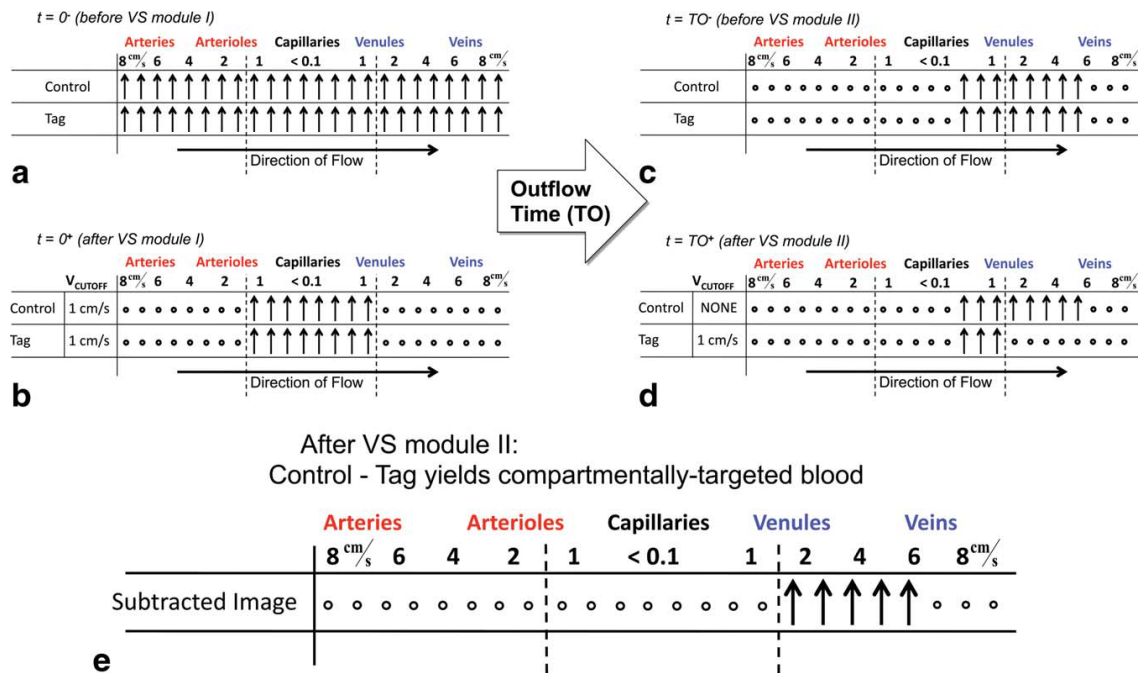


**Figure 13. QUIXOTIC**

Idealized cartoon of venular blood signal targeting in QUIXOTIC approach, as told via spin configuration throughout the experiment. Relaxed spins are denoted by upright arrows; dephased spins by hollow circles. Dotted vertical lines correspond to 1 cm/s blood velocity (i.e., the cutoff velocity in b and d). This figure and its caption were reproduced from (Bolar et al. 2011b).

$T_2$  relaxation can be converted to venous saturation using a biophysical model and relaxation parameters measured using bovine blood (van Zijl et al. 1998; Golay et al. 2001). Venous saturation is then converted to OEF and  $CMRO_2$  using the same principles as for the TRUST approach (Xu et al. 2009) (Equation 9). The QUIXOTIC method yielded very promising early results, with maps of  $CMRO_2$  and OEF values within the expected range (Bolar et al. 2011b). However, the one drawback of the QUIXOTIC method is that it requires knowledge of the flow

velocity range required to selectively image the venular signal, a value which is likely to change with age and health status.

A further approach consists of using phase information to determine the susceptibility difference between a blood vessel and the surrounding tissue (Jain et al. 2010; Fan et al. 2011). Since this susceptibility effect arises from the paramagnetic effects of deoxyhemoglobin, it can be related to venous saturation which can, in turn, be used to measure  $CMRO_2$  using Fick's principle of arteriovenous saturation differences (Equation 9). The initial implementation of this idea was used to obtain a global brain measure in the superior sagittal sinus (Jain et al. 2010). A more recent implementation, called phase-based regional oxygen metabolism (PROM) can be used to obtain a measure in single cortical veins (Fan et al. 2011). These techniques however are limited to single vessels and for them to work using the current models, the vessels chosen must be oriented parallel to the main magnetic field.

Finally, an alternative approach to estimating baseline OEF and  $CMRO_2$  using MRI was devised to use the information provided by the hypercapnia and hyperoxia calibration techniques (Bulte et al. 2011). For this approach, both a hyperoxia and a hypercapnia breathing manipulations are performed. The  $M$  parameter is determined using the hypercapnia manipulation as in Equation 1 (Davis et al. 1998). The hypercapnia  $M$  parameter is then used in the expression originally derived to determine  $M$  in the hyperoxia calibration technique (Equation 8) (Chiarelli et al. 2007b) but now solving for OEF. This OEF can then be used to derive absolute baseline  $CMRO_2$  when combined with measures of baseline CBF and end-tidal  $O_2$  concentrations. Though this technique is somewhat similar to the one presented in Chapter 3 of this thesis, some additional assumptions make the modeling used in the method presented by Bulte and colleagues less exact and more prone to systematic errors (see Chapter 2). Furthermore, since these assumptions differ between the hypercapnia and hyperoxia techniques, the results suffer from an additional source of physiological ambiguity.

While MRI-based measures of metabolism are just starting to emerge, PET estimates can also be obtained using  $^{15}O$  labeled PET tracers. These PET

measures of  $CMRO_2$  require three separate acquisitions with injection of  $^{15}O$  labeled  $O_2$ ,  $H_2O$  and  $CO$ . These three measurements are necessary to take into account the combined contribution of  $O_2$  diffusion into tissue, its conversion to water during oxidative metabolism, as well as the dependence on blood volume, assessed with  $C^{15}O$  (Mintun et al. 1984; Buxton 2010). However, the use of three separate injections of positron emitting tracers greatly increases the radiation dose associated with this measurement. Furthermore, the short half-life (about two minutes) of  $^{15}O$  means that this technique is not possible without an on-site cyclotron (Miller et al. 2008).

### **1.7. Quantitative studies of brain aging**

There have been few attempts to quantify the effects of vascular and metabolic aging using MRI. Only two calibrated studies of aging can currently be found in the literature. One study looked at the effects of aging on hemodynamic and metabolic parameters during a visual task using the hypercapnia method (Ances et al. 2009) and the other investigated the effects of aging on these parameters during a cognitive task using the hyperoxia calibration method (Mohtasib et al. 2012). While the two studies do not agree on all fronts, both report significant changes in the hemodynamic components underlying the BOLD contrast. The study by Ances and colleagues found differences in reactivity,  $M$  and BOLD signal responses to visual stimulation. However, these differences did not translate into changes in  $CMRO_2$  (Figure 14). The study by Mohtasib and colleagues did not find as clear a difference in  $M$ , but did find a difference both in task-evoked BOLD and  $CMRO_2$  (Figure 15). While each study is subject to different confounds and investigate the effects of aging on different parts of the brain, both studies warrant caution when interpreting BOLD signal differences in aging.

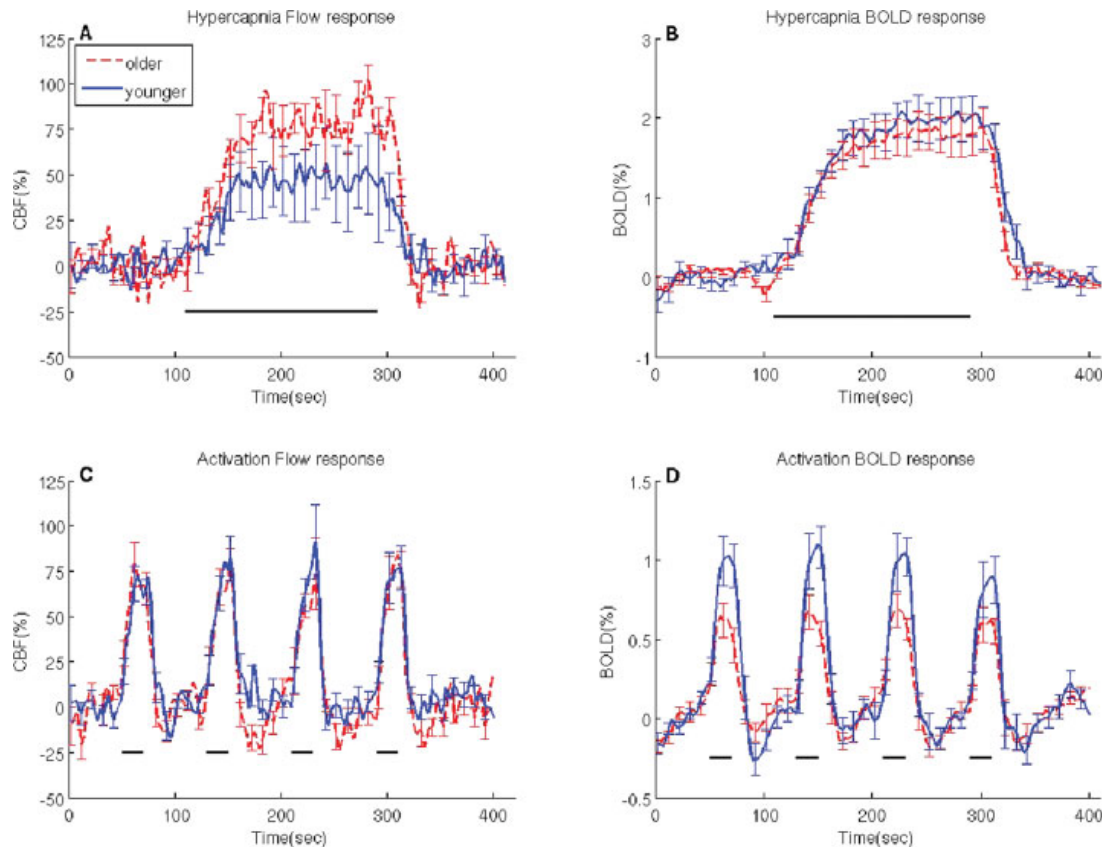


**Figure 14. Calibrated fMRI of visual activation in aging**

Functional changes in the blood oxygen level dependent (BOLD) and cerebral blood flow (CBF) response in the VC (visual cortex) for mild hypercapnia and functional activation. The panels show average response curves and standard errors for the CBF activated voxels within healthy younger (n 5 10) and older (n 5 10) subjects. (A) Fractional changes in the CBF responses to hypercapnia, (B) Changes in the BOLD responses to hypercapnia, (C) Fractional changes in the CBF responses to activation, and (D) Changes in the BOLD responses to activation. This figure and its caption are reproduced from (Ances et al. 2009).

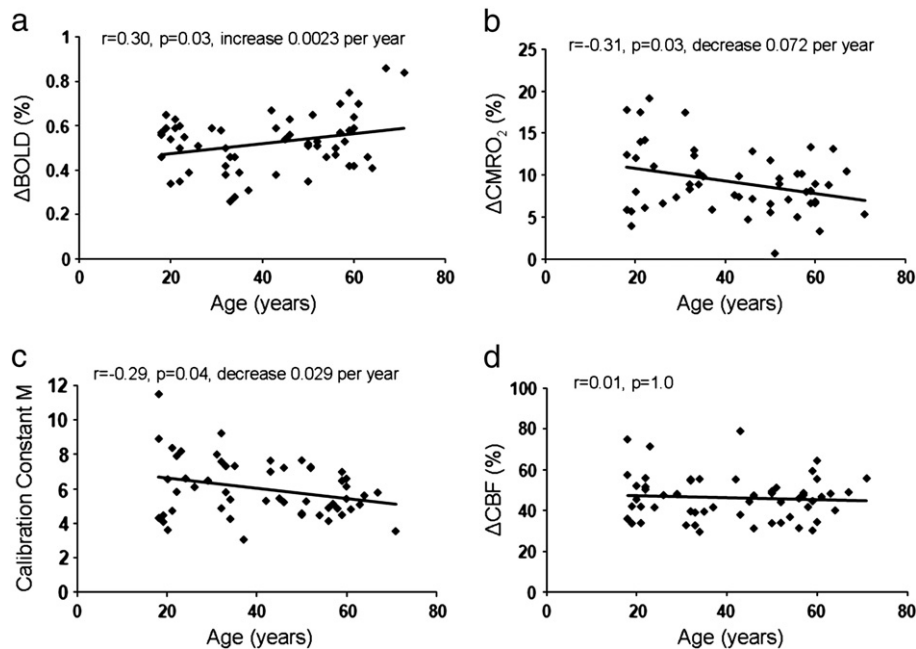


**Figure 15. Calibrated fMRI of Stroop activation in aging**

The age-related change in the measured/estimated parameters ((a)  $\Delta$ BOLD, (b)  $\Delta$ CMRO<sub>2</sub>, (c) M and (d)  $\Delta$ CBF), averaged over the ten activated regions. Each point shows the average value for an individual over the ten activated regions. This figure and its caption are reproduced from (Mohtasib et al. 2012).

While calibrated fMRI studies of aging are still rare, other groups have sought to quantify some of the hemodynamic parameters underlying the BOLD signal across the lifespan, showing important differences with age in various BOLD signal components. A rigorous quantification of age-related absolute baseline CBF changes using ASL has shown that, while CBF showed decreases with increasing age throughout the brain, some regions may be more vulnerable than others (Chen et al. 2011). Furthermore, the observed CBF decreases were not found to be an effect of atrophy as there was little overlap between regions showing the greatest rate of atrophy and the regions showing the greatest rate of CBF decrease (Figure 16). However, an interesting finding of this study was that the regions most affected by age-related atrophy largely overlapped with the areas with highest absolute baseline CBF during early adulthood. Some of the regions with significant CBF decreases with age were found to be the regions involved in the default-mode network. Overall, CBF decreases across all regions was found to be 0.38% per year. This value is similar to the estimated decrease of 0.45% found in an earlier study (Parkes et al. 2004).

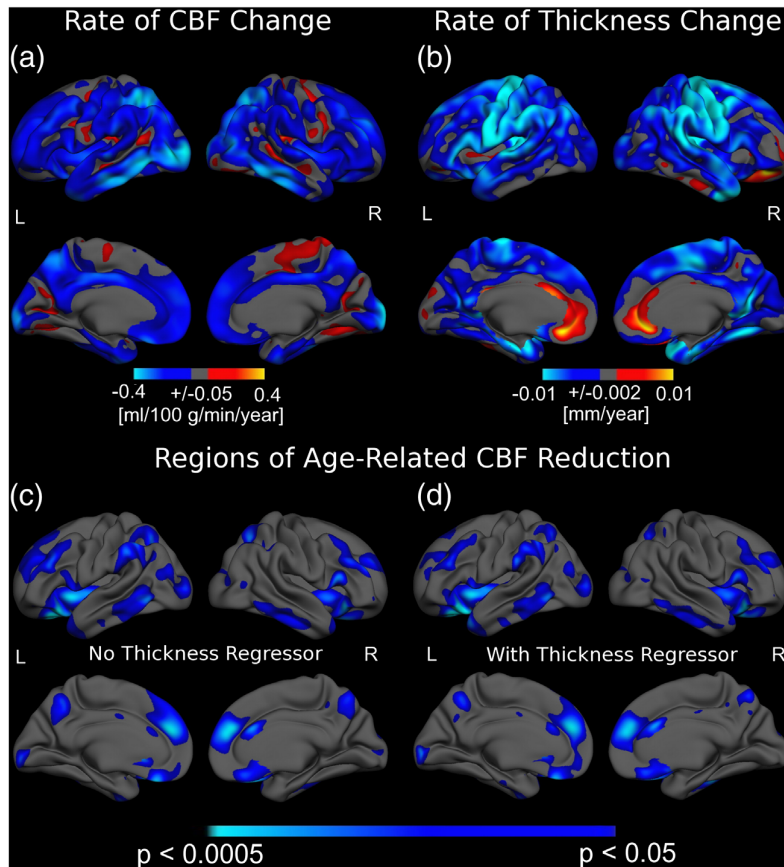


**Figure 16. The association between age and regional CBF as well as cortical thickness.**

The colour scale in (a) indicates the amplitude of age-associations in CBF, while those in (b) and (c) indicate statistical significance, with light blue and yellow denoting the strongest negative and positive associations, respectively. Regions exhibiting the largest magnitude of CBF reduction (a) and cortical thinning with age (b) did not spatially coincide. The significance map of CBF reductions before (c) and after vertex-wise covariation for age-associations in cortical-thickness (d) only subtly differed. Greatest statistical effects were found in the left supramarginal and occipital gyri, and the right anterior cingulate, as well as bilaterally in the right rostral middle-frontal, superior parietal, middle-inferior temporal and insular regions, medial superior frontal, orbito-frontal and precuneus regions. Furthermore, the localization of regions exhibiting the most rapid age-related CBF decline appeared to coincide with regions showing the highest statistical effects of age on CBF. This figure and its caption were reproduced from (Chen et al. 2011).

Baseline CBF is one of the components that help determine the amplitude of the BOLD response and differences in baseline can lead to erroneous conclusions about neuronal signaling. For example, a similar flow increase from a lower baseline CBF may lead to overestimation of the neural response, since the percent CBF increase from this lower baseline will be higher for an absolute increase of similar amplitude (a 10% increase from a baseline of 50 ml/100g/min will be smaller in absolute terms than a 10% increase from a baseline of 100 ml/100g/

min). This will lead to an inflated BOLD response and the conclusion that neuronal signaling is larger in the group with lower baseline CBF. This can easily be accounted however, as baseline CBF is a robust measurement that can be obtained using a short ASL acquisition.

Age-related changes in baseline CMRO<sub>2</sub> have also been investigated in the whole brain using the TRUST technique in a large cohort of 152 healthy participants between the ages of 20 and 90 (Lu et al. 2011). Venous saturation was found to decrease by about 1.4% per decade while global CBF, measured using phase contrast imaging of the carotids, was found to decrease by about 0.8 ml/100g/min per decade. Together, these measurements indicate that global oxidative metabolism is increased by about 2.6 μmol/100g/min in healthy aging, when corrected for grey matter volume loss (Figure 17). This finding could have a significant impact on the BOLD signal, by determining the amount of dHb present before any task-specific increase. This would affect the baseline state from which a task-evoked fractional BOLD signal change would arise, as well as the dynamic range of BOLD signal. However, this result is somewhat surprising given previous PET results showing the opposite trend in CMRO<sub>2</sub> (Yamaguchi et al. 1986; Leenders et al. 1990; Marchal et al. 1992). It may be that the difficulties in accounting for partial volume effects in PET images lead to an underestimation or inadequate correction for volume loss. The results of this study indicate that, as we age, an increased oxygen demand is met with a reduced baseline CBF, leading to a decrease in venous oxygenation.

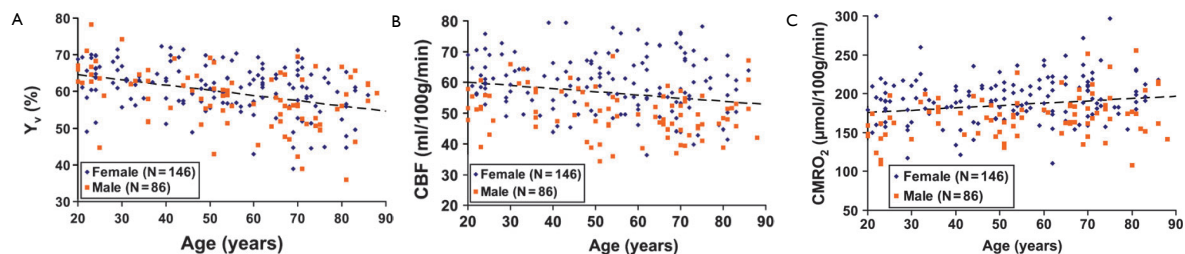


**Figure 17. Whole brain hemodynamic age-related changes**

Each dot represents data from one subject ( $n = 232$ ). The data from women and men are shown with different symbols. The dashed line is a linear fitting of the experimental data from both sexes. A. Scatter plot between global venous oxygenation ( $Y_v$ ) and age. B. Global CBF alterations with age. C. Scatter plot between global CMRO<sub>2</sub> and age. This figure and its caption were reproduced from (Lu et al. 2011).

This study also investigated possible changes in cerebrovascular reactivity (CVR) with age by acquiring ASL data during a hypercapnic challenge. Age-dependent effects on flow reactivity were larger and more pervasive than baseline flow decreases, which affected mostly the frontal areas of the brain. However, the largest CVR decreases were also found in frontal areas. CVR is also of importance when investigating BOLD changes with aging, since reactivity will determine the amplitude of CBF increase for a given amount of vasodilatory signaling and therefore the amplitude of the BOLD signal change evoked by a given amount of metabolism.

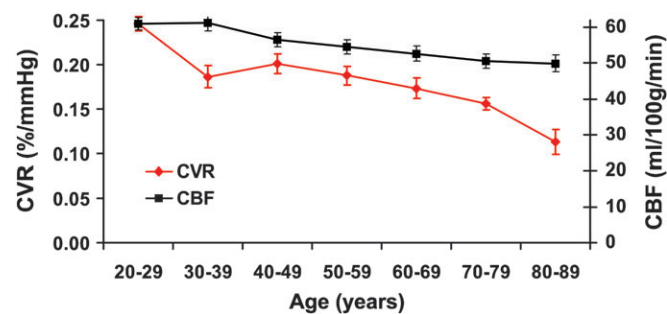


**Figure 18. Decade-by-decade alterations in prefrontal CVR and CBF.**

Display scales for CVR and CBF are shown on the left and right axis, respectively. The display scales were set such that the first points of the 2 curves overlapped. It can be seen that CVR manifests a more rapid decay with age compared with CBF. The subjects in each decade were grouped, and the data shown are the mean and standard error of the group. This figure and its caption were reproduced from (Lu et al. 2011).

While the quantitative studies presented here suggest that simple group comparisons of BOLD signal changes in participants of different ages may lead to errors and systematic biases, together they provide only a fragmentary window into this problem. In the aging study presented in Chapter 4 of this thesis, we have sought to go further in bringing all these observations together in an integrated set of experiments to probe into vascular changes with aging. The effects of these changes on hemodynamic measures are addressed in the context of a calibrated fMRI investigation in Chapter 4.

In summary, the BOLD signal is a physiologically-relevant, but ambiguous measure of neuronal activity. This limits the specific physiological inferences that can be made in the context of studies in young and healthy adults, a challenge that is

exacerbated in the case of comparisons between groups of different ages and health status. Chapter 2 of this thesis presents a generalization of previous techniques for the extraction of fractional changes in  $CMRO_2$  (a quantity more physiologically-specific and comparable between groups) from the BOLD signal evoked by a task. Chapter 3 presents a technique that allows estimation of baseline  $CMRO_2$  and OEF, which are not only highly relevant clinical parameters but will also allow a more in-depth investigation of age-related vascular and metabolic changes. Chapter 4 presents the results of a subset of these techniques in groups of younger and older adults. This allows a discussion of the physiological changes that occur with aging and the confounds present in the conclusions drawn from BOLD-only studies of cognitive aging. Finally, Chapter 5 will explore some of the central and cerebral vascular changes that occur with aging and their relationship with cognitive performance and cardiovascular fitness.

## **2. A generalized procedure for calibrated MRI incorporating hyperoxia and hypercapnia**

Gauthier, C.J.<sup>1,2</sup>, Hoge, R.D.<sup>1,2</sup>

<sup>1</sup> Physiology/Biomedical Engineering, Université de Montréal, Montreal, Quebec, Canada, <sup>2</sup> CRIUGM, Montreal, Quebec, Canada

Human Brain Mapping, Accepted 22 September 2011, in press

DOI: 10.1002/hbm.21495

### **2.1. Preface**

Calibrated fMRI was developed almost fifteen years ago by Davis et al. (Davis et al. 1998) and the original technique uses a hypercapnia manipulation combined with a biophysical model to decompose a task-evoked BOLD response into its vascular and oxidative metabolism components. This original technique uses the flow and BOLD responses to a hypercapnia manipulation to estimate the calibration factor  $M$ , corresponding to the maximal possible BOLD signal change from baseline. This calibration parameter is then used to estimate relative task-evoked increases in the cerebral metabolic rate of  $O_2$  consumption ( $CMRO_2$ ). Because hypercapnia may cause discomfort when given in higher concentrations, other groups have developed alternative techniques using instead either hyperoxia (Chiarelli et al. 2007b) or the information present in gradient and spin echoes, without any gas manipulation (Blockley et al. 2011b), to calibrate the BOLD signal. Despite this decreased discomfort however, these two methods may be more sensitive to errors from misassignment of assumed parameters than the original method (Blockley et al. 2011b).

In this chapter, an extension of the hypercapnia and hyperoxia calibration models is presented, which can take into account both arbitrary changes in blood flow and

in blood O<sub>2</sub> content. This generalized model, combined with a simultaneous hypercapnia and hyperoxia breathing manipulation (carbogen inhalation), is compared to the hypercapnia and hyperoxia methods. The generalized model was not compared to the method by Blockley et al. however, since the last method was not published at the time of this study. The generalized model, combined with carbogen inhalation is shown to compare advantageously to the hypercapnia and hyperoxia methods, in terms both of accuracy of the  $M$  parameter and robustness to measurement error.

## 2.2. Abstract

Calibrated MRI techniques use the changes in cerebral blood flow (CBF) and blood oxygenation level-dependent (BOLD) signal evoked by a respiratory manipulation to extrapolate the total BOLD signal attributable to deoxyhemoglobin at rest ( $M$ ). This parameter can then be used to estimate changes in the cerebral metabolic rate of oxygen consumption (CMRO<sub>2</sub>) based on task-induced BOLD and CBF signals. Different approaches have been described previously, including addition of inspired CO<sub>2</sub> (hypercapnia) or supplemental O<sub>2</sub> (hyperoxia). We present here a generalized BOLD signal model that reduces under appropriate conditions to previous models derived for hypercapnia or hyperoxia alone, and is suitable for use during hybrid breathing manipulations including simultaneous hypercapnia and hyperoxia. This new approach yields robust and accurate  $M$  maps, in turn allowing more reliable estimation of CMRO<sub>2</sub> changes evoked during a visual task. The generalized model is valid for arbitrary flow changes during hyperoxia, thus benefiting from the larger total oxygenation changes produced by increased blood O<sub>2</sub> content from hyperoxia combined with increases in flow from hypercapnia. This in turn reduces the degree of extrapolation required to estimate  $M$ . The new procedure yielded  $M$  estimates that were generally higher ( $7.6 \pm 2.6$ ) than those obtained through hypercapnia ( $5.6 \pm 1.8$ ) or hyperoxia alone ( $4.5 \pm 1.5$ ) in visual areas. These  $M$  values and their spatial distribution represent a more accurate and robust depiction of the underlying distribution of tissue deoxyhemoglobin at rest, resulting in more accurate estimates of evoked CMRO<sub>2</sub> changes.

### 2.3. Introduction

The blood oxygenation level-dependent (BOLD) MRI signal reflects local changes in blood flow, blood volume, and oxygen consumption. The amplitude of the signal measured depends on both the baseline value and the reactivity of these physiological quantities. Increases in neuronal signaling are associated with local increases in arterial blood flow, which in turn cause a reduction in deoxygenated hemoglobin (dHb) concentration in the venous circulation serving the activated region. This increase in the local arterial blood flow raises the mean  $O_2$  saturation along the capillary bed, increasing the diffusion-limited delivery of  $O_2$  to neural tissues (Buxton et al. 1997). Given that virtually all dHb in the venous circulation of healthy individuals is generated as a result of metabolic  $O_2$  extraction, the relative change in venous dHb level measured through BOLD during stimulation should depend partly on the relative change in the cerebral metabolic rate of  $O_2$  consumption, or  $CMRO_2$  (Buxton et al. 1997).

The dependence of the BOLD signal on baseline physiology complicates the comparison of BOLD response amplitudes between groups or individuals. This is particularly problematic for groups expected to have different vascular tone and reactivity (such as elderly populations or cardiovascular patients), because baseline blood flow, oxygenation, and cerebrovascular reactivity (CVR) will greatly affect the dynamic range of the BOLD signal (Gauthier et al. 2011b). The dissociation of metabolic and vascular factors contributing to the BOLD response is thus essential for meaningful comparisons between populations with disparate physiology.

If the vascular contribution to the BOLD signal can be quantified and factored out, then in theory it should be possible to obtain a quantitative estimate of the fractional change in  $CMRO_2$  evoked by stimulation. This notion is the foundation for various MRI-based methods for  $CMRO_2$  estimation (Davis et al. 1998; Chiarelli et al. 2007b; Gauthier et al. 2011b). The BOLD signal change observed during activation is not itself sufficient to determine the relative change in venous dHb concentration. Such a determination requires expressing the activation-induced BOLD signal as a fraction of the total attenuation of  $T2^*$ -weighted signal

attributable to dHb at baseline (equivalent to the maximum possible BOLD signal increase, usually denoted  $M$ ). For this reason, various calibration methods have been proposed in which the maximal BOLD increase  $M$  is estimated through extrapolation of BOLD signal increases observed during mild hypercapnia (Davis et al. 1998), hyperoxia (Chiarelli et al. 2007b) or a combination of the two (Gauthier et al. 2011b). Note that, although  $M$  is commonly referred to as the "maximal BOLD signal", it could also be described as the "resting BOLD signal" in the same sense that the baseline ASL difference signal represents resting cerebral blood flow. That is, it is the factor by which activation-induced changes must be normalized to recover the fractional change in a specific physiological quantity (i.e. blood flow or venous deoxyhemoglobin content). Unlike ASL however, there is no simple subtractive scheme allowing isolation of the  $T_2^*$ -weighted signal component associated specifically with deoxygenated hemoglobin at rest (although methods based on  $T_2'$  show some promise (Blockley et al. 2011a)). Current quantitative BOLD approaches thus rely on extrapolative blood-gas manipulation techniques.

In the hypercapnia method, small amounts of carbon dioxide (typically 5-10%  $\text{CO}_2$  by volume) are added to the air breathed by subjects during acquisition of BOLD and CBF image series. The vasodilatory properties of  $\text{CO}_2$  lead to increases in cerebral blood flow and tissue oxygen delivery, producing BOLD signal increases throughout grey matter as well as in large veins. The maximal BOLD signal  $M$  at a given location can then be extrapolated using the Davis model of BOLD as a function of CBF, assuming a constant arterial saturation of 100% and unchanged metabolism during hypercapnia. This is the original calibration method, introduced by Davis et al. and since used in a number of studies (Davis et al. 1998; Hoge et al. 1999b; Stefanovic et al. 2006; Leontiev et al. 2007b; Ances et al. 2008; Lin et al. 2008; Perthen et al. 2008; Ances et al. 2009; Bulte et al. 2009; Chen et al. 2009b; Mark et al. 2011).

In the hyperoxia method, subjects inhale high levels of oxygen (typically 50-100%  $\text{O}_2$  with balance nitrogen where applicable) during acquisition of BOLD image series and recordings of expired oxygen concentration (a surrogate for the arterial partial pressure of  $\text{O}_2$ ). The enriched  $\text{O}_2$  raises the total oxygen content of the arterial blood, leading to increases in venous hemoglobin saturation (SVO<sub>2</sub>) and

hence increases in BOLD signal. The maximal BOLD signal  $M$  can then be extrapolated using the hyperoxia calibration model of BOLD as a function of  $SVO_2$ , with an approximated correction for the small decreases in CBF known to occur during hyperoxia (Chiarelli et al. 2007b; Goodwin et al. 2009; Mark et al. 2011). Due to the difficulty of measuring small CBF changes with the somewhat noisy ASL method, a fixed value for the hyperoxia-induced CBF decrease is generally assumed.

The hyperoxia model (Chiarelli et al. 2007b) can be generalized for arbitrary changes in cerebral blood flow during hyperoxia (Gauthier et al. 2011b), rendering it valid for conditions such as simultaneous hyperoxia and hypercapnia (as would be produced during breathing of carbogen, a mixture composed largely of  $O_2$  with a balance of 5-10%  $CO_2$ ). This article presents a detailed description of this generalized calibration model (GCM), examines the sensitivity of the different methods to errors in CBF measurement, and compares values of visually-evoked  $CMRO_2$  change obtained using the different calibration approaches.

### 2.3.1. Theory

Oxygen is a mild vasoconstrictor, and hyperoxia during inhalation of 100%  $O_2$  has been associated with small reductions in cerebral blood flow (Bulte et al. 2007). The hyperoxia calibration method introduced by Chiarelli *et al.* (Chiarelli et al. 2007b), was thus derived for conditions where cerebral blood flow would be expected to undergo little or no change. To generalize the model to be valid under an arbitrary change in cerebral blood flow, Equation 12 in Chiarelli *et al.* can be replaced with the following expression:

$$CBF \cdot Cv_{O_2} = CBF \cdot Ca_{O_2} - CBF_0 \cdot \left( Ca_{O_2}|_0 \cdot OEF_0 \right) \quad [1]$$

where, as in Chiarelli, CBF is the cerebral blood flow in milliliters per second,  $Cv_{O_2}$  is the venous oxygen content in milliliters of  $O_2$  per deciliter of blood,  $Ca_{O_2}$  is the arterial oxygen content (also in ml  $O_2$ /dl blood), and OEF is the oxygen extraction fraction (dimensionless, and assumed here to be 0.3 as in Chiarelli *et al.*). The subscript '0' is used to denote resting values for  $Ca_{O_2}$ , OEF, and CBF. The value  $OEF_0$  used in this equation reflects the resting value, which is assumed to be

constant throughout the brain and across individuals (Frackowiak et al. 1980; Ito et al. 2004; Ashkanian et al. 2008; Bremmer et al. 2010; Sedlacik et al. 2010).

Whereas the expression proposed by Chiarelli balances O<sub>2</sub> concentrations, the new expression balances the temporal fluxes of O<sub>2</sub> at the level of the capillaries.

The above expression can be readily solved for the venous O<sub>2</sub> content during an arbitrary change in blood flow and oxygenation:

$$Cv_{O_2} = Ca_{O_2} - \frac{\left( Ca_{O_2}|_0 \cdot OEF_0 \right)}{\left( \frac{CBF}{CBF_0} \right)} \quad [2]$$

Values for Ca<sub>O<sub>2</sub></sub> at baseline and during the breathing manipulations are obtained using the end-tidal O<sub>2</sub> measurements as in Chiarelli *et al.* End-tidal O<sub>2</sub> values are used here as a surrogate for Pa<sub>O<sub>2</sub></sub>, the arterial partial pressure of O<sub>2</sub>. The total arterial O<sub>2</sub> content during carbogen inhalation is obtained from Equation 11 of Chiarelli:

$$Ca_{O_2} = \left( \phi \cdot [Hb] \cdot Sa_{O_2} \right) + \left( Pa_{O_2} \cdot \varepsilon \right) \quad [3]$$

where  $\phi$  is the O<sub>2</sub> carrying capacity of hemoglobin (1.34 ml<sub>O<sub>2</sub></sub>/g<sub>Hb</sub>), [Hb] is the concentration of hemoglobin in blood (15 g<sub>Hb</sub>/dl), Sa<sub>O<sub>2</sub></sub> is the hemoglobin saturation, and  $\varepsilon$  represents the solubility of O<sub>2</sub> in plasma (0.0031 ml<sub>O<sub>2</sub></sub>/ (dl<sub>blood</sub>\*mmHg)). The constants used here are the same as those in Chiarelli *et al.* The measured end-tidal O<sub>2</sub> values were considered equivalent to Pa<sub>O<sub>2</sub></sub>, and used to determine Sa<sub>O<sub>2</sub></sub> using the Severinghaus equation:

$$Sa_{O_2} = \frac{1}{\left( \frac{23400}{\left( Pa_{O_2} \right)^3 + 150 \left( Pa_{O_2} \right)} + 1 \right)} \quad [4]$$

The value for Ca<sub>O<sub>2</sub></sub>|<sub>0</sub>, used above in Equation 2, is determined using the Pa<sub>O<sub>2</sub></sub> value at normoxia, the OEF<sub>0</sub> value of 0.3 is assumed from literature, and the baseline-normalized CBF value is measured during pCASL imaging.

As a penultimate step, we can estimate the venous O<sub>2</sub> saturation using Equation 14 from Chiarelli *et al.* (assuming that plasma O<sub>2</sub> content in venous blood is zero as long as there is any dHb available for binding) and the CvO<sub>2</sub> value computed above:

$$Sv_{O_2} = \frac{Cv_{O_2} - (Pv_{O_2} \cdot \epsilon)}{\varphi \cdot [Hb]} \quad [5]$$

We can now estimate an *M* value based on values for SvO<sub>2</sub>, BOLD signal increase, and CBF increase during simultaneous hypercapnia and hyperoxia. With variable CBF incorporated explicitly in our revised expression for CvO<sub>2</sub>, we no longer need the CBF correction term ‘C’ from Equation 8 in Chiarelli *et al.*, and the expression becomes:

$$\begin{aligned} \frac{\Delta BOLD}{BOLD_0} &= M \left( 1 - \left( \frac{CBF}{CBF_0} \right)^\alpha \left( \frac{[dHb]}{[dHb]_0} \right)^\beta \right) \\ &= M \left( 1 - \left( \frac{CBF}{CBF_0} \right)^\alpha \left( \frac{(1 - Sv_{O_2})}{(1 - Sv_{O_2}|_0)} \right)^\beta \right) \end{aligned} \quad [6]$$

where the term (CBF/CBF<sub>0</sub>)<sup>α</sup> is used to model cerebral blood volume, assuming *α* = 0.38 (Grubb *et al.*, 1974), and *β* = 1.5 is used to model the influence of deoxygenated hemoglobin on transverse relaxation (Boxerman *et al.*, 1995). The above expression can be readily solved for *M*:

$$M = \frac{\frac{\Delta BOLD}{BOLD_0}}{1 - \left( \frac{CBF}{CBF_0} \right)^\alpha \left( \frac{(1 - Sv_{O_2})}{(1 - Sv_{O_2}|_0)} \right)^\beta} \quad [7]$$

Calculation of relative CMRO<sub>2</sub> during a task can then be performed using the expression proposed by Davis *et al.* (Davis *et al.* 1998):

$$CMRO_2 = \left( \frac{CBF}{CBF_0} \right)^{1-\alpha/\beta} \left( 1 - \frac{\left( \frac{\Delta BOLD}{BOLD_0} \right)}{M} \right)^{1/\beta} \quad [8]$$

A detailed theoretical comparison of the different models is given in the Appendix.

## 2.4. Methods

Acquisitions were conducted in eight healthy subjects (seven male and one female, aged 21 to 38 years) on a Siemens TIM Trio 3T MRI system (Siemens Medical Solutions, Erlangen, Germany) using the Siemens 32-channel receive-only head coil for all acquisitions. All subjects gave informed consent and the project was approved by the Comité mixte d'éthique de la recherche du Regroupement Neuroimagerie/Québec.

### 2.4.1. Image acquisition

Sessions included an anatomical, 1mm<sup>3</sup> MPRAGE acquisition with TR/TE/alpha = 2300ms/3ms/9°, 256x240 matrix and a GRAPPA acceleration factor of 2 (Griswold et al. 2002).

Functional image series were acquired using a dual-echo pseudo-continuous arterial spin labeling (pCASL) acquisition (Wu et al. 2007) to measure changes in cerebral blood flow (CBF). The parameters used include: TR/TE1/TE2/alpha = 3000ms/10ms/30ms/90° with 4x4mm in-plane resolution and 11 slices of 7mm (1mm slice gap) on a 64x64 matrix (at 7/8 partial Fourier), GRAPPA acceleration factor = 2, post-labeling delay = 900ms, label offset = 100mm, Hanning window-shaped RF pulse with duration/space = 500µs/360µs, flip angle of labeling pulse = 25°, slice-selective gradient = 6mT/m, tagging duration = 2s (Wu et al. 2007).

In one subject, five susceptibility-weighted images (SWI) (Reichenbach et al. 2001; Rauscher et al. 2005a) were obtained to provide a qualitative assessment of the venous oxygenation increase with each breathing manipulation. One image was acquired during inhalation of, respectively: air, 7% CO<sub>2</sub>/93% air (HC), 100% O<sub>2</sub> (HO), 7% CO<sub>2</sub>/93% O<sub>2</sub> (HO-HC 7%) and 10% CO<sub>2</sub>/90% O<sub>2</sub> (HO-HC 10%). For all

images, the acquisition was started after an initial one minute period of gas breathing to allow oxygen saturation and vasodilation to reach a plateau. Parameters used for the SWI acquisition were: TR/TE/alpha = 27ms/20ms/15° with 0.9x0.9mm in-plane resolution with 56 slices of 1.5mm on a 256x192 matrix.

## **2.4.2. Manipulations**

Each session consisted of four functional runs: one run with visual stimulation and three runs each including a different gas manipulation. During each gas manipulation run, a single three-minute block of gas inhalation was preceded with one minute and followed by two minutes of medical air breathing. The three gas manipulations used were: 100% O<sub>2</sub> (hyperoxia, or HO), 7% CO<sub>2</sub>/93% air (hypercapnia, or HC) and 7% CO<sub>2</sub>/93% O<sub>2</sub> (simultaneous hyperoxia and hypercapnia, or HO-HC). The latter gas is a specific formulation of carbogen, which in general may contain different O<sub>2</sub>/CO<sub>2</sub> ratios.

### *2.4.2.1. Visual stimulus*

The visual stimulus used was a black and white radial checkerboard, with annuli scaled logarithmically with eccentricity, luminance modulated in a temporal squarewave at 8 Hz (equivalent to 16 contrast reversals per second) presented using an LCD projector (EMP-8300, Epson, Toronto, ON, Canada) onto a translucent screen viewed by subjects through a mirror integrated into the Siemens head coil. This stimulation was initiated one minute into the acquisition and lasted three minutes, followed by two minutes of rest.

### *2.4.2.2. Gas manipulations*

At the beginning of the experiment, subjects were fitted with a non-rebreathing face mask (Hudson RCI, #1059, Temecula, California, USA). To avoid discomfort from outward gas leakage blowing into the subject's eyes, skin tape (Tegaderm Film, #1626W, 3M Health Care, St-Paul, MN, USA) was used to seal the top of the mask to the face. Plastic tubing (Airlife™ Oxygen tubing #001305, Cardinal Health, McGraw Park, IL, USA) and a series of two Y-connectors were used to connect pressure/flow-meters for medical air, 100% O<sub>2</sub> (hyperoxia, or HO), 7% CO<sub>2</sub>/93% air (hypercapnia, or HC) and 7% CO<sub>2</sub>/93% O<sub>2</sub> (simultaneous hyperoxia and

hypercapnia, or HO-HC) tanks (Vitalaire, Mississauga, ON, Canada) to the mask. Gas flows were adjusted manually on the pressure/flow-meters (MEGS, Ville St-Laurent, QC, Canada) to keep a total flow rate of 16L/min. Gas flow was kept at 16L/min at all times except during administration of the HO-HC and the HC gas mixtures. To accommodate the hyperventilation caused by CO<sub>2</sub> breathing, gas flow rates were increased to the maximal possible rate (25L/min) achievable with our pressure/flowmeters. Pulse rate and arterial O<sub>2</sub> saturation were monitored in all subjects using a pulse-oximeter (InVivo Instruments, Orlando, USA) as a safety measure and to observe the effects of carbogen breathing.

End-tidal O<sub>2</sub> and CO<sub>2</sub> values were monitored during all acquisitions. Gases were sampled via an indwelling nasal cannula (Airlife™ Nasal Oxygen Cannula #001321, Cardinal Health, McGraw Park, IL, USA) using the CO2100C and O2100C modules of the MP150 BIOPAC physiological monitoring unit (BIOPAC Systems Inc., Goleta, CA, USA). Calibration of the unit was done by taking into account an expired partial pressure of water of 47mmHg (Severinghaus 1989). Subjects were instructed to breathe through their nose, which ensured that only expired gas was sampled by the nasal cannula. End-tidal CO<sub>2</sub> and O<sub>2</sub> values were selected manually from continuous respiratory traces sampled at 200 Hz. The first 10 breaths of the first baseline period and the last 10 breaths of the gas-inhalation block were averaged to give baseline values and gas manipulation values respectively.

Following acquisition, all subjects were debriefed to assess the level of discomfort associated with the manipulation. The subjects were asked to rate the air hunger and breathing discomfort associated with the HO-HC and HC mixtures on a french language version of the scale proposed by Banzett *et al.* (Banzett et al. 1996).

### **2.4.3. Data analysis**

Individual subject analyses for ROI quantifications, absolute CBF,  $M$  and CMRO<sub>2</sub> mapping were done using the NeuroLens data analysis software package ([www.neurolens.org](http://www.neurolens.org)). Time-series data from each echo were motion corrected (Cox et al. 1999) and spatially smoothed with a 6 mm 3D Gaussian kernel. ASL data were similarly processed, and the CBF signal was isolated from the first echo

(TE = 10ms) through surround subtraction using linear interpolation between neighboring points (Liu et al. 2005). A BOLD time series was isolated through surround addition using linear interpolation of neighboring points of the second echo (TE = 30ms). A general linear model (GLM) including a single-block response, a linear drift, and constant offset terms was applied, to obtain effect sizes and T-maps for each condition. The first 60s after each transition in gas composition were excluded from the analyses by zeroing out relevant rows in the GLM computational matrices, to select responses at (or close to) steady-state.

Fractional changes were then calculated by dividing effect sizes over the visual ROI by the constant DC term from the GLM averaged within the same region. Group average values  $\pm$  standard deviation are reported.

Uncertainties on the estimates for  $M$  and  $CMRO_2$  were computed through numerical propagation of errors. This was performed by evaluating  $M$  and  $CMRO_2$  for all combinations of input values evaluated at the upper and lower bounds of their respective confidence intervals (based on  $\pm$  SE). The resultant ranges of  $M$  and  $CMRO_2$  values were then taken as the uncertainty for the respective parameter.

Absolute CBF maps were generated as in (Wang et al. 2003b). A binary mask was generated from the absolute flow map to remove all voxels with an absolute baseline CBF below 25 mL/100g/min, as a means of selecting cortical grey matter. Percent CBF and BOLD maps in response to the breathing manipulations as well as the visual task were multiplied by this mask to exclude white matter and CSF, as the low resting CBF levels in these tissue compartments preclude stable estimation of fractional CBF changes required by the model.

Arterial spin-labeling measurements acquired during hyperoxia alone and combined hyperoxia and hypercapnia were corrected for T1 changes using the approach described in (Chalela et al. 2000; Zaharchuk et al. 2008). Arterial blood T1 values were estimated based on measured  $PETO_2$  (partial end-tidal pressure of  $O_2$ ) values for each subject and T1 vs.  $PETO_2$  values tabulated in Bulte *et al.* (Bulte et al. 2007). Since the T1 depends specifically on the level of dissolved  $O_2$  in the plasma, and since we obtained different  $Pa_{O_2}$  (arterial partial pressure of  $O_2$ )

values at a given  $F_{iO_2}$  (fraction of inspired  $O_2$ ) than the latter study (their  $Pa_{O_2}$  values were higher, likely due to the use of a tightly sealed face mask), the values were interpolated to account for this difference (i.e. the table from Bulte was converted to T1 vs. group average  $Pa_{O_2}$ , and the T1 corresponding to each subject's  $PET_{O_2}$  during hyperoxia manipulations was interpolated). Values for the absolute blood flow at the air-breathing baseline were computed using Equation 1 from Wang *et al.* (Wang *et al.* 2003b), assuming the same constant values as in this reference.

The resultant values of percent change in ASL and BOLD signals (and where appropriate  $PET_{O_2}$ ) were input to the applicable BOLD signal models to generate maps of the  $M$  parameter. More specifically, ASL and BOLD responses during hypercapnia were input to the hypercapnia model (Davis *et al.* 1998), while BOLD, and  $PET_{O_2}$  data were input to the hyperoxia model (Chiarelli *et al.* 2007b) with an assumed flow decrease of 5% (based on  $PET_{O_2}$  values obtained in our subjects and the flow decrease observed by Bulte *et al.* for similar  $PET_{O_2}$  levels (Bulte *et al.* 2007). The generalized calibration model (GCM) was applied to ASL, BOLD, and  $PET_{O_2}$  data for all manipulations.

#### 2.4.3.1. Visual

Regions of interest (ROIs) were derived from the intersection of the flow and BOLD thresholded ( $p \leq 0.01$  corrected) (Worsley *et al.* 2002) visual activation T-maps for each individual subject from the NeuroLens analysis. One subject (subject 1) fell asleep during the visual task and was therefore excluded from all analyses requiring a visual ROI.

#### 2.4.3.2. Grey matter

A grey matter ROI was defined for each subject using the automatic tissue segmentation functionality of the CIVET software package (Tohka *et al.* 2004).

#### 2.4.3.3. Analysis of sensitivity to errors in CBF

One of the limiting factors in the application of calibrated MRI methods has been the low signal-to-noise ratio of ASL measurements. To assess the sensitivity of different  $M$  estimation methods to possible errors in cerebral flow change, we

computed  $M$  values based on group average ROI and respiratory measures with simulated errors in the gas-induced CBF response. In these simulations, the input value of baseline-normalized CBF was varied over a range corresponding to the measurement uncertainty exhibited by our data while other input parameters (BOLD response and, where applicable, end-tidal  $O_2$  values) were held constant. This computation was carried out for the Davis model with HC data, for the Chiarelli model with HO data, and for the GCM with HC, HO, and HO-HC data.

## 2.5. Results

End-tidal partial pressures of  $O_2$  ( $PETO_2$ ) and  $CO_2$  ( $PETCO_2$ ) achieved during each gas manipulation for each subject are shown in Table 1. While  $PETCO_2$  values were very similar between HC and HO-HC,  $PETO_2$  values tended to be lower for HO-HC than for HO alone (possibly reflecting the 90% vs. 100%  $O_2$  content of the two gases).

	Subject 1	Subject 2	Subject 3	Subject 4	Subject 5	Subject 6	Subject 7	Subject 8	Average
$PETCO_2$ baseline	37.7	41.7	38.3	41.9	39.3	42.0	40.4	34.5	39.5
$PETCO_2$ HC	51.2	52.2	47.5	46.9	51.9	46.9	47.8	42.3	48.3
$PETO_2$ baseline	113.9	114.1	113.0	139.0	125.4	125.0	92.3	106.3	116.1
$PETO_2$ HO	578.4	621.6	509.3	569.8	583.6	380.0	560.8	513.1	539.6
$PETCO_2$ baseline	41.8	42.0	37.2	40.8	41.2	41.3	40.1	35.1	40.0
$PETCO_2$ HO-HC	48.9	51.0	46.1	46.9	50.8	46.7	45.9	45.5	47.7
$PETO_2$ baseline	102.9	104.0	135.7	125.2	114.0	130.3	106.4	105.4	115.5
$PETO_2$ HO-HC	447.5	480.8	400.8	425.1	486.7	303.8	403.5	375.6	415.5

**Table 1. End-tidal values for each breathing manipulation**

Average end-tidal values for individual subjects. The top subsection shows end-tidal partial pressures of  $CO_2$  ( $PETCO_2$ ) for the hypercapnia (HC) breathing manipulation during baseline (top row) and during the hypercapnia block (second row). The second subsection shows end-tidal partial pressures of  $O_2$  ( $PETO_2$ ) for the hyperoxia (HO) breathing manipulation during baseline (third row) and during the hyperoxia block (fourth row). The third section shows  $PETCO_2$  and  $PETO_2$  (baseline and block) for combined hypercapnia and hyperoxia (HO-HC).

The changes in blood oxygenation resulting from these three gas manipulations can be appreciated from the ROI-average values for BOLD signal change (Figure 1B), while the vasodilatory effect of CO<sub>2</sub> is demonstrated by the CBF changes within the same ROI's (Figure 1A). Percent changes in CBF (Figure 1A) for HC and HO-HC were not found to be significantly different (paired two-tailed Student's T-test,  $p > 0.3$ ) in both visual and GM ROI's. Average CBF changes in the visual ROI were  $63.3 \pm 6.7\%$  and  $68.9 \pm 12.2\%$ , while average changes throughout GM were  $37.3 \pm 4.8\%$  and  $40.7 \pm 3.7\%$  for HC and HO-HC respectively. Average flow changes for HO in visual and GM ROI's were, respectively,  $-7.3 \pm 3.7\%$  and  $-3.1 \pm 3.1\%$ . BOLD percent changes (Figure 1B) for HC and HO were similar, with averages of  $2.3 \pm 0.2\%$  and  $1.9 \pm 0.2\%$  in the visual ROI and  $2.3 \pm 0.1\%$  and  $1.7 \pm 0.2\%$  in GM for HC and HO respectively. Average ROI values for HO-HC were about double those of HO and HC alone, with averages of  $4.1 \pm 0.4\%$  and  $3.6 \pm 0.4\%$  respectively for visual and GM ROI's.

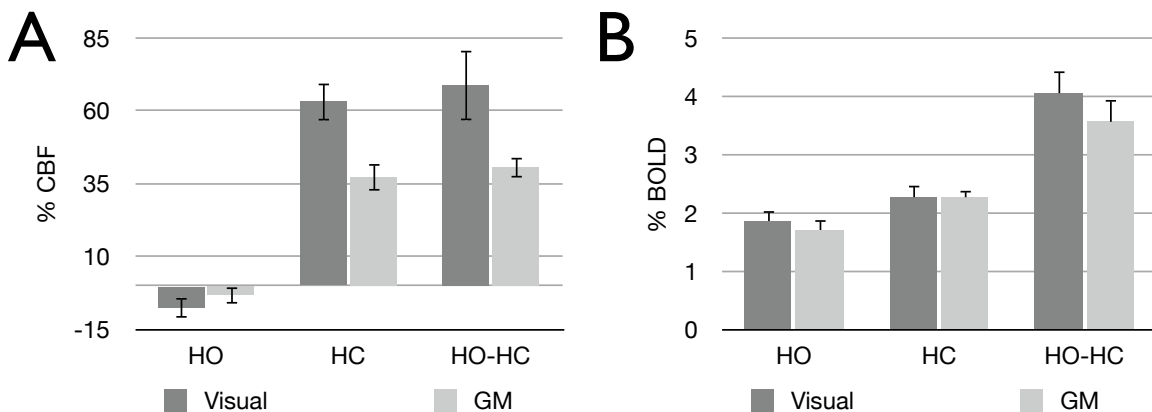


**Figure 1. Group average percent CBF and BOLD for each breathing manipulation**

Group average percent CBF (A) and percent BOLD (B) changes over visual and grey-matter ROI's for hyperoxia (HO), hypercapnia (HC) and combined hypercapnia and hyperoxia (HO-HC).

Individual subjects' ROI-based *M* values for visual cortex are summarized in Figure 2A and Table 2. Values of *M* are shown for each gas manipulation (HC, HO and HO-HC), calculated with the original model for that manipulation. Group average *M* values were  $5.6 \pm 1.8\%$ ,  $4.5 \pm 1.5\%$ , and  $7.6 \pm 2.6\%$  for HC, HO and HO-HC respectively over the visual ROI. The *M* values estimated using the HO-HC technique were generally found to be the highest, while HO tended to give the lowest values. Application of the GCM to ROI-average CBF and BOLD signals as

well as  $PETO_2$  values measured during hypercapnia yielded slightly lower values than those of the Davis model ( $M$  values with GCM were on average lower by  $0.5 \pm 0.2\%$ ). On the other hand, application of the GCM to the BOLD and  $PETO_2$  values recorded during hyperoxia (with an assumed flow decrease of 5%) yielded systematically higher  $M$  values than the Chiarelli model ( $M$  values with GCM were on average  $1.7 \pm 1.1\%$  higher; data not shown).

Some similarities were observed when  $M$  was estimated over all grey matter (Figure 2B). Group average  $M$  values were  $7.9 \pm 0.8\%$ ,  $4.0 \pm 0.8\%$  and  $7.9 \pm 0.6\%$  for HC, HO and HO-HC respectively. The tendency toward higher  $M$  values with HO-HC and lower  $M$  values with HO is clearer here with a lower inter-subject variability. Application of the GCM to data obtained during HC yielded lower  $M$  values than the Davis model (values computed with GCM were on average  $0.8 \pm 0.3\%$  lower than those from the Davis model). On the other hand,  $M$  values estimated using the GCM during HO were higher than those obtained using the Chiarelli model ( $1.3 \pm 0.4\%$  higher for GCM as compared to the Chiarelli model; data not shown).

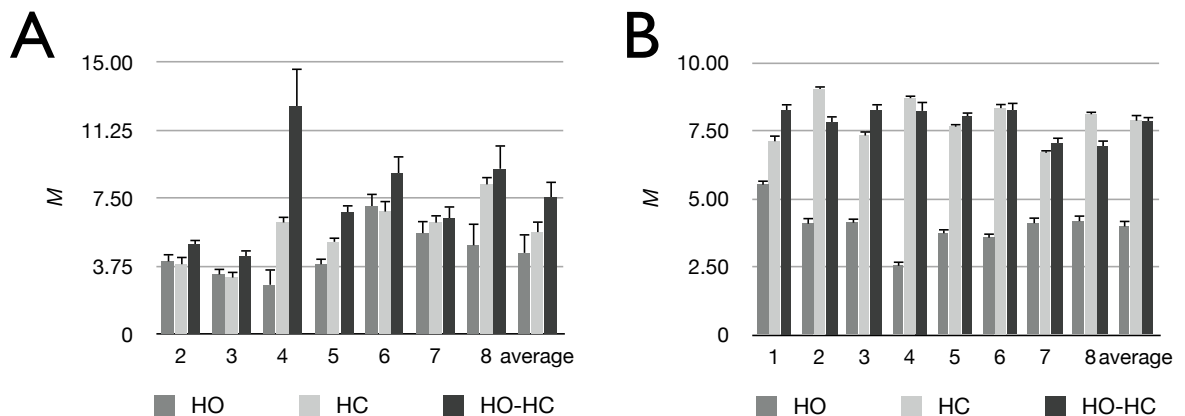


**Figure 2. Individual and average  $M$  values over the visual and grey-matter ROI's for each breathing manipulation**

Individual and group average  $M$  values over visual (A) and grey-matter (B) ROI's for hyperoxia (HO), hypercapnia (HC) and combined hypercapnia and hyperoxia (HO-HC). The Chiarelli, Davis and GCM formulae were used to process data from the respective gas manipulations.

Maps of  $M$  for each breathing manipulation using the model originally derived for the respective procedures are shown in Figure 3. A similar pattern may be observed between subjects whereby HO yields lower and more uniform maps of  $M$

values, with few localized enhancements compared to HC and HO-HC. The maps created using HC show a speckled pattern of focal  $M$  hotspots, some of which appear (based on placement with respect to sulcal anatomy) to be veins, while others appear artifactual, likely from instabilities in the model under high CBF errors (Figure 4). Maps from HO-HC exhibit an intermediate pattern with more uniform  $M$  values throughout cortex combined with local enhancements associated with larger veins. The reduced prevalence of questionable hot spots in the HO-HC maps, as compared to the HC maps can be appreciated in the example maps shown in Figure 4. In this figure, the window display levels were adjusted to highlight the differences in the high amplitude local enhancements in these maps, as opposed to the scale used in Figure 3, chosen to show general trends over all techniques and subjects.

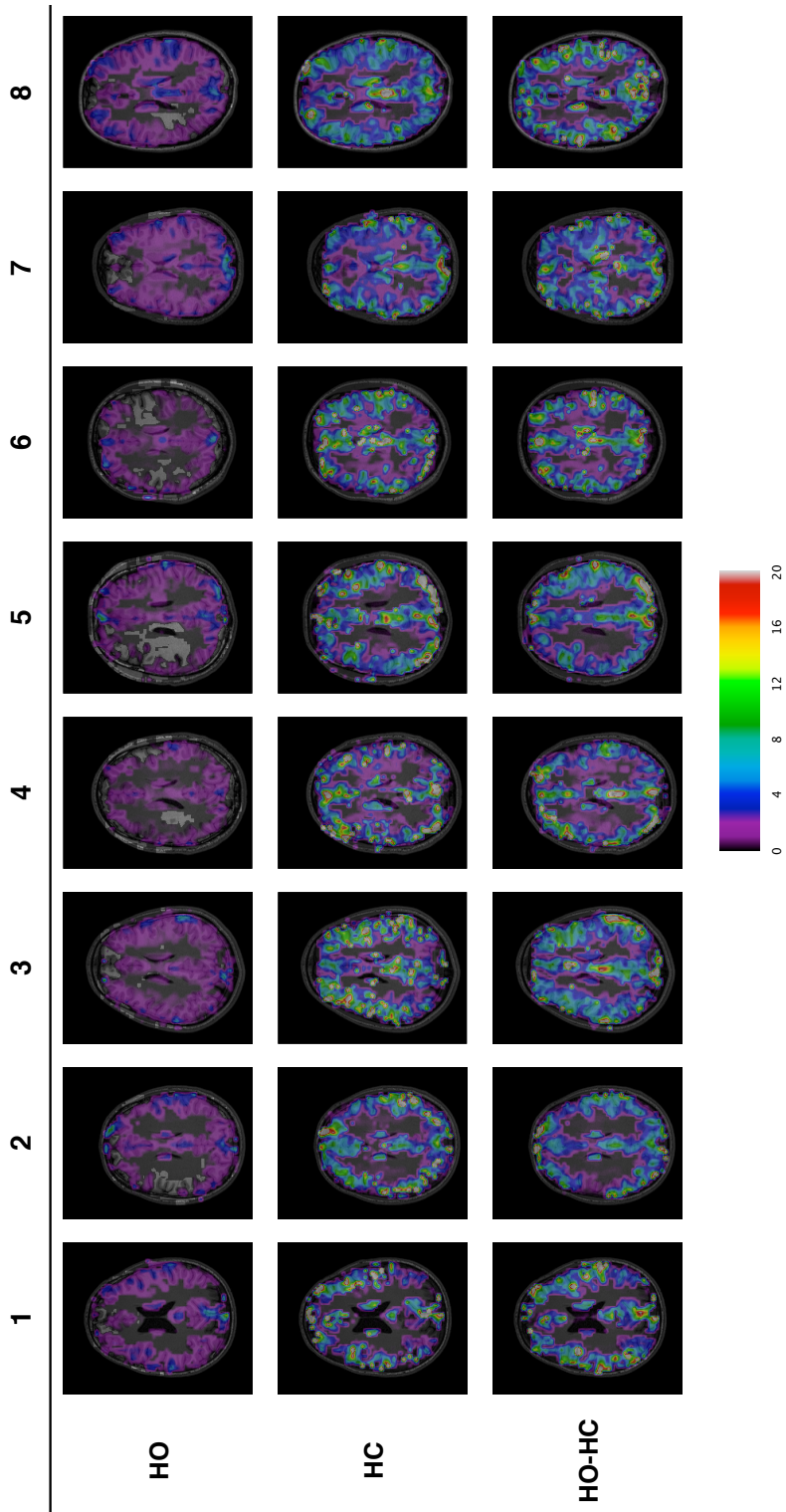


**Figure 3. Individual  $M$  maps for each breathing manipulation**

Individual  $M$  maps for hyperoxia (HO) (top row), hypercapnia (HC) (second row) and combined hypercapnia and hyperoxia (HO-HC) (third row). The Chiarelli, Davis, and GCM expressions were used to process data from the respective gas manipulations. Display window levels have been adjusted to emphasize detail in all maps.

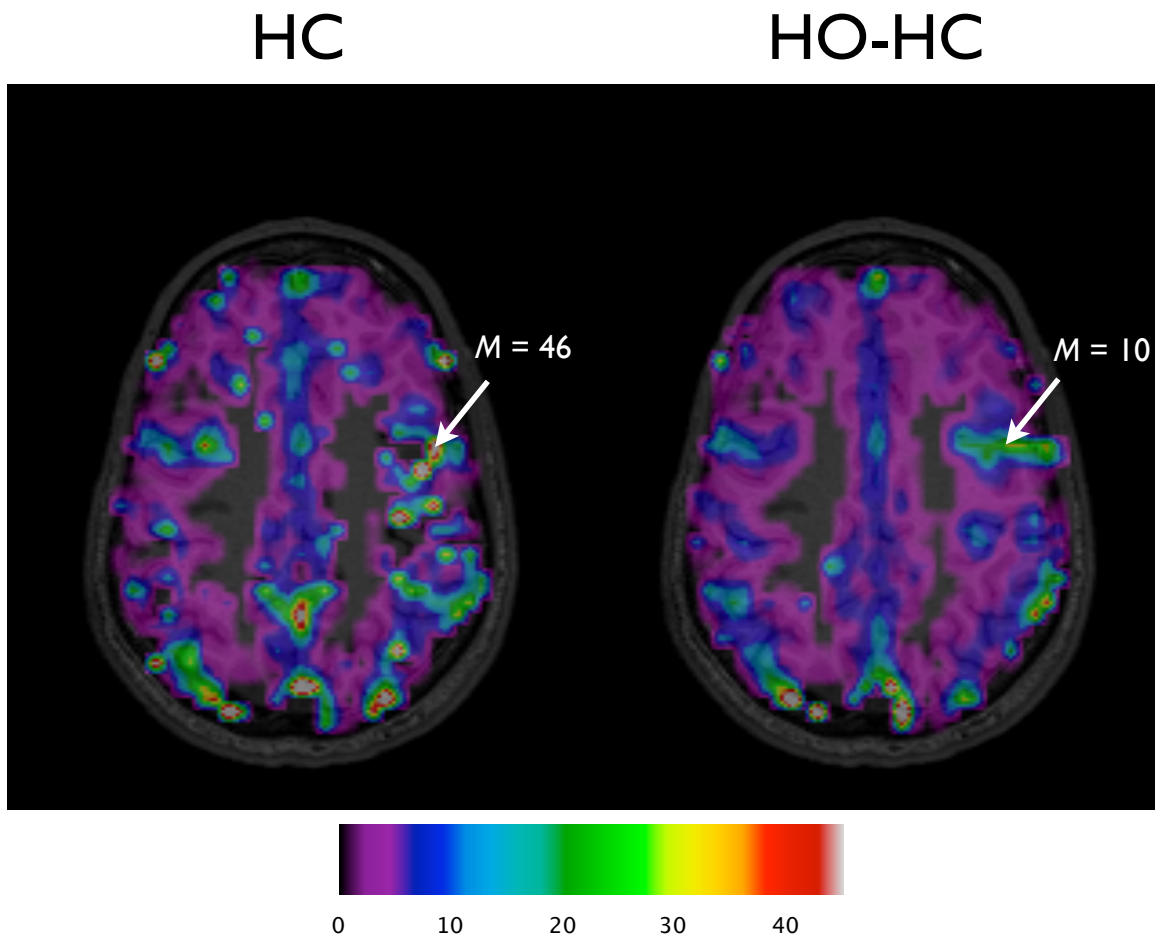


**Figure 4. Spatial heterogeneity of  $M$  maps**

Maps of  $M$  from one subject for HC and HO-HC (using Davis model and GCM, respectively). The display window levels have been adjusted to highlight the differences in the magnitude of  $M$  estimates within local enhancements.

The susceptibility-weighted venograms acquired in one subject provide a qualitative depiction of the venous saturation provided by each breathing manipulation (Figure 5). In this subject, the prominent veins visible in the baseline image acquired during air breathing can be seen to fade due to increasing levels of oxygen saturation for 100%  $O_2$  (HO) breathing and 7%  $CO_2$ /93% air (HC) mixtures. While a carbogen mixture with 10%  $CO_2$ /90%  $O_2$  (HO-HC 10%) composition yields a complete loss of venous contrast, the carbogen mixture with 7%  $CO_2$ /93%  $O_2$  (HO-HC 7%) shows an intermediate pattern with complete loss of venous contrast in smaller veins, but some residual contrast in the largest veins.

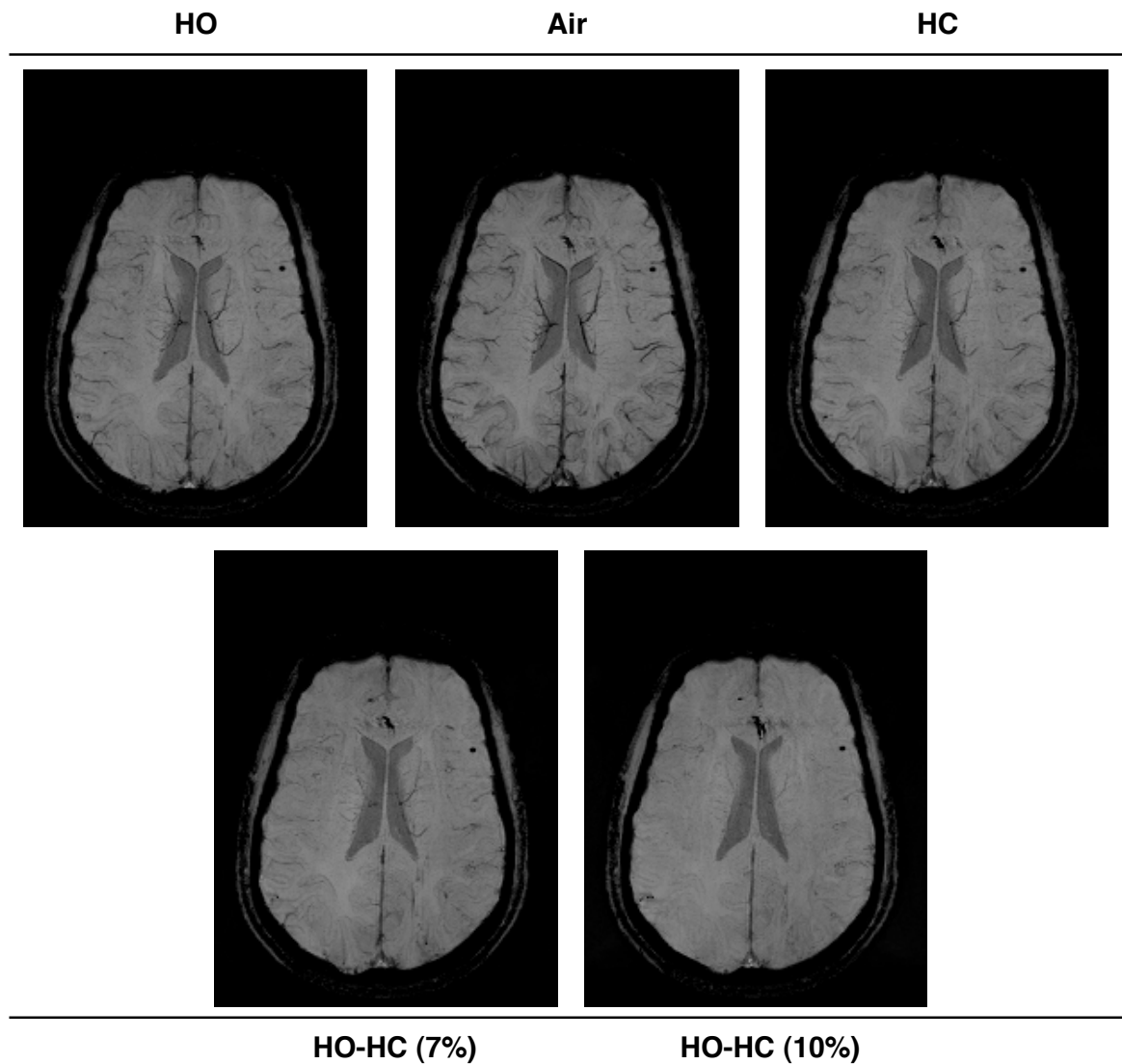


**Figure 5. Susceptibility-weighted venograms during each breathing manipulation**

Susceptibility-weighted venograms acquired in a single subject during breathing of either air, 100% O<sub>2</sub> (HO), 7% CO<sub>2</sub>/93% air (HC), 7% CO<sub>2</sub>/93% O<sub>2</sub> (HO-HC 7%) and 10% CO<sub>2</sub>/90% O<sub>2</sub> (HO-HC 10%).

Simulations of the effect of CBF error on apparent  $M$  value are shown in Figure 6. Estimates of  $M$  based on manipulations including hypercapnia exhibited greater-than-linear increases in the error on  $M$  as a function of CBF underestimation (for both Davis model and GCM). However this non-linearity and resultant errors on  $M$  were far smaller, over the entire range of CBF errors examined, for GCM in combination with HO-HC than for other methods (Figure 6A). Estimates of  $M$  based on hyperoxia alone exhibited marked instabilities for relatively small errors in CBF (for both the Chiarelli model and GCM) (Figure 6B).

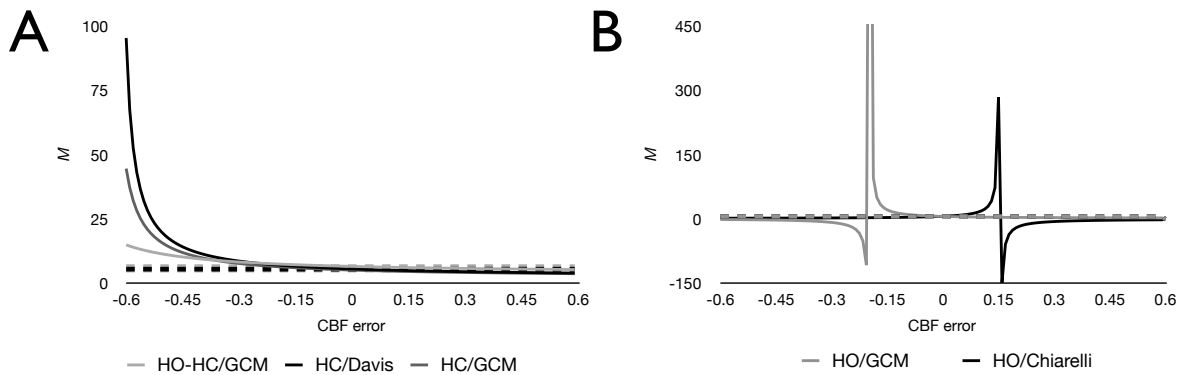


**Figure 6. Effect of CBF errors on  $M$  estimates from different models and breathing manipulations**

Solid lines show  $M$  estimates as a function of the error in CBF, while the broken lines (nearly overlapping) show the values of the actual  $M$  estimates from the group average visual ROI flow response (i.e. without error) for the different methods. All estimates use group average values for BOLD and respiratory measures, as well as for the central (zero error) value of CBF. For manipulations and models with a HC component (A), HC/Davis, HC/GCM and HO-HC/GCM, greater-than-linear error occurs with progressive underestimation of the flow response to hypercapnia. The combination of HO-HC with the GCM yielded  $M$  estimates with the greatest immunity to errors in CBF. The hyperoxia-only manipulation, when used with either the GCM and Chiarelli model (B) shows a singularity at flow estimates within the typical error bounds on ASL measurements.

Percent changes in  $CMRO_2$  over visual cortex were computed for each subject using ROI-average values for CBF and BOLD increases during the visual task and  $M$  values obtained from each breathing manipulation (Figure 7 and Table 2). While group average values for each technique were similar and a pattern for large inter-subject variability can be seen, some patterns nevertheless emerge from this analysis. The HO-HC technique yielded physiologically plausible estimates of relative  $CMRO_2$  change in all subjects. HC, on the other hand, yielded very low and non-physiological  $\Delta\%CMRO_2$  estimates in two subjects (subjects 2 and 3 in Figure 7). HO also resulted in a non-physiological, negative  $\Delta\%CMRO_2$  estimate in one subject (subject 3 in Figure 7).

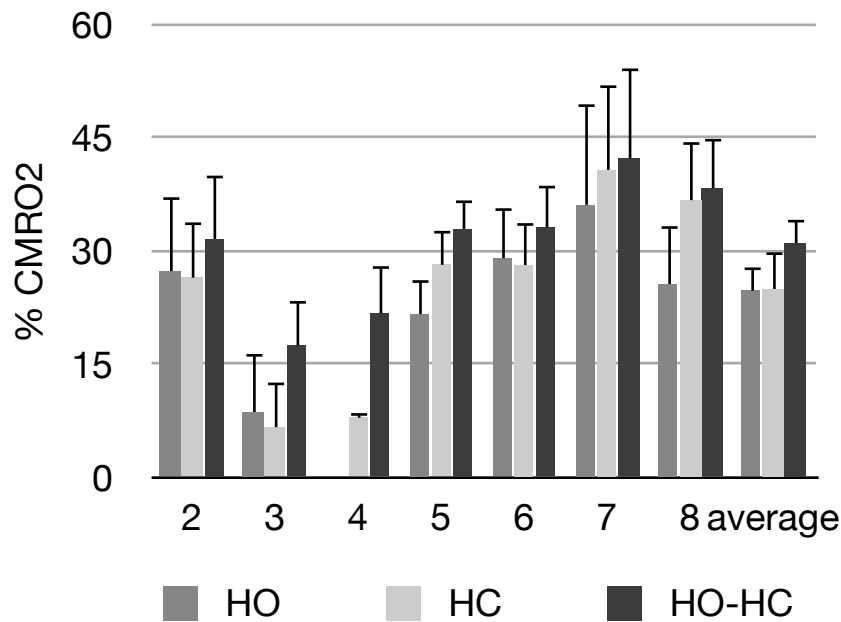


**Figure 7. Individual and average CMRO<sub>2</sub> estimates over the visual ROI**

Individual and group average evoked CMRO<sub>2</sub> estimates for the visual task, calculated using  $M$  values from hyperoxia (HO), hypercapnia (HC) and combined hypercapnia and hyperoxia (HO-HC) manipulations (and respective models).

Calibrated fMRI parameters, including cerebrovascular reactivity during HC and HO-HC,  $M$ , CMRO<sub>2</sub> and the coupling parameter  $n$  are shown for each subject in Table 2. Vascular reactivities were similar in most subjects for HC and HO-HC, except in subjects 3 and 7, who exhibited lower flow responses to HO-HC than to HC alone. The coupling constant  $n$  is defined here as the magnitude of the fractional flow change during a stimulus divided by the corresponding fractional change in CMRO<sub>2</sub>. Values for  $n$  are expected to be between 2 and 4 (Buxton 2010). While most  $n$  values fall within this range, some values obtained using either HC or HO calibration exhibited physiologically suspect values with either very high (subjects 2 and 3) or one negative value (subject 3) in the case of HO calibration.

	Subject 1	Subject 2	Subject 3	Subject 4	Subject 5	Subject 6	Subject 7	Average
Reactivity HC	6.5	8.5	8.3	6.0	8.7	10.7	6.1	7.8
Reactivity HO-HC	9.3	10.3	2.3	8.3	8.4	10.1	2.9	7.4
<i>M</i> HC	3.8	3.1	6.1	5.1	6.8	6.2	8.3	5.6
<i>M</i> HO	4.0	3.3	2.7	3.9	7.1	5.6	4.9	4.5
<i>M</i> HO-HC	5.0	4.3	12.6	6.7	8.9	6.4	9.1	7.6
CMRO <sub>2</sub> HC	26.5	6.7	7.9	28.2	28.2	40.8	36.8	25.0
CMRO <sub>2</sub> HO	27.3	8.7	-30.8	21.6	29.1	36.1	25.6	16.8
CMRO <sub>2</sub> HO-HC	31.6	17.5	21.7	32.9	33.1	42.3	38.3	31.1
<i>n</i> HC	2.7	9.4	6.1	2.4	2.5	3.0	2.0	4.0
<i>n</i> HO	2.6	7.2	-1.6	3.2	2.4	3.4	2.9	3.0
<i>n</i> HO-HC	2.2	3.6	2.2	2.1	2.1	2.9	2.0	2.4

**Table 2. Calibrated fMRI results**

Individual subjects' and average values for vascular and metabolic parameters. The first section shows vascular reactivity (% change CBF/mmHg change in PETCO<sub>2</sub>) values for hypercapnia (HC) and combined hypercapnia and hyperoxia (HO-HC). The second section shows average *M* values over the visual ROI for each breathing manipulation. The third section shows estimates of visually-evoked CMRO<sub>2</sub> using *M* values calculated with the *M* value associated with each breathing manipulation. Finally, the fourth section shows the coupling constant between CBF and CMRO<sub>2</sub> associated with the estimates obtained from each breathing manipulation. The Chiarelli, Davis and GCM formulae were used to process data from the respective gas manipulations.

## 2.6. Discussion

### 2.6.1. Estimation of *M* parameter

Comparison of functional MR calibration methods based respectively on hypercapnia, hyperoxia and combined hypercapnia and hyperoxia indicates that the hybrid technique may yield more robust and accurate *M* estimates thanks to the reduced range of extrapolation required from the higher measured BOLD signals. In the latter assessment we define robustness as the relative immunity from physically invalid results such as negative, imaginary, or artifactually large values, and accuracy in terms of agreement with the lower bound on *M* values set

by previous direct measures in which high levels of venous saturation were produced. Estimates of  $M$  based on HO-HC show a trend toward higher values than the individual HC and HO approaches (the latter yielding the lowest values).

#### *2.6.1.1. ROI analysis*

Group average  $M$  values obtained with the HO-HC method in visual cortex ( $7.6 \pm 2.8$ ) were similar to the average value of  $7.5 \pm 1.0$  measured directly in a previous study using simultaneous hypercapnia and hyperoxia with a higher CO<sub>2</sub> content (10% CO<sub>2</sub>/90% O<sub>2</sub>) to reach very high venous O<sub>2</sub> saturation from a larger flow response (Gauthier et al. 2011b). The value of 7.5% BOLD signal increase measured in Gauthier *et al.* can be considered a direct measurement of (or at least a lower bound on)  $M$ , as venous saturation levels exceeding 90% were reached in this experiment. Both the HC and HO calibration techniques, on the other hand, yielded  $M$  estimates of  $5.6 \pm 1.8$  for HC and  $4.5 \pm 1.5$  for HO, well below the directly measured lower bound for  $M$  cited above. The agreement between directly measured BOLD signal changes at very high venous saturations and the  $M$  value extrapolated here from the smaller HO-HC changes provided by the 7%CO<sub>2</sub>/93%O<sub>2</sub> carbogen mixture used here indicates that the values obtained with this technique may be more accurate.

The accuracy of  $M$  has been shown to have an important impact on the validity of task-induced CMRO<sub>2</sub> responses estimated through calibrated MRI (Chiarelli et al. 2007a). The higher BOLD signal values obtained from the combined sources of increased oxygen saturation and the larger (and thus more readily measurable) flow values obtained from the 7% CO<sub>2</sub> content reduce the range of extrapolation required to estimate the maximal BOLD response.

#### *2.6.1.2. Susceptibility-weighted venograms*

The distance of measured BOLD responses from (or their proximity to) the maximal BOLD signal change can be demonstrated qualitatively by SWI venograms acquired during the different breathing manipulations. In one subject we acquired venograms during breathing of the following gases: air, 100% O<sub>2</sub> (HO), 7%CO<sub>2</sub>/93% air (HC), 7% CO<sub>2</sub>/93% O<sub>2</sub> (HO-HC 7%) and 10% CO<sub>2</sub>/90% O<sub>2</sub> (HO-HC 10%) (Figure 5). This last mixture, 10% CO<sub>2</sub>/ 90% O<sub>2</sub> has been shown in

previous studies (Sedlacik et al. 2008; Gauthier et al. 2011b) to yield an almost complete loss of venous contrast in SWI due to a very large increase in venous oxygenation. This supports use of the BOLD change produced by this manipulation as a direct measurement of  $M$  and a ground truth against which to compare other manipulations (including carbogen breathing at lower  $\text{CO}_2$  levels). The SWI venograms in Figure 5 demonstrate different degrees of reduced susceptibility contrast in veins, with the effect of HO-HC at 7%  $\text{CO}_2$  exceeding those of HC or HO alone by a considerable margin. The venogram acquired during HO-HC at 10%  $\text{CO}_2$  demonstrates a complete loss of susceptibility contrast.

#### 2.6.1.3. $M$ mapping

Estimates of  $M$  have, in the past, typically been expressed as average values over regions of interest. Here we show maps of  $M$  values over all voxels in which an absolute baseline CBF above 25 mL/100g/min was measured (chosen to exclude CSF and white matter), allowing an investigation into the spatial distribution of  $M$  values.

Maps of  $M$  obtained from the hypercapnia manipulation included numerous isolated voxels with very high  $M$  values (Figure 3 and 4). While  $M$  values in larger veins are expected to be high, some of these high values obtained with this approach appear to be artifactual. This may be due to amplification of noise inherent in the broad range over which extrapolation is required, as well as an inherent instability of the model for low flow estimates (see Appendix and Figure 6). Maps of  $M$  generated using hyperoxia alone with the hyperoxia model (Figure 3) showed a tendency toward lower  $M$  values and appeared to underestimate the values in larger veins (which were essentially absent in the maps). Note that many of the hyperoxic  $M$  maps included large zones in which the grey-matter  $M$  was negative, which are shown as fully transparent in the image overlays of Figure 5.

#### 2.6.1.4. Spatial heterogeneity of $M$ values

Mark *et al.* have compared the hypercapnia and hyperoxia manipulation techniques. They found the  $M$  values obtained with the hyperoxia technique to show less inter-subject variability than hypercapnia. Given that the hyperoxia technique assumes a fixed flow value in response to hyperoxia and a uniform

venous saturation based on end-tidal PO<sub>2</sub> measurements, the main contribution to noise comes from the BOLD measurement. The hypercapnia method, on the other hand, uses the noisier flow response to hypercapnia in its model.

Though the greater uniformity of hyperoxia-derived  $M$  values could be viewed as an advantage, it may in fact reflect bias in the technique - particularly where large veins are concerned. It is known *a priori* that veins must have a higher  $M$  value than parenchyma, since their dHb content is higher. Such veins do in fact show higher BOLD increases than grey matter during hyperoxia, but application of the hyperoxia model results in  $M$  values considerably below those detected using the other techniques. This may be due to the assumption of a single fixed flow change throughout the brain, or a breakdown of the model in regions with a high venous blood volume fraction.

The  $M$  parameter maps generated from the combined hypercapnia-hyperoxia manipulation with GCM analysis accurately captured the high  $M$  values in large veins while remaining free of the artifactual hot spots due to model instability seen in the hypercapnia maps and the zones of negative  $M$  value observed in the hyperoxia maps.

#### *2.6.1.5. Robustness of $M$ estimates*

As noted above, maps of  $M$  generated using the GCM in conjunction with the HO-HC manipulation appeared to be relatively immune to artifactual hot spots compared with maps generated using the Davis model and the hypercapnia manipulation. Detailed analysis of  $M$  maps together with input maps of CO<sub>2</sub>-induced BOLD and CBF responses indicated that improbably high  $M$  values in the Davis/HC maps tended to occur in voxels where the apparent CBF change was atypically low compared with surrounding voxels. Such low flow values in individual voxels may reflect a combination of noise excursions from the 'true' grey-matter value and bias caused by partial volume with white matter or large veins. The simulation results presented in Figure 6 reveal that estimates of  $M$  exhibit non-linear errors for increasing errors in CBF. The degree of error was found to depend both on the model used and the gas manipulation employed.

Both the Davis model and the GCM can be used to compute  $M$  from data acquired

during hypercapnia. Simulation results indicated that hypercapnic  $M$  estimates using the GCM were somewhat more stable (i.e. non-linearity of the error in  $M$  was reduced) than those obtained using the Davis model (Figure 6A). This is due to the moderating effect of terms in the GCM reflecting arterial  $O_2$  content at rest and during hypercapnia. While the details of this are presented in the appendix, it is interesting to note that incidental increases in arterial  $PO_2$  from  $CO_2$ -induced hyperventilation actually tend to stabilize estimates of  $M$  derived from hypercapnic measures with the GCM.

Data acquired during pure hyperoxia can be analyzed using either the Chiarelli model or the GCM. Although the Chiarelli model is often applied using an assumed value of the  $O_2$ -induced CBF decrease, it was important to assess the impact of any mis-assignment of this parameter (whether through measurement error or incorrect assumption). Our simulations showed that relatively modest errors in the  $O_2$ -induced CBF change could result in extremely large bias in the apparent  $M$  value (culminating in singularities at CBF errors well within the typical standard deviation). This was the case for both the Chiarelli model and the GCM formulation, although the specific range of CBF errors where singularity arose was different for the two models (Figure 6B). As discussed in the Appendix, this instability is due to the lower range of flow values obtained in the hyperoxia manipulation, which fall in regimes for both models where division by zero can readily occur with typical values of other parameters. It should be noted that practical applications of the hyperoxia approach typically use a fixed value for the  $O_2$ -induced decrease in CBF that lies within the stable range for both models.

The simulation results for the GCM in conjunction with the combined hypercapnia/hyperoxia manipulation demonstrate the relative immunity of this approach to typical errors in CBF. The mathematical basis for this stability is discussed in the appendix, but it can also be understood on intuitive grounds by considering that, in the limit, complete saturation of venous blood would completely eliminate the dependence of  $M$  on the CBF and CBV terms. Because the combined effects of simultaneous hypercapnia and hyperoxia drive the venous system considerably closer to this endpoint than other manipulations, and because the GCM is valid for such simultaneous manipulations, it offers improved accuracy and robustness in

the estimation of  $M$  over previous methods.

### **2.6.2. CMRO<sub>2</sub>**

The  $M$  parameters obtained using each breathing manipulation were used as intermediate results in the estimation of fractional CMRO<sub>2</sub> changes evoked during a visual task. While most CMRO<sub>2</sub> estimates fell within the range reported in the literature for similar visual paradigms (Davis et al. 1998; Hoge et al. 1999a; Stefanovic et al. 2006; Leontiev et al. 2007a; Leontiev et al. 2007b; Ances et al. 2008; Lin et al. 2008; Perthen et al. 2008), some physiologically implausible estimates of CMRO<sub>2</sub> were also calculated using the hypercapnia and hyperoxia calibration methods (Figure 7, Table 2). In Figure 7, subjects 3 and 4 have either non-physiological (subject 4) or atypically low (subject 3) CMRO<sub>2</sub> responses associated with the visual task. In these two subjects,  $M$  values estimated with combined hypercapnia and hyperoxia were larger than those estimated using the other two methods. In the case of subject 3, the  $M$  value from HO-HC was about 1% higher than with the other two methods and this led to the estimation of a CMRO<sub>2</sub> value around 17.5%, much closer to the expected range (between 15 and 35%) than the values of 6.7 and 8.7% found by HC and HO respectively. In subject 4, the very high estimate for  $M$  obtained by HO-HC (12.6%) is however the only value for  $M$  that, when coupled with the task-related signal changes in CBF and BOLD, yields a plausible CMRO<sub>2</sub> estimate (21.7% as opposed to 7.9 or -30.8% for HC and HO respectively). Furthermore, this high  $M$  value is within the range of values reported in previous studies (Perthen et al. 2008) and is not inconceivable for an individual endowed with unusually prominent venous anatomy.

### **2.6.3. Limitations of the study**

#### *Breathing manipulations*

High inspired CO<sub>2</sub> concentrations are known to be associated with air hunger and dyspnea (Banzett et al. 1996). In the present study, we used 7% CO<sub>2</sub> for both the HC and HO-HC conditions. While this CO<sub>2</sub> content is somewhat higher than the 5% CO<sub>2</sub>/air mixture often used in the calibrated fMRI literature, it was chosen here to ensure high flow increases and venous saturation levels. The discomfort associated with this CO<sub>2</sub> concentration was, furthermore, found to be mild with an

average discomfort rating of  $2.1 \pm 0.6$  on a 7-point scale (Banzett et al. 1996). In the future, the high flow and BOLD signal responses measured with combined hypercapnia and hyperoxia could be utilized, in frail populations, to reduce CO<sub>2</sub> concentrations while achieving sufficient BOLD and ASL signal levels for adequate sensitivity.

Previous studies have, for similar fixed inspired gas concentrations, detected higher end-tidal values during hyperoxia (Bulte et al. 2007; Chiarelli et al. 2007b) than those reported here. This is probably due to air being entrained into the partially unsealed mask used here, especially during breathing manipulations involving CO<sub>2</sub> and therefore leading to increased minute ventilation. A setup allowing the accommodation of larger breathing volumes and rates (including a mask with a larger bag and flow regulators allowing larger volumes to be given) would allow the mask to be sealed and prevent contamination from room air. This would be desirable as it would provide higher oxygenation increases for the same inspired gas O<sub>2</sub> and CO<sub>2</sub> gas concentrations. However the validity of the methods presented here depends only on the ability to accurately record the evoked changes in end-tidal O<sub>2</sub> and CO<sub>2</sub>, which is ensured by instructing subjects to exhale through their nose and sampling via an indwelling nasal cannula. The requirement for breathing through the nose could be removed in future patient studies using a more closely sealed mask and the use of a one-way valve to prevent mixing of inspired and expired gases.

#### *2.6.3.1. M value confounds*

The dual-echo pCASL technique used here gave reliable flow and BOLD estimates in the grey matter that allowed the GCM to provide consistently plausible *M* values. The relatively higher noise levels in flow and BOLD signal changes measured in white matter voxels however yield clearly invalid estimates of *M* and CMRO<sub>2</sub>. This technique (like the pure hypercapnia and hyperoxia methods) is thus not currently suitable for calculating maximal BOLD signal or CMRO<sub>2</sub> in white matter.

Because of the low spatial resolution, bias in flow and BOLD estimates from partial volume effects is clearly a concern at the interfaces between grey matter and white matter or cerebrospinal fluid. Inspection of the *M* parameter maps indicates that

there is indeed a zone in which  $M$  falls smoothly to zero along the grey-white matter interface. Parameter estimates in regions of homogeneous grey matter are thus likely to be more quantitative. Also, caution is needed when interpreting the  $M$  values that appear to fall in pure white matter as seen in Figure 3, since these in fact arise from a partial volume effect of adjacent slices during the resampling of the functional data to the anatomical resolution.

A potential advantage of the combined hyperoxia and hypercapnia calibration is the reduced dependence on the assumptions of a fixed flow-volume coupling relationship and that  $CMRO_2$  does not change during changes in arterial  $O_2$  or  $CO_2$  levels (Kety et al. 1948; McPherson et al. 1991; Horvath et al. 1994; Hino et al. 2000; Jones et al. 2005; Zappe et al. 2008; Chen et al. 2010b; Xu et al. 2011b). This can be appreciated by considering the limiting case in which concurrent flow and oxygenation increases drive venous  $O_2$  saturation to 100%. Under such conditions, venous blood volume is no longer relevant since venous blood does not contain any deoxygenated hemoglobin. Moreover if venous oxygenation is driven to 100%, this means that all metabolic oxygen consumption has been satisfied by a combination of  $O_2$  carried on hemoglobin and dissolved in blood plasma, regardless of whether  $CMRO_2$  was constant during the calibration. While this is not the case for the submaximal values of venous saturation achieved in the present study, it is clear that the influence on  $M$  of systematic errors in the CBV term (estimated from CBF) and  $CMRO_2$  change (assumed to be zero) must become progressively smaller with increasing venous saturation (ultimately having no effect at 100% saturation as mentioned above). The group average venous saturation during combined hyperoxia and hypercapnia in the present study was computed to be  $87 \pm 4\%$  in visual cortex, leaving relatively little deoxyhemoglobin (approximately 13% desaturation) and thus considerably reducing the impact of venous blood volume. A modest decrease in  $CMRO_2$  caused by the administered  $CO_2$  (Xu et al. 2011b) would imply a slightly higher true saturation value, with minimal effect on the computed  $M$  value.

In the present study, the model parameters alpha and beta were assigned the same values as in prior calibrated MRI literature (e.g. Davis, Chiarelli) (Davis et al. 1998; Chiarelli et al. 2007b). While the purpose here was to highlight the different

model formulations, it should be noted that recent studies have attempted to refine these parameters to values that more specifically reflect venous blood volume and its regional variations ( $\alpha$ ), and more realistically describe the concentration-relaxation behavior applicable in gradient-echo EPI at 3 Tesla ( $\beta$ ) (Chen et al. 2009a; Buxton 2010; Chen et al. 2010c; Mark et al. 2011). As noted above, the higher venous saturation values attained during combined HO-HC reduce the impact of slight mis-specifications of  $\alpha$  and  $\beta$ .

## 2.7. Conclusion

The combined hypercapnia and hyperoxia procedure with the generalized model was found to yield  $M$  values that were robust at the individual voxel level and consistent with the lower bound determined in a previous study in which  $M$  was determined during near-complete arterialization of venous blood.

The combined sources of increased venous saturation, in conjunction with the added stability of the GCM over previous models, allow a more robust estimation of  $M$ , with a reduced range of extrapolation. We believe that this provides more accurate and robust estimates of stimulus-evoked increases in  $CMRO_2$  than previous methods.

## 2.8. Acknowledgements

We thank Carolyn Hurst, André Cyr, Tarik Hafyane and Élodie Boudes for help with data acquisition, Cécile Madjar for help with data acquisition, data analysis and helpful discussions. We would also like to thank Jiongjiong Wang, who provided the pseudo-continuous arterial spin-labeling sequence used. This work was supported by the Canadian Institutes for Health Research (MOP 84378, Banting and Best Scholarship held by CJG), the Canadian Foundation for Innovation (Leaders Opportunity Fund 17380), and the Ministère du développement économique, de l'innovation et de l'exportation (PSR-SIIRI-239).

## 2.9. Appendix

The Davis, Chiarelli, and generalized models all use the same basic expression, originally derived by Davis, to compute the resting BOLD signal  $M$  from CBF and BOLD changes measured during a respiratory manipulation:

$$M = \frac{\frac{\Delta BOLD}{BOLD_0}}{1 - \left(\frac{CBV}{CBV_0}\right) \left(\frac{[dHb]}{[dHb]_0}\right)^\beta} . \quad [9]$$

All approaches also use Grubb's relation to model the change in venous cerebral blood volume:

$$\frac{CBV}{CBV_0} = \left(\frac{CBF}{CBF_0}\right)^\alpha \quad [10]$$

where the exponent  $\alpha$  may be assigned a value of 0.38 as in the original Grubb study, or an alternate value to better reflect the venous portion of blood volume (Chen et al. 2009a; Chen et al. 2010c).

Where the models differ is in how they express the baseline-normalized concentration of deoxygenated hemoglobin (dHb) in Equation 9. To consider how the models differ, we introduce the variable  $D$  to represent this dHb term:

$$D = \frac{[dHb]}{[dHb]_0} \quad [11]$$

In the discussion that follows, we will use the term *desaturation* to describe the fraction of hemoglobin that is deoxygenated (equivalent to one minus the saturation expressed as a decimal fraction). We can now proceed to analyze the different models.

### 2.9.1. Davis model with hypercapnia manipulation

We start by considering the original Davis model, which was intended for use with data acquired during a hypercapnic manipulation without changes in arterial oxygen tension. In the Davis model, it is assumed that there is no deoxygenated hemoglobin in arterial blood (*i.e.* arterial O<sub>2</sub> saturation is 100%), and that metabolic oxygen extraction does not change during hypercapnia. In this case the relative level of dHb can be expressed simply as

$$D_{Davis} = \frac{CBF_0}{CBF} \cdot \quad [12]$$

That is, doubling CBF will reduce the venous concentration of dHb by a factor of two. There has been considerable discussion of whether oxygen extraction can really be assumed to be constant during hypercapnia (McPherson et al. 1991; Horvath et al. 1994; Hino et al. 2000; Jones et al. 2005; Zappe et al. 2008; Chen et al. 2010b). Moreover, typical arterial O<sub>2</sub> saturation values in young volunteers are actually slightly less than 100%, and this value could be considerably lower in individuals with impaired cardiopulmonary function (e.g. the elderly, respiratory patients). Finally it is possible that arterial O<sub>2</sub> tension will increase during a hypercapnic manipulation, due to CO<sub>2</sub>-induced hyperventilation.

### 2.9.2. Chiarelli model with hyperoxia manipulation

The Chiarelli model was conceived for use during a hyperoxic manipulation, during which metabolic oxygen extraction is also assumed constant. In this formulation of the model, the relative concentration of deoxygenated hemoglobin is expressed as the sum of two additive terms:

$$D_{Chiarelli} = \left( \frac{1 - \frac{1}{\varphi[Hb]} \left( Ca_{O_2} - \left( Ca_{O_2}|_0 \cdot OEF_0 \right) \right)}{1 - \frac{1}{\varphi[Hb]} \cdot Ca_{O_2}|_0 \cdot (1 - OEF_0)} \right) + \left( \frac{CBF_0}{CBF_c} - 1 \right), \quad [13]$$

where  $\phi$  is the  $O_2$  capacity of hemoglobin in ml  $O_2$ /g Hb,  $[Hb]$  represents the concentration of hemoglobin in the blood in g Hb/dl blood,  $OEF_0$  is the oxygen extraction fraction at rest, and  $Ca_{O_2}$  is the total arterial oxygen content in ml  $O_2$ /dl blood (determined from measurements of end-tidal  $O_2$ ). The above expression groups  $D$  into two key terms depending, respectively, on end-tidal gas measures ( $B$ ) and cerebral blood flow ( $C$ ). The term  $B$  represents the increase in saturation attributable directly to the rise in arterial  $O_2$  content from breathing the hyperoxic gas mixture, while  $C$  reflects variable dilution of venous dHb associated with reduced CBF during hyperoxia.

### 2.9.3. Generalized calibration model (GCM) with hyperoxia and hypercapnia

While the expression for  $D_{Chiarelli}$  above is reasonably accurate for the small changes in CBF expected during normocapnic hyperoxia, the GCM incorporates arbitrary CBF changes in a modified version of the  $B$  term, resulting in a more general and accurate expression for relative deoxyhemoglobin concentration and obviating the need for term  $C$ . With some reorganization, the modified expression that distinguishes the GCM can be expressed as

$$D_{GCM} = \left( \frac{\frac{Ca_{O_2}|_0 \cdot OEF_0}{\phi[Hb]}}{1 - \frac{Ca_{O_2}|_0}{\phi[Hb]}(1 - OEF_0)} \right) \left( \frac{CBF_0}{CBF} \right) + \left( \frac{1 - \frac{Ca_{O_2}}{\phi[Hb]}}{1 - \frac{Ca_{O_2}|_0}{\phi[Hb]}(1 - OEF_0)} \right). \quad [14]$$

In the above expression, the term  $X$  is equivalent to the hemoglobin desaturation due specifically to resting metabolism, expressed as a fraction of the total resting hemoglobin desaturation in the venous compartment. It thus serves to modulate the CBF term of the Davis model, accounting for the fact that the arterial  $O_2$  saturation may not be 100% (if resting arterial saturation is 100% then all venous dHb comes from metabolism and the term  $X$  reduces to unity).

The term  $Y$ , which is equivalent to the hyperoxic arterial desaturation as a fraction of total resting venous desaturation, reflects additional oxygen available from hyperoxic arterial blood for augmenting venous saturation. During hyperoxia, it is

possible for the effective arterial desaturation (the numerator in  $Y$ ) to be negative, which reflects the fact that even at 100% arterial Hb saturation, additional  $O_2$  dissolved in arterial plasma will eventually bind to venous dHb (thus reducing the venous desaturation). If the total arterial  $O_2$  content during the respiratory manipulation corresponds exactly to 100% saturation, then the term  $Y$  reduces to zero.

Since the  $X$  and  $Y$  terms respectively reduce to unity and zero for a constant arterial  $O_2$  content corresponding exactly to 100% arterial saturation, the GCM is equivalent to the Davis model under the specific assumptions of that model. The GCM is also equivalent to the Chiarelli model in the specific case where there is no change in CBF during hyperoxia.

#### **2.9.4. Stability of the models during hypercapnic manipulations**

The largest source of error in estimates of  $M$  obtained from hypercapnia data is the high noise level of the CBF measurements. Because all of the models examined here include a CBF term in the denominator of the expression for  $M$ , moderate in CBF result in very high errors on  $M$  due to the non-linearity inherent in the reciprocal function. However the degree of non-linearity and resultant stability under noisy CBF data vary between the different models.

Both the Davis model and GCM can be used to estimate the resting BOLD signal based on measurements during hypercapnia (end-tidal  $O_2$  measurements are additionally required for the GCM). In the case where end-tidal  $O_2$  measurements indicate an unchanging arterial saturation of exactly 100%, both models will yield identical results. As illustrated in Figure 6A, the Davis model results in a significant overestimation of  $M$  when CBF is sufficiently underestimated. When the GCM is used to analyze the same data, as shown in Figure 6A, the non-linearity of  $M$  with CBF underestimation is considerably less pronounced. This is due to a slight attenuation of the CBF factor in  $D_{GCM}$  from the  $X$  term (since resting arterial saturation is slightly less than 100%) and to the damping effect of the additive  $Y$  term (which is slightly negative since arterial  $O_2$  content actually increases slightly due to hyperventilation during  $CO_2$  breathing).

This finding has the interesting consequence that small, incidental increases in arterial  $\text{Pa}_{\text{O}_2}$  during hypercapnia may actually be advantageous (helping to stabilize the model) if they are recorded and input to the GCM. As discussed below, the same effect accounts for the dramatic improvement in estimation stability when the GCM is used in conjunction with simultaneous hypercapnia and hyperoxia.

Note that, while it is theoretically possible to apply the Chiarelli model to measurements of hypercapnically-induced changes in CBF, BOLD, and end-tidal  $\text{O}_2$ , the resultant estimates of  $M$  are physiologically implausible (negative for the input data used here).

### **2.9.5. Stability of the models during hyperoxia manipulations**

Either the Chiarelli model or GCM can be used to compute  $M$  from data acquired during a hyperoxic manipulation. Figure 6B indicates that  $M$  estimates produced in this way are also vulnerable to significant bias from measurement errors on CBF, regardless of the model used. In this case, the problem arises due to an interaction between the lower range of flow values encountered with the hyperoxia manipulation and the form of the denominator for  $M$  in Equation 9. Moderate excursions in CBF can result in a combination of terms for baseline-normalized CBV and [dHb] which lead to division by zero. With the Chiarelli formulation, this only occurs for values of baseline-normalized CBF exceeding one. Because such values may readily arise in noisy ASL measures of small CBF changes, a physiologically plausible fixed value is typically assumed.

#### *Stability of GCM during combined hyperoxia and hypercapnia manipulations*

As noted above in the comparison with the Davis model, small increases in arterial  $\text{O}_2$  content tend to moderate the sensitivity of  $M$  to errors in CBF when the GCM is used to process data from hypercapnia manipulations. While this is a somewhat subtle effect when hypercapnia is induced under near-normoxic conditions, the stabilizing influence of increased arterial  $\text{Pa}_{\text{O}_2}$  becomes considerable in a combined hyperoxia/hypercapnia manipulation due to the influence of the additive  $Y$  term (negative) in Equation 14. The hypercapnia component of such manipulations tends to reduce the term  $(\text{CBF}_0/\text{CBF})$ , further increasing the relative

importance of the term based on relatively stable end-tidal measurements. These effects lead to considerably lower values of  $D$  than can be achieved with hypercapnia or hyperoxia alone. Because the term  $(CBV/CBV_0)$  in Equation 9 is multiplied by  $D$ , low values of  $D$  also serve to reduce the impact of uncertainty on the exact exponent  $\alpha$  used in Equation 10.

### **3. Magnetic resonance imaging of resting OEF and CMRO<sub>2</sub> using a generalized calibration model for hypercapnia and hyperoxia**

Gauthier, C.J.<sup>1,2</sup>, Hoge, R.D.<sup>1,2</sup>

<sup>1</sup> Physiology/Biomedical Engineering, Université de Montréal, Montreal, Quebec, Canada, <sup>2</sup> Centre de recherche de l'institut de gériatrie de Montréal, Montreal, Quebec, Canada

NeuroImage, 60 (2012) 1212–1225

#### **3.1. Preface**

Calibrated fMRI techniques allow the quantification of task-evoked fractional CMRO<sub>2</sub> change. While this is an important physiologically-specific quantity that can be directly compared between groups with different vascular properties, it nevertheless suffers from several limitations. Because calibrated fMRI yields a relative change from an unknown baseline, groups with different baselines could show similar relative changes but in reality consume different quantities of O<sub>2</sub> in absolute units. Aging and some diseases such as dementia may be associated with changes in baseline oxidative metabolic activity (Yamaguchi et al. 1986; Leenders et al. 1990; Nagata et al. 2000; Yamauchi et al. 2002; Lu et al. 2011) and an MRI measure of this quantity would allow future studies to combine this metric with other informative MRI techniques such as measures of blood flow, atrophy or white-matter lesions to gain a better understanding of normal and pathological physiology.

Also, techniques requiring a task may be more limited in many clinical contexts. Task paradigms are difficult to control and differences in performance or hemodynamic signals may reflect confounding effects such as anxiety from the imaging setting, strategy choice, differences in motivation, arousal and physical discomfort (Bonfond et al. 2011; Satterthwaite et al. 2012; Worthy et al. 2012).

Furthermore, some patient groups may experience difficulty in complying with the complex instructions of many task paradigms.

For all these reasons, an MRI technique that allows measurement of resting-state  $CMRO_2$  would be useful both for basic and clinical research. Several groups have recently proposed MRI-based methods to quantify resting  $CMRO_2$  (He et al. 2007; He et al. 2008; Lu et al. 2008; Xu et al. 2009; Jain et al. 2010; Bolar et al. 2011b; Bulte et al. 2011; Fan et al. 2011). While several of these techniques quantify resting  $CMRO_2$  in a single vessel (He et al. 2007; He et al. 2008; Lu et al. 2008; Xu et al. 2009; Jain et al. 2010; Fan et al. 2011), some recent methods can be used for mapping of this parameter (Bolar et al. 2011b; Bulte et al. 2011). Here we propose an alternative technique based on our generalized calibration model presented in Chapter 2. Because this model can be used for any arbitrary change of blood oxygen content and flow, different combinations of hypercapnia and hyperoxia can be used to derive an experimentally determined value for  $M$  and resting oxygen extraction fraction (OEF). Resting OEF can then be used with measured blood flow and arterial oxygen content to obtain a value for baseline  $CMRO_2$ . Since its publication, we have dubbed the method "QUO2". The use of the QUO2 technique to obtain accurate estimates of these parameter in complete grey matter is demonstrated here.

### **3.2. Abstract**

We present a method allowing determination of resting cerebral oxygen metabolism ( $CMRO_2$ ) from MRI and end-tidal  $O_2$  measurements acquired during a pair of respiratory manipulations producing different combinations of hypercapnia and hyperoxia. The approach is based on a recently introduced generalization of calibrated MRI signal models that is valid for arbitrary combinations of blood flow and oxygenation change. Application of this model to MRI and respiratory data during a predominantly hyperoxic gas manipulation yields a specific functional relationship between the resting BOLD signal  $M$  and the resting oxygen extraction fraction  $OEF_0$ . Repeating the procedure using a second, primarily hypercapnic, manipulation provides a different functional form of  $M$  vs.  $OEF_0$ . These two equations can be readily solved for the two unknowns  $M$  and  $OEF_0$ . The procedure

also yields the resting arterial O<sub>2</sub> content, which when multiplied by resting cerebral blood flow provides the total oxygen delivery in absolute physical units. The resultant map of oxygen delivery can be multiplied by the map of OEF<sub>0</sub> to obtain a map of the resting cerebral metabolic rate of oxygen consumption (CMRO<sub>2</sub>) in absolute physical units.

Application of this procedure in a group of seven human subjects provided average values of  $0.35 \pm 0.04$  and  $6.0 \pm 0.7\%$  for OEF<sub>0</sub> and *M*, respectively in grey-matter (*M* valid for 30 ms echo-time at 3 Tesla). Multiplying OEF<sub>0</sub> estimates by the individual values of resting grey-matter CBF (mean  $52 \pm 5$  ml/100g/min) and the measured arterial O<sub>2</sub> content gave a group average resting CMRO<sub>2</sub> value of  $145 \pm 30$  μmol/100g/min. The method also allowed the generation of maps depicting resting OEF, BOLD signal, and CMRO<sub>2</sub>.

### **3.2.1. Keywords**

Calibrated MRI, BOLD, OEF, CMRO<sub>2</sub>, hypercapnia, hyperoxia, carbogen, oxygen, metabolism

## **3.3. Introduction**

Oxygen is a key molecule for metabolic energy production in higher organisms, and the brain accounts for a significant fraction of the human body's total resting oxygen consumption. Conversely, interruption of the brain's oxygen supply - for example through occlusion of the carotid arteries - leads to unconsciousness within seconds and irreversible tissue damage within minutes (Levy et al. 1975). Much of this voracious appetite for oxygen is thought to support ATP-dependent ion pumping proteins which are essential for the maintenance of neuronal membrane potentials during ongoing synaptic activity (Erecinska et al. 1990). It is thus easy to understand how deficits in oxygen delivery might lead to impaired neuronal function. Conversely, reductions in synaptic activity from neuronal degeneration lead to a decrease in overall cerebral metabolism. This overall reduction in metabolism can be manifested as a reduction in the consumption of both oxygen and glucose, the substrates used in aerobic metabolism. Thanks to the latter postulate, imaging of brain glucose uptake with positron emission tomography

(PET) in the diagnosis of dementia has become one of the largest clinical applications of any functional neuroimaging method (detection of metabolically active metastatic brain lesions being another). PET measures of glucose metabolism and resting oxygen extraction fraction (OEF) have been used to diagnose and evaluate the prognosis of diseases such as Alzheimer's disease (Nagata et al. 2002; Herholz et al. 2007; Lo et al. 2011; Rodriguez et al. 2011), Parkinson's disease (Hirano et al. 2009; Poston et al. 2010) and stroke (Yamauchi et al. 1999; Yamauchi et al. 2009; Zipfel et al. 2009; Isozaki et al. 2010).

PET imaging of  $^{18}\text{F}$ FDG (fluorodeoxyglucose) uptake offers good sensitivity and spatial resolution and, due to the relatively long half-life of  $^{18}\text{F}$ , can be performed in clinics without an on-site cyclotron. Its disadvantages include ionizing radiation exposure from the positron emitting  $^{18}\text{F}$  tracer, additional radiation when an integrated x-ray CT scanner is employed to provide anatomic information, and the need to have access to a regional source of  $^{18}\text{F}$  close enough to allow delivery given the 110 minute half-life (Miller et al. 2008). The radiation dose considerations preclude serial imaging studies that could be of interest in clinical trials of drug efficacy, and the necessity of a regional source poses a problem for clinics situated in smaller municipalities.

Although used less frequently in clinical applications, the cerebral metabolic rate of oxygen consumption ( $\text{CMRO}_2$ , which may reflect total ATP yield more directly than glucose uptake) can be obtained using  $^{15}\text{O}$  labeled PET tracers. As opposed to the straightforward single measurement required for FDG-PET, PET measures of  $\text{CMRO}_2$  require three separate acquisitions with injection of  $^{15}\text{O}$  labeled  $\text{O}_2$ ,  $\text{H}_2\text{O}$  and  $\text{CO}$ . These three measurements are necessary to take into account the combined contribution of  $\text{O}_2$  diffusion into tissue, its conversion to water during oxidative metabolism, as well as the dependence on blood volume, assessed with  $\text{C}^{15}\text{O}$  (Mintun et al. 1984; Buxton 2010). However, the use of three separate injections of positron emitting tracers greatly increases the radiation dose associated with this measurement. Furthermore, the short half-life (about two minutes) of  $^{15}\text{O}$  means that this technique is not possible without an on-site cyclotron (Miller et al. 2008).

Because of the above concerns, an MRI-based alternative to PET-FDG and CMRO<sub>2</sub>-PET for imaging resting brain metabolism would be extremely attractive. While CMRO<sub>2</sub> can be measured in MRI using <sup>17</sup>O<sub>2</sub> labeling methods (Fiat et al. 1992; Fiat et al. 1993; Fiat et al. 2004), these techniques are impractical due to the limited availability and high cost of <sup>17</sup>O. In recent years, efforts to develop proton MRI alternatives to PET have yielded some promising avenues to measure OEF and oxidative metabolism (CMRO<sub>2</sub>). While some of the techniques proposed yield whole-brain or single vessel estimates (An et al. 2000; Xu et al. 2009; Jain et al. 2010; Fan et al. 2011), more recent efforts have focussed on mapping of these parameters (He et al. 2007; He et al. 2008; Bolar et al. 2011a). In the present article we propose a new and straightforward method for generating images of resting CMRO<sub>2</sub> on a clinical MRI scanner. The technique proposed here is an extension of calibrated fMRI methods described previously (Davis et al. 1998; Hoge et al. 1999a; Chiarelli et al. 2007b; Gauthier et al. 2011b). Calibrated fMRI is an established technique to determine changes in CMRO<sub>2</sub> associated with a task based partly on measurements acquired during a respiratory manipulation. We have previously described a generalization of calibrated MRI methods based individually on hypercapnia (Davis et al. 1998) and hyperoxia (Chiarelli et al. 2007b). This generalized calibration model (GCM), which is valid for arbitrary combinations of hypercapnia and hyperoxia, was used to estimate evoked changes in CMRO<sub>2</sub> during neuronal stimulation (Gauthier et al. 2011a). In the present article we demonstrate that, in addition to the calibration parameter *M* required to estimate task-induced changes in CMRO<sub>2</sub>, the GCM can also be used to estimate resting OEF and ultimately resting CMRO<sub>2</sub> in absolute micromolar units. The resultant calibration approach also yields resting cerebral blood flow (CBF) and cerebrovascular reactivity (CVR). These attributes offer the possibility of a comprehensive neurofunctional workup providing rich detail about vascular function, oxygen delivery, and tissue integrity in the brain.

### **3.3.1. Theory**

A key component of all calibrated MRI approaches has been estimation of the parameter *M*, which has been commonly described as the maximal BOLD signal increase that would be observed upon elimination of all deoxygenated hemoglobin

(dHb) in tissues. We prefer the term resting BOLD signal, which reflects the fact that  $M$  isolates the purely dHb-dependent component of the total MRI signal at rest in the same way that arterial spin-labeling (ASL) difference signals isolate the purely flow-dependent component of MRI signals at rest. Similarly to ASL difference signals, a task-induced change in BOLD signal can be normalized to the resting BOLD signal to obtain a physiologically meaningful quantity: the fractional change in tissue dHb concentration (although unlike ASL and CBF the relationship between BOLD and dHb ratios is a power law rather than linear). This information, together with fractional flow changes from ASL, can then be used to determine the task-induced fractional change in CMRO<sub>2</sub>. The latter output is a relative quantity, which does not include information about the actual absolute baseline.

Here we present a further extension of our generalized method which allows estimation of both the resting BOLD signal  $M$  and the resting oxygen extraction fraction (OEF<sub>0</sub>). We then describe how the MRI and respiratory measures acquired during this procedure can be combined to estimate resting oxygen consumption.

### 3.3.1.1. Determination of resting BOLD signal $M$ and OEF

Our initial description of the CGM in Gauthier et al. (Gauthier et al. 2011a; Gauthier et al. 2011b) describes its application for providing robust estimates of the MRI calibration parameter  $M$  during hypersaturation of venous blood produced by carbogen inhalation. The extension presented here allows simultaneous determination of  $M$  and resting OEF using two gas manipulations: one hyperoxic and the other hypercapnic. The procedure is based on the original calibrated BOLD formulation proposed by Davis (Davis et al. 1998), in which  $M$  is modeled as

$$M = \frac{\frac{\Delta BOLD}{BOLD_0}}{1 - \left(\frac{CBV}{CBV_0}\right) \left(\frac{[dHb]}{[dHb]_0}\right)^\beta}, \quad \left(\frac{CBV}{CBV_0}\right) \approx \left(\frac{CBF}{CBF_0}\right)^\alpha \quad [1]$$

where the numerator is the fractional change in BOLD signal produced by a gas manipulation, and the denominator includes terms representing cerebral blood volume (CBV) and blood concentration of deoxygenated hemoglobin [dHb] during

the manipulation normalized to their respective baseline values. The exponent  $\alpha$  (most recently estimated to be  $\sim 0.18$  (Chen et al. 2010c)) models the non-linear coupling between flow and venous volume changes, while  $\beta$  ( $\sim 1.5$  (Boxerman et al. 1995)) represents the non-linear dependence of changes in  $R_2^*$  on deoxyhemoglobin concentration.

The Davis formulation modeled the deoxyhemoglobin term in Equation 1 as the reciprocal of the increased relative CBF during hypercapnia (from the Fick principle of mass conservation), while the subsequent adaptation by Chiarelli estimated the same term by modeling increases in blood oxygen content during hyperoxia (assuming minimal flow changes). The GCM is an extension of Davis and Chiarelli's methods that is valid for arbitrary combinations of changes in arterial oxygen content and flow, allowing the baseline-normalized deoxyhemoglobin term to be expressed as

$$\frac{[dHb]}{[dHb]_0} = \left( \frac{\frac{Ca_{O_2}|_0 \cdot OEF_0}{\phi[Hb]}}{1 - \frac{Ca_{O_2}|_0}{\phi[Hb]}(1 - OEF_0)} \right) \left( \frac{CBF_0}{CBF} \right) + \left( \frac{1 - \frac{Ca_{O_2}}{\phi[Hb]}}{1 - \frac{Ca_{O_2}|_0}{\phi[Hb]}(1 - OEF_0)} \right) \quad [2]$$

where  $CBF_0/CBF$  is the reciprocal of the baseline-normalized cerebral blood flow during the gas manipulation (taken directly in the original Davis model to represent  $[dHb]/[dHb]_0$ ),  $\phi$  is the  $O_2$  capacity of hemoglobin in ml  $O_2/g$  Hb,  $[Hb]$  represents the concentration of total hemoglobin (oxygenated or deoxygenated) in the blood in g Hb/ml blood (which can be determined by blood test),  $OEF_0$  is the oxygen extraction fraction at rest,  $Ca_{O_2}$  is the total arterial oxygen content in ml  $O_2/ml$  blood during the manipulation, and  $Ca_{O_2}|_0$  is the resting value of the latter. The baseline and gas-manipulated values for  $Ca_{O_2}$  are determined from measurements of end-tidal  $O_2$  using the Severinghaus equation (Severinghaus 1989) and plasma solubility of  $O_2$  as described by Chiarelli et al. (Chiarelli et al. 2007b). While the oxygen saturation curve described by the Severinghaus equation can be significantly altered during hypercapnia, all measurements

involved in this calibration procedure take place at very high saturations where shifts in the curve with CO<sub>2</sub> concentration are negligible.

The factor (henceforth referred to as  $X$ ) applied to  $(CBF/CBF_0)$  in Equation 2 represents the fraction of resting venous deoxyhemoglobin that is generated through local metabolism (as opposed to delivered in arterial blood; typically close to 100% of  $[dHb]$  in healthy individuals, but less if arterial O<sub>2</sub> saturation is abnormally low), while the second additive term (which we will call  $Y$ ) represents reductions in total (arterial plus venous) deoxyhemoglobin due to increased arterial O<sub>2</sub> content during the gas manipulation. The expression reduces to the Davis model when arterial O<sub>2</sub> saturation remains constant at exactly 100% ( $CaO_2/(\phi[Hb])=CaO_{2|0}/(\phi[Hb])=1$ , so  $X=1$ ,  $Y=0$ ), and to the Chiarelli model when the gas-induced CBF change approaches zero (Gauthier et al. 2011a). The GCM thus encompasses previous models under the specific assumptions of those models.

In the original Chiarelli method for hyperoxia-calibrated fMRI, a specific fixed value of  $OEF_0$  was assumed in their counterpart to Equation 2. Substitution of CBF, BOLD, and end-tidal quantities measured during a single gas manipulation would then yield a unique value of  $M$ . If  $OEF_0$  is not fixed, one nonetheless obtains a specific functional relationship between  $M$  and  $OEF_0$ :

$$M = f(OEF_0) \quad [3]$$

where the shape of the function  $f$  is determined by the measured MRI and end-tidal quantities. In the method proposed here, two gas manipulations (hyperoxia and hypercapnia) are performed and the two resultant equations for  $M = f(OEF_0)$  are solved to give a unique combination of  $M$  and  $OEF_0$  corresponding to the intersection of the two functions. The solution to such a system of two equations for two unknowns can be readily solved to arbitrary precision using numerical methods.

### 3.3.1.2. Determination of resting $CMRO_2$

Once the resting value of OEF is determined via the above procedure, resting  $CMRO_2$  in ml O<sub>2</sub>/100g/min can then be computed as

$$CMRO_2|_0 = Ca_{O_2}|_0 \cdot CBF_0 \cdot OEF_0 \quad [4]$$

where  $CBF_0$  is the resting cerebral blood flow expressed in ml/100g/min. It can be seen that the product of the first two terms is equivalent to the rate of  $O_2$  delivery, which is converted to the rate of  $O_2$  consumption after multiplication by the third extraction fraction term. Conversion from milliliters to micromolar units can be carried out using the following conversion factor:

$$\frac{\left[ \frac{1000000 \mu mol}{mol} \right] \cdot \left[ \frac{273.15 K}{310.0 K} \right]}{\left[ \frac{22.4 L}{mol} \cdot \frac{1000 ml}{L} \right]} = 39.34 \left[ \frac{\mu mol}{ml} \right] \quad [5]$$

based on the ideal gas law adjusted for physiological temperature.

### 3.4. Methods

Acquisitions were conducted in eight healthy subjects (seven male and one female, aged 21 to 38 years) on a Siemens TIM Trio 3T MRI system (Siemens Medical Solutions, Erlangen, Germany) using the vendor-supplied 32-channel receive-only head coil for all acquisitions. All subjects gave informed consent and the project was approved by the Comité mixte d'éthique de la recherche du Regroupement Neuroimagerie/Québec.

#### 3.4.1. Image acquisition

Sessions included an anatomical, 1mm<sup>3</sup> MPRAGE acquisition with TR/TE/alpha = 2300ms/3ms/9°, 256x240 matrix and a GRAPPA acceleration factor of 2 (Griswold et al. 2002).

Functional image series were acquired using a dual-echo pseudo-continuous arterial spin labeling (pCASL) acquisition (Wu et al. 2007) to measure changes in cerebral blood flow (CBF). The parameters used include: TR/TE1/TE2/alpha = 3000ms/10ms/30ms/90° with 4x4mm in-plane resolution and 11 slices of 7mm (1mm slice gap) on a 64x64 matrix (at 7/8 partial Fourier), GRAPPA acceleration factor = 2, post-labeling delay = 900ms, label offset = 100mm, Hanning window-

shaped RF pulse with duration/space = 500 $\mu$ s/360 $\mu$ s, flip angle of labeling pulse = 25°, slice-selective gradient = 6mT/m, tagging duration = 1.5s (Wu et al. 2007).

### 3.4.2. Gas manipulations

Each session included three functional runs each including a different gas manipulation. During each gas manipulation run, a single three-minute block of gas inhalation was preceded with one minute and followed by two minutes of medical air breathing. The three gas manipulations used were: 100% O<sub>2</sub> (hyperoxia), 7% CO<sub>2</sub>/21%O<sub>2</sub>/72%N<sub>2</sub> (hypercapnia) and 7% CO<sub>2</sub>/93% O<sub>2</sub> (simultaneous hyperoxia/hypercapnia). The latter gas is a specific formulation of carbogen, which in general may contain different O<sub>2</sub>/CO<sub>2</sub> ratios.

At the beginning of the experiment, subjects were fitted with a non-rebreathing face mask (Hudson RCI, #1059, Temecula, California, USA). To avoid discomfort from outward gas leakage blowing into the subject's eyes, skin tape (Tegaderm Film, #1626W, 3M Health Care, St-Paul, MN, USA) was used to seal the top of the mask to the face. Plastic tubing (Airlife™ Oxygen tubing #001305, Cardinal Health, McGraw Park, IL, USA) and a series of two Y-connectors were used to connect pressure/flow-meters for medical air, 100% O<sub>2</sub> (hyperoxia), 7% CO<sub>2</sub>/93% air (hypercapnia) and 7% CO<sub>2</sub>/93% O<sub>2</sub> (simultaneous hyperoxia/hypercapnia) tanks (Vitalaire, Mississauga, ON, Canada) to the mask. Gas flows were adjusted manually on the pressure/flow-meters (MEGS, Ville St-Laurent, QC, Canada) to keep a total flow rate of 16L/min. Gas flow was kept at 16L/min at all times except during administration of the hyperoxia/hypercapnia and the hypercapnia gas mixtures. To accommodate the elevated minute ventilation caused by CO<sub>2</sub> breathing, gas flow rates were increased to the maximal possible rate (25L/min) achievable with our pressure/flowmeters. Pulse rate and arterial O<sub>2</sub> saturation were monitored in all subjects using a pulse-oximeter (InVivo Instruments, Orlando, USA) as a safety measure and to observe the effects of carbogen breathing.

End-tidal O<sub>2</sub> and CO<sub>2</sub> values were monitored during all acquisitions. Gases were sampled via an indwelling (15 mm) nasal cannula (Airlife™ Nasal Oxygen Cannula #001321, Cardinal Health, McGraw Park, IL, USA) using the CO2100C and O2100C modules of the MP150 BIOPAC physiological monitoring unit

(BIOPAC Systems Inc., Goleta, CA, USA). Calibration of the unit was done by taking into account an expired partial pressure of water of 47mmHg (Severinghaus 1989). Subjects were instructed to breathe through their nose, which ensured that only expired gas was sampled by the nasal cannula. End-tidal CO<sub>2</sub> and O<sub>2</sub> values were selected manually from continuous respiratory traces sampled at 200 Hz. The first 10 breaths of the first baseline period and the last 10 breaths of the gas-inhalation block were averaged to give baseline values and gas manipulation values respectively.

Following acquisition, all subjects were debriefed to assess the level of discomfort associated with the manipulation. The subjects were asked to rate the air hunger and breathing discomfort associated with the hypercapnia and carbogen mixtures on a French language version of the scale proposed in (Banzett et al. 1996).

### **3.4.3. Data analysis**

The raw EPI series acquired during the three gas manipulation runs were preprocessed by motion correction (Cox et al. 1999) and spatial smoothing with a 3D Gaussian kernel (10 mm FWHM). The CBF signal was isolated from the series of first echoes using linear surround subtraction (Liu et al. 2005), while the BOLD signal was extracted using linear surround addition of the second echo series (multiplicative error on BOLD signal due to ASL contamination is less than 1% of the BOLD response with this approach and all time points are utilized).

Fractional changes in BOLD and CBF signals were then determined for each gas manipulation by fitting a GLM to the respective signals and dividing the estimated effect size by the estimated constant term. Model fits used a single-gamma hemodynamic response function (HRF) with parameters described by Glover et al. (Glover 1999) and included a first order polynomial to represent baseline signal and linear drift (higher order polynomial fits were deemed unsuitable due to the single long block during the gas runs). Because the canonical HRF cited above actually bears little resemblance to the impulse response describing transitions between respiratory states, the first 60 seconds after each transition in gas composition were excluded from the analyses by zeroing out relevant rows in the GLM computational matrices, to select responses at steady-state. While the

transition data might add statistical power if properly modeled, mis-specification of the shape would have the opposite effect and satisfactory results were obtained with the simple approach described here.

Image datasets were masked prior to smoothing, based on the intensity of the baseline EPI scans, to ensure that only intra-cerebral voxels were analyzed. Additional masking was performed to remove large veins that could be readily identified as very large (>10%) BOLD increases in unsmoothed EPI data during CO<sub>2</sub> inhalation. Large arteries exhibited implausibly large decreases in pre-T1-correction absolute CBF (>50 ml/100g/min decrease, likely due to T1 shortening) during O<sub>2</sub> inhalation, allowing them to be similarly masked out. All masks were generated based on unsmoothed data, and were applied before smoothing in subsequent analyses to avoid "bleeding" of large vessel responses into parenchymal voxels. Basing masks on the unsmoothed data had the added advantage that the contrast of vascular responses against background was greatly enhanced at the higher spatial resolution (less partial volume averaging), considerably improving specificity. In practice this measure reduced the incidence of macrovascular "hot spots" without substantially affecting the distribution of grey matter values.

Because the flow changes produced by hyperoxia were considerably smaller than the noise level in our ASL acquisitions, a constant fixed value of -3.11% was assumed for this CBF change (only for hyperoxia). This value was the average flow change determined by first averaging the O<sub>2</sub>-induced change in ASL signal (after correction for T1 changes as described below) over all cortical and sub-cortical grey matter in each subject, and then pooling average values from the seven subjects. The use of a fixed value for the O<sub>2</sub>-induced flow response is also advocated in the Chiarelli method, as these changes are generally agreed to be too small for reliable measurement at the single voxel level with current ASL methods and within the range of measurement error they do not contribute significantly in the model.

As noted above, it was necessary to correct maps of the fractional CBF change during hyperoxic manipulations to account for changes in the T1 of blood known to

occur during changes in the plasma concentration of O<sub>2</sub> (which is paramagnetic). This was carried out using the approach described in (Chalela et al. 2000; Zaharchuk et al. 2008). We estimated arterial blood T1 values based on the end-tidal O<sub>2</sub> (ETO<sub>2</sub>) measurements obtained in each subject, along with T1 vs. ETO<sub>2</sub> values tabulated in Bulte *et al.* (Bulte et al. 2007). Since the exact T1 depends on the level of dissolved O<sub>2</sub> in plasma, and because we obtained slightly different ETO<sub>2</sub> values at a given fraction of inspired O<sub>2</sub> than the latter study, the values were interpolated to account for this difference.

Following determination of average end-tidal O<sub>2</sub> values as described above, the latter were converted to arterial O<sub>2</sub> content in ml O<sub>2</sub>/ml blood as described in Chiarelli et al (Chiarelli et al. 2007b). In this approach, end-tidal O<sub>2</sub> respiratory measures are taken to represent the arterial partial pressure of O<sub>2</sub> (PaO<sub>2</sub>). These are translated to arterial hemoglobin saturation (SaO<sub>2</sub>) using the Severinghaus equation (Severinghaus 1979):

$$SaO_2 = \frac{1}{\left( \frac{23400}{(PaO_2)^3 + 150 \cdot PaO_2} + 1 \right)}. \quad [6]$$

The total arterial O<sub>2</sub> content CaO<sub>2</sub> is then determined as the sum of O<sub>2</sub> bound to hemoglobin and O<sub>2</sub> dissolved in plasma:

$$CaO_2 = (\phi \cdot [Hb] \cdot SaO_2) + (PaO_2 \cdot \varepsilon). \quad [7]$$

The following parameters were assumed for all subjects in the latter conversion:  $\phi = 1.34$  mlO<sub>2</sub>/gHb, [Hb] = 15 gHb/dl blood, and  $\varepsilon = 0.0031$  mlO<sub>2</sub>/dl blood/mmHg (the solubility of O<sub>2</sub> in plasma) (Chiarelli et al. 2007b; Rhoades et al. 2009). In two of the subjects, [Hb] was also determined through a blood draw as part of their participation in another study. It can be seen that the first additive term represents O<sub>2</sub> bound to hemoglobin, while the second term represents O<sub>2</sub> dissolved in plasma. Prior to modeling of the data, region-of-interest (ROI) masks selecting cortical and sub-cortical grey matter were generated based on the high-resolution T1 scan using the automated segmentation capabilities of the CIVET software package

(Tohka et al. 2004). These ROI masks were then resampled to the resolution of the functional EPI scans for use in subsequent analyses.

For the hyperoxic and hypercapnic manipulations, the corresponding fractional changes in BOLD and CBF along with arterial  $O_2$  content values were substituted into the generalized calibration model to determine the  $M$  vs.  $OEF_0$  curve for each gas (the averaging performed on the measured MRI and respiratory values is described below). The intersection point of the two curves was then determined numerically using the bisection method (Press et al. 1992). A third curve was also generated based on the MRI and respiratory responses during carbogen inhalation (combined hyperoxia and hypercapnia), and used to confirm the existence of a unique intersection point. To assess both the validity of the procedure as well as its stability under progressively more challenging SNR conditions, the solution of the model was carried out on data generated at three levels of averaging: 1) the group average of individual grey-matter ROI averages and respiratory values; 2) individual ROI averages and respiratory values; and 3) single voxels in individual scans and individual respiratory values.

The group average curves for the three conditions (hyperoxia, hypercapnia, and combined) were plotted to confirm intersection at or near a common point. To assess the sensitivity of  $M$  and  $OEF_0$  estimates on the assumed model parameters  $\alpha$  and  $\beta$ , this procedure was repeated with a range of values for each parameter, bracketing the nominal literature values used in the actual analysis. The range of  $\alpha$  was 0.1 to 0.38, with the upper value being the original Grubb value for total (arterial plus venous) blood volume. The range of  $\beta$  parameters was one to two (centered on the nominal value of 1.5). To investigate the effect of possible changes in  $CMRO_2$  during hypercapnia, we conducted additional analyses in which both increases (Horvath et al. 1994; Jones et al. 2005) and decreases (Zappe et al. 2008; Xu et al. 2011b) of 15% in cerebral oxygen consumption were simulated during the hypercapnic component of calibrations. This was effectuated by applying the appropriate factor (1.15 or 0.85) to the terms in Eq. 2 representing oxygen consumption (normally assumed to be constant at the resting value). The value of  $\Delta\%CMRO_2 = \pm 15\%$  was chosen because it spans the range of values suggested in the literature cited above during comparable hypercapnic manipulations.

Individual ROI data from hyperoxia and hypercapnia were used to determine average cortical  $M$  and  $OEF_0$  solutions for each subject, while voxel-wise analyses were used to generate images of  $M$  and  $OEF_0$  for each subject. Because of the reduced signal-to-noise ratio in the voxel-wise case, parameter images were computed as the average of the solutions for the hypercapnia-hyperoxia and combined-hyperoxia combinations. In cases where one of the latter combinations did not intersect (i.e. no solution) the other solution was taken if it existed. To aid in assessing anatomic contrast in the computed parameters, individual parametric maps were also spatially normalized using FSL (Jenkinson et al. 2001) to allow computation of the arithmetic mean image over all seven subjects. To account for the fact that images of some subjects contained regions with no solution, the averaging procedure took into account the actual number of values (true solutions) contributing in the average to prevent bias.

Computation of resting  $CMRO_2$  required the absolute resting CBF, which was determined from the pCASL data using the approach described by Wang et al. (Wang et al. 2003a) assuming blood brain partition coefficient = 0.9, labeling efficiency = 0.80, blood  $T_1 = 1.49$  s, and grey matter  $T_1 = 1.4$  s. For this computation, the baseline ASL difference signal estimated in the GLM fit for each gas manipulation was divided by an estimate of the baseline (raw) EPI signal computed in a similar GLM fit and the resultant ratio converted to absolute CBF units based on the parameters above. Maps of resting  $CMRO_2$  were obtained by computing the product of the resting arterial  $O_2$  content for that subject, resting CBF, and  $OEF_0$ . For each of the latter terms, averaging was performed at the three levels described above.

Other than the coordinates for intersection of group average  $M$  vs.  $OEF_0$  curves, for which the range of intersection coordinates was used, all uncertainties are provided as  $\pm$  standard deviation.

### 3.5. Results

#### 3.5.1. Gas manipulations

Hyperoxic gas manipulations led to increases in end-tidal O<sub>2</sub> in all subjects. Hypercapnia led to slight increases in some subjects (likely due to modest increases in minute ventilation), but overall the change was non-significant. The mean resting ETO<sub>2</sub> value over all seven subjects, in all gas manipulations, was 117±14 mmHg. Mean increases in ETO<sub>2</sub> were: 424±79 mmHg for hyperoxia, 14±22 mmHg for hypercapnia, and 300±65 mmHg for combined hyperoxia and hypercapnia. The average resting ETCO<sub>2</sub> value over all gas manipulation scans was 39±3 mmHg. The mean changes in ETCO<sub>2</sub> were: -3±5 mmHg during hyperoxia, 9±4 mmHg during hypercapnia, and 8±4 mmHg during combined hyperoxia and hypercapnia.

Quantity		Value
Hyperoxia	Resting ETO <sub>2</sub>	116±14 mmHg
	Manipulated ETO <sub>2</sub>	540± 74 mmHg
	Δ%CBF	-3.1±9%
	Δ%BOLD	1.71±0.4%
Hypercapnia	Resting ETO <sub>2</sub>	120±17 mmHg
	Manipulated ETO <sub>2</sub>	134±14 mmHg
	Δ%CBF	37±8%
	Δ%BOLD	2.3±0.4%
Hyperoxia + Hypercapnia (Carbogen)	Resting ETO <sub>2</sub>	115±13 mmHg
	Manipulated ETO <sub>2</sub>	415± 60 mmHg
	Δ%CBF	41± 12%
	Δ%BOLD	3.5±0.8%

**Table 1**

Group average MRI and respiratory measures used to compute GCM solutions for *M* and OEF<sub>0</sub>.

## 3.5.2. ROI analyses

### 3.5.2.1. MRI responses

All hypercapnic manipulations led to significant increases in grey-matter CBF. Average percent changes in CBF were  $37\pm 8\%$  for hypercapnia (mean  $\Delta\text{ETCO}_2 = 9\pm 4$  mmHg), and  $41\pm 12\%$  for combined hyperoxia/hypercapnia ( $\Delta\text{ETCO}_2 = 8\pm 4$  mmHg). Hyperoxia produced a mean flow decrease of  $3.1\pm 9\%$ , after correction for T1 changes. Average resting cerebral blood flow in grey matter was  $52\pm 5$  ml/100g/min. The average  $\text{CO}_2$ -mediated cerebrovascular reactivity during hypercapnia was  $5.3\pm 1.6 \Delta\% \text{CBF}/\text{mmHg CO}_2$ .

All gas manipulations, both hypercapnic and hyperoxic, led to increases in BOLD signal. These were:  $1.7\pm 0.4\%$  for hyperoxia,  $2.3\pm 0.4\%$  for hypercapnia, and  $3.5\pm 0.8\%$  for combined hyperoxia/hypercapnia.

### 3.5.2.2. Group average $M$ vs. $\text{OEF}_0$ curves

Figure 1 shows plots of the  $M$  vs.  $\text{OEF}_0$  curves for hyperoxia, hypercapnia, and combined hyperoxia/hypercapnia, computed by first averaging end-tidal  $\text{O}_2$  changes and MRI responses within grey-matter ROI's from all subjects and then inputting these group average measurements into the model. The three curves intersected very close to a common point situated at  $\text{OEF}_0 = 0.37\pm 0.01$  and  $M = 6.200\pm 0.005\%$  (uncertainties are based on distances of individual intersections from midpoint). Curves were generated over the physically possible range of  $\text{OEF}_0$  values: zero to one (the trivial solution at  $\text{OEF}_0 = 0$  is ignored). Values of  $\text{OEF}_0$  below 0.1 (which are extremely unlikely to arise in practice) resulted in complex values of  $M$  for the two manipulations that included hyperoxia (only the real part is shown - values of  $\text{OEF}_0$  above 0.1 gave purely real  $M$  values in all cases). It can be seen that the curve for hyperoxia is somewhat orthogonal to those for the manipulations including hypercapnia, which are relatively similar. Because of this, we found that solutions between the purely hyperoxic manipulation and the two other (solely or partly) hypercapnic conditions were more robust. Group average measurements used as inputs to the model are listed in Table 1.

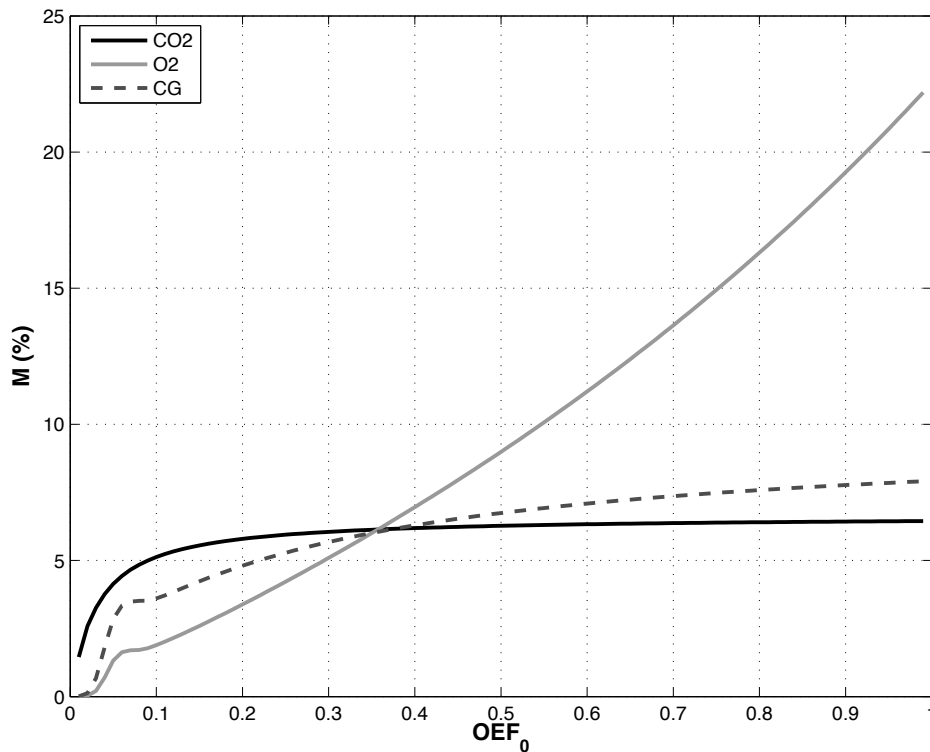


**Figure 1**

Grey matter  $M$  vs.  $OEF_0$  curves computed with GCM using group average input data for hyperoxia (grey), hypercapnia (black), and combined hyperoxia/hypercapnia (dashed). The three intersection points coincide closely, centered on  $OEF_0 = 0.37 \pm 0.01$ ,  $M = 6.200 \pm 0.005\%$ .

### 3.5.2.3. Individual grey matter ROI values of $OEF_0$ , $M$ , and $CMRO_2$

Figure 2A shows a scatter plot of  $OEF_0$  and  $M$  values computed from the intersection of the hyperoxia curve with those for hypercapnia (circles) and the combined manipulations (crosses), generated using input MRI and respiratory data averaged over grey matter in each of seven individual subjects. Axis scaling is based on the range of  $OEF_0$  and  $M$  values spanned by the different  $M$  vs.  $OEF_0$  curves plotted for group average data in Figure 1. Considering the range of values physically possible, the individual values cluster closely around physiologically plausible values for  $M$  ( $6.0 \pm 0.7$ ) and  $OEF_0$  ( $0.35 \pm 0.04$ ). Multiplying individual grey-matter  $OEF_0$  estimates by the corresponding values of  $CaO_{2l_0}$  and  $CBF_0$  gave similarly close distributions of  $CMRO_2$  estimates (Figure 2B) with an average value of  $140 \pm 28 \mu\text{mol}/100\text{g}/\text{min}$  for hypercapnia and  $150 \pm 34 \mu\text{mol}/100\text{g}/\text{min}$  for the combined manipulation (the average of the two manipulations gave  $145 \pm 30 \mu\text{mol}/$

100g/min). Parameter estimates for individual subjects, including cerebrovascular reactivity (CVR), are shown in Table 2.

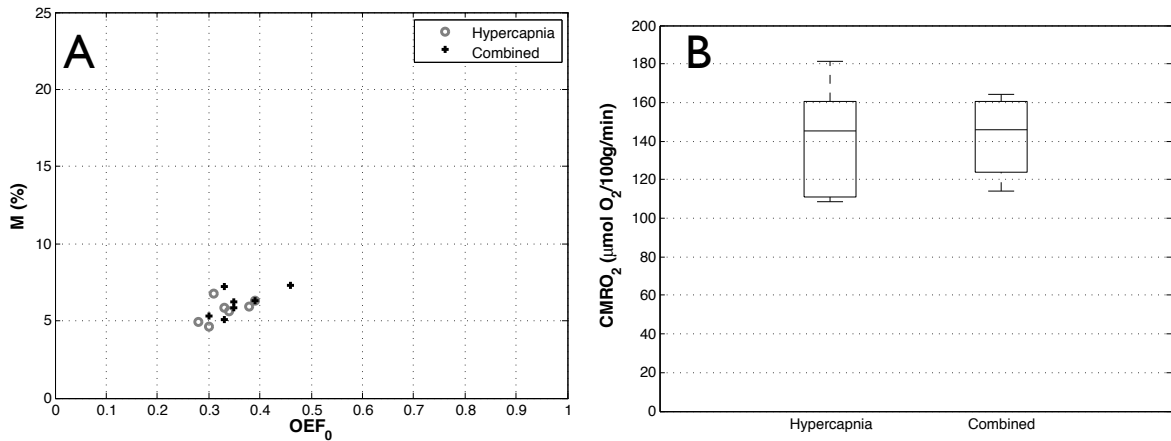


**Figure 2**

A) Coordinates for intersections of hyperoxia/hypercapnia curves (grey circles) and hyperoxia/combined curves (black crosses) in grey matter for seven individual healthy subjects. Axis scaling is the same as Figure 1, covering the physically possible range of OEF<sub>0</sub> and corresponding *M* values for the different gases. Individual solution values are clustered around the average coordinates OEF<sub>0</sub> = 0.35±0.05, *M* = 6.0±0.8%. B) Box and whisker plot showing median, quartile, and adjacent value ranges of computed CMRO<sub>2</sub> for the seven subjects using the solutions between hyperoxia and hypercapnia (left) or combined hyperoxia/hypercapnia (right). Average CMRO<sub>2</sub> values were 138±28 µmol/100g/min for hypercapnia, and 149±34 µmol/100g/min for the combined manipulation.

Subject	Resting CBF (ml/100g/min)	CVR (Δ%CBF/mmHg CO <sub>2</sub> )	<i>M</i>	OEF <sub>0</sub>	Resting CMRO <sub>2</sub> (µmol/100g/min)
1	44.0	4.2	7.0	0.32	111.6
2	53.4	3.6	6.3	0.39	164.6
3	52.1	5.0	5.8	0.33	135.7
4	59.8	4.0	6.6	0.42	199.6
5	53.4	7.1	5.9	0.35	149.2
6	46.5	7.6	4.9	0.32	116.8
7	56.2	5.4	5.6	0.32	139.5
average	52±5	5.3±1.6	6.0±0.7	0.35±0.04	145±30

**Table 2**

Physiological parameters computed in individual subjects.

### 3.5.3. Parametric maps

#### 3.5.3.1. Resting BOLD signal $M$

Figure 3A shows the maps of resting BOLD signal  $M$  obtained for the seven subjects by solving the GCM at each voxel and averaging (or merging) the solutions for hypercapnia and carbogen as described above. The  $M$  maps demonstrate the expected contrast between grey and white matter (due to the higher blood volume in grey matter) and the distribution of values in grey matter corresponds well to those obtained above in ROI analyses as well as in previous studies (Gauthier et al. 2011a; Gauthier et al. 2011b). The qualitative appearance of the maps is good, with plausible grey-white matter contrast and few venous hot spots or improbably high values that can result from non-linear amplification of noise in BOLD calibration models (Gauthier et al. 2011a). Black patches in grey matter (e.g. subject 4) indicate regions in which neither the hypercapnic nor carbogen GCM curves intersected with the curve for hyperoxia.

#### 3.5.3.2. Resting oxygen extraction fraction $OEFO$

Figure 3B shows maps of resting OEF for the seven subjects. Although previous PET studies (Frackowiak et al. 1980; Ito et al. 2004; Ashkanian et al. 2008; Bremmer et al. 2010; Ibaraki et al. 2010) indicate that OEF is very constant throughout the resting brain, the individual  $OEFO$  maps exhibited a degree of apparently random spatial heterogeneity as well as a modest grey-white matter contrast in most subjects. Nonetheless the values within grey matter tended to be distributed within a physiologically plausible range (e.g. the literature standard 0.3 assumed for healthy tissue in the Chiarelli method (Chiarelli et al. 2007b)) consistent with the ROI analyses presented above.

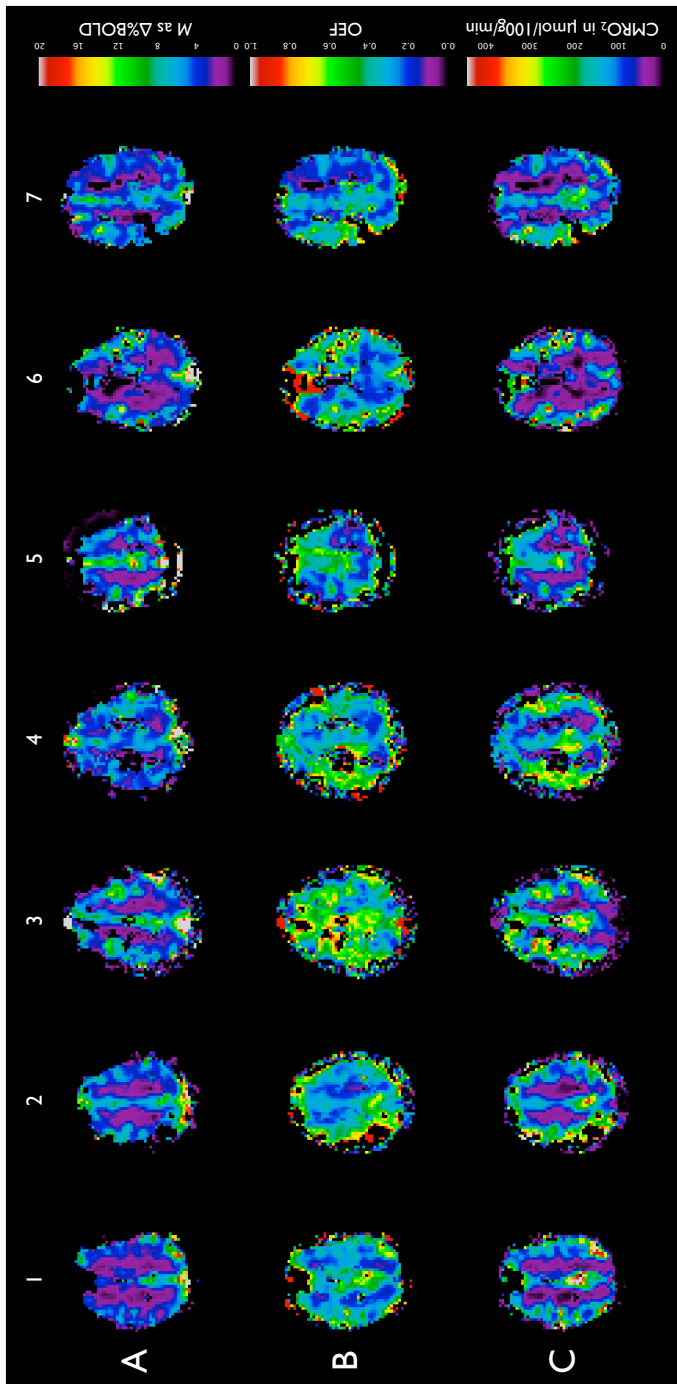


**Figure 3**

Individual maps of (A) resting BOLD signal  $M$ , (B) resting OEF, and (C) resting  $CMRO_2$  for seven subjects, computed as average of hyperoxia-hypercapnia and hyperoxia-combined solutions (image left is subject left). When only one out of the two pairs of equations could be solved, that value was used. Voxels where no solutions existed were assigned a value of zero (black patches visible in some subjects, *e.g.* #4).

### 3.5.3.3. Resting oxygen metabolism $CMRO_2$

Figure 3C shows maps of resting  $CMRO_2$  computed for the seven subjects. While the effect of noise in the  $OEF_0$  maps is apparent, the distribution of grey matter  $CMRO_2$  values is generally in very good agreement with the ROI values computed above.

### 3.5.3.4. Group average maps

Figure 4 shows average images from spatially normalized individual maps. All maps exhibited plausible pattern of anatomic contrast, with quantitative values tending towards group average ROI estimates. Grey-white matter contrast is absent in the map of resting  $OEF$ , as expected for this parameter.

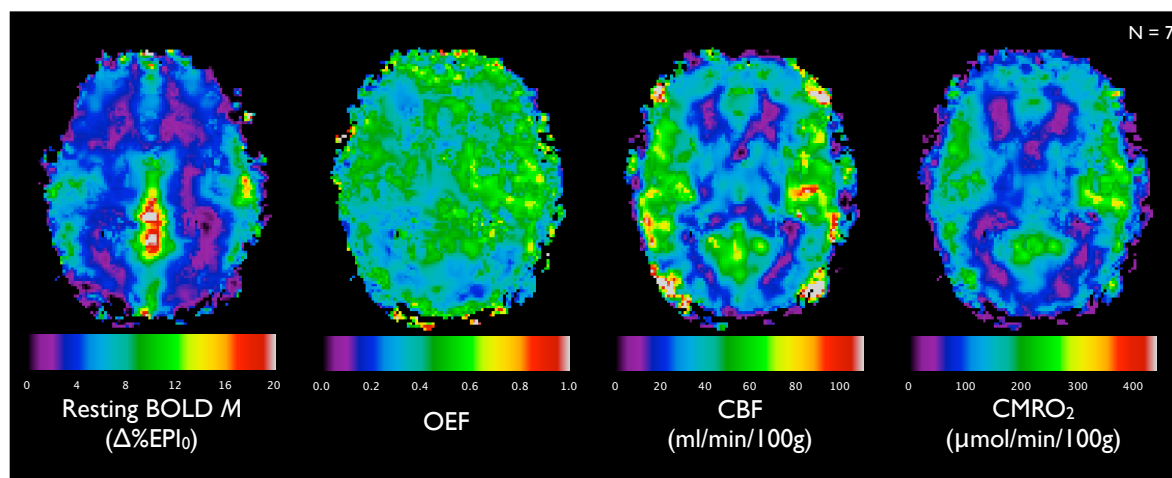


**Figure 4**

Group average (N=7) maps of estimated parameters. Images of  $M$ ,  $OEF$ ,  $CBF$ , and  $CMRO_2$  exhibit plausible pattern of anatomic contrast, with quantitative values matching group average ROI estimates. Grey-white matter contrast is absent in the map of resting  $OEF$ , consistent with previous PET studies.

### 3.5.3.5. Sensitivity to model parameters, possible $CMRO_2$ changes during hypercapnia

Figure 5 shows model three-gas model solutions for group average ROI data and a range of values for  $\alpha$  and  $\beta$ . Some parameter combinations (such as  $\alpha = 0.38$ ,  $\beta = 1$ ) gave widely divergent solution points for the different gases, while others gave coincident solution points but at slightly different values of  $M$  and  $OEF_0$  from the nominal parameters.

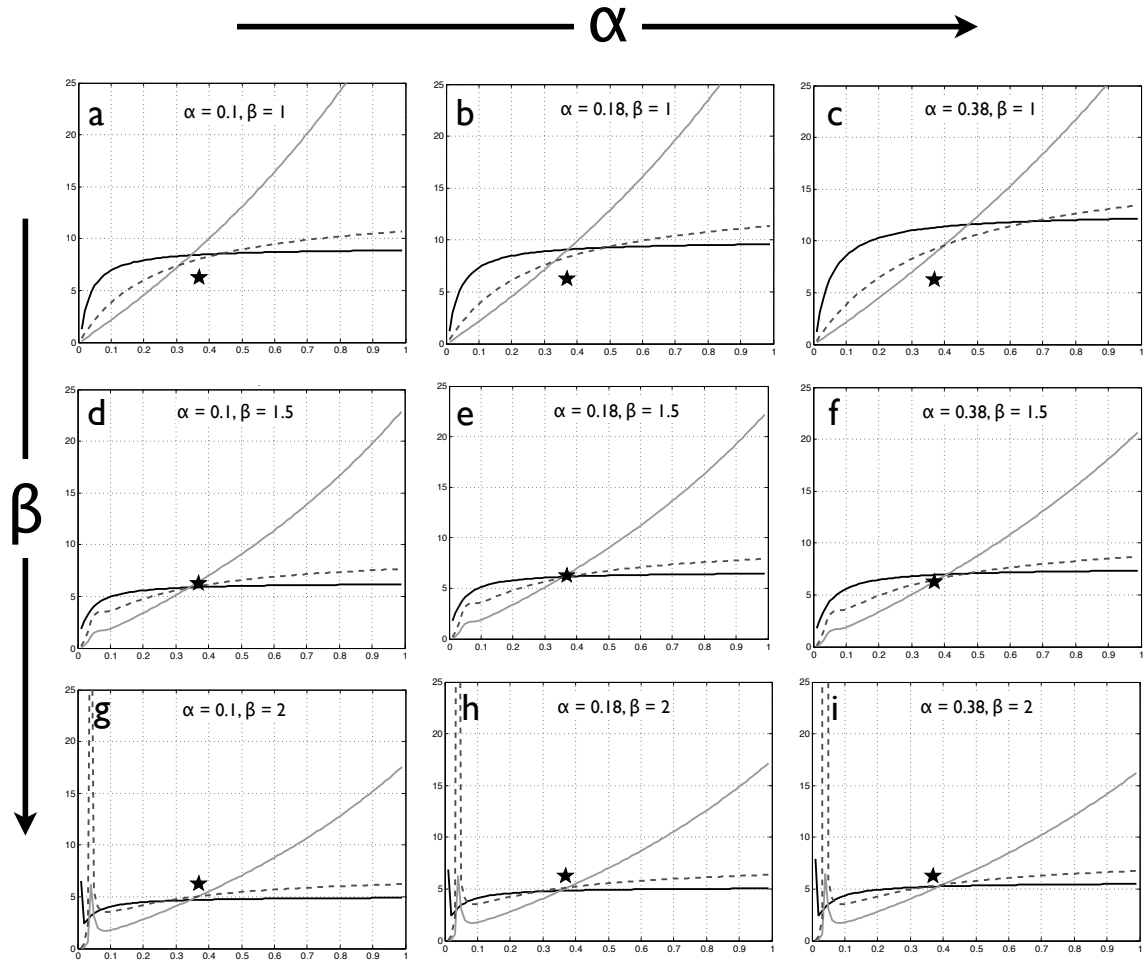


**Figure 5**

Dependence of solution coordinates on assumed model parameters  $\alpha$  and  $\beta$  with the same group average data plotted in Figure 1. The values used,  $\alpha = 0.18$  and  $\beta = 1.5$ , are in the central plot (e). The intersection yielded by these nominal values is indicated by the star (same coordinates) in each plot. Some parameter combinations (such as c) lead to widely divergent solution points for the different gases, while others give coincident solution points but at slightly different values of  $M$  and  $OE_{F_0}$  from the nominal parameters. Axis scaling and units for all plots are as in Figure 1 and 2: the horizontal axis is resting  $OE_{F_0}$ , and the vertical axis is  $M$ .

Figure 6 shows three-gas solutions for group average ROI data and hypercapnia-induced  $CMRO_2$  changes of -15%, 0, and +15%. Modeling the increase in  $CMRO_2$  during hypercapnia resulted in widely divergent model curves, with the midpoint of intersections falling at  $OE_{F_0} = 0.68$  and  $M = 11\%$ . Modeling a 15% decrease in  $CMRO_2$  resulted in a more convergent intersection of the three curves. The solution coordinates in this case were centered at  $OE_{F_0} = 0.25$  and  $M = 4.5\%$ .

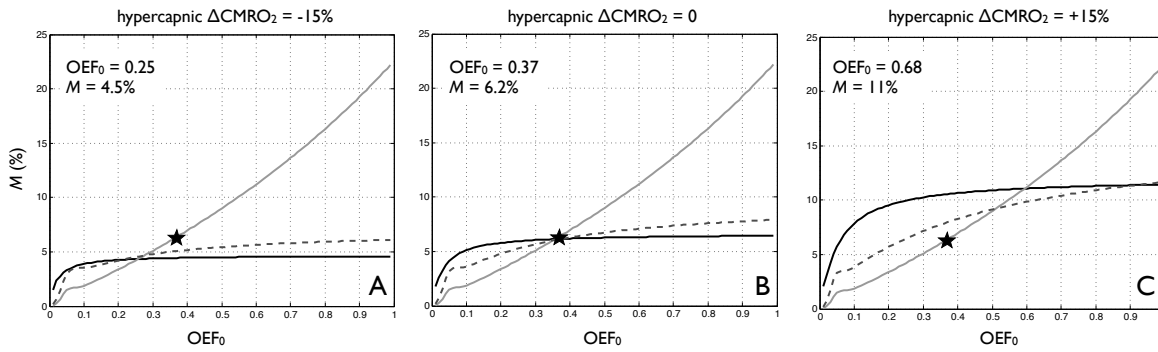


**Figure 6**

Variation of model curves with simulated decreases (A) and increases (C) in  $CMRO_2$  during hypercapnic phases of calibration. Curves with no  $CMRO_2$  change (B) are shown for comparison (solution coordinates for  $\Delta CMRO_2 = 0$  indicated by star on all plots). Simulated  $CMRO_2$  increases prevented convergence of curves (C), while decreases resulted in very low apparent solution values for  $OEF_0$  and  $M$ .

### 3.6. Discussion

We have demonstrated GCM-based estimation of resting BOLD signal  $M$ ,  $OEF_0$ , and  $CMRO_2$  in seven healthy volunteers. The intersection of group average  $M$  vs.  $OEF_0$  curves at almost exactly coincident points, as well as the correspondence between the coordinates of this point and previous literature values for the above parameters, lend strong support for the validity of this method. The individual ROI analyses indicate that the approach is feasible at the single-subject level. While generating maps of MRI calibration parameters at the single voxel level has proven in the past to be quite challenging (the vast majority of calibrated MRI studies have reported ROI values rather than maps), the relative stability of individual and group average maps of  $M$ ,  $OEF$ , and  $CMRO_2$  obtained with the GCM in combination with the three-gas calibration approach is also encouraging.

#### 3.6.1. Accuracy

Here we define accuracy as the tendency for data with sufficiently high SNR (regional, group averaging) to converge towards physiologically plausible values that are in agreement with independent measurements using other techniques from literature.

The parameters estimated in the present study from group average data are in good agreement with literature values. Grey-matter average values for  $M$  at 3 Tesla

(adjusted to TE = 30 ms) have been reported as  $7.0\pm 0.7\%$  (hyperoxia (Chiarelli et al. 2007b)),  $7.9\pm 0.6\%$  (GCM with carbogen (Gauthier et al. 2011a)),  $8.8\pm 0.8\%$  (hypercapnia (Mark et al. 2011)), and  $6.6\pm 0.4\%$  (hyperoxia (Mark et al. 2011)). The group average value of  $6.0\pm 0.7\%$  overlaps with this range, although at the lower end. This is likely due to the fact that, in the present study, we masked out the largest veins as described in the methods section, which will remove a slight source of upward bias on the average  $M$  value over all grey matter. Other differences include the fact that the studies by Chiarelli and Mark used pulsed ASL, with the additional incorporation of background suppression in the Mark study (BOLD acquisitions were interleaved without background suppression). The use of background suppression is likely to be an effective means of improving the low signal-to-noise ratio in ASL image series.

While OEF values ranging from  $0.26\pm 0.02$  (Bolar et al. 2011a) through 0.3 (Perlmutter et al. 1985) to  $0.45\pm 0.06$  (Ibaraki et al. 2010) have been reported, the average value of  $0.35\pm 0.04$  in the present study falls solidly in the center of this range.

Values obtained for resting  $CMRO_2$  in grey-matter were also in good agreement with literature data. A recent study by Xu et al. (Xu et al. 2009) used the TRUST method to estimate the mean whole-brain  $CMRO_2$  in healthy volunteers at  $132\pm 20$   $\mu\text{mol}/100\text{g}/\text{min}$ , which is slightly lower than our group average grey-matter value of  $145\pm 30$   $\mu\text{mol}/100\text{g}/\text{min}$ . The latter study also included a survey of literature values obtained primarily using PET, for which grey-matter values of 147 and 157  $\mu\text{mol}/100\text{g}/\text{min}$  were cited in subjects of various ages (Ishii et al. 1996; Ibaraki et al. 2010). Other estimates cited in Xu's survey ranged from 118 to 157  $\mu\text{mol}/100\text{g}/\text{min}$ , corresponding very closely to the average value of  $145\pm 30$   $\mu\text{mol}/100\text{g}/\text{min}$  for grey-matter determined with MRI in the present study. Whole brain values are expected to be somewhat lower than grey-matter values, given that the bulk of synaptic membrane activity takes place in grey matter. An alternate MRI-based method, QUIXOTIC, recently proposed by Bolar et al. (Bolar et al. 2011a) yielded an average grey-matter  $CMRO_2$  value of  $125\pm 15$   $\mu\text{mol}/100\text{g}/\text{min}$ , which is somewhat lower than the grey-matter measurements cited for PET.

While the agreement with literature values in healthy volunteers is very encouraging, potential sources of bias include the possibility that functional ASL measurements during the carbogen manipulation are biased by blood T1 changes. However we have taken steps to correct for T1 shortening, using a procedure that has been validated in CGM-calibrated MRI with carbogen (Gauthier et al. 2011a) against more direct calibration using near-total saturation of venous blood (Gauthier et al. 2011b). Moreover in future applications of this approach we believe that the carbogen manipulation can be omitted, leaving only hyperoxia and hypercapnia. Hypercapnia is not significantly affected by T1 changes, while the CBF changes during hyperoxia are so minimal that they can be modeled with a small fixed constant value (as done here based on group average data with T1 correction).

The correct choice of constant model parameters have been another area of ongoing concern in calibrated MRI. In particular the parameter  $\alpha$ , used to model venous blood volume, has been the topic of considerable debate. Recent work indicates that the long-assumed value of 0.38 determined by Grubb for the aggregate arterio-venous blood volume (Grubb et al. 1974) is too high and should be replaced with the lower value of 0.18 measured specifically for the venous circulation in which deoxygenated hemoglobin resides. The value of  $\beta$  used here is also derived from older literature, having been estimated by Boxerman using Monte Carlo simulations and microsphere phantoms (Boxerman et al. 1995). To assess the sensitivity of our physiological estimates to these model parameters, we repeated the graphical solution originally shown in Figure 1 using a range of different  $\alpha$  and  $\beta$  values (Figure 5). Performing this analysis with the three gas curves had the interesting benefit that it allowed us to rule out some combinations of  $\alpha$  and  $\beta$ , since they resulted in intersection points for the different curves that were widely divergent (*e.g.*  $\beta = 1$  did not appear to converge for any value of  $\alpha$ ). For the parameter combinations that did converge, the resultant estimates of  $M$  and OEF deviated only slightly from the results obtained using the nominal values.

Given the complexities of multi-compartment modeling of susceptibility-based contrast, it should be understood that  $\alpha$  and  $\beta$  are more appropriately viewed as lumped constants, respectively modeling multiple effects associated with CBV or

[dHb], when applied to the low spatial-resolution single TE data typically acquired in calibrated MRI. This issue has recently been explored by Griffeth et al. (Griffeth et al. 2011), who used numerical optimization of a multi-compartment model for measured data to estimate the values of  $\alpha$  and  $\beta$ . The latter study found that alternate values of  $\alpha = 0.14$  and  $\beta = 0.91$  might be more appropriate for the measurement conditions considered. While we were able to verify (in separate analyses; data not shown) that the latter value of  $\alpha$  (0.14) was compatible with a unique ( $M, OEF_0$ ) solution for the three gases tested, our data and model appeared to be inconsistent with Griffeth's  $\beta$  value (i.e. no combination of other parameters gave a unique solution with  $\beta = 0.91$ ). While further exploration will be required to reconcile these findings, the GCM and Griffeth models provide complementary means of exploring the biophysics of BOLD contrast.

In addition to the above MRI parameters, modeling of the arterial and venous oxygen contents and saturations are an important component of the method presented. Fortunately the parameters involved (hemoglobin  $O_2$  capacity  $\phi$ , plasma  $O_2$  solubility  $\epsilon$ , and blood concentration of hemoglobin [Hb]) are highly conserved in healthy individuals (Rhoades et al. 2009). The only potentially uncertain parameter is [Hb], which can vary with gender (due to differences in hematocrit), disease (*e.g.* anemia), and acclimation to altitude. Individual values for [Hb] can however be readily determined using a simple blood test at the time of the exam. Two subjects in the present study had undergone recent blood tests as part of their participation in another study. Their respective values for [Hb] were 14.5 and 15.2 g Hb/dl blood, very close to the assumed value of 15 gHb/dl blood. Given the ease with which [Hb] can be measured, we recommend that future imaging studies adopting this method include a blood draw.

A potential concern related to oxygen content modeling is that the hemoglobin dissociation curve described by the Severinghaus equation may be incorrect during hypercapnia. However it is important to note that  $CO_2$ -dependent shifts in the Hb- $O_2$  binding curve (the Bohr effect) are mainly significant in the linear middle region of this sigmoidal curve. Hypercapnic manipulations in our method occur at very high arterial  $O_2$  saturation levels (>98% for all conditions; >99.9% for carbogen), where the Bohr effect is negligible. We should also emphasize that the

Severinghaus equation is only used to estimate arterial saturation, so although the venous saturation may be within the range where the Bohr effect is relevant, this does not impact the model. In the healthy subjects used in the present study, replacing the Severinghaus equation with a constant value of one would result in minimal change to the results. However it is quite possible to encounter much lower arterial saturation values in patient populations (e.g. impaired cardiopulmonary function). To account for this, it would be necessary to use an extended form of the Severinghaus equation that that adjusts for variations in  $PCO_2$  (Dash et al. 2004; Dash et al. 2010).

In the design of the present study, we chose to use a fairly simple gas manipulation approach based on switching between different fixed concentrations of inspired gases. While this is known to result in variable end-tidal gas responses achieved in different individual subjects, our model does not require prospective targeting of specific end-tidal values, relying instead on the ability of our model to control retrospectively for a wide range of changes in blood flow and end-tidal  $O_2$  which are measured during the experiment. Moreover there is no requirement that hypercapnic manipulations be isoxic, or that hyperoxic manipulations be isocapnic, since all manipulations are treated identically and the model is valid for arbitrary combinations of flow and oxygenation change. The approach used here does lead to a degree of inter-individual variability in the evoked gas responses, and this could be reduced by using available technology for prospective targeting of end-tidal values (Slessarev et al. 2007). Nevertheless, group average measurements in our study converged to values that we feel were adequately stable and representative for the calculations presented here. It should be noted that modeling of  $M$ ,  $OEF_0$ , and  $CMRO_2$  based on group average MRI and respiratory measures yielded results that were very close to the valued obtained by modeling data in individual subjects (whose end-tidal values varied) and then averaging individual values of  $M$ ,  $OEF$ , and  $CMRO_2$ .

Another area of discussion has been the impact of hypercapnic manipulations on neuronal  $CMRO_2$ . Currently a variety of findings on this topic have been reported including increases in metabolism (Horvath et al. 1994; Jones et al. 2005), decreases (Zappe et al. 2008; Xu et al. 2011b), and no detectable change

(McPherson et al. 1991; Hino et al. 2000; Chen et al. 2010a). The modeling shown in Figure 6 simulating CO<sub>2</sub>-induced changes in CMRO<sub>2</sub> of ±15% allows us to assess the impact of these on the model solutions. Our model and data would appear to rule out a CMRO<sub>2</sub> increase, as the  $M$  vs. OEF<sub>0</sub> curves for this case are widely divergent with pairwise solutions centered over physiologically implausible values of OEF<sub>0</sub> and  $M$ . Although the set of curves modeled with a CMRO<sub>2</sub> decrease are more convergent, the implied values for OEF<sub>0</sub> and  $M$  bring the validity of this scenario into question. The OEF<sub>0</sub> value of 0.25 is at the very low end of physiologically plausible values cited in prior literature (Perlmutter et al. 1985; Ibaraki et al. 2010; Bolar et al. 2011a). Moreover the associated  $M$  value of 4.5% is well below the value measured directly in grey matter using high CO<sub>2</sub>-content carbogen (Gauthier et al. 2011b). The agreement, in the  $\Delta$ CMRO<sub>2</sub> = 0 case, between  $M$  values obtained using our previous application of the Davis model during hypercapnia (Gauthier et al. 2011a) and  $M$  values determined using direct hypersaturation of venous blood with 10%CO<sub>2</sub>/90%O<sub>2</sub> (Gauthier et al. 2011b) suggests that bias from changes in CMRO<sub>2</sub> during hypercapnia is likely to be minimal. The agreement between implied values for resting OEF and CMRO<sub>2</sub> modeled with hypercapnic  $\Delta$ CMRO<sub>2</sub> = 0 and prior PET literature also tends to rule out such an effect.

Strongly hyperoxic manipulations could also create confounding effects by altering the MRI signal in the cerebrospinal fluid (CSF) due to T1 shortening (Hajnal et al. 1995). However inspection of both smoothed and unsmoothed statistical maps for both ASL and BOLD revealed no significant responses in either the ventricles or sulci. We also examined regions of susceptibility artifact in our T2\*-weighted image series for evidence of variability associated with high O<sub>2</sub> concentrations in the sinuses. There was no indication that hyperoxia modified the pattern of susceptibility artifact in these areas, in which fMRI responses are generally unreliable even under normoxic conditions. A recent numerical simulation study has suggested that hyperoxia may result in pronounced arterial BOLD effects (Schwarzbauer et al. 2011). Although we were able to find evidence of T1 shortening during hyperoxia in voxels containing larger arteries in our short-TE ASL data, careful inspection of the same voxels in the long TE image series

revealed no discernible modulation of the arterial T2\*-weighted signal during hyperoxia. Moreover such macrovascular voxels were excluded from analysis using masks generated by thresholding maps of hyperoxic response generated from unsmoothed ASL data (clearly revealing large arteries).

It should be noted that the accuracy of a unique solution for  $M$  and  $\text{OEF}_0$  will depend in part on the degree of orthogonality between the two  $M$  vs.  $\text{OEF}_0$  curves implied by the two calibrations used. Pairs of curves that are nearly parallel, such as the ones shown in Figure 1 for hypercapnia and carbogen (hyperoxia +hypercapnia), are likely to less well defined solutions than curves that cross at larger angles. Figure 1 also shows that, for a given set of BOLD and ASL measurements during hypercapnia, the implied  $M$  value has little dependence on the associated value of  $\text{OEF}_0$ . In the limit of a 'pure' hypercapnic manipulation, the situation can be understood as one in which  $\text{CO}_2$ -induced flow increases result in proportional dilution of venous deoxyhemoglobin, all of which is assumed to be deposited by local metabolism during capillary transit. The actual rate of metabolism (and thus OEF) is unimportant - all that matters is that any increase in CBF by a factor  $F$  will result in a decrease in venous [dHb] by  $1/F$ , bringing the BOLD signal correspondingly closer to the asymptotic value  $M$ . Note that, at very low  $\text{OEF}_0$  values, the small amount of deoxyhemoglobin present in arterial blood becomes significant, resulting in lower  $M$  values and some dependence on  $\text{OEF}_0$ . In the limit of 'pure' hyperoxia, the flow-related dilution (the term  $X$  applied to  $(\text{CBF}/\text{CBF}_0)$  in Eq. 2) is negligible, and all decreases in blood dHb arise due to increases in  $\text{CaO}_2$ . Because  $\text{CaO}_2$  is expressed as the quantity of  $\text{O}_2$  in absolute physical units (introduced by the end-tidal gas measurement), it can only be linked to venous Hb saturation by also modeling  $\text{CMRO}_2$  in absolute units. OEF thus represents the link between measured quantities (respiratory and MRI) and the relative value of tissue [dHb] required to estimate  $M$ . This explains the relatively strong variation in  $M$  value with  $\text{OEF}_0$  for hyperoxia. Although carbogen is an intermediate case, it can be seen that the flow effects tend to dominate and its behavior is more similar to that of pure hypercapnia alone over most of the range of  $\text{OEF}_0$ . This is due to the fact that fractional changes in CBF are considerably

larger than the fractional changes in  $\text{CaO}_2$  produced by the hyperoxic component of this manipulation.

### **3.6.2. Stability**

While the regionally and group-averaged data indicate that the calibration method proposed here is capable of yielding valid estimates of resting BOLD signal and OEF, the random fluctuations in the OEF maps and the patches in some subject where the GCM functions could not be solved indicates that the SNR of single voxels is close to the threshold where the stability of the method breaks down. Qualitatively, the parametric maps of  $M$  demonstrated good stability (immunity from hot spots) although these maps are affected by the lack of a solution in some regions. Group average maps with seven subjects showed improved stability, resulting particularly in a better depiction of the relative invariance of OEF across the resting brain. Based on prior PET literature (Frackowiak et al. 1980; Ito et al. 2004; Ashkanian et al. 2008; Bremmer et al. 2010; Ibaraki et al. 2010), we believe that OEF in these young healthy subjects is in fact 'flat' across the brain, lacking the pronounced grey-white matter contrast evident in maps of resting CBF and  $\text{CMRO}_2$ . However in cases of pathology, increases in OEF may indicate insufficiency of the local blood supply relative to local oxygen demand. For future clinical applications, it will thus be important to improve the image stability to the point where healthy brain  $\text{OEF}_0$  exhibits minimal noise fluctuations.

The limiting factor in the stability of our approach is the quality of fractional change maps for CBF during the various gas manipulations. Since this is a ratio calculation, regions with a low denominator (such as white matter) are particularly problematic. Fortunately there are a number of strategies that could be used to improve this; for example physiological noise correction methods such as RETROICOR (Glover et al. 2000; Restom et al. 2006) may help improve signal stability and thus the quality of fractional change maps. More sophisticated modeling of the gas-induced response, based on the actual end-tidal traces, may improve GLM fitting. Background suppression techniques (Garcia et al. 2005) may also help reduce uncontrolled physiological fluctuations in the ASL signal. In general any factor affecting ASL performance and accuracy, such as sensitivity

profiles in multi-channel receive coils, must be carefully evaluated to achieve optimal results with the method proposed here.

### **3.6.3. Similar methods**

Two other MR techniques have recently been proposed to measure baseline OEF and CMRO<sub>2</sub>. The technique described by He and Yablonskiy, termed quantitative BOLD (qBOLD), uses the MR signal modeling of the static dephasing regime to determine baseline hemodynamic parameters from a GESSE signal (He et al. 2007; He et al. 2008). The alternate approach (QUIXOTIC) proposed by Bolar et al. uses velocity-sensitive ASL (Bolar et al. 2011a) to target directly the oxygenation signal from small venules. By specifically measuring the signal from this compartment, a localized measure of oxygen extraction and metabolism can be obtained. While both methods have shown promising early results, both techniques present complexities which constitute potential obstacles to clinical adoption. The qBOLD method depends on a fitting procedure involving a large number of parameters, some of which are simultaneously optimized as part of the model fit, and others which must be assumed based on previously determined values. The uniqueness of parameter combinations yielding convergent fits can be difficult to guarantee, and the remaining fixed parameters reflect fundamental magnetic properties of tissue which are difficult to measure directly on an individualized basis. The QUIXOTIC method requires knowledge of the flow velocity range required to selectively image the venular signal, a value that could change considerably depending on the age and health of the subject. In spite of the above concerns, the emergence of a variety of distinct, MRI-based methods for imaging OEF and CMRO<sub>2</sub> that yield converging values for these parameters based on different aspects of BOLD signal modeling can only serve to improve our understanding of brain physiology and neuroimaging signals.

### **3.6.4. Applications**

The method proposed here could be applied in settings where FDG PET is currently used, with the added benefit that a rich array of vascular (resting CBF, cerebrovascular reactivity) and anatomic (T1, T2 scans) information would be provided in a single imaging session of similar duration and comfort to that of a

PET exam. The approach may thus be of particular interest in discriminating between vascular dementias and other etiologies such as Alzheimer's disease (Nagata et al. 2002; Herholz et al. 2007; Lo et al. 2011; Rodriguez et al. 2011). The method could also prove interesting for determining physiological changes in the brain during chronic ischemia such as that observed in carotid artery disease and in the identification and characterization of penumbral tissue in acute ischemia (Yamauchi et al. 1999; Yamauchi et al. 2009; Zipfel et al. 2009; Isozaki et al. 2010).

Although high levels of CO<sub>2</sub> can cause intense discomfort, the levels administered here (average increase in end-tidal CO<sub>2</sub> of 8.8 mmHg for hypercapnia and 7.7 mmHg for carbogen) while perceptible did not produce significant discomfort in our subjects. It should be remembered that it is the actual change in ETCO<sub>2</sub> that determines discomfort, and that this can be strongly modulated by factors like the maximum minute ventilation allowed given the gas flow rates. Also the ETCO<sub>2</sub> endpoints attained will vary considerably, even for a given gas mixture, depending on the exact mode of delivery. Fluctuations over a moderate range are of no significant consequence for the method described here, as long as end-tidal measurements are performed.

The need for patients to breathe through their nose to ensure that exhaled gases are sampled by the nasal cannula could pose a problem in patients for whom such compliance is difficult. This requirement could be alleviated by using a more sophisticated valve assembly on the face mask to ensure that expired gas being sampled does not mix with the inflowing mixture. We have verified the end-tidal O<sub>2</sub> and CO<sub>2</sub> data yielded by the setup used in the present study against alternate approaches (Slessarev et al. 2007), and found the values to be in consistent agreement with more rigorous reference standards (which were not used here because carbogen inhalation was not supported). Whatever approach is used, it will be desirable to minimize the need for patients to follow special breathing directives for this technique to achieve the broadest applicability.

In addition to possible clinical applications, the non-invasive method proposed may prove useful in basic neuroimaging research. Baseline properties are of considerable interest for the comparison of fMRI results between groups in aging

and disease. Task-induced BOLD signal changes cannot, in standard fMRI protocols, be related to a known baseline state. This reduces the strength of inferences that can be made about the signal changes measured, since BOLD changes are expressed as a function of an unknown baseline with an unknown inter-subject and inter-group variability. While we have emphasized resting metabolism in this report, the  $M$  values provided can still be used to calibrate task-induced changes in BOLD and ASL signals measured in functional studies. Such a study would benefit from access to both the resting  $CMRO_2$  and the percent functional change.

The emergence of commercially available hybrid PET-MRI instruments also creates interesting possibilities for the proposed technique. Given that  $^{18}F$ FDG PET can be performed without an on-site cyclotron, research and clinical sessions providing both glucose and oxygen uptake would be feasible. The combination of these two measures may allow more detailed inferences about cellular dysfunction (i.e. distinguishing between aerobic and anaerobic metabolism). Moreover the impending regulatory approval of  $^{18}F$ -based amyloid imaging agents such as florbetapir would allow, on a PET-MRI scanner, a combined amyloid/metabolic/vascular exam that could offer considerable improvements in diagnostic specificity between vascular and Alzheimer's etiologies. Such a tool would be invaluable in treatment selection and ongoing assessment of drug efficacy in clinical drug trials and personalized medicine.

### **3.7. Conclusion**

We have demonstrated in seven subjects a relatively simple MRI calibration procedure allowing estimation of the resting BOLD signal  $M$ , resting OEF, and resting  $CMRO_2$ . Considering that the method yielded a rich set of resting physiological estimates in excellent agreement with literature values, the number of parameters assumed in the approach is remarkably small, and consists of simple quantities whose values can be determined with a high degree of certainty.

### **3.8. Acknowledgements**

We thank Carolyn Hurst, André Cyr, Tarik Hafyane and Élodie Boudes for help with

data acquisition, Cécile Madjar for help with data acquisition, data analysis and helpful discussions. We would also like to thank Jiongjiong Wang, who provided the pseudo-continuous arterial spin-labeling sequence used. This work was supported by the Canadian Institutes for Health Research (MOP 84378, Banting and Best Scholarship held by CJG), the Canadian Foundation for Innovation (Leaders Opportunity Fund 17380), and the Ministère du développement économique, de l'innovation et de l'exportation (PSR-SIIRI-239).

## **4. Age-dependence of hemodynamic response characteristics in human fMRI**

Gauthier, C.J.<sup>1,2</sup>, Madjar, C.<sup>2</sup>, Desjardins-Crépeau, L.<sup>2,3</sup>, Bellec, P.<sup>2,4</sup>, Bherer, L.<sup>2,3</sup>, Hoge, R.D.<sup>1,2</sup>

<sup>1</sup> Physiology/Biomedical Engineering, Université de Montréal, Montreal, Quebec, Canada, <sup>2</sup> CRIUGM, Montreal, Quebec, Canada, <sup>3</sup>UQAM, Psychology Department, Montreal, Quebec, Canada, <sup>4</sup>Computer Science and Operations Research, Université de Montréal, Montreal, Quebec, Canada

Neurobiology of aging, Accepted November 2nd 2012, in press

### **4.1. Preface**

Aging is known to be associated with changes in cognitive performance. Older adults typically perform cognitive tasks more slowly and make more mistakes than younger adults. Furthermore, though this is true of many tasks, cognitive paradigms including an executive function component may be preferentially affected (Langenecker et al. 2004; Cabeza et al. 2005; Spreng et al. 2010). When fMRI is used to probe into the neuronal underpinnings of these behavioral differences, a series of common patterns emerge for many task paradigms, whereby older adults tend to show lower responses in posterior brain regions, and higher and more bilateral signal increases in frontal regions. These patterns have lead to a series of hypotheses on the mechanisms of cognitive aging (Cabeza 2002; Davis et al. 2008; Reuter-Lorenz et al. 2008; Park et al. 2009; Reuter-Lorenz et al. 2010; Schneider-Garces et al. 2010).

However, all these theories are based on direct comparisons of hemodynamic response amplitude between younger and older adults, with most recent studies using the BOLD contrast. While there is solid evidence for a link between BOLD

signal amplitude and underlying neuronal activity (Logothetis et al. 2001; Shmuel et al. 2002; Logothetis et al. 2004; Magri et al. 2012), the neurovascular coupling that determines the amplitude of the hemodynamic response is complex and may be affected by age (Girouard et al. 2006; Lecrux et al. 2011; Lu et al. 2011). The BOLD response is in other words an ambiguous signal that arises from a combination of changes in oxidative metabolism, blood flow and blood volume increase, and every component of the response may be affected by age-related changes (Yamaguchi et al. 1986; Chen et al. 2011; Lu et al. 2011). Therefore, before direct comparison of BOLD signal changes may be used to determine age-dependent changes in neuronal usage, the age-related biases inherent to the contrast mechanism must be identified.

The study presented in Chapter 4 is an investigation of the physiological changes in the brain associated with healthy aging. A calibrated fMRI framework was used to probe into these physiological changes and their impact on hemodynamic measures of brain activity. While the techniques presented in Chapters 2 and 3 would have allowed us to obtain some additional physiological information and a more robust measurement of  $M$ , these techniques were developed in parallel with the data acquisition phase of the study presented in this chapter. The design used here is therefore that of a hypercapnia calibrated fMRI experiment. Although this data did not allow application of the full generalized model for estimation of resting-state  $CMRO_2$ , the experiment did provide numerous physiologically-relevant parameters in addition to the blood flow and BOLD response to a modified Stroop task, including baseline blood flow, cerebrovascular reactivity to  $CO_2$ ,  $M$  and percent evoked  $CMRO_2$ . These physiological quantities are used to investigate the effects of aging and the confounds present in BOLD-only studies of cognitive aging.

## **4.2. Abstract**

Functional MRI studies of cognitive aging have generally compared the amplitude and extent of BOLD signal increases evoked by a task in older and younger groups. BOLD is thus used as a direct index of neuronal activation and it is assumed that the relationship between neuronal activity and the hemodynamic

response is unchanged across the lifespan. However, even in healthy aging, differences in vascular and metabolic function have been observed that could affect the coupling between neuronal activity and the BOLD signal. Here we use a calibrated fMRI method to explore vascular and metabolic changes that may bias such BOLD comparisons. While BOLD signal changes evoked by a cognitive task were found to be similar between a group of younger and older adults (e.g.  $0.50 \pm 0.04\%$  vs.  $0.50 \pm 0.05\%$  in right frontal areas), comparison of BOLD and ASL responses elicited in the same set of structures by a controlled global hypercapnic manipulation revealed significant differences between the two groups. Older adults were found to have lower responses in both BOLD and flow responses to hypercapnia (e.g.  $1.48 \pm 0.07\%$  vs.  $1.01 \pm 0.06\%$  over grey matter for BOLD and  $24.92 \pm 1.37\%$  vs.  $20.67 \pm 2.58\%$  for blood flow), as well as a generally lower maximal BOLD response  $M$  ( $5.76 \pm 0.2\%$  vs.  $5.00 \pm 0.3\%$ ). This suggests that a given BOLD response in the elderly may represent a larger change in neuronal activity than the same BOLD response in a younger cohort. The results of this study highlight the importance of ancillary measures such as ASL for the correct interpretation of BOLD responses when fMRI responses are compared across populations who may exhibit differences in vascular physiology.

### **4.3. Introduction**

Aging is associated with a variety of changes in the brain. While atrophy and white matter lesions are observable at the later stages in life (Salat et al. 2004; Brown et al. 2011), functional changes can also be observed (Chen et al. 2011; Lu et al. 2011). The effect of aging on the BOLD signal evoked by a variety of tasks has been the subject of intense research in recent years and typical patterns of change are starting to emerge. While several theories have been put forward to categorize and explain these patterns (Cabeza 2002; Davis et al. 2008; Reuter-Lorenz et al. 2008; Park et al. 2009; Reuter-Lorenz et al. 2010; Schneider-Garces et al. 2010), the complexity of the age-related changes observed indicate that there may be several mechanisms at play (Cabeza et al. 2005; Reuter-Lorenz et al. 2010). One of the most frequently observed pattern of change is a decreased lateralization of frontal BOLD responses, often detected as a decreased left frontal activation but

an increased right frontal BOLD signal increase in older participants (Cabeza 2002; Reuter-Lorenz et al. 2010). These differences in BOLD signal patterns have typically been explained by some form of compensatory neuronal activity in older participants to counterbalance the effects of loss of function and decreased primary perception or processing capacity (Cabeza 2002; Cabeza et al. 2005; Davis et al. 2008; Reuter-Lorenz et al. 2008; Park et al. 2009; Reuter-Lorenz et al. 2010). Implied in this type of theory is the fact that the additional recruitment should provide an advantage in terms of reduced age-related effects, usually observed as lower error rates or faster reaction times.

However, most of the results used to devise these theories are based on hemodynamic imaging techniques, with BOLD contrast at the forefront. Therefore, one of the main sources of potential confounds in functional MRI studies of aging stems from the ambiguous nature of the BOLD signal, which makes it difficult to draw physiologically specific conclusions from the amplitude and spatial extent of observed changes. The increases in BOLD signal observed during tasks arise from concomitant local changes in blood flow, blood volume and oxidative metabolism. This complicates the direct, quantitative comparison of BOLD signal changes between groups, especially when changes in hemodynamic function across groups are suspected (Samanez-Larkin et al. 2008; Ances et al. 2009; Chen et al. 2011; Lu et al. 2011; Mohtasib et al. 2012). Because BOLD can only be expressed as a fractional change from an unknown baseline, differences in the extent or amplitude of the BOLD signal may simply reflect an altered baseline state rather than a change in neuronal activity. For example, a similar metabolic change or vascular response from a lower metabolic or cerebral blood flow (CBF) baseline could artificially inflate the BOLD response.

Changes in BOLD signal may also reflect a decreased vascular reactivity (Lu et al. 2011). Aging is known to be associated with hardening of blood vessels throughout the body (O'Rourke et al. 2007; Brown et al. 2011). Increased rigidity in vessels of the brain could lead to a decreased vascular response to a given metabolic demand. This would then result in a lower BOLD signal change in older individuals with neuronal activity levels similar to those seen in younger individuals. All these potential sources of confounds make the interpretation of BOLD signal

comparisons between groups more difficult. However, some of these difficulties in interpretation could be alleviated by obtaining more physiologically-specific signals. The framework of calibrated fMRI, in which ASL and controlled vascular manipulations are added to BOLD, may be ideal for this as both the end-result and intermediate steps can be informative in determining the sources of age-related changes in hemodynamic properties (Gauthier et al. 2012a).

Calibrated fMRI techniques allow quantitative comparisons between groups by isolating the oxidative metabolic component of the BOLD response to a task, which can be expressed as the percent change in cerebral metabolic rate of O<sub>2</sub> consumption (CMRO<sub>2</sub>) (Davis et al. 1998; Chiarelli et al. 2007b; Blockley et al. 2011b; Gauthier et al. 2012b). The most widely adopted techniques have used respiratory manipulations to determine the change in BOLD signal produced by a controlled vascular challenge. The gas manipulations used have included hypercapnia (Davis et al. 1998; Hoge et al. 1999a) (breathing increased concentrations of CO<sub>2</sub>), hyperoxia (Chiarelli et al. 2007b) (breathing increased concentrations of O<sub>2</sub>) or a combination of both (Gauthier et al. 2011b; Gauthier et al. 2012b). Hyperoxia increases the O<sub>2</sub> content of blood, while hypercapnia leads to large and well characterized changes in blood flow throughout grey matter from the vasodilatory properties of CO<sub>2</sub>. Both these manipulations give rise to substantial increases in BOLD signal throughout the brain that can, in combination with quantification of the concomitant CBF change evoked, be used to characterize the vascular component of the BOLD signal (Hoge et al. 1999b; Stefanovic et al. 2006; Ito et al. 2008; Goode et al. 2009b; Mark et al. 2010; Tancredi et al. 2012). More specifically, calibrated fMRI experiments use the CBF and BOLD response to a gas manipulation to estimate the maximum possible BOLD signal change,  $M$ . This calibration factor  $M$  corresponds to the BOLD signal that would be obtained from complete elimination of deoxygenated hemoglobin from cerebral veins. Once this vascular component is estimated, it can be factored out of the BOLD response evoked by an experimental task, to yield an estimate of the CMRO<sub>2</sub> component of the task-evoked BOLD signal change measured. We have recently described an extension of previous models (Davis et al. 1998; Chiarelli et al. 2007b) that takes into account arbitrary changes in both blood flow and oxygen content (Gauthier et

al. 2012b). This model will be used here to more accurately take into account both blood flow and oxygenation changes caused by the breathing manipulation.

In the present study, we have used hypercapnically calibrated fMRI to investigate the effects of aging on the different components of the hemodynamic response, in the context of a cognitive task that has often been used to assess age-related cognitive deficits. Several studies have reported a larger Stroop effect (increases in reaction time and error rates to conflicting textual cues) and task switching cost in older compared to younger adults (DiGirolamo et al. 2001; Milham et al. 2002; Langenecker et al. 2004; Zysset et al. 2007; Jimura et al. 2010; Prakash et al. 2011; Wasylyshyn et al. 2011; Yun et al. 2011; Mohtasib et al. 2012). A modified Stroop task previously used by our group (Gauthier et al. 2012a) and involving both an element of interference and of switching is used here to identify the brain regions where age-related effects may be expected. This study therefore investigates the effects of two functional challenges: the modified Stroop task, which is typical of cognitive tasks that might be explored in a BOLD aging study, and a hypercapnic respiratory manipulation. The combination of acquisitions during these two functional challenges is used to investigate possible biases and confounds associated with BOLD studies of cognitive aging. Calibrated fMRI is used to estimate a number of vascular and metabolic parameters that jointly determine the final BOLD signal compared between young and old in typical fMRI studies of aging. These parameters may be used to assess the validity of direct BOLD signal comparisons between age groups. Because baseline blood flow and vascular reactivity are both expected to decrease with age (Chen et al. 2011; Lu et al. 2011), it may be that the maximal BOLD signal change is lower in older individuals, leading to bias in the interpretation of age-related BOLD signal differences.

## **4.4. Methods**

### **4.4.1. Participants**

Acquisitions were conducted in 31 young (10 female, with mean age of  $24 \pm 3$  years) and 31 older (14 female, with mean age of  $64 \pm 5$  years) healthy participants on a Siemens TIM Trio 3T MRI system (Siemens Medical Solutions, Erlangen,

Germany) using the vendor-supplied 32-channel receive-only head coil for all acquisitions. All subjects gave informed consent and the project was approved by the local ethics committee (Comité mixte d'éthique de la recherche du Regroupement Neuroimagerie/Québec).

Exclusion criteria for this study included claustrophobia, cardiac disease, hypertension or taking blood pressure lowering medication, neurological or psychiatric illness, smoking, excessive drinking (more than two drinks per day), thyroid disease, diabetes, asthma and being under a regular treatment known to be vasoactive or psychoactive. Participants were all non-smoking and older participants had all been non-smoking for at least five years. Additionally, every participant had a fasting blood draw on the morning of the MR acquisition day to ensure that their fasting blood glucose and cholesterol levels were normal, and older participants met with a geriatric MD to ensure that they did not meet any of the exclusion criteria for the study.

All participants completed a short neuropsychological screening battery to assess verbal reasoning (Similarities subtest of the Wechsler Adult Intelligence Scale III (WAIS-III) (Wechsler 1997), short-term memory (Digit span forward of WAIS-III), working memory (Digit span backward of WAIS-III), psychomotor speed (Digit Symbol of WAIS-III), attention, and executive functions (Trail Making Test, Part A and B and Color-Word Interference Test of the Delis-Kaplan Executive Function System (D-KEFS) (Reitan 1958; Delis 2001). Older adults participants also completed the Mini-mental state examination (MMSE) (Folstein et al. 1975) to screen for global cognitive decline. Participants who scored less than 26 on the MMSE were excluded. None of the participants was excluded based on this criterion. Table 1 shows the mean scores for each test in both groups. The results are within the normal range of performance for all clinical tests.

Whenever possible, participants needing eyesight correction were asked to wear contact lenses on the day of the MRI experiment. For those without contact lenses, eyesight was corrected to the nearest possible 0.50D using MRI-compatible glasses for the modified Stroop acquisition only. For participants with significant

hearing losses, written instructions were projected onto a screen at the end of the bore that could be seen by participants through a mirror.

#### **4.4.2. MR Image acquisition**

Sessions included two anatomical, 1mm<sup>3</sup> MPRAGE acquisitions with TR/TE/flip angle = 2300ms/3ms/9°, 256x240 matrix and a GRAPPA acceleration factor of 2 (Griswold et al. 2002). Older participants had an additional FLAIR acquisition to estimate the presence and severity of white-matter lesions. FLAIR acquisition parameters included TR/TE/flip angle=9000ms/107ms/120 with echo train length of 15, an inversion time of 2500 ms, 512x512 matrix for an in-plane resolution of 0.43 x 0.43mm and 25 slices of 4.8mm. White matter hyperintensities were quantified using the scale from Wahlund and colleagues (Wahlund et al. 2001). Only participants with scores of 0 or 1, corresponding to no or few small lesions, were included in this study. The score average and standard deviation was  $0.67 \pm 0.48$  in the older group.

Functional image series were acquired using a dual-echo pseudo-continuous arterial spin labeling (pCASL) acquisition (Wu et al. 2007) to measure simultaneously changes in cerebral blood flow (CBF) and BOLD signal. The parameters used include: TR/TE1/TE2/flip angle = 3000ms/10ms/30ms/90° with 4x4mm in-plane resolution and 11 slices of 7mm (1mm slice gap) on a 64x64 matrix (at 7/8 partial Fourier), GRAPPA acceleration factor = 2, post-labeling delay = 900ms, label offset = 100mm, Hanning window-shaped RF pulse with duration/space = 500μs/360μs, flip angle of labeling pulse = 25°, slice-selective gradient = 6mT/m, tagging duration = 1.5s (Wu et al. 2007).

Imaging sessions were divided into in two parts. During one part, an MPRAGE, FLAIR and modified Stroop functional acquisition was acquired. During the other, an MPRAGE and the hypercapnia functional acquisition was performed. Participants were taken out of the scanner in between these two acquisition segments to either put on, or take off the hypercapnia mask depending on the order of acquisitions. Participants were allowed to move or stretch during this pause to ensure greater comfort, especially in the older participants.

#### **4.4.3. Hypercapnic manipulation**

Hypercapnic manipulations were achieved using a computer-controlled gas delivery system in combination with a sequential gas delivery circuit (RespirAct™, Thornhill Research Inc., Toronto, Canada). The Respiract™ system allows independent control of end-tidal PCO<sub>2</sub> and PO<sub>2</sub> using a feed-forward physiological model, using as input the measured or predicted baseline O<sub>2</sub> consumption and CO<sub>2</sub> production of a subject (Slessarev et al., 2007). End-tidal partial pressure of CO<sub>2</sub> (ETCO<sub>2</sub>) was targeted to be 40mmHg at baseline and 45 mmHg during the hypercapnia blocks. End-tidal partial pressure of O<sub>2</sub> (ETO<sub>2</sub>) was targeted to be 100mmHg throughout the experiment. Gas was sampled continuously at the mouth and analyzed for partial pressure of CO<sub>2</sub> (PCO<sub>2</sub>) and O<sub>2</sub> (PO<sub>2</sub>). Respiract™ software calculated ETCO<sub>2</sub> and ETO<sub>2</sub> from the continuous partial pressure data. These calculations were confirmed manually in post hoc analysis. During the hypercapnic stimulation, volunteers breathed through the circuit via a soft plastic mask sealed to the face using adhesive dressing (Tegaderm 3M Healthcare, St. Paul MN), as necessary to prevent gas leakage. Participants were asked to breathe deeply enough to empty the fresh gas compartment of the breathing circuit at every breath during the functional acquisitions (to ensure delivery of the entire gas dose delivered by the machine). Generally, subjects did not have difficulty complying with this requirement.

Participants underwent the manipulation twice during the study, once outside the scanner before the imaging session to acclimatize the participant to the manipulation and once during the MRI session. Subjects were interviewed after the acclimatization session to assess their level of respiratory discomfort using the seven-point scale published by Banzett and colleagues (Banzett et al. 1996). Subjects reporting subjective rating of 5 or higher (significant discomfort) were not invited to continue in the study (two cases).

#### **4.4.4. Stroop task**

The Stroop task (Gauthier et al. 2012a) consisted of two 60-second blocks each of control and Stroop conditions, interspersed with 60-second rest blocks. In total, there were four task and five resting blocks, for a total acquisition length of nine

minutes (Figure 1). During task blocks, control or Stroop events always lasted 2.5 seconds, preceded by 1.5 seconds with a fixation cross to maintain a constant gaze direction. The task was presented and the responses recorded using the Eprime software (version 1.2, Psychology software tools, inc., Sharpsburg, PA, USA). The task was presented to participants using an LCD projector (EMP-8300, Epson, Toronto, ON, Canada) onto a translucent screen viewed by subjects through a mirror integrated into the Siemens head coil. In all cases, subjects had only two possible answers (blue or green), selected using an MRI-compatible button box (FIU-005 interface with 8 buttons bimanual response pads, Current Designs, Philadelphia, PA, USA). Most subjects were native French speakers or had been speaking French on a daily basis for more than thirty years and the color words were written in French ('BLEU' and 'VERT'). An English version of this task was also available for native English speakers (two in the younger and one in the older group).

During the Stroop/switching condition blocks, two different types of events were given in random order. In all cases, letter color and word semantic were non-congruent. In ten of fifteen cases, when the color word appeared, the correct answer was letter color. In five cases out of fifteen, a large white rectangle appeared around the word for the whole event, starting during the two seconds with the fixation cross. This rectangle indicated to the subject that the rule had changed and that the right answer now corresponded to word semantic rather than letter color. During the control task blocks (color naming), a series of four X's were written either in blue or green and the participant was asked to give the color of the letters.

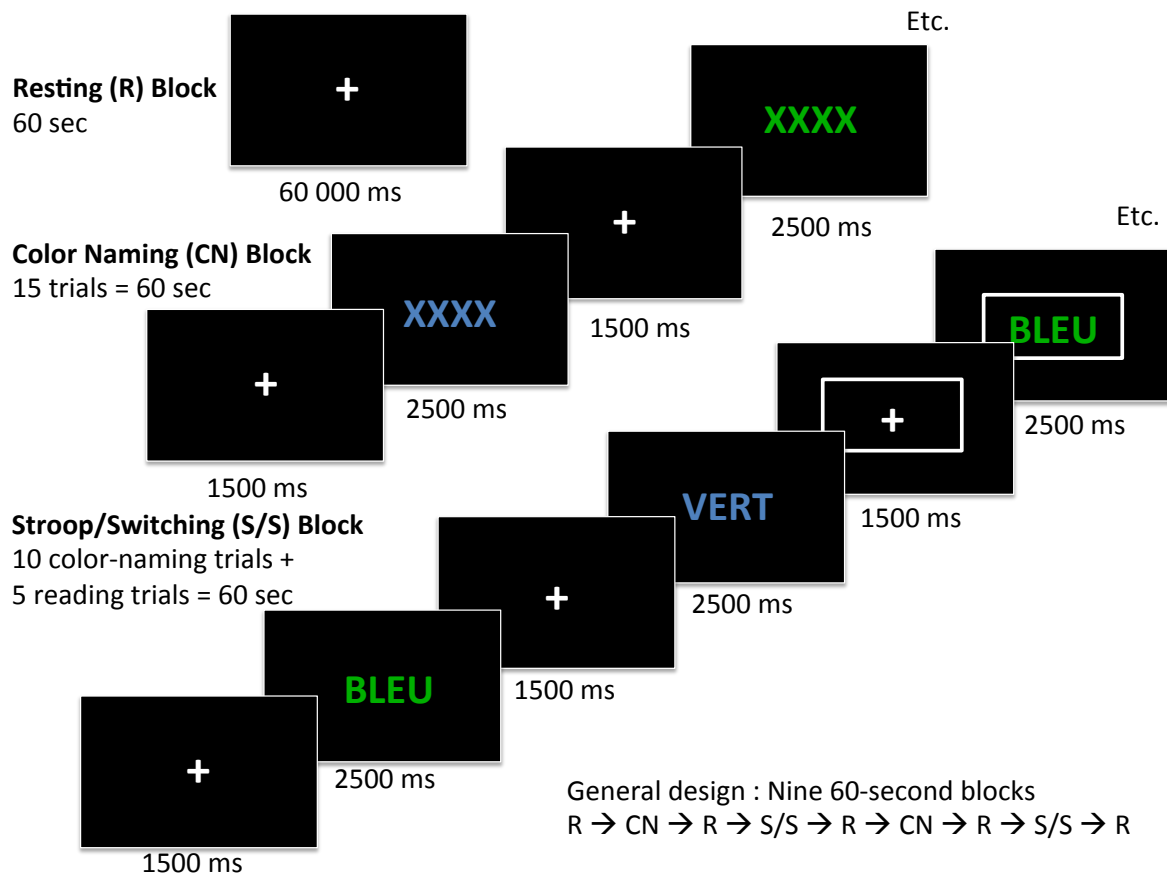


**Figure 1. Modified Stroop task paradigm**

This figure shows the different task conditions and block order of the modified Stroop task used during functional acquisition.

#### 4.4.5. Data analysis

All analyses except for group analysis, definition of Stroop ROIs, and registration of images to the MNI152 template were done using the NeuroLens data analysis software package ([www.neurolens.org](http://www.neurolens.org)). All raw EPI series were preprocessed by motion correction (Cox et al. 1999) and spatial smoothing with a 3D Gaussian kernel (6 mm FWHM). The CBF signal was isolated from the series of first echoes using linear surround subtraction (Liu et al. 2005), while the BOLD signal was extracted using linear surround addition of the second echo series (Liu et al. 2005; Gauthier et al. 2012a; Gauthier et al. 2012c).

Fractional changes in BOLD and CBF signals were then determined for hypercapnia by fitting a GLM to the respective signals and dividing the estimated effect size by the estimated constant term. Model fits used a single-gamma

hemodynamic response function (HRF) with parameters described by Glover et al. (Glover, 1999) and included linear, quadratic and third order polynomials to represent baseline signal and drifts. CBF and BOLD data for the Stroop task were treated similarly. For the Stroop task, a contrast was used to isolate the signal changes during the inhibition/switching blocks. Temporal SNR maps were derived from the CBF and BOLD datasets for the modified Stroop task. These were obtained by dividing the beta of the linear baseline term (DC) by the residuals from the GLM at each voxel. The temporal SNR represents the ratio between the baseline functional signal and the temporal fluctuations arising from hardware thermal noise and physiological sources of fluctuations (Kruger et al. 2001; Triantafyllou et al. 2005).

The average time course for CBF and BOLD of both hypercapnia and modified Stroop tasks were determined using a finite impulse response (FIR) analysis, which is a parsimonious method for averaging blocked responses within the context of a GLM fit that can be used to remove spurious drift terms. For purposes of the FIR fit, the 'events' were defined as being the block onsets, shifted earlier in time as needed to capture a brief interval of baseline before the task block. The number of FIR regressors was then chosen to adequately cover the initial baseline period, the task block, and a brief period after the task block. Using this approach, the temporal response was measured for 15 seconds before the beginning and after the end of each block (either hypercapnia or modified Stroop), to capture the rising, plateau and descending phases of the response. All other parameters were as in the previously described GLM analysis. The time course amplitudes of the regressor of interest (hypercapnia or modified Stroop) were divided by the baseline term from the GLM to obtain the time course in units of percent change CBF or BOLD. Individual time courses were averaged over all subjects in each group. To facilitate comparisons between groups and because the FIR trace does not always have an initial baseline of zero as expected, the first five TRs (minus 15 seconds to zero) were averaged and the whole trace was shifted by this average offset to bring the traces to a baseline of zero.

Absolute resting CBF was determined from the pCASL data using the approach described by Wang *et al.* (Wang et al. 2003a) assuming blood brain partition

coefficient = 0.9, labeling efficiency = 0.80, blood T1 = 1.49 s, and grey matter T1 = 1.4 s. For this computation, the baseline ASL difference signal estimated in the GLM fit for each gas manipulation was divided by the corresponding un-subtracted baseline EPI signal from the ASL series, computed in a similar GLM fit carried out on the un-subtracted EPI series. The un-subtracted baseline EPI signal from the ASL series is used here as a surrogate for the fully relaxed magnetization that can alternately be acquired in the form of what is termed an  $M_0$  scan. To account for incomplete recovery of longitudinal magnetization during the sequence TR of 3 seconds, baseline EPI estimates from grey-matter ROI's were corrected using the grey matter T1 value cited above. The resultant ratio was converted to absolute CBF units based on the parameters above. Cerebrovascular reactivity was obtained by dividing the percent BOLD and CBF signal changes during the hypercapnia manipulation by the increase in end-tidal  $PCO_2$  values during this manipulation (Graham et al. 1994; Forbes et al. 1997; Gauthier et al. 2012a).

The GCM method was used as in Gauthier *et al.* (Gauthier et al. 2012a; Gauthier et al. 2012b) to obtain  $M$  estimates for each subject. Under the conditions of this study, the results should be very similar to those obtained using the hypercapnia calibration model (Davis et al. 1998). Small differences may arise if arterial saturation is estimated to be below 100% (Gauthier et al. 2012b), but saturation values are expected to be very high in healthy individuals. Evoked  $CMRO_2$  values were obtained using group average values for all input parameters (percent CBF and BOLD change during the modified Stroop task and  $M$  value). One older participant was excluded from this analysis since their CBF response to  $CO_2$  and the modified Stroop task were found to be outliers.

ROI quantification was done by weighted averaging of voxels in EPI space, taking into account the grey matter volume fraction from automated tissue segmentation (described in the next section) at each voxel. All uncertainties are provided as  $\pm$  standard error. Uncertainties on evoked  $CMRO_2$  were computed from propagation of uncertainties on  $M$ , CBF and BOLD as described in Davis *et al.* (Davis et al. 1998).

#### 4.4.6. Regions-of-interest definition

Regions of interest were defined independently for each age-group using their respective areas of significant signal changes in the group analysis maps. Group analyses and normalization for ROI definition were done using FSL (version 4.1.9). All functional data were motion corrected with MCFLIRT (Jenkinson et al. 2002) and the brain was extracted using BET (Brain Extraction Tool, version 2.1) (Smith 2002). A 6mm<sup>3</sup> FWHM 3D Gaussian smoothing kernel, high-pass filter (100s cutoff) and pre-whitening (FILM) (Woolrich et al. 2001) were applied to the time series. Spatial normalization to standard space (MNI152 template) (Jenkinson et al. 2001; Jenkinson et al. 2002) was performed (12 degrees of freedom) on the 30ms echo time series. Spatial transformation matrices for the 30ms echo time-series were used for the 10ms time series, to minimize normalization errors from the bright scalp signal in the shorter echo. The flow-dependent component of the first echo time series (TE = 10ms) was isolated through sinc interpolation subtraction between neighboring points. The BOLD time series was extracted from the second echo time series (TE = 30ms) by isolating the control images from the original time series. A GLM was performed with the main experimental paradigm convolved with a dual gamma function. Temporal derivatives were included in the model. Fixed effect group analysis was performed using FLAME1 (Beckmann et al. 2003; Woolrich et al. 2004; Woolrich 2008) to generate group average statistical maps for the contrast representing the significant BOLD signal increases during the inhibition/switching blocks. The intersection of group average maps with Gaussian random field voxel-wise thresholding corrected at  $p = 0.01$  for each echo (i.e. the intersection of significant CBF and BOLD peaks) was used to derive the individual ROIs. Four ROIs were drawn using the map of the intersection of significant BOLD and ASL maps for the group (Figure 1). Two ROIs focused on significant activation over left and right frontal areas. A third ROI was drawn over significantly activated bilateral parietal areas. Because changes in laterality of activations is predominantly discussed in the context of frontal BOLD signal changes in the literature (Cabeza 2002; Park et al. 2009; Cappell et al. 2010; Reuter-Lorenz et al. 2010), only the frontal component of the activation was separated in lateral ROIs. The fourth ROI was derived from automated tissue segmentation of all grey matter.

The transformation matrix used to register individual functional acquisitions to MNI space was inverted and this inverted transform was applied to each ROI derived from the group activation map to obtain ROIs in native space using linear interpolation.

In order to account for the fact that our large EPI voxels inevitably contained a mixture of grey matter, white matter, and CSF, average BOLD and ASL responses were determined by computing weighted-averages within ROIs, with the weighting provided by the estimated grey matter volume fraction in each voxel. The grey matter volume fraction was determined using automatic tissue segmentation of anatomical images using the FAST module of FSL (Zhang et al., 2001). Grey matter probability maps generated by FAST were projected into native EPI space using linear interpolation. Binarized individual ROI maps (Stroop task-derived) were multiplied by grey matter probability. This approach assumes that the responses in white matter and CSF are negligible compared with the grey matter response, which is supported by our observations in these tissue compartments (data not shown).

#### **4.4.7. Statistical analysis**

Statistical analysis of the Stroop behavioral data was done using an analysis of variance (ANOVA) as implemented in the SPSS 19.0 software (IBM, Armonk, New York, USA). The inhibition/switching cost was calculated by dividing the difference in reaction time between the inhibition/switching and control conditions by the reaction time of the control task.

The difference between age groups across physiological measure, functional challenge and ROIs was tested using a general linear model analysis, as implemented in the Neuroimaging Analysis Kit (<http://www.nitrc.org/projects/niak>). First, the effect of age was investigated using a model pooling the measures from all the ROIs. The purpose of this model was to test the overall effect of age across all the ROIs, regardless of its significance at any particular ROI. The explanatory variables of the model included a dummy variable coding for the age group of each subject. In addition, the differences between the mean value for each of the four ROI were coded using an intercept and 3 dummy variables,

following the method described in (Gujarati 2002). The intercept captured the mean across all four ROIs. The first variable dummy variable coded for the difference between the mean of ROI 1 (grey matter) and the mean of ROI 2 to 4 (left and right frontal, and parietal). The second dummy variable coded for the difference between the mean of ROIs 1 and 2 and the mean of ROIs 3 and 4. The third dummy variable coded for the difference between the mean of ROIs 1 to 3 and the mean of ROI 4. The significance level of the overall effect of age across all regions was corrected for multiple comparisons across contrasts and experiments using Bonferroni's procedure (significance threshold  $p$  of 0.05 divided by 11 types of estimation,  $p = 0.0045$ ). For those combinations of physiological measure/functional challenge where age had an overall effect across ROIs, we further tested the significance of age effects at each ROI. This means that for each ROI, we used a reduced model including only the measurements coming from this ROI, as well as an intercept and age groups coded as a dummy variable for explanatory variables. The significance of the effect of age for each region was corrected for multiple comparisons across ROIs using the Bonferroni procedure (significance threshold  $p$  of 0.05 divided by 4 ROIs,  $p = 0.0125$ ). We did not correct for multiple comparisons across physiological measure/functional challenge at this level, as we already assumed that the omnibus test for the overall effect of age was significant for this particular combination of physiological measure/functional challenge.

	Younger	Older
Gender (M/F)	21/10	17/14
Age	23.74 ± 0.52	63.53 ± 0.87
Education (years)	17.03 ± 0.38	16.01 ± 0.57
MMSE (score)	-	28.81 ± 0.20
Similarities (score)	26.16 ± 0.86	23.69 ± 0.85
Digit span forward (score)	9.87 ± 0.41	10.69 ± 0.40
Digit span backward (score)	7.39 ± 0.41	7.06 ± 0.40
Digit symbol (score)	92.48 ± 2.13	66.09 ± 2.32
CWIT – Color naming (s)	25.65 ± 0.74	29.65 ± 0.94
CWIT – Reading (s)	19.15 ± 0.49	20.23 ± 0.64
CWIT – Inhibition (s)	41.89 ± 1.33	57.12 ± 2.22
CWIT – Switching (s)	49.46 ± 2.14	58.33 ± 3.71
TMT – Part A (s)	26.00 ± 1.45	34.15 ± 1.65
TMT – Part B (s)	56.55 ± 3.66	78.45 ± 5.14

**Table 1. Neuropsychological battery results**

This table shows the average ± standard error in each group for all tests included in the battery administered to participants. MMSE : Mini-Mental State Examination, CWIT : Color-Word Interference Test, TMT : Trail Making Test. The results are within the normal range of performance for all clinical tests.

## 4.5. Results

### 4.5.1. Modified Stroop task behavioral results

This study explores the hemodynamic and vascular changes in regions implicated in a modified Stroop task (Figure 1) thought to be associated with age-related changes. Reaction times (RT) and error rates were found to be significantly higher in the older group, both during the control and during the inhibition/switching blocks ( $p < 0.0001$ ). Reaction times during the control block were  $575.52 \pm 25.14$  ms and  $696.78 \pm 19.63$  ms in younger and older adults for the control task, and  $898.20 \pm 38.08$  ms and  $1239.91 \pm 34.26$  ms for the inhibition/switching blocks in younger and older adults respectively (Figure 2A). The group by condition interaction ( $p <$

0.0001) showed that the RT increase from the inhibition/switching compared to control condition was larger in older than younger adults. The cost in terms of reaction time for the inhibition/switching condition was  $56.07 \pm 4.92\%$  and  $77.95 \pm 4.67\%$  for the younger and older adults respectively, indicating a larger age-related slowing for inhibition/switching beyond the general slowing seen with age. A significant group by condition interaction was also observed in accuracy ( $p = 0.007$ ) (Figure 2B) with older adults showing larger decline in accuracy in the switching condition. Percent correct responses in younger and older adults respectively for the control task were  $99.52 \pm 0.24\%$  and  $97.58 \pm 1.61\%$ . Accuracy during the inhibition/switching blocks was  $96.19 \pm 0.82\%$  and  $87.39 \pm 2.41\%$  in the younger and older groups respectively.

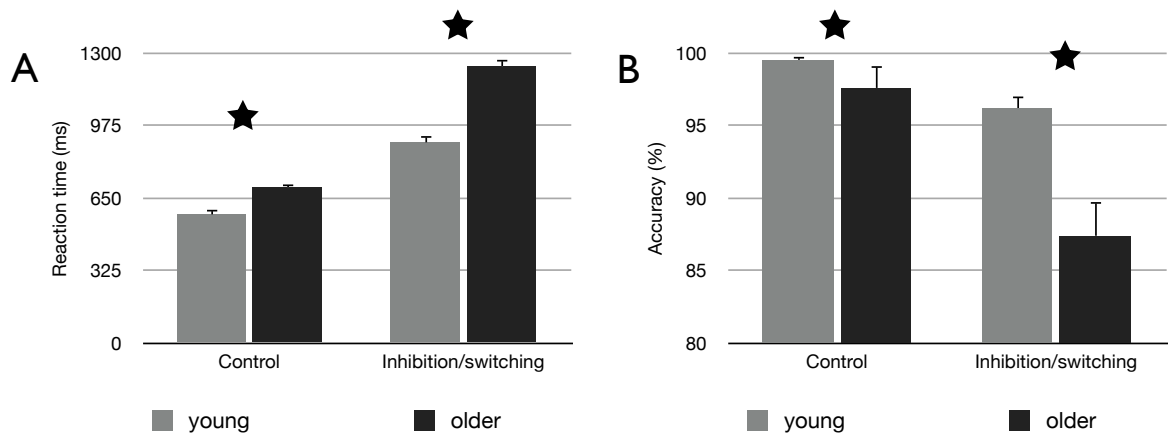


**Figure 2. Modified Stroop behavioral response**

Reaction time in ms (A) and accuracy in percent correct responses (B) were both significantly different between the younger and older groups ( $p < 0.0001$ ). The interaction between age group and block type (control or inhibition/switching) were also statistically significant ( $p < 0.0001$  for reaction time and  $p = 0.007$  for accuracy) and the cost of inhibition/switching was found to be higher in older than younger adults, indicating that the inhibition/switching is affected by age beyond the general effects of slowing and decreased accuracy seen in the control task (color naming). Statistical significance is indicated by a star.

#### 4.5.2. Modified Stroop activation maps

Group analysis of the inhibition/switching blocks revealed significant BOLD and ASL signal increases in similar areas for both groups. Significant BOLD and ASL increases (Figure 3) were found in several regions over cortex including anterior cingulate, part of the frontal, parietal and occipital lobes, as well as some sub-cortical structures covering mainly the putamen. Frontal activation foci were

bilateral and covered part of the middle frontal and inferior frontal gyri. This area of activation also extended partially over pre-central gyrus. Activation over parietal areas was extensive, covering areas 40 and 7 and extending down into occipital areas.

However, no significant difference was detected in a group average map for the contrast old minus young, for either the CBF or BOLD data. ROIs were drawn over the frontal and parietal areas significantly activated within each group during the inhibition/switching blocks (Figure 4). Responses within these ROI's are discussed below.

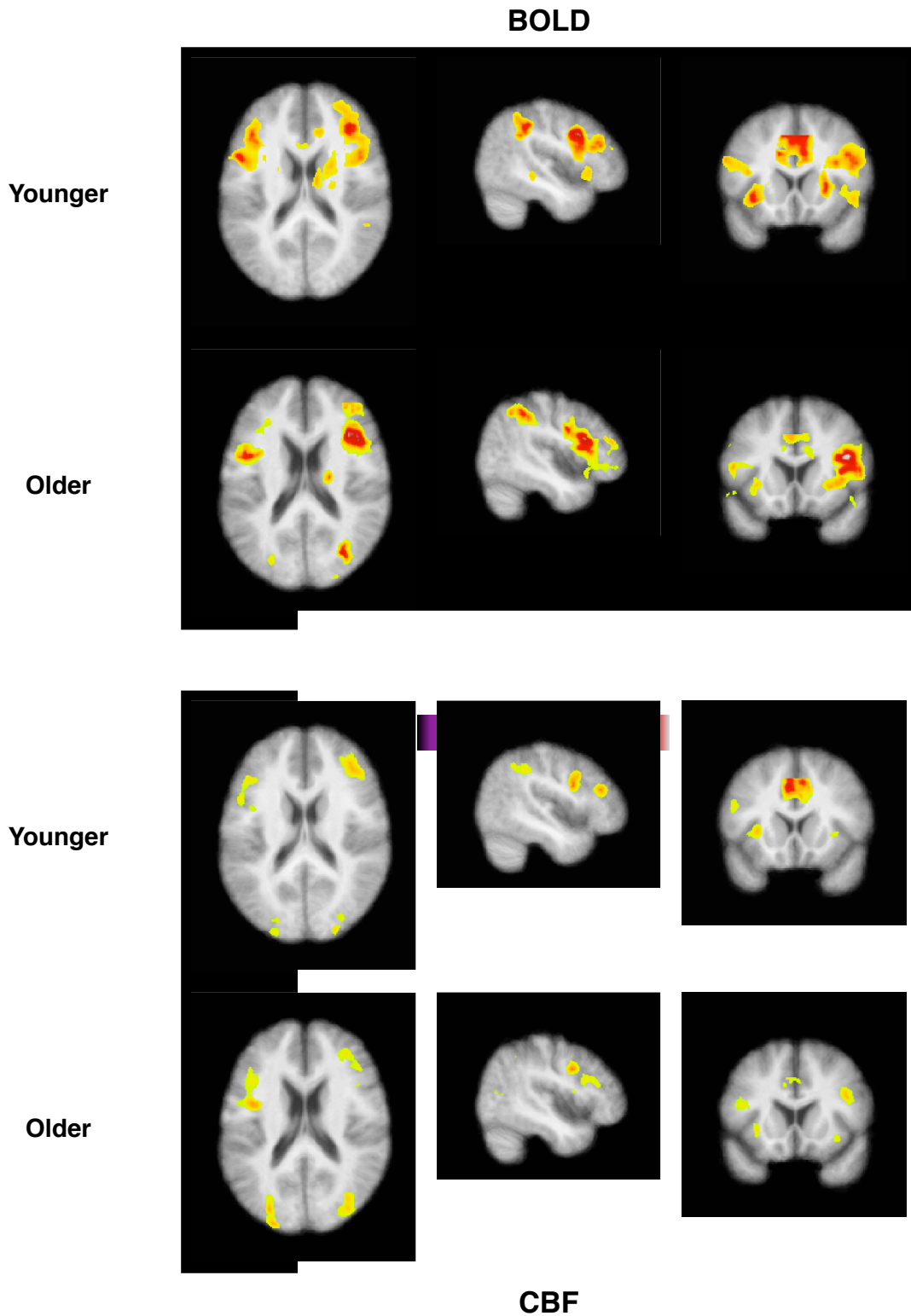


**Figure 3. Modified Stroop Z-score maps**

Group activation maps for BOLD and ASL in response to the Stroop task. These maps show the significant signal changes in response to the inhibition/switching blocks of the task. No significant difference was detected between maps from younger and older adults.

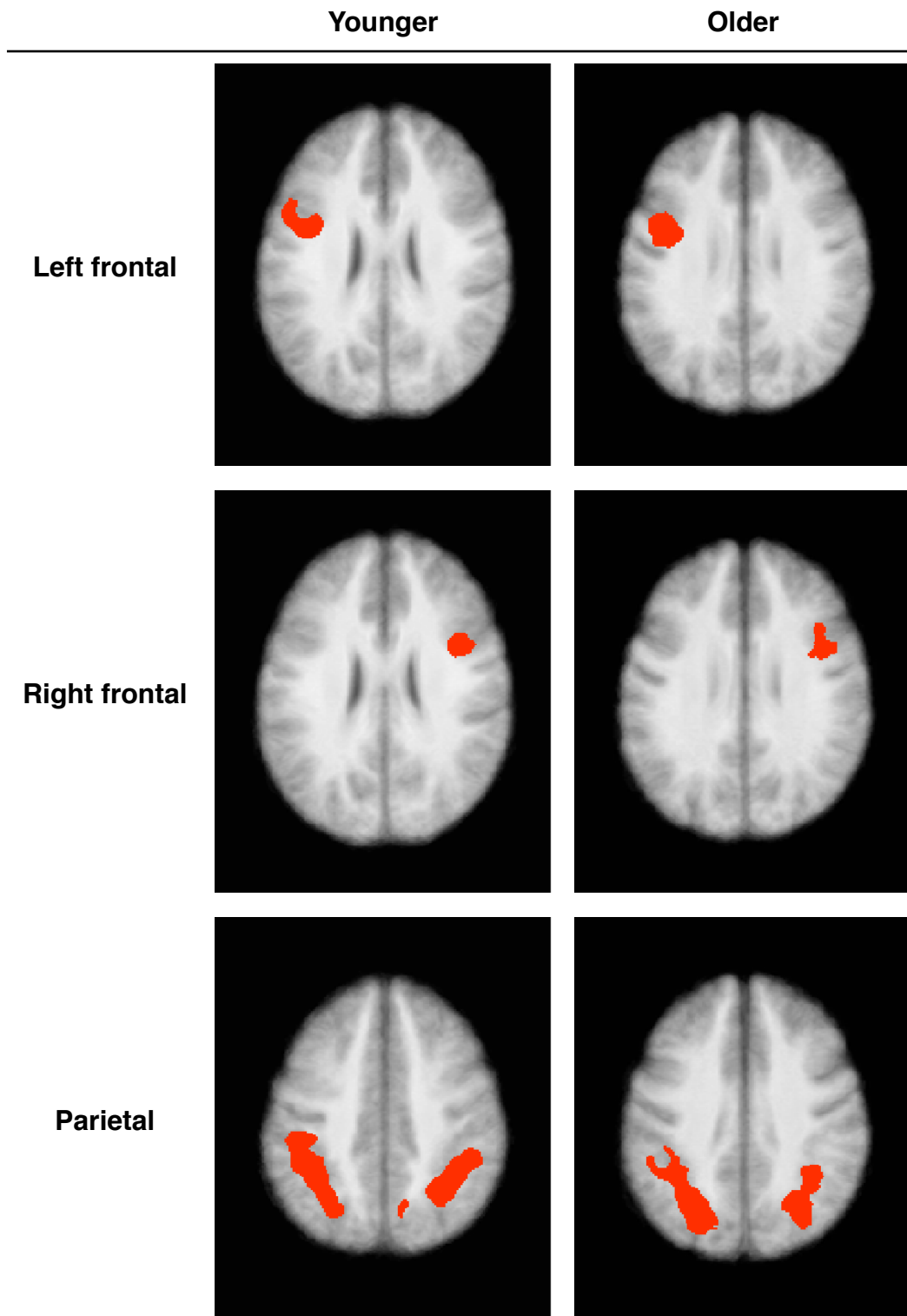


**Figure 4. Modified Stroop task ROIs**

Group activation maps for the modified Stroop task yielded three main foci of cortical significant signal changes. These were used to delineate three ROIs in left frontal, right frontal and parietal cortex. Signal changes and other physiological estimates were quantified within these ROIs for each participant.

### 4.5.3. Stroop evoked responses

Percent BOLD and CBF responses to the inhibition/switching blocks of the modified Stroop task were quantified in three ROIs: left frontal, right frontal and parietal areas. BOLD response amplitude during the task was similar ( $p = 0.85$ ) between the two groups (Figure 5A and Table 2). Percent BOLD signal responses quantified over individual ROIs are shown in Figure 5A and Table 2.

ASL data shows a somewhat different picture, with a significant general age effect ( $p < 0.0001$ ) (Figure 5B and Table 2). Percent changes have been converted to absolute increase in CBF, in units of ml/100g/min for each individual using ROI-average value of resting blood flow for this comparison. The values in percentage, which are used as input into the calibrated fMRI model are shown in Table 2. CBF responses were similar between the two groups in the left frontal ROI ( $p = 0.26$ ), while right frontal ROI showed higher responses in the older group ( $p = 0.002$ ). Finally, the parietal CBF change showed a trend towards higher responses in the older group ( $p = 0.04$ , threshold to account for multiple comparisons of  $p = 0.013$ ).

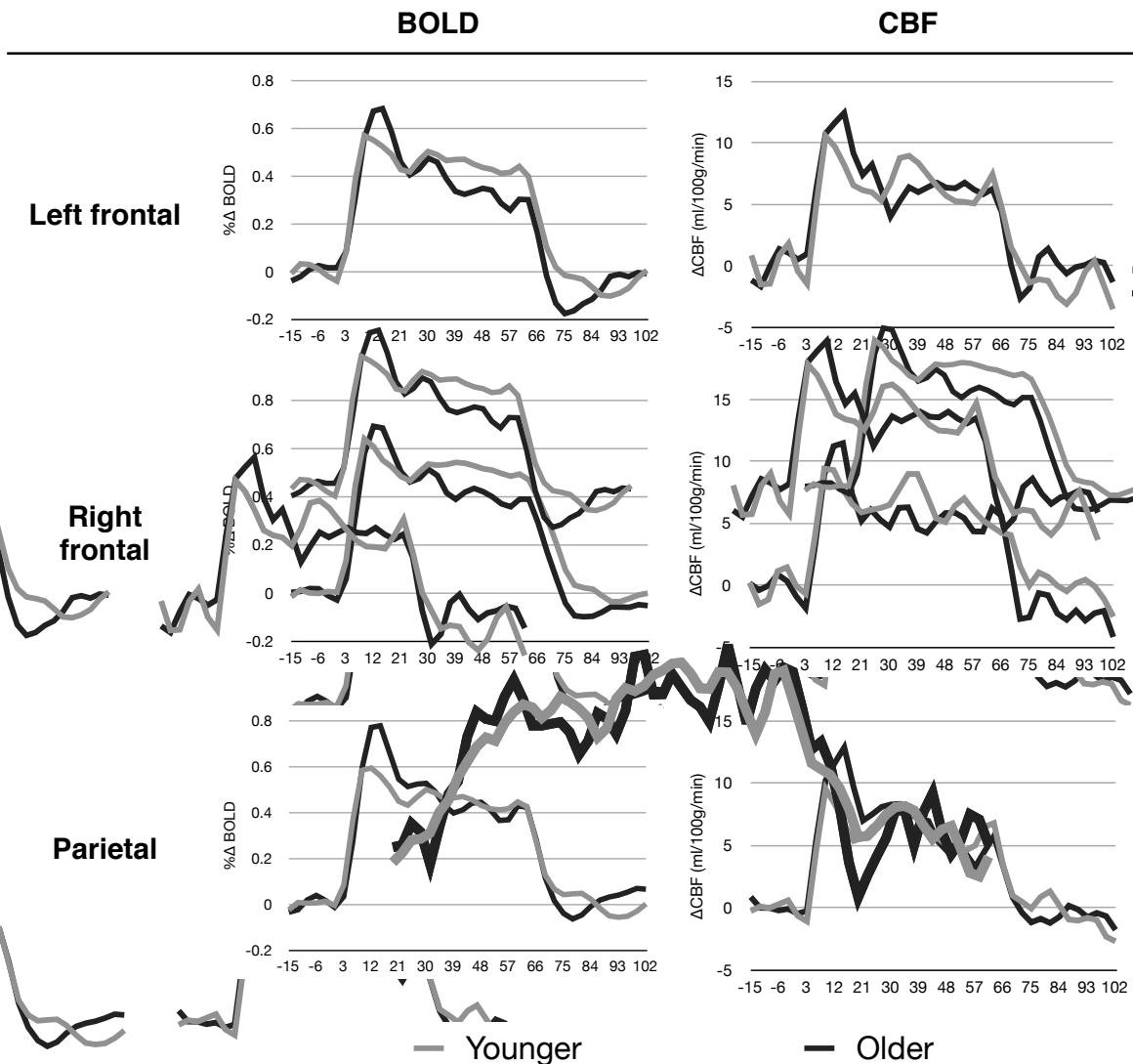


**Figure 5. Percent BOLD and CBF responses to the modified Stroop task**

Time courses showing BOLD and CBF responses to the modified Stroop task over the three functionally-defined ROIs: left frontal, right frontal and parietal areas. Similar BOLD and CBF changes were observed in younger and older adults over all ROIs.

#### 4.5.4. Respiratory manipulation

The hypercapnia protocol led to the expected increase in CO<sub>2</sub>, with stable plateaus within a few breaths. End-tidal values were increased by 4.81 ± 0.15 mmHg in the younger group and 4.49 ± 0.21 mmHg in the older group, from baseline values of 38.50 ± 0.23 mmHg and 39.31 ± 0.33 mmHg in the younger and older groups respectively. End-tidal CO<sub>2</sub> change between the baseline and the hypercapnia block did not differ significantly between the two groups. End-tidal O<sub>2</sub> values increased slightly during the hypercapnia going on average from 106.04 ± 1.12

mmHg to  $109.32 \pm 1.10$  mmHg in the younger group and from  $101.61 \pm 0.99$  mmHg to  $105.54 \pm 0.94$  mmHg in the older group. The manipulation was tolerable for participants of both age groups, with discomfort ratings of  $2.16 \pm 0.17$  and  $2.26 \pm 0.19$  for the younger and older groups respectively on a possible range of seven points (Banzett et al. 1996).

#### **4.5.5. Vascular parameters**

In contrast to the BOLD and CBF responses to the Stroop task, which were similar in both groups, other hemodynamic signals were found to be generally decreased in the older group. More specifically, BOLD responses to hypercapnia were found to be significantly lower in pooled ROIs ( $p < 0.0001$ ) in the older group as compared to the young (Figure 6 and Table 2). Individual ROIs were also associated with a significantly lower BOLD signal change in the older adults. Responses to the hypercapnia challenge were quantified over the three Stroop ROIs, as well as in complete grey matter. Average BOLD signal changes to  $\text{CO}_2$  in grey matter were found to be  $1.48 \pm 0.07\%$  and  $1.01 \pm 0.06\%$  for younger and older adults respectively ( $p < 0.0001$ ). All individual ROI average values are shown in Table 2.

Blood flow responses showed the same trend and average CBF responses in units of ml/100g/min were generally lower in the older group and the main effect of age over all ROIs was found to be significant ( $p < 0.0001$ ) (Figure 7). Individual ROI averages can be found in Table 2. CBF changes over gray matter were found to be significantly lower in the older group, with values of  $14.32 \pm 1.01$  ml/100g/min in the younger and  $10.00 \pm 1.24$  ml/100g/min in the older group ( $p < 0.01$ ). Left frontal estimates were on the other hand similar between the two groups ( $p = 0.13$ ), while right frontal estimates showed the largest difference between groups ( $p < 0.0002$ ). Finally, results in the parietal ROI showed a trend towards lower values in the older group ( $p = 0.02$ ). While flow changes in terms of absolute flow represent a more physiologically meaningful quantity, these changes are often reported as percentages in the extant literature. To facilitate comparisons with previous literature and since percent change values in CBF are used as input into the calibrated fMRI model, these values are reported in Table 2.

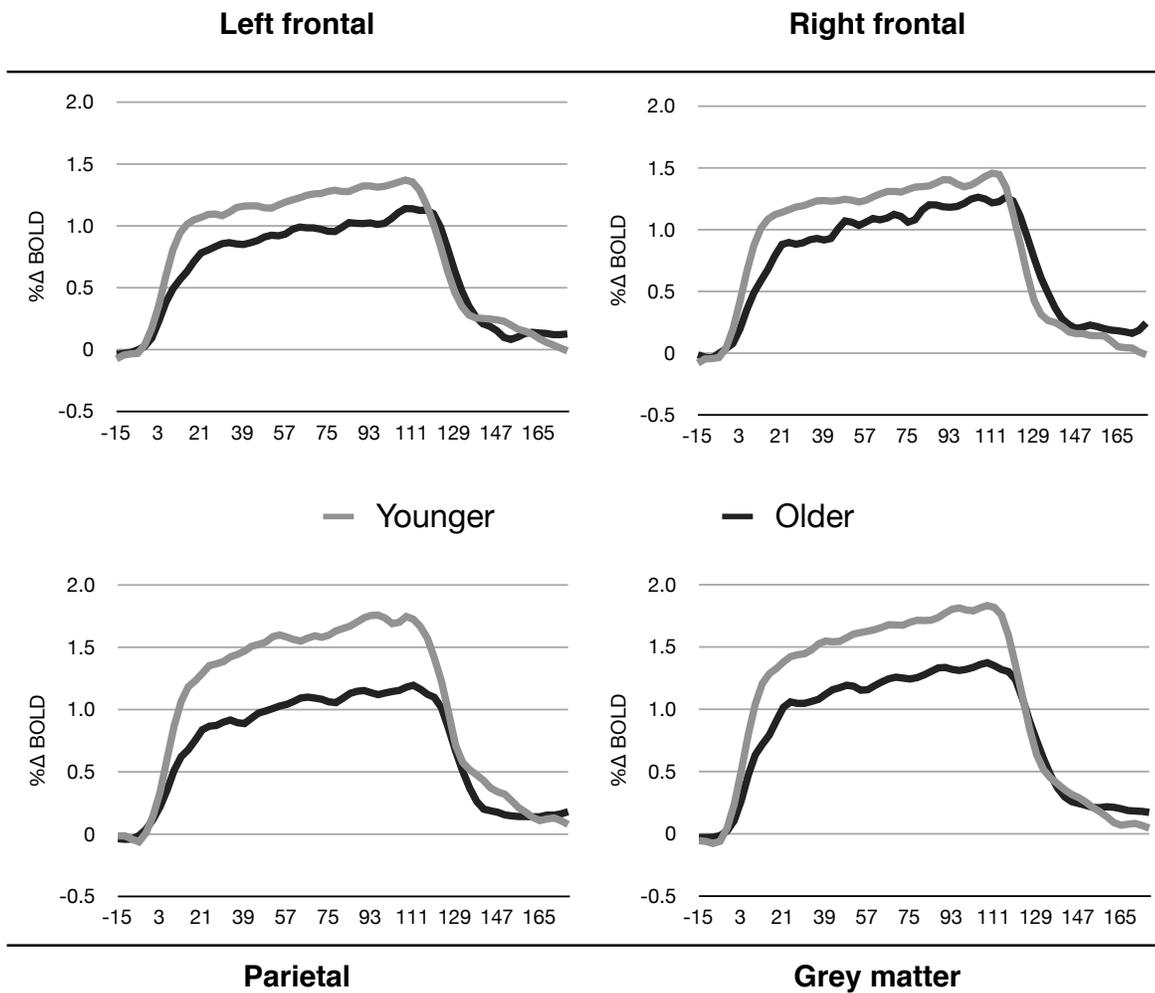


**Figure 6. BOLD hypercapnia time courses**

Time courses of percent BOLD signal change in response to hypercapnia over all functionally determined ROIs (left frontal, right frontal, parietal) and over all grey matter. BOLD responses to hypercapnia were lower in all ROIs in the older group ( $p < 0.0001$ ).

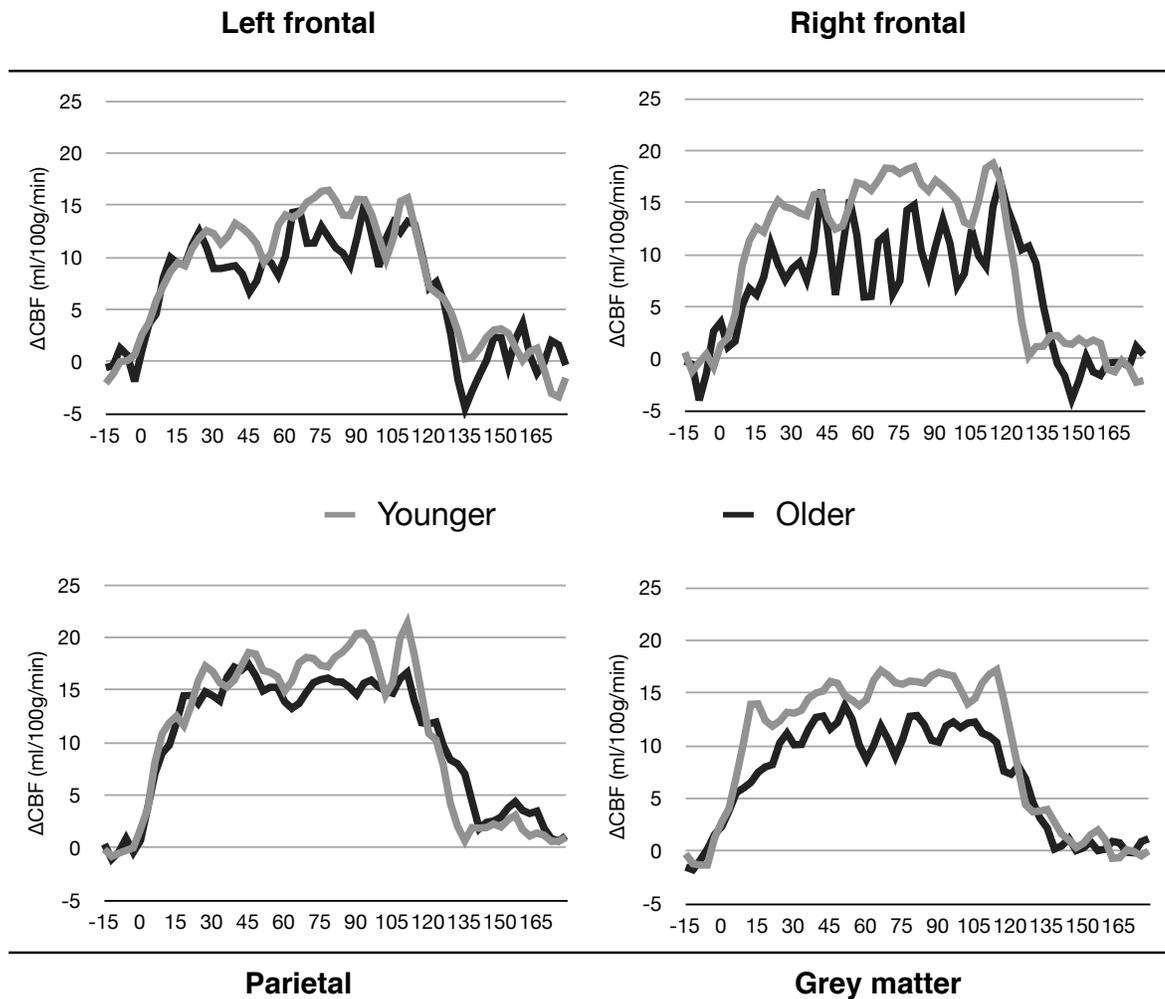


**Figure 7. CBF hypercapnia time courses**

Time courses of CBF change with hypercapnia, in absolute units of ml/100g/min over all functionally determined ROIs (left frontal, right frontal, parietal) and over all grey matter. Though an overall effect of age was found and CBF response to hypercapnia was found to be generally lower in the older group ( $p < 0.003$ ), individual ROIs did not show a significant difference.

Percent BOLD and CBF changes during hypercapnia can also be converted to cerebrovascular reactivity (CVR) by dividing the percent change in CBF or BOLD by the change in end-tidal PCO<sub>2</sub> (Graham et al. 1994; Forbes et al. 1997; Mandell et al. 2008; Gauthier et al. 2012a). CVR is likely to be a factor in determining the amplitude of task-induced changes in BOLD and CBF, since it quantifies the increase in signal per unit of vasodilatory signal. Because end-tidal PCO<sub>2</sub> increases were similar between the two groups, CVR values follow the same trend as percent changes. BOLD CVR was found to be significantly lower in the older group in pooled ROIs ( $p < 0.0001$ ), with values of  $0.31 \pm 0.06$  % $\Delta$ BOLD/mmHg in

the younger group and  $0.23 \pm 0.01$  % $\Delta$ BOLD/mmHg in the older group over grey matter. BOLD CVR was also significantly lower in all others individual ROIs ( $p < 0.003$  in all cases), as shown in Figure 8B and Table 2.

CBF vascular reactivity was more similar between the two groups than BOLD reactivity measured, though generally also significantly lower over all ROIs in the older group ( $p < 0.0001$ ) (Figure 8C and Table 2 for individual ROI quantifications). Grey matter and right frontal CVR were found to be significantly lower in the older group ( $p < 0.004$ ), with values of  $3.00 \pm 0.18$  (ml/100g/min)/mmHg in the younger and  $2.14 \pm 0.22$  (ml/100g/min)/mmHg in the older group over grey matter. The left frontal estimates were similar between the two groups however ( $p = 0.26$ ), and parietal estimates showed a trend towards lower values in the older participants ( $p = 0.04$ ). CVR is often expressed as percentage CBF change in the literature and, to facilitate comparison with other studies, these values expressed as percentages are included in Table 2.

Baseline CBF was also found to be significantly lower across all ROIs in the older group as compared to the younger ( $p < 0.0001$ ) (Figure 8A and Table 2). Average grey matter baseline CBF was  $57.94 \pm 2.51$  ml/100g/min in younger and  $50.20 \pm 1.90$  ml/100g/min in the older group. Individual ROI averages are shown in Table 2 and these generally show a trend towards lower values in the older group, with  $p$  values slightly above the multiple comparison threshold ( $p$  values between 0.02 and 0.05, with threshold for multiple comparisons at  $p = 0.013$ ).

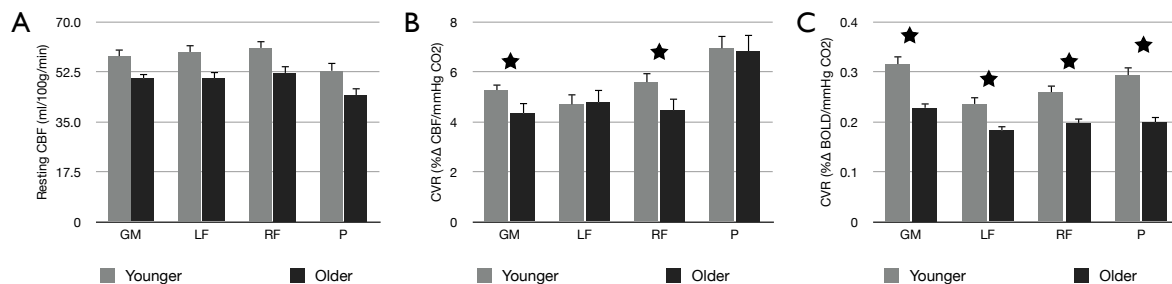


**Figure 8. Baseline CBF and CVR**

This figure shows baseline CBF values in units of ml/100g/min (A), CBF CVR in units of percent CBF change per mmHg end-tidal PCO<sub>2</sub> increase (B), and BOLD CVR in units of percent BOLD signal change per mmHg end-tidal PCO<sub>2</sub> increase (C) for all ROIs, where GM is grey matter, LF is left frontal, RF is right frontal and P is parietal. Baseline CBF showed a trend towards a lower

baseline flow in the older group over pooled ROIs ( $p < 0.0001$ ), while only BOLD CVR differed significantly over all ROIs ( $p < 0.002$ ). Significance at the individual ROI level is indicated by a star.

#### 4.5.6. Calibrated fMRI estimates

BOLD and CBF percent changes in response to  $\text{CO}_2$  can be combined to estimate the maximum possible BOLD signal change, also called  $M$  in the calibrated fMRI literature. The calibration parameter  $M$  was quantified in individual subjects and ROIs (Figure 9A and Table 2). Values pooled over all ROIs showed a significant decrease in  $M$  values in the older group ( $p = 0.003$ ). In individual ROIs, the average values in the older group were generally lower than in the younger, and a tendency towards significance was identified in grey matter, with values of  $5.72 \pm 0.22\%$  and  $5.00 \pm 0.30\%$  for younger and older participants respectively ( $p = 0.05$ ). Parietal estimates in the older group were found to be significantly lower than in the younger group ( $p = 0.003$ ). Frontal estimates did not differ significantly between the two groups ( $p \geq 0.09$ ).

Task-evoked  $\text{CMRO}_2$  in each ROI was determined using group average values for all input parameters to benefit from additional averaging. Evoked  $\text{CMRO}_2$  estimates during the modified Stroop task over individual ROIs can be found in Figure 9B and Table 2. These estimates are associated with high variance since they are derived from a combination of three noisy measurements (percent BOLD and CBF evoked by the task and  $M$ ) and no significant age effect was found across ROIs.

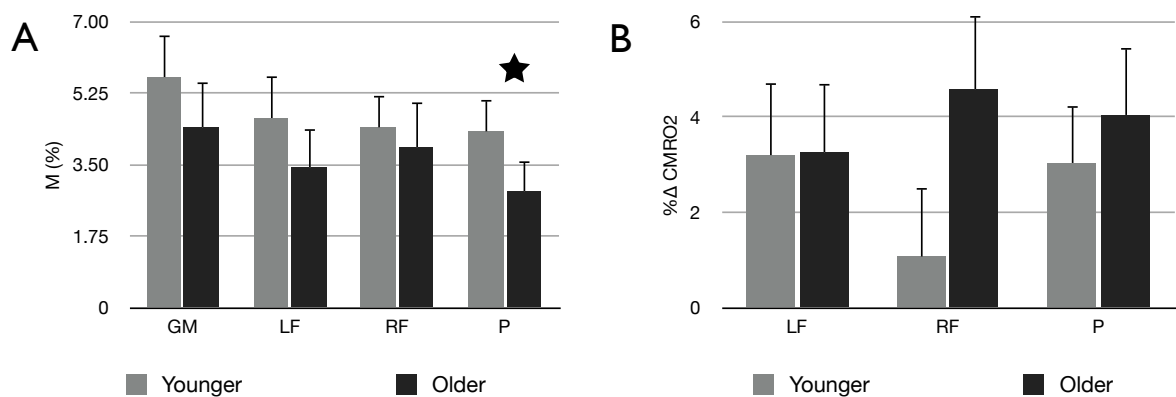


**Figure 9.  $M$  and  $\text{CMRO}_2$  values**

This figure compares the calibrated fMRI parameters  $M$  (A) and percent evoked  $\text{CMRO}_2$  to the modified Stroop task (B) between the younger and older groups.  $\text{CMRO}_2$  was only quantified in the

functionally-determined ROIs (LF = left frontal, RF = right frontal and P = parietal), while  $M$  was quantified over an additional grey matter ROI (GM) since it is not a task-based measurement. Values of  $M$  were found to be generally lower in the older group ( $p = 0.0002$  for pooled ROIs). Similar  $CMRO_2$  estimates may reflect the fact that variance on this estimate is high since it is a composite estimate from four measurements. Significance at the individual ROI level is indicated by a star.

#### 4.5.7. Temporal SNR

Temporal SNR of BOLD and CBF was quantified using the Stroop time series. This quantity represents the average baseline term over each time series, divided by the residuals from the GLM fit, averaged over all participants within each group. Temporal SNR is a measure of the signal to noise ratio associated with temporal fluctuations in the signal, arising from a combination of instrumental thermal noise and fluctuations from physiological sources (e.g. cardiac and respiratory). As can be qualitatively ascertained in the maps shown in Figure 9A, tSNR of the ASL data was lower in the older group as compared to the younger. This decrease seems especially pronounced in more frontal areas. BOLD tSNR however, was similar between the two groups (Figure 10A). Quantifications within the different ROIs confirmed that tSNR was significantly lower in all ROIs used in this study for ASL ( $p < 0.0001$ ) (Figure 10B and Table 2), but no significant difference was identified for BOLD data ( $p = 0.48$ ) (Figure 10C and Table 2). BOLD temporal SNR values were  $225.55 \pm 7.71$  and  $205.35 \pm 9.25$  in grey matter for young and older respectively. ASL temporal SNR was generally fairly low and even lower across all ROIs in the older group ( $p < 0.0001$ ), with values of  $2.80 \pm 0.13$  and  $1.81 \pm 0.13$  in the younger and older group respectively in the grey matter ROI ( $p < 0.0001$ ). All ROI average values can be found in Table 2.

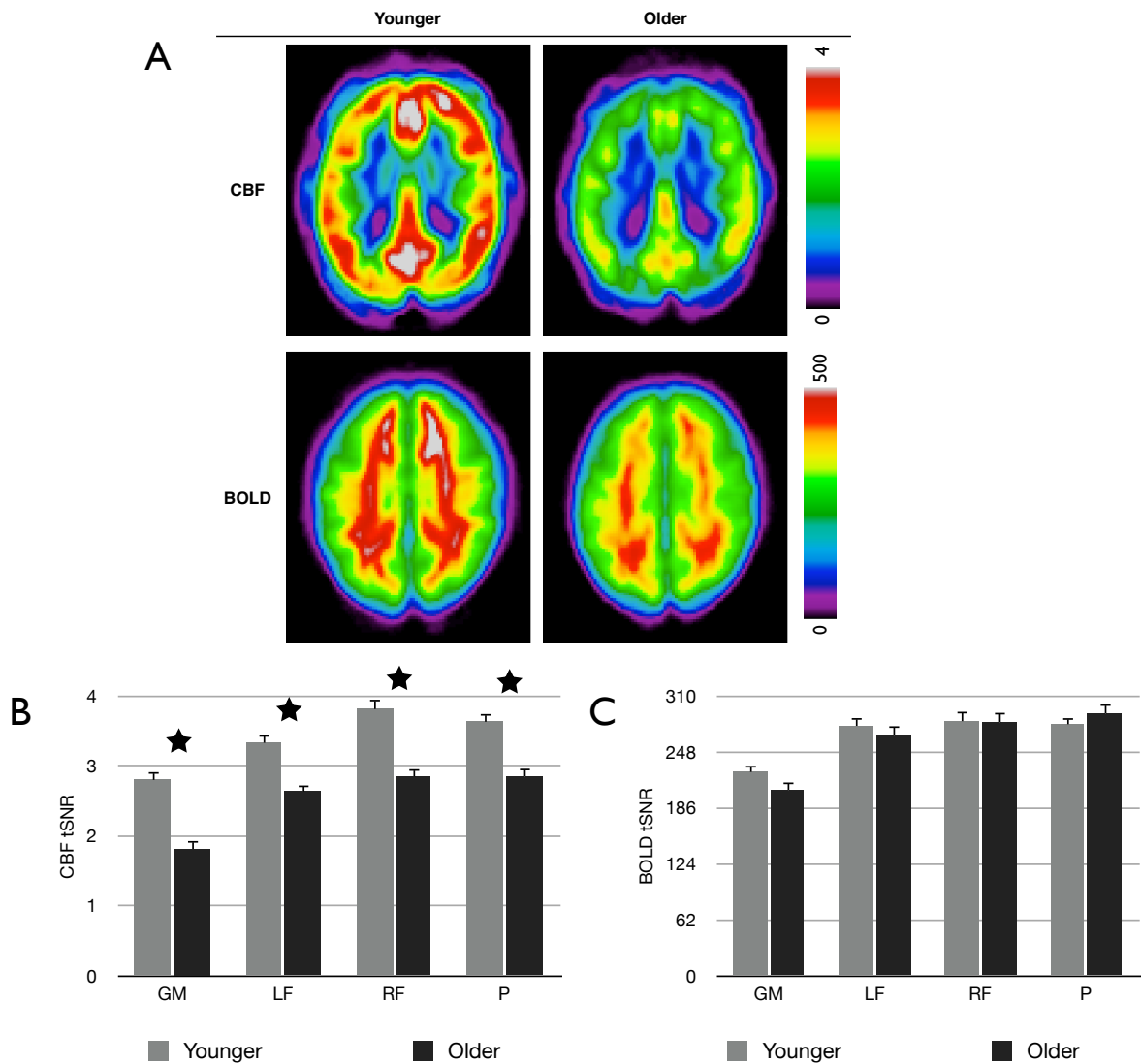


**Figure 10. Temporal SNR of CBF and BOLD measurements**

Temporal SNR maps of ASL and BOLD (A) show a decrease in ASL tSNR over all grey matter in the older group, with some spatial heterogeneity. Quantification of tSNR in functionally-defined and grey matter ROIs show that ASL tSNR (A) was significantly lower in all ROIs ( $p < 0.0001$ ), while BOLD tSNR (B) was found to be fairly stable across age. Significance at the individual ROI level is indicated by a star.

	Younger			Older				
	Left frontal	Right frontal	Parietal	Grey matter	Left frontal	Right frontal	Parietal	Grey matter
<b>Stroop</b>								
%Δ BOLD	0.50 ± 0.04	0.50 ± 0.04	0.47 ± 0.04	1.48 ± 0.07	0.48 ± 0.03	0.50 ± 0.05	0.49 ± 0.04	
%Δ CBF	11.92 ± 1.73	9.47 ± 1.70	12.18 ± 1.40	24.92 ± 1.37	13.80 ± 1.53	14.21 ± 1.52	17.56 ± 1.44	
%Δ CMRO <sub>2</sub>	3.20 ± 1.54	1.07 ± 1.46	3.04 ± 1.23	0.31 ± 0.06	3.25 ± 1.48	4.57 ± 1.58	4.04 ± 1.43	
<b>Hypercapnia</b>								
%Δ BOLD	1.11 ± 0.07	1.21 ± 0.07	1.37 ± 0.07	1.48 ± 0.07	0.81 ± 0.05	0.86 ± 0.06	0.87 ± 0.06	1.01 ± 0.06
%Δ CBF	22.16 ± 2.17	26.56 ± 2.08	32.78 ± 2.67	24.92 ± 1.37	21.62 ± 2.60	19.55 ± 1.96	30.55 ± 3.52	20.67 ± 2.58
%Δ BOLD/ mmHg	0.24 ± 0.02	0.26 ± 0.02	0.29 ± 0.02	0.31 ± 0.06	0.18 ± 0.01	0.20 ± 0.01	0.20 ± 0.01	0.23 ± 0.01
%Δ CBF/ mmHg	4.69 ± 0.44	5.58 ± 0.39	6.93 ± 0.53	5.26 ± 0.26	4.77 ± 0.55	4.47 ± 0.51	6.83 ± 0.70	4.34 ± 0.44
<b>Baseline</b>								
CBF	59.46 ± 2.85	60.87 ± 2.77	52.86 ± 3.09	57.94 ± 2.51	50.07 ± 2.58	52.12 ± 2.76	44.39 ± 2.74	50.20 ± 1.90
M	5.24 ± 0.48	4.78 ± 0.31	4.67 ± 0.03	5.72 ± 0.22	4.78 ± 0.31	4.33 ± 0.36	3.41 ± 0.27	5.00 ± 0.30
<b>SNR</b>								
BOLD	276.71 ± 10.69	281.86 ± 11.14	278.44 ± 8.47	225.55 ± 7.71	265.87 ± 11.30	280.69 ± 12.28	290.18 ± 11.06	205.35 ± 9.25
ASL	3.33 ± 0.13	3.81 ± 0.15	3.63 ± 0.13	2.80 ± 0.13	2.63 ± 0.12	2.84 ± 0.13	2.85 ± 0.12	1.81 ± 0.13

## **Table 2. ROI quantification results**

This table compiles all the group average ROI results. BOLD responses to the Stroop and hypercapnia are expressed as percent changes, CBF responses to the Stroop and hypercapnia challenges are expressed in ml/100g/min and percent change, evoked CMRO<sub>2</sub> is expressed in percent change, baseline CBF in ml/100g/min and the *M* value represents a percent. Temporal SNR values are also shown for each ROI. Stroop responses were only quantified in the three functionally-defined ROIs (left frontal, right frontal and parietal), while responses to the hypercapnia challenge and baseline properties were additionally quantified in complete grey matter. Significance of results are expressed using stars with one, two and three stars being used to show  $p < 0.05$ , 0.01 and 0.001 respectively. An alpha level equivalent to 0.013 is used to assess significance when correcting for multiple comparisons across all measures (CBF changes where only compared between groups in ml/100g/min) (following page).

## **4.6. Discussion**

Neuroimaging studies of cognition typically use the BOLD signal to localize brain regions involved in the performance of a task. Cognitive studies of aging often compare the BOLD signal changes in groups of young and older adults in the context of tasks known to be associated with significant behavioral age-related differences. The assumption made in such studies is that the BOLD signal can be taken as a direct index of neuronal activity. However, there is reason to believe that this simplifying assumption may not be valid when comparing groups of widely different age, given that significant vascular changes are known to occur during adult life (O'Rourke et al. 2007; Samanez-Larkin et al. 2008; Chen et al. 2011; Lu et al. 2011). The results of the present study indicate that caution must be exercised when making these direct comparisons and that there are in fact profound vascular biases associated with age. Age-related vascular changes may mask some metabolic differences and lead to erroneous conclusions when only BOLD results are taken into account to make inferences about the neuronal resources used during performance of a task.

### **4.6.1. BOLD measurement of the cognitive task**

The results presented here go beyond the standard sets of measures usually collected in the context of a cognitive imaging study of aging, but do in fact include them. If one were to look simply at the BOLD data evoked by the modified Stroop task collected here (Figures 3 and 5), one would draw the conclusion that older adults use similar neuronal resources to perform this task as younger individuals,

but that this similarity stands in contrast to the widely differing behavioral responses (Figure 2). The lower behavioral performance of older adults in the context of similar brain responses could be suggestive of a ceiling effect, possibly due to brain atrophy in older adults (Reuter-Lorenz et al. 2008; Schneider-Garces et al. 2010). This task is fairly difficult, since a set of two rules and two possible answers must be kept in mind at all times, and any set of rules and answer may be required at any time during the inhibition/switching blocks. It could therefore be that the older adults have reached their own maximal usage of neuronal resources and that they in fact perform more poorly on the task because they could not recruit the additional resources they needed to match the performance of younger adults (Park et al. 2009; Reuter-Lorenz et al. 2010). One could speculate this to be due to atrophy or other changes such as decreased perceptual acuity and dedifferentiation from changes in neuromodulatory system (Baltes et al. 1997; Li et al. 2002; Park et al. 2009).

The results obtained from a BOLD-only acquisition of a cognitive task do not however allow us to answer these questions, given the physiological ambiguity of the BOLD signal. While studies have shown that the amplitude and shape of the BOLD response is related to synaptic activity in individual primate subjects (Logothetis et al. 2001; Shmuel et al. 2002), the relationship between synaptic activity measured using local field potential electrophysiology and BOLD signal amplitude and shape is complex and non-linear (Magri et al. 2012). Neuronal activity leads to the release of a variety of vasoactive signals (Girouard et al. 2006; Lecrux et al. 2011) that determine the characteristics of the hemodynamic response measured using the BOLD contrast. Though the main mediators of neurovascular coupling are fairly well established, the quantitative relationship between these molecules and the blood flow and volume increase is unknown (Girouard et al. 2006; Lecrux et al. 2011). Furthermore, we do not as yet know how all these mechanisms are affected by aging. More specific vascular and metabolic information is needed to better interpret the observed BOLD responses in terms of neuronal activity, since BOLD alone cannot be readily converted into a quantitative measure of synaptic activity and since the factors that determine this relationship are likely to be affected by age.

#### **4.6.2. Blood flow measurements during the cognitive task**

While these questions cannot all be answered with the present dataset, the additional information provided does improve our understanding of the physiological events occurring. One pertinent piece of information is provided by blood flow changes during the task. ASL techniques allow the measurement of changes in cerebral blood flow (Williams et al. 1992), which represents a more physiologically-specific quantity and can inform us on one of the factors contributing to the BOLD signal. Here we can see that the CBF change evoked by the task was in most ROIs, as seen for BOLD, similar between the two groups in terms of amplitude and shape (Figure 3 and 5). Therefore, this measurement also leads us to believe that similar neural resources are used by younger and older adults for the performance of this task. A modest trend towards higher CBF increases in all ROIs and a statistically significant difference in the right frontal ROI indicate, however, that there may be a tendency for older individuals to have a larger increase in metabolism and hence, presumably, in neuronal activity during the task. This higher response may furthermore be highest in some regions, which agrees well with previous literature on lateralization changes in cognitive studies of aging (Cabeza 2002; Park et al. 2009; Cappell et al. 2010; Reuter-Lorenz et al. 2010; Schneider-Garces et al. 2010).

#### **4.6.3. Hypercapnic responses**

It may, however, be that similar signal changes in younger and older adults reflect different metabolic expenditures if the hemodynamic properties of older brains are changed due to vascular impairments. Aging has been shown to be associated with vascular impairments such as arterial hardening from increased collagen content of arterial walls and decreased vascular density (Sonntag et al. 1997; O'Rourke et al. 2007; Brown et al. 2011). Because these have the potential to profoundly affect cerebral blood flow, they could also affect the BOLD signal amplitude measured in response to the task. The clearest indication that this may be the case is that the BOLD response to a hypercapnia challenge was found to be significantly reduced in the older adults. CO<sub>2</sub> has vasodilatory properties and its inhalation triggers an increase in blood flow throughout grey matter. Furthermore,

previous studies have shown that this increase in blood flow, and hence in BOLD signal, is linearly proportional to the concentration of CO<sub>2</sub> in the inspired air, when CO<sub>2</sub> is given as here in small concentrations (Hoge et al. 1999b; Stefanovic et al. 2006; Mark et al. 2010). The reduced BOLD responses to hypercapnia in older adults confirm the capability of BOLD to capture age-related physiological differences in the brain regions probed in the present study. It also indicates that there are some underlying hemodynamic changes in the elderly, not visible from BOLD measurements of task alone. A reduced reactivity to CO<sub>2</sub> could indicate that the coupling of vasodilatory signal to flow increase is degraded in older subjects. This could be because of vessel hardening, especially since the brain is known to be one of the only organs in the body without protection against the pulsatile effects of flow, and may hence be more sensitive to long-term damage (O'Rourke et al. 2007). However, because the BOLD signal is intrinsically ambiguous and arises from a combination of sources, we cannot know from this alone which components of the response is affected by aging.

Once again, we can turn to the ASL data to get a more physiologically specific measurement. An additional advantage of ASL over BOLD measurements is that resting blood flow in absolute units of ml/100g/min can readily be obtained. This is not only an important parameter of itself, but can also be used to convert percent changes into flow change in absolute units. This allows quantitative comparisons between groups, such as in younger and older adults, known to exhibit differences in baseline flow (Chen et al. 2011). Both baseline blood flow and absolute changes in response to hypercapnia were found to be lower in older adults across pooled ROIs. This may be indicative of a lower vascular tone in the older adults, possibly due to damage to blood vessel walls from the pulsatile effect of blood (O'Rourke et al. 2007). This finding is furthermore in agreement with previous literature also showing age-related decreases in flow CVR (Ances et al. 2009; Lu et al. 2011).

#### **4.6.4. Calibrated fMRI measurements**

Taken together, CBF and BOLD response to hypercapnia can be used to calculate the BOLD calibration factor  $M$ . This corresponds to the BOLD signal attenuation at rest, attributable to the baseline deoxyhemoglobin (dHb) brain content. Because

this is calculated using a ratio of BOLD and CBF, this measurement suffers however from having a low SNR. Values of  $M$  were found to be significantly lower in the older group than in the younger group for pooled ROI values. A similar trend towards lower  $M$  values in older adults has been observed in other calibrated fMRI studies of aging (Ances et al. 2009; Mohtasib et al. 2012). This means that in the older group, the amplitude scaling of BOLD for a given fractional change in dHb is reduced due to a lower initial dHb content of venous blood. Because blood flow increases more than metabolism following neuronal activity (Hoge et al. 1999a; Buxton 2010), it is in part the dHb concentration present at rest that determines how much BOLD signal can increase during performance of a task (since baseline dHb is one of the sources of decreased BOLD signal that is diluted by activity-dependent flow increases). Because the BOLD amplitude scaling is reduced, it may therefore be that a larger amount of oxidative metabolism is needed to evoke a similar CBF and BOLD response.

The measurement of BOLD and CBF responses to the task, combined with the  $M$  parameter estimated before, can be used to estimate the fractional change in  $CMRO_2$  evoked by the task. This parameter represents a more specific physiological property than the BOLD signal, and may be compared between groups. Furthermore, since the greater part of the metabolism evoked following neuronal activity is thought to be oxidative (Ishii et al. 1996; Mintun et al. 2002; Yamauchi et al. 2002; Hattori et al. 2004; Ito et al. 2005; Ibaraki et al. 2008; Ibaraki et al. 2010), it is also a quantity more directly related to neuronal function than BOLD signal or measurements of CBF. The precision of this estimate is unfortunately limited, given that it is computed as a function of four low-SNR measures. Although no significant differences were thus detected in this group, the differences in BOLD and CBF responses to  $CO_2$  were consistent with a trend towards an increase in  $CMRO_2$  in the older group in response to the task, despite the similarity in the measured responses to the task.

#### **4.6.5. Potential confounds**

In this study, we sought to isolate the effects of age and selected our older cohort using very strict selection criteria to exclude older adults with vascular risk factors

such as high blood pressure (including medically-controlled blood pressure), hypercholesterolemia and smoking. However, the Canadian Health Measure Survey indicates that adults in the age range included in this study (55 to 75 years) may be at a vulnerable time of life for developing heart conditions. Within this age range the incidence of high blood pressure increases very steeply from 18.4% in the 40-69 years population to 53.2% observed for the next two decades. Adults included in this study were also highly educated, with an average number of years of education at  $16.3 \pm 3.4$ , corresponding to five years of post-secondary education in the province of Quebec. This is above the national average of 13.2 years for adults between the ages of 25 and 54 years reported from the 1996 Canadian census. Therefore, the results of this study likely represent an underestimation of the effects observable in the general aging population, given that these individuals are in better health and more educated than the general population within the same age range. If the effects of age on BOLD signal properties are expected to stem from deteriorating vascular health, then the healthier the arteries, the smaller the effects of age will be. In this case, since our exclusion criteria ensured that none of our participants had the usual hallmarks of poor vascular health, such as high blood pressure, high blood cholesterol and fasting glucose levels, we expect these older adults to be much more similar in terms of vascular health to young participants than less healthy older adults.

The relatively small amplitude of difference between the two groups may also be attributable to several other factors. The sample sizes used here, though larger than those used in most other calibrated fMRI studies, may still be too small to detect the small differences present in a group of very healthy older adults, particularly when only a single scanning run of the modified Stroop task was performed. In typical cognitive fMRI studies, several repetitions of the task are usually performed to maximize statistical power. However, time constraints in this comprehensive imaging protocol, which also included a thoracic MRI exam to be discussed in a separate publication, precluded the acquisition of additional modified Stroop runs. Finally, baseline  $CMRO_2$  may be different in the two groups. There is some indication that baseline  $CMRO_2$  may be changed in older adults, though the existing literature does not agree on the direction of the change, with

PET results showing a decrease with age (Yamaguchi et al. 1986; Leenders et al. 1990; Marchal et al. 1992) and results from a recent MRI study showing an increase (Lu et al. 2011). Therefore, even if equivalent fractional changes in  $CMRO_2$  are estimated, it may be that there is in fact a difference in evoked  $CMRO_2$  in absolute units between the two groups, when expressed in terms of micromolar  $O_2$  usage for a given tissue volume. While we cannot determine here if this is the case, future studies using a method recently developed in our group will address this issue (Gauthier et al. 2012c).

Another parameter that was noted to be significantly different in the two age groups was the temporal signal-to-noise ratio of ASL (tSNR) as illustrated in Fig 10B. Temporal SNR takes into account the temporal fluctuations in time series. These fluctuations are thought to be a combination of instrumental thermal noise and fluctuations from physiological sources such as heart beats and respiration changes (Kruger et al. 2001; Triantafyllou et al. 2005). This difference in ASL tSNR can be contrasted to the BOLD tSNR in grey matter, which was much more comparable between the two groups and for which the difference did not attain statistical significance (Fig. 10C). As the variance of BOLD signals in grey matter is believed to be dominated by physiological noise under the conditions of our study (3 Tesla, large voxels), it would appear that the age-related differences ASL tSNR might be due to physical noise sources that affect the actual MRI signal strength and instrumentation noise. This is also supported by the observation that BOLD tSNR in the young group was substantially higher in white matter (Fig. 10A), where instrumental noise is likely to be more predominant. Higher instrumental noise in older subjects could be associated with differences in coil loading or shimming associated with systematic postural and anatomical differences that were noted (*e.g.* kiphotic spine, higher body fat). Alternatively, the lower ASL tSNR could reflect an increased variability in the ASL labeling signal, in addition to a reduction in its mean amplitude. Such an increase in variability might be due to differences in heart rate and blood flow velocity in the two groups, or other physiological factors. The impact of age on ASL labeling parameters for pseudo-continuous ASL sequences are unknown, but reduced labeling efficiency has been previously demonstrated for pulsed ASL sequences (Campbell et al. 2006). This means that

age-dependent comparisons of neuronal activation based solely on the spatial extent of significant ASL response in a functional study must be treated with caution as this metric may be biased by the different tSNR levels.

#### **4.6.6. Limitations**

The sample size and limited data averaging possible in this study did not permit the investigation of the difference contrast between the inhibition/switching and control components of the task. While this does not prevent asking questions about the physiological properties of the areas of the brain involved in the task, it allows only a limited discussion of their implications in the context of cognitive aging.

Furthermore, it may be that the task used in this study was not optimal for finding differences between young and old adults. Tasks with a switching component, such as the modified Stroop task used here, are expected to yield bilateral prefrontal activation, since these areas are involved both in inhibition and task switching (Dove et al. 2000; Leung et al. 2000; MacDonald et al. 2000; DiGirolamo et al. 2001; Milham et al. 2002; Langenecker et al. 2004; Yeung et al. 2006; Zysset et al. 2007; Prakash et al. 2011). Studies of aging using the Stroop task have generally found an increased extent or amplitude of the hemodynamic response in the older group than in the younger group during inhibition (Langenecker et al. 2004; Zysset et al. 2007; Prakash et al. 2011), though at least one study found the opposite trend (Milham et al. 2002). There are few fMRI studies of switching tasks with aging, but one study (DiGirolamo et al. 2001) found that both older and younger adults recruit similarly DLPFC and MFC areas. However, while younger adults did not recruit these areas during non-switch trials, older adults did. In this case, we also found similar BOLD signal patterns during inhibition/switching blocks in both age groups. We cannot however, with the mixed block design used here, identify differences in activation patterns during non-switch trials. Furthermore, since our control task was a color naming, rather than a block of incongruous Stroop task trials, we cannot use it to uncover the type of patterns shown by DiGirolamo *et al.* Another study of switching during aging found however older adults to show smaller BOLD signal changes in response to the task both in frontal and parietal regions (Gold et al. 2010), which is not the pattern observed here. The task used in

that study was however different and the group of participants smaller, with less stringent selection criteria, indicating a perhaps less healthy cohort.

Different breathing manipulations may be used for calibrated fMRI and a common concern with hypercapnia is that it may lead to breathing discomfort in participants. Breathing discomfort was rated using the seven-point rating scale presented by Banzett *et al.* (Banzett *et al.* 1996) and average ratings were  $2.16 \pm 0.17$  and  $2.26 \pm 0.19$  in the younger and older groups respectively. This corresponds to a rating of between no discomfort and mild discomfort. Therefore, discomfort of the breathing manipulation is unlikely to have acted as a significant confound in our data.

Another subject of debate with hypercapnia is whether it causes any changes in oxidative metabolism when small doses are administered. Results from the literature are unclear, with some reports of increases in metabolism (Horvath *et al.*, 1994; Jones *et al.*, 2005), decreases (Xu *et al.*, 2011b; Zappe *et al.*, 2008), and no detectable change (Chen and Pike, 2010a; Hino *et al.*, 2000; McPherson *et al.*, 1991). Because the literature lacks consensus on this topic, we have elected to preserve the assumption of no evoked metabolism usual for this type of study. However, were a consensus to be reached or a way of measuring a potential change in metabolism arise, this could be taken into account in the modeling in future studies.

#### **4.6.7. Future directions**

The present study identifies potential sources of bias in BOLD studies of cognitive aging and suggests that simple BOLD signal comparisons may not fully reflect the metabolic response elicited by a task in older brains. Interpretation would be further aided if absolute measures of resting CMRO<sub>2</sub> were available in our subjects. Since the calibrated fMRI method used here yields a fractional change from an unknown and possibly population-dependent baseline, we cannot determine from this result if the oxidative metabolism in micromolar units is truly different between groups. We have recently reported a technique, dubbed QUO<sub>2</sub>, which allows determination of resting OEF and CMRO<sub>2</sub> using two breathing manipulations (Gauthier *et al.* 2012c). Future studies using this or other related techniques (Bulte *et al.* 2011) will

add much-needed information on the metabolic aspects of aging and the possible impact of these changes on hemodynamic imaging techniques.

#### **4.7. Conclusion**

The present study indicates that BOLD-only studies of cognitive aging may be subject to biases that lead to underestimation of the oxidative metabolism underlying the BOLD signal changes seen in the elderly. BOLD and CBF responses to a hypercapnia functional challenge indicate that the reactivity and range of these imaging contrasts in older adults, masking to some extent increases in oxidative metabolism. These results warrant greater caution in the interpretation of BOLD signal changes observed in different age groups and highlight the importance of ancillary measures such as baseline blood flow and CO<sub>2</sub> reactivity provide important information for the understanding of age-related functional imaging changes.

#### **4.8. Acknowledgments**

We thank Carollyn Hurst and André Cyr for help with data acquisition, Christopher Steele for help with data analysis and presentation, and Felipe Tancredi for helpful discussions on data analysis. We would also like to thank Jiongjiong Wang at UCLA, who provided the pseudo-continuous arterial spin-labeling sequence used. This work was supported by the Canadian Institutes for Health Research (MOP 84378, Banting and Best Scholarship held by CJG), the Canadian Foundation for Innovation (Leaders Opportunity Fund 17380), the Canadian National Sciences and Engineering Research Council (R0018142), and the Ministère du développement économique, de l'innovation et de l'exportation (PSR-SIIRI-239).

## **5. Relationship between cardiovascular health, cerebral physiology and cognition in healthy aging**

Gauthier, C.J.<sup>1,2</sup>, Lefort, M.<sup>3</sup>, Mekary, S.<sup>2,4</sup>, Desjardins-Crépeau, L.<sup>2,5</sup>, Madjar, C.<sup>2</sup>, Bherer, L.<sup>2,3</sup>, Frouin, F.<sup>3</sup>, Hoge, R.D.<sup>1,2</sup>

<sup>1</sup>Physiology/Biomedical Engineering, Université de Montréal, Montreal, Canada, <sup>2</sup>CRIUGM, Montreal, Canada, <sup>3</sup>Inserm 678, UPMC, CHU Pitié Salpêtrière, Paris, France, <sup>4</sup>Kinesiology, Université de Montréal, Montreal, Canada, <sup>5</sup>UQAM, Psychology Department, Montreal, Canada

### **5.1. Preface**

The brain is known to undergo vascular and cognitive changes with age (Cabeza et al. 2005; Chen et al. 2011; Lu et al. 2011). These changes may be preceded by arterial hardening starting at the aorta (Redheuil et al. 2010), then spreading to other organs including the brain as pulsations become less efficiently absorbed by the aorta. Therefore, there may be a link between age-related arterial stiffening and loss of elasticity in the brain vasculature (O'Rourke et al. 2007). Some of these processes may furthermore underly the decreased cognitive performance and changes in patterns of hemodynamic signal changes observed in fMRI studies of cognitive aging (Brown et al. 2011). While these effects may contribute to even healthy aging, cardiovascular fitness may act as modulator to slow down the progression towards stiffer vessels (Churchill et al. 2002; Brown et al. 2010; Davenport et al. 2012).

The study presented in Chapter 5 seeks to address these questions by combining measures of central and cerebral vascular health, cognitive performance on an executive function task and cardiovascular fitness in a group of younger and older adults. Parameters found to differ significantly between young and old are then examined to identify correlations within the older group and identify links between vascular health, fitness and cognition.

The data presented here represents a subset of a larger dataset. The data from 31 younger and 31 older adults is presented, but this same set of measures was acquired in an additional 25 older participants not included in this preliminary analysis. Furthermore, the measures presented here is also a subset of the measures acquired in this cohort, which included also a series of blood tests (fasting glucose, cholesterol, triglycerides, hemoglobin and C-reactive protein), body mass index, a neuropsychological battery, additional aortic metrics, fMRI of the Stroop task, time domain near-infrared measure of baseline hemoglobin (oxygenated and deoxygenated), and a near-infrared acquisition during the Stroop task. These additional measures and participants will be included in the final analysis of this study. Despite its preliminary nature, this study was included since it demonstrates the breadth of experimental work carried out in the thesis project. Although the additional statistical power provided by the complete cohort will be necessary to confirm the correlations noted in the present analysis and uncover other important relationships between different aspects of vascular and cognitive health, the smaller cohort is nevertheless indicative of interesting age-related changes and confirms some of the expected links between central vascular health, cerebral vascular and metabolic function, cognition and cardiovascular fitness.

## **5.2. Abstract**

The aging brain exhibits both vascular and cognitive changes. While arteries throughout the body are known to become stiffer with age, this vessel hardening is believed to start at the level of the aorta and progress to other organs, including the brain. The progression of this vascular impairment may contribute to cognitive changes observed with aging. Furthermore, it may be that regular exercise acts as a modulator to partially attenuate the effects of age on vascular and metabolic physiology. The present study seeks to address these questions by identifying vascular, metabolic and cognitive properties that change within a cohort of thirty-one younger and older adults. We then sought to identify cardiovascular and neurological parameters exhibiting significant correlations within the older group. Decreases in aortic elasticity were found in the older group, both in terms of aortic pulse-wave velocity (PWV) and augmentation index (AI). The older group was

furthermore found to have a lower cerebrovascular BOLD reactivity to hypercapnia and a lower baseline BOLD signal (measured as the parameter  $M$  from calibrated fMRI methods). Finally, older adults were found to show a lower performance on an executive function task and show reduced cardiovascular fitness (VO<sub>2</sub>max).

Results within the older group indicate that there may be a relationship between VO<sub>2</sub>max, AI and cognitive performance, as well as between AI and  $M$ . The results of this study therefore support the hypothesis that greater cardiovascular fitness is associated with improvements in central vascular function, contributing in turn to improved brain vascular health and cognition.

### **5.3. Introduction**

The arterial network has two main functions: to deliver blood to all tissues in the body and dampen heart pulsations so that when blood reaches the capillaries, flow is continuous rather than pulsatile (O'Rourke et al. 2007). The dampening of pulsatile flow is achieved by laminae of the protein elastin in blood vessel walls. This protein acts like rubber to allow vessel walls to be distended during the systolic phase of the cardiac cycle and return to their original shape during the diastolic phase (O'Rourke et al. 2007; Fritze et al. 2012). Elastin has a half-life of decades but, like all material, it undergoes mechanical fatigue (Rigby 1964). Over a lifetime of stretching at every heart beat, the elastin laminae fracture and lose efficiency (Quaglino et al. 1996; Fritze et al. 2012). The laminae become thinner and the space created between laminae is filled with collagen. Collagen is not elastic, so decreased elastin to collagen ratio results in stiffer blood vessels with a larger diameter and prevents large deformations of blood vessel walls (Fritze et al. 2012).

Arterial hardening is a general process that affects the arteries of the whole body, though not all at the same pace. The aorta is the first artery to be affected since much of the pulsatile flow absorption and therefore the mechanical damage to elastin laminae occurs at this level (Laurent et al. 2007; Redheuil et al. 2010). Furthermore, measures of aortic stiffening (including pulse-wave velocity and augmentation index) have been shown to be independent risk factor for all cause mortality and a variety of conditions including cardiovascular events and fatal

stroke (Boutouyrie et al. 2002; Laurent et al. 2003; Laurent et al. 2006). Therefore, it may be that measures of aortic stiffening are the most sensitive test of general hardening.

The brain may be particularly vulnerable to the effects of arterial hardening and there may be a link between arterial stiffening and cognitive decline (Waldstein et al. 2008; Elias et al. 2009; Brown et al. 2011). The brain is one of the only organs without protection against the pulsatile nature of blood flow and cerebral arteries may therefore be more sensitive to loss of elastin (Laurent et al. 2007; O'Rourke et al. 2007). Furthermore, animal studies have shown that the brain experiences an age-related decrease in microvascular density (Sonntag et al. 1997). The increased pulsatility associated with less elastic arteries may lead to distal cerebral lesions and impaired microcirculation (O'Rourke et al. 2007), and vascular lesions in white matter have been shown to be associated with cognitive decline and dementia (Sierra et al. 2004). Finally, impaired endothelial function leading to circulation of cellular debris may contribute to microvascular lesions and hence cognitive deficits (O'Rourke et al. 2007; Wang et al. 2007; Wang et al. 2009).

### **5.3.1. Effects of cardiorespiratory fitness**

A healthy diet and regular exercise are the most widely recognized means to preserving autonomy and quality of life during aging (Wallace 2005). Physically fit older adults have been shown to have lower blood pressures and higher cerebrovascular reserve (Brown et al. 2010). Cross-sectional studies have suggested that regular exercise may be partly protective against dementia (Podewils et al. 2005; Larson et al. 2006) and cognitive decline (Rogers et al. 1990; Yaffe et al. 2001; Churchill et al. 2002; Etnier et al. 2006; Kramer et al. 2006; Brown et al. 2010; Brown et al. 2011). A meta-analysis of fitness training studies has showed that fitness training results in improved cognitive scores, especially for tasks requiring executive control processes (Colcombe et al. 2003). The improvement may, however, depend on many factors including the time spent exercising on the day of the experiment and genetic polymorphisms (Hopkins et al. 2012).

In a recent study on the hemodynamic properties of the aging brain, we have shown that older adults show a reduced hemodynamic response to a global CO<sub>2</sub> challenge, as well as reduced baseline blood flow and baseline BOLD signal throughout the brain (Chapter 4). The participants included in that study also underwent MRI scanning of the aorta to assess hardening in this major artery, as well as a test of cardiorespiratory fitness. Here we document age-related differences in aortic elasticity, in cerebral vascular and metabolic properties, as well as changes in fitness and cognition within these older adults. Furthermore, correlations between these changes indicate that there may be a link between central vascular health and fitness, cerebral hemodynamics, and cognition.

## **5.4. Methods**

### **5.4.1. Participants**

Acquisitions were conducted in 31 young (10 female, with mean age of  $24 \pm 3$  years) and 31 older (14 female, with mean age of  $64 \pm 5$  years) healthy participants on a Siemens TIM Trio 3T MRI system (Siemens Medical Solutions, Erlangen, Germany). All subjects gave informed consent and the project was approved by the Comité mixte d'éthique de la recherche du Regroupement Neuroimagerie/Québec.

Exclusion criteria for this study included claustrophobia, cardiac disease, hypertension or taking blood pressure lowering medication, neurological or psychiatric illness, smoking, excessive drinking (more than two drinks per day), thyroid disease, diabetes, asthma and being under a regular treatment known to be vasoactive or psychoactive. Participants were all non-smoking and older participants had been non-smoking for at least five years. All older participants met with a geriatric MD to ensure that they did not meet any of the exclusion criteria for the study. Furthermore, all participants underwent a neuropsychological battery to ensure the absence of cognitive impairment.

### **5.4.2. Maximal continuous graded exercise test**

All participants underwent an exercise test to estimate their cardiorespiratory fitness at the time of the study. All tests were done within one month of the MRI session. Initial workload was set at the individual body weight and increased by 15

W every minute until voluntary exhaustion. Strong verbal encouragement was given throughout the test. Oxygen uptake (in ml/min/kg) was determined continuously on a 30-second basis using an automated cardiopulmonary exercise system (Moxus, AEI Technologies, Naperville, IL). The highest over a 30-second period during the test was considered as the peak oxygen uptake (peak, in ml/min/kg). For older participants, a cardiologist was available in case of difficulties during the test and the ECG trace was reviewed by the cardiologist to ensure that it was normal.

#### **5.4.3. Modified Stroop task**

The modified Stroop task consisted of two 60-second blocks each of control and inhibition/switching Stroop conditions, interspersed with 60-second rest blocks. The details of this task have been described in a previous study (see Chapter 4).

#### **5.4.4. MR Image acquisition**

The imaging session was divided in two segments: one for the acquisition of brain images and the other for aortic images. Participants were taken out of the scanner in between these two acquisition segments to change the equipment. Participants were allowed to move or stretch during this pause to ensure greater comfort.

##### *5.4.4.1. Brain exam*

The vendor-supplied 32-channel receive-only head coil was used for all acquisitions. Sessions included an anatomical, 1mm<sup>3</sup> MPRAGE acquisition and older participants had an additional FLAIR acquisition to assess the presence and severity of white-matter lesions. MPRAGE and FLAIR acquisition parameters have been described in a previous study using the same protocol (Chapter 4). White matter hyperintensities were quantified using the scale from Wahlund and colleagues (Wahlund et al. 2001). Only participants with scores of 0 or 1 were included in this study, for an average and standard deviation of  $0.67 \pm 0.48$  in the older group.

Functional image series were acquired using a dual-echo pseudo-continuous arterial spin labeling (pCASL) acquisition (Wu et al. 2007) to measure

simultaneously changes in cerebral blood flow (CBF) and BOLD signal. The parameters for this sequence have been previously described (Chapter 4).

#### *5.4.4.2. Aortic exam*

The session also included an aortic exam with simultaneous brachial pressure recording (Model 53000, Welch Allyn, Skaneateles Falls, NY, USA). Aortic images were acquired using the six-element body matrix and 24-element spine matrix coils. All acquisitions were ECG gated and acquired during cued breath holding. A series of black blood turbo spin echo (TSE) images were acquired to visualize the aortic arch with parameters: TR/TE/alpha: 700ms/6.5ms/180°, with 1.4x1.4mm in-plane resolution and two slices of 7.0mm. Once these images were acquired, a plane perpendicular to the ascending and descending aorta was defined, at the level of the pulmonary artery. In this plane, a phase-contrast velocity encoded series was acquired with parameters: TR/TE/alpha: 28.6 ms/1.99 ms/30°, with 1.5x1.5 mm in-plane resolution and a single slice of 5.5 mm, during 60 phases of the cardiac cycle, acquired in three segments, with a velocity encoding of 180 cm/s through plane. Brachial pressures were acquired at the beginning of the aortic exam, and before and after the phase-contrast sequence.

#### **5.4.5. Tonometry**

Carotid applanation tonometry was performed right after the MRI session in an adjoining room. Participants were supine and the data was acquired using a Pulsepen device (DiaTecne, Milan, Italy). Simultaneous pulse waveform and ECG trace was acquired on both carotids. Brachial blood pressure measure was taken right before leaving the MR room. Post-processing was done using the manufacturer's software. Augmentation index (AI; in %) was determined for both carotids as the ratio of augmented pressure (determined as the height of the last systolic peak above the inflection point) to the pulse pressure (the difference between systolic and diastolic pressure).

#### **5.4.6. Hypercapnic manipulation**

Hypercapnic manipulations were achieved using a computer-controlled gas delivery system in combination with a sequential gas delivery circuit (RespirAct™,

Thornhill Research Inc., Toronto, Canada). For details on the hypercapnia manipulation, see Chapter 4. Subjects underwent the manipulation twice during the study, one outside the scanner before the imaging session to acclimatize the participant to the manipulation and once during the MRI session. Subjects were debriefed after the acclimatization session to assess their level of respiratory discomfort using the seven-point scale published by Banzett and colleagues (Banzett et al. 1996). All participants had a rating below 5 (significant discomfort).

#### **5.4.7. Data analysis**

##### *5.4.7.1. Brain data*

All analyses were done using the NeuroLens data analysis software package ([www.neurolens.org](http://www.neurolens.org)). Functional data analyses were done as described in Chapter 4.

##### *5.4.7.2. Aortic data*

The aortic data was analyzed using the ARTFUN software (Herment et al. 2010). Pulse wave velocity (PWV) was regionally computed between ascending and descending aorta from phase contrast and cine images. Using amplitude phase contrast cine images, the aortic lumen contours of the ascending aorta and descending aorta were automatically segmented and flow profiles were estimated using the phase information within these contours (Herment et al. 2010). Delay times ( $\Delta t$ ) between the two flow profiles were computed by least squares minimization of the delay between the up slopes of the two curves. The 3D length of the aortic arch ( $L_a$ ) between the ascending and descending aorta was computed using additional TSE images (including coronal views and axial views) by manually selecting markers in the central line of the aorta. PWV was defined as the ratio between  $L_a$  and  $\Delta t$  (Dogui et al. 2011).

#### **5.4.8. Statistical analysis**

Statistical analysis of all data was done using SPSS 19.0 (IBM, Armonk, New York, USA). Comparisons between groups were done using one-tailed Student's t-tests. One-tailed partial correlations were done using only the 31 participants in the older

group, taking into account the effects of age and gender. All measures reported in the text are average values  $\pm$  standard error.

## 5.5. Results

Aging is known to be associated both with decreases in cognitive performance and in vascular health. Here we quantify reductions in aortic elasticity and cardiorespiratory fitness in older participants, as well as cognitive performance on an executive function task and brain vascular and metabolic function. The results presented here indicate that measures of central vascular health and cardiorespiratory fitness may be predictive of an individual's level of cerebral and cognitive health.

### 5.5.1. Central vascular health and fitness

Aortic elasticity was assessed using pulse-wave velocity and augmentation index measures. Results show that there was a significant difference between younger and older participants in both these measures ( $p < 0.0001$  for both). PWV was found to be  $3.95 \pm 0.15$  cm/s in the younger group and  $8.92 \pm 0.58$  cm/s in the older group (Figure 1A), while AI was found to be  $-9.32 \pm 3.53$  and  $19.43 \pm 2.44$  in the younger and older group respectively (Figure 1B).

Cardiorespiratory fitness was assessed using a VO<sub>2</sub>max test. VO<sub>2</sub>max was also found to be different between the two groups ( $p < 0.0001$ ) with values of  $42.32 \pm 1.31$  ml/min/kg in the younger and  $31.66 \pm 1.26$  ml/min/kg in the older group (Figure 1C).

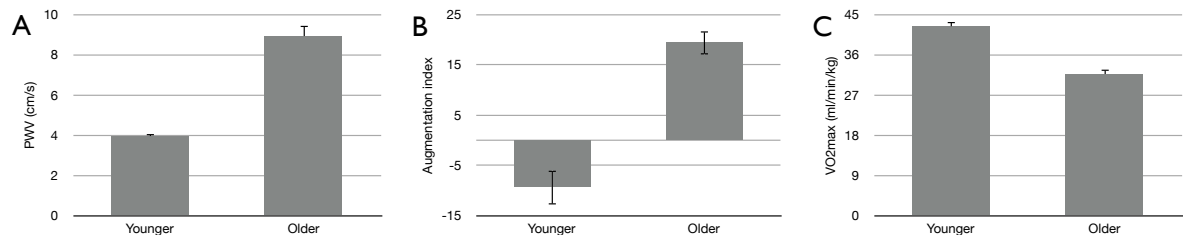


**Figure 1. Central vascular health and cardiorespiratory fitness**

Measures of central arterial elasticity including aortic pulse-wave velocity (PWV) (A) and augmentation index (B) were found to be significantly affected by age ( $p < 0.0001$ ). Cardiorespiratory fitness, measured in terms of VO<sub>2</sub>max (C), was also found to be significantly decreased with age ( $p < 0.0001$ ).

### 5.5.2. Cerebral measures

Cerebral measures included both reaction time in responding to a cognitive task and measures of cerebrovascular and metabolic health. Imaging parameters, including baseline BOLD hypercapnia reactivity and the baseline BOLD signal  $M$  were quantified globally within grey matter.

The modified Stroop task used here included two types of blocks: inhibition/switching blocks and control blocks. The reaction times presented here correspond to the subtraction between inhibition/switching reaction times and control task reaction times. These were found to be significantly different between the two groups ( $p < 0.0001$ ), with values of  $322.67 \pm 24.53$  ms in the younger and  $543.13 \pm 28.74$  ms in the older group (Figure 2). Average values for each task component are also shown in Figure 2.

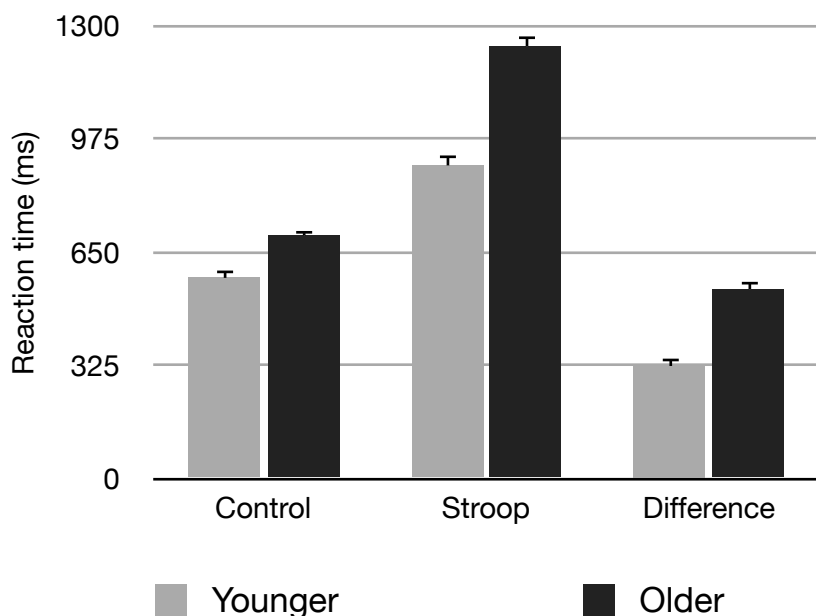


**Figure 2. Stroop task performance**

Performance on the modified Stroop task was assessed using reaction time. Older adults were found to have slower reaction times for both the control and inhibition/switching (Stroop) parts of the task. The difference in reaction time between these two parts was furthermore significantly different between the two groups ( $p < 0.0001$ ).

Group average maps of vascular reactivity and baseline BOLD signal show that these properties may be lower throughout grey matter in the older adults (Figure 3). BOLD CVR was obtained by dividing the group average percent BOLD signal

change in response to a hypercapnia stimulus by the change in expired CO<sub>2</sub> concentration in mmHg. The amplitude of this response is thought to be related to the distensibility of cerebral arteries. BOLD CVR measures were found to be significantly lower in the older group ( $p < 0.0001$ ), with values of  $0.31 \pm 0.02$  % $\Delta$ BOLD/mmHg and  $0.23 \pm 0.01$  % $\Delta$ BOLD/mmHg in the younger and older participants respectively (Figure 3).

The  $M$  parameter is defined as the maximal theoretical possible BOLD signal change. It represents the BOLD signal attenuation from paramagnetic deoxyhemoglobin present in venous blood. It is therefore an indirect measure of baseline metabolism, with a contribution from baseline blood flow and volume. Values for this parameter were found to be marginally significantly different between the two groups ( $p = 0.048$ ), with values of  $5.76 \pm 0.22\%$  in the younger and  $5.00 \pm 0.30$  in the older group (Figure 3).

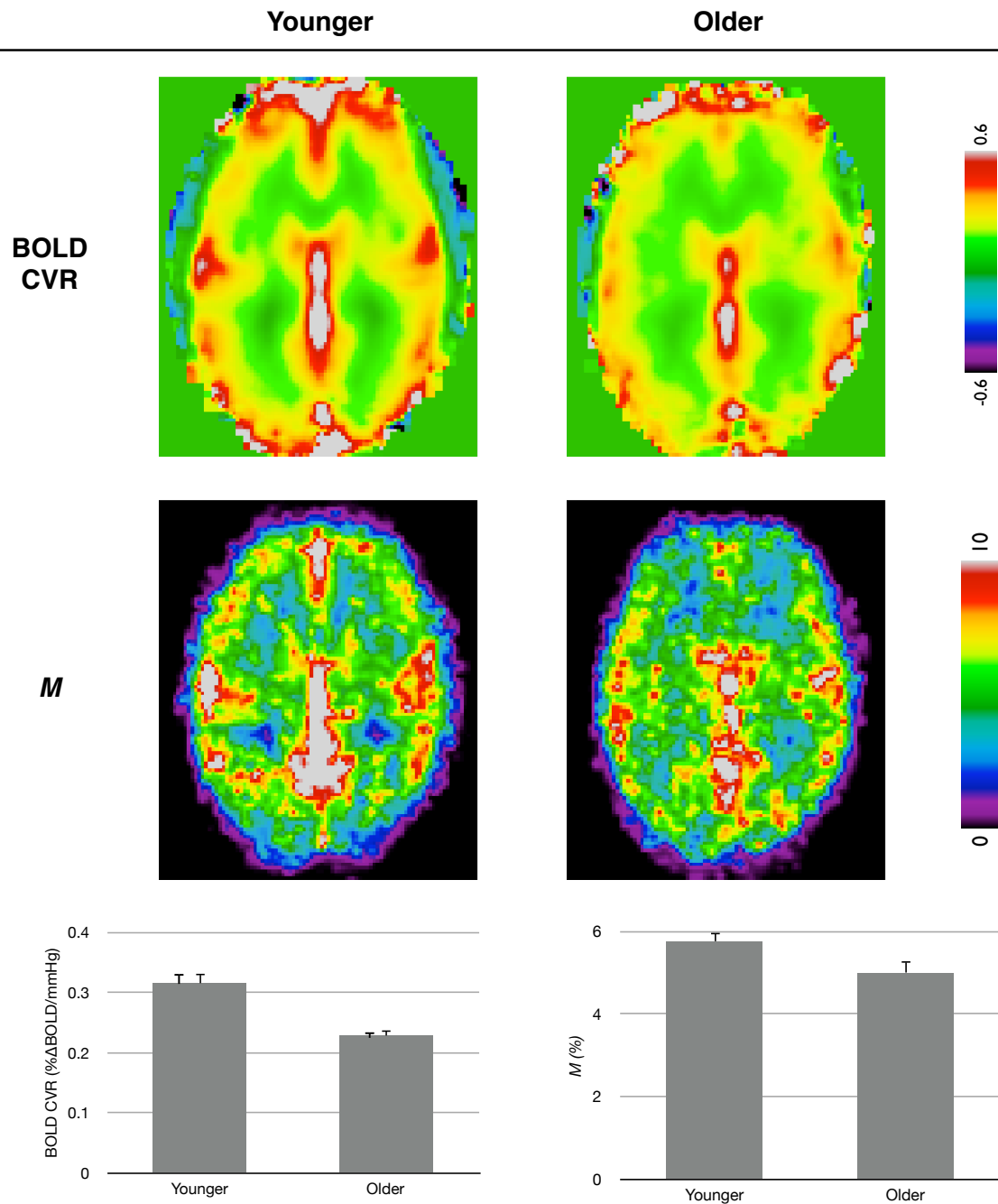


**Figure 3. Cerebral hemodynamic properties**

This figure shows average BOLD CVR maps in younger and older adults, as well as maps of the  $M$  parameter for these two groups. Quantification of these two parameters over all grey matter for younger and older adults are shown in the bottom part of this figure. BOLD CVR was found to be significantly lower in older adults ( $p < 0.001$ ), while a marginally significant decrease in  $M$  parameter was also seen in the older group ( $p = 0.048$ ).

### 5.5.3. Correlations between parameters

Partial correlations between the above-mentioned parameters showing age-related differences were assessed within the older group, taking into account the effects of age and gender (Table 1).

	AI	VO2max	Stroop RT	BOLD CVR	M	
<b>AI</b>	1.000	-0.314	0.290	0.057	-0.336	Cor
	.	0.052	0.067	0.387	0.040	Sig
<b>VO2max</b>		1.000	-0.494	-0.310	0.079	Cor
		.	0.004	0.054	0.345	Sig
<b>Stroop RT</b>			1.000	0.215	0.006	Cor
			.	0.135	0.488	Sig
<b>BOLD CVR</b>				1.000	-0.017	Cor
				.	0.465	Sig
<b>M</b>					1.000	Cor
					.	Sig

**Table 1. Partial correlations between health indices in the older subjects**

This table shows the results of a partial correlation analysis within the 31 older participants showing the relationship between various vascular, metabolic and cognitive health indices. This analysis was done taking into account the effects of age and gender. For each combination of parameters, the strength of the correlation (cor) and significance (sig) of the association is given. Parameters included are augmentation index (AI), VO2max (in ml/min/kg), reaction time difference between the inhibition/switching and control parts of the modified Stroop task (Stroop RT; in ms), cerebrovascular reactivity to CO<sub>2</sub> measured using the BOLD signal (BOLD CVR; in %ΔBOLD/mmHg CO<sub>2</sub>) and the *M* parameter (in %).

VO2max was found to be correlated significantly with the difference between inhibition/switching reaction time and reaction time on the control task (Stroop RT in Table 1) with a coefficient of  $r = -0.494$  ( $p = 0.004$ ). A trend towards significance was observed between the augmentation index and VO2max ( $r = -0.314$ ;  $p =$

0.052), as well as with the  $M$  parameter ( $r = -0.336$ ;  $p = 0.040$ ) and, to a lesser extent, Stroop reaction time ( $r = 0.290$ ;  $p = 0.067$ ). Finally, VO<sub>2</sub>max was also found to have a trend towards an association with BOLD CVR ( $r = -0.310$ ;  $p = 0.054$ ). Pulse-wave velocity was not found to be associated with any other measures within the older group.

## **5.6. Discussion**

Results shown here indicate that there may be a link between central vascular health, cardiorespiratory fitness, cerebral vascular and metabolic health with aging. There may additionally be a link between these measures of vascular and metabolic health and cognitive performance on a type of task thought to be affected by age.

### **5.6.1. Differences between age groups**

The data presented here show that age is associated with a variety of vascular and metabolic changes centrally and in the brain. Aging is associated with increased pulse-wave velocity and augmentation index at the level of the aorta. This agrees well with literature showing progressive hardening of central vessels with age (Boutouyrie et al. 2002; Binder et al. 2006; Laurent et al. 2007; Waldstein et al. 2008; Redheuil et al. 2010). Vascular changes are also known to occur in the brain during aging (Chen et al. 2011; Lu et al. 2011). This was ascertained in our sample, with older adults showing lower BOLD reactivity to CO<sub>2</sub>. CO<sub>2</sub> is a potent vasodilator and inhaling increased concentrations of CO<sub>2</sub> leads to a global increase in blood flow throughout grey matter which may be sensitively captured using the BOLD technique (Leontiev et al. 2007a; Mandell et al. 2008; Goode et al. 2009b). A lower BOLD reactivity to CO<sub>2</sub> may be indicative of vessel hardening at the level of the brain (Mandell et al. 2008; Goode et al. 2009a; Goode et al. 2009b). Furthermore, the parameter  $M$  was also found to be lower in the older group, in agreement with previous calibrated fMRI studies of aging (Ances et al. 2009; Mohtasib et al. 2012). The  $M$  parameter represents the maximum possible BOLD signal change from baseline and arises from the deoxyhemoglobin content of venous blood at rest (Davis et al. 1998; Hoge et al. 1999a). As such, it is an indirect composite measure of baseline oxidative metabolism, with contributions from baseline blood flow and

volume. It can be taken to be the baseline BOLD signal, since it represents BOLD attenuation at rest. While not as physiologically-specific as a direct measure of oxidative metabolism, it nevertheless provides some information on baseline metabolic and vascular health.

Two other measures were assessed for changes with aging. The capacity to metabolize O<sub>2</sub> during exercise was found, as elsewhere, to be affected by age (Lazarus et al. 2010; Andersson et al. 2011). This physiological property, while generally thought to be decreased with age is, however, highly dependent on lifestyle and the type and amount of regular exercise done by older adults (Colcombe et al. 2006; Hagner et al. 2009; Sergi et al. 2010; Davenport et al. 2012). Because vascular health is thought to be at least partly determined by lifestyle and because vascular health is thought to improve with greater fitness (Binder et al. 2006; Arena et al. 2009; Davenport et al. 2012), this change in O<sub>2</sub> metabolic capacity with exercise may be an important modulating factor of the effects of aging. Finally, performance on a cognitive task including an executive function component was assessed and found to be lower in the older group. While performance in terms of reaction time and accuracy on a wide variety of cognitive tasks has been found to be decreased with aging, executive functions may be particularly sensitive to the effects of aging (Langenecker et al. 2004; Cabeza et al. 2005; Spreng et al. 2010). Performance on this task was measured in terms of reaction time difference between the inhibition/switching blocks (which contain an executive function component) and the control blocks.

### **5.6.2. Correlations within older participants**

While the different vascular, metabolic and cognitive properties assessed here have all been used in previous studies to investigate the effects of aging, this is the first time that these were assessed within a single cohort. The fact that all these properties differ within the same group of individuals allows a more in depth investigation of the relationships between these parameters during healthy aging. Therefore, partial correlations between these parameters were assessed within the older group, while taking into account the confounding effects of age and gender. Because the group of subjects included in this analysis was fairly small (31

participants) and because the inclusion and exclusion criteria for this study were very strict (and hence make the population more homogeneous in terms of vascular health), the correlations remain, however, somewhat modest. We are in the process of extracting quantitative measures from additional older subjects, who will be added to the cohort analyzed here with the hope of increasing statistical power.

The augmentation index, a measure of aortic elasticity thought to be an early indicator of arterial hardening (Pase et al. 2010; Redheuil et al. 2010), was found here to correlate with cardiorespiratory fitness in terms of VO<sub>2</sub>max. While we cannot establish a causal link, this is consistent with the well-established link between preservation of vascular health in the elderly and regular cardiovascular exercise (Binder et al. 2006; Arena et al. 2009). The data presented here confirm the results by Binder *et al.* showing an association between augmentation index and VO<sub>2</sub>max (Binder et al. 2006). Augmentation index was furthermore found to correlate with the *M* parameter, establishing a link between central vascular health and cerebral hemodynamic properties. This may indicate that older adults with less healthy central arteries may also show reduced metabolic equilibrium in the brain, since a reduced *M* may be indicative of a change in metabolic production of deoxyhemoglobin or a changed balance between deoxyhemoglobin concentration and the baseline cerebral blood flow that dilutes it. Further research is, however, needed to explore this link, given the ambiguous nature of the *M* parameter. Finally, augmentation index was found to have a trend towards an association with reaction time difference between the inhibition/switching and control blocks of the modified Stroop task. The addition of data from more study participants may help confirm this link, in agreement with other studies showing a link between measures of central vascular health and cognition (Pase et al. 2010; Gorelick et al. 2011; Mitchell et al. 2011; Sahathevan et al. 2012).

The strongest association found here was between VO<sub>2</sub>max and the reaction time difference in the cognitive task. This association could, however, be related to motivation, since voluntary exhaustion is used to interrupt the VO<sub>2</sub>max test and since motivation and attention will influence performance on the cognitive task (Bonfond et al. 2011; Satterthwaite et al. 2012). But other associations between

vascular parameters support the conclusion this effect is at least partly vascular in nature. VO<sub>2</sub>max was also found to show a trend towards an association with BOLD CVR. This would be consistent with another study showing lower hypercapnia blood flow response in sedentary older adults (Brown et al. 2010; Davenport et al. 2012). Furthermore, the study by Brown and colleagues also identified a link between cardiovascular fitness and cognitive function. This association between fitness and cognition has also been seen in several other studies (Rogers et al. 1990; Yaffe et al. 2001; Churchill et al. 2002; Etnier et al. 2006; Kramer et al. 2006; Brown et al. 2010; Hopkins et al. 2010; Brown et al. 2011; Hopkins et al. 2012).

The results presented here support the view that with age comes a general arterial hardening, beginning at the aorta and progressing to other organs including the brain (O'Rourke et al. 2007; Waldstein et al. 2008; Redheuil et al. 2010). This vessel hardening is thought to be a contributing factor in the cognitive decline observed with aging (Waldstein et al. 2008; Brown et al. 2010; Iadecola 2010; Brown et al. 2011; Gorelick et al. 2011). Finally, the results of this cross-sectional study agree with the view that lifestyle factors, such as cardiorespiratory fitness, act as modulators of these vascular effects and that regular exercise may help mitigate the detrimental effects of aging on cognition (Rogers et al. 1990; Yaffe et al. 2001; Churchill et al. 2002; Etnier et al. 2006; Kramer et al. 2006; Brown et al. 2010; Hopkins et al. 2010; Brown et al. 2011; Hopkins et al. 2012). Improved statistical power with the larger final cohort will hopefully allow a more nuanced discussion of these effects. Furthermore, the addition of more physiologically-specific measures, such as blood flow and baseline oxidative metabolism could in the context of a future study, help improve our understanding of these effects.

## **5.7. Conclusion**

The results of this study support a link between aging and degradations in vascular and metabolic health, both centrally and in the brain, as well as an association between declining vascular health and decreased cognitive performance. The results presented here also support the notion that regular exercise, by increasing cardiorespiratory fitness, may help prevent some of the negative effects of aging

on the vasculature and on cognition. However, more work is needed to firmly establish these relationship and future longitudinal work including more physiologically-specific parameters may help establish the mechanisms by which these effects arise.

## **5.8. Acknowledgments**

We thank Carollyn Hurst and André Cyr for help with data acquisition, Élie Mousseau, Alban Redheuil and Alain Herment for help with setup of the aortic acquisition protocol and Mélanie Renaud for help with logistics of subjects' participation. We would also like to thank Jiongjiong Wang, who provided the pseudo-continuous arterial spin-labeling sequence used. This work was supported by the Canadian Institutes for Health Research (MOP 84378, Banting and Best Scholarship held by CJG), the Canadian Foundation for Innovation (Leaders Opportunity Fund 17380), and the Ministère du développement économique, de l'innovation et de l'exportation (PSR-SIIRI-239).

## 6. General Discussion

Functional magnetic resonance imaging has been steadily gaining in popularity from its first description in 1992 (Kwong et al. 1992; Ogawa et al. 1992). The BOLD contrast is a sensitive measure of the hemodynamic response that follows synaptic activity and offers advantages in terms of spatial resolution over competing functional imaging methods such as near-infrared spectroscopy and PET. Unfortunately however, the BOLD signal suffers from being physiologically unspecific. Increases in BOLD signal during tasks arise from an ambiguous combination of increases in oxidative metabolism, blood flow and blood volume. While this may not be an overly detrimental limitation when assessing the localization of brain activity within a group of homogeneous participants, it does however limit the inferences that may be drawn from group comparisons of signal amplitudes and extent when these groups are suspected to differ in vascular or metabolic function (Samanez-Larkin et al. 2008).

The present thesis is an attempt to explore the ways in which MRI methods may be used to make the BOLD contrast more physiologically specific and understand the physiological differences that underly changes in BOLD signals. An extension of previous calibrated fMRI techniques is first presented in Chapter 2 to extract more robust and accurate estimates of task-evoked oxidative metabolism. Chapter 3 presented a method to estimate baseline  $CMRO_2$  based on combinations of gas manipulations and the calibrated fMRI model described in Chapter 2. In Chapter 4, the more traditional hypercapnia calibrated fMRI frame was used to explore age-related changes in brain physiology and the possible biases that BOLD-only studies of cognitive aging are subject to. Finally, an investigation into the possible underlying vascular causes of age-related changes are presented in Chapter 5. In summary, this thesis presents methods to extract more physiologically-specific information from the BOLD signal, then uses the concepts provided by these methods to explore the physiological changes associated with healthy aging and the confounds that BOLD studies of aging are subject to.

All the manuscripts included in this thesis use concepts adapted from prior calibrated fMRI work to explore the meaning of BOLD signal changes. Calibrated

fMRI techniques have existed and been used for now almost fifteen years. Though the original Davis approach using hypercapnia was for long the only method available (Davis et al. 1998), other techniques have started to emerge in the last few years. The second technique to be proposed was the hyperoxia calibration method (Chiarelli et al. 2007b). The purported advantage of this technique is a reduced discomfort of the breathing manipulation since changes in O<sub>2</sub> composition is not perceived by participants. However, this technique comes with its own set of assumptions and it may be more susceptible to systematic biases than other techniques (Blockley et al. 2011b; Gauthier et al. 2012b). In the last year, two more techniques were proposed. One uses the information in spin and gradient echoes to calibrate the signal without the need for a separate breathing manipulation (Blockley et al. 2011b) and the other is an extension of the hyperoxia calibration model that can be used with any combination of hypercapnia and hyperoxia. This second method is presented in Chapter 2 and used throughout all the thesis's manuscripts.

## **6.1. Calibrated fMRI method comparisons**

The Davis method has stood the test of time and has been shown to provide a set of robust simplifications that compare well with more complex modeling approaches (Buxton 2010; Blockley et al. 2011b; Griffeth et al. 2011). While these studies have demonstrated the robustness of the method in the context of observations made in healthy young subjects, the assumptions made by the model may not hold as well in the context of older individuals. More specifically, this model includes the implicit assumption that arterial blood is completely saturated with oxygen, which may not hold true as aging results in decreases in gas exchange and perfusion efficiency (Janssens et al. 1999; Sharma et al. 2006).

The hyperoxia calibration model generated much enthusiasm from the reduced discomfort associated with hyperoxia as opposed to hypercapnia. While the M values obtained using this technique show reduced variance (Mark et al. 2011), this arises from the fact that the amplitude of the CBF decrease in response to hyperoxia is generally assumed. This flow assumption is made because the real flow change is too small to be measured using standard CBF measurements in

most experimental contexts (Bulte et al. 2007). However, since ASL of gas changes is the lowest SNR measure in any of these techniques, assuming a CBF change artificially lowers the variance across subjects and creates the impression that the intra- and inter-individual differences are lower than they really are. In Chapter 2 of this thesis, we have shown that this technique is highly sensitive to misassignment of this CBF change. Even modest errors within the physiological range in the CBF value input into the model can result in large errors and even singularities in the computed  $M$  value (Figure 6B in Chapter 2). Blockley et al. have also shown that this model is very sensitive to errors in the assignment of baseline OEF (Blockley et al. 2011b).

The Generalized calibration model (GCM) was devised to take into account both arbitrary changes in blood flow and blood oxygenation. It is based on a modification of the hyperoxia calibration model to take into account blood flow changes in the equation relating changes arterial content of  $O_2$  to venous content of  $O_2$  (Equation 2, Chapter 2). While the hyperoxia model formulation used by Chiarelli et al. (Chiarelli et al. 2007b) is correct for manipulations, such as mild hyperoxia, which are not thought to result in changes in CBF, it is not appropriate for manipulations including a substantial change in CBF. Because the GCM takes into account both arterial oxygenation and changes in CBF, it may in fact be more robust to measurement error in CBF than either of the two original model (Chapter 2, Figure 6). Furthermore, because it can be used in combination with breathing manipulations that include simultaneous hypercapnia and hyperoxia (carbogen breathing) the  $M$  value can be estimated more robustly using higher SNR measurements as input.

## **6.2. Accuracy of measurement**

In a previous study, we have performed a direct measurement of the  $M$  parameter (Appendix A). Since  $M$  corresponds to the BOLD signal change from complete removal of all baseline dHb, this was achieved using a breathing manipulation that greatly increases both CBF and arterial oxygenation. Participants were asked to breathe a mixture of 10%  $CO_2$  in 90%  $O_2$  (carbogen-10), ensuring both a very large CBF increase (around 100%), as well as a substantial amount of dissolved oxygen

in arterial blood. This study worked under the hypothesis that it is possible to increase arterial saturation enough so that the dissolved  $O_2$  in arteries will meet all  $O_2$  extraction from metabolism. In other words, venous blood would become almost or completely saturated with  $O_2$  and be the virtual equivalent of arterial blood. The BOLD signal increase observed during such a manipulation would correspond to  $M$ .

In this manuscript (Appendix A) we have shown, by titrating the BOLD signal with increasing fractions of carbogen-10 in the presence and absence of a visual stimulation, that we could saturate the BOLD signal. BOLD data was acquired while subjects breathed four different fractional concentrations of carbogen-10 (25%, 50%, 75% and 100%). This led to an increased BOLD signal at each concentration step, up to a maximal BOLD signal change of 7.5% when subjects breathed 100% carbogen-10. The experiment was then repeated with a single minute of visual stimulation using a flashing checkerboard in the middle of the carbogen-10 breathing blocks (Figure 3, Appendix A). As an ever larger fraction of inspired gas was composed of carbogen-10 instead of air, the BOLD signal evoked by a flashing checkerboard decreased to finally completely disappear at a 100% carbogen-10 inhalation (Figure 3 and 5, Appendix A). In other words, as more and more  $O_2$  was present from the carbogen inhaled, it could fill the binding sites on hemoglobin as  $O_2$  was extracted to fill sustain metabolic activity from visual stimulation. At 100% carbogen-10 inhalation, BOLD measurements within visual cortex with and without visual stimulation was identical at 7.5%. Furthermore, the fact that the CBF response to the visual stimulation was maintained even during breathing of 100% carbogen-10 (even while there is no more measured BOLD response) indicates that BOLD signal saturation does not arise from an absence of CBF response some feedback mechanism in situations of  $O_2$  overabundance (Figure 7, Appendix A).

Because the BOLD signal measure during carbogen-10 inhalation is a direct measurement of  $M$ , this BOLD measurement can be used as a 'gold standard' against which to compare the three methods mentioned above. As shown in Chapter 2, hypercapnia and hyperoxia with their respective models resulted in an underestimation of the value of  $M$  in visual cortex. The combination of GCM with

carbogen inhalation (simultaneous hypercapnia and hyperoxia) resulted in  $M$  estimates in closer agreement to the values measured in Appendix A (Figure 2A). While the hyperoxia method still resulted in the underestimation of  $M$  in grey matter, hypercapnia yielded similar values as the GCM with combined carbogen inhalation in this ROI (Figure 2B). This however may stem from averaging of lower parenchymal values with hotspots of putative venous origin with hypercapnia, to yield similar end results as the new technique (Figure 4). These hotspots may arise from flow measurement error (Figure 6) and may become problematic if large veins are not removed when drawing ROIs.

It seems therefore that the GCM provides advantages over previous models in that it more accurately takes into account individual physiology to yield more robust  $M$  estimates from a reduced sensitivity to error in flow measurement. The GCM used in combination with combined hypercapnia and hyperoxia provides the further advantage of more accurate  $M$  estimates from a reduced degree of extrapolation towards the limit.

### **6.3. Baseline metabolism**

While the task-evoked percent  $CMRO_2$  change is a useful measure to compare group responses, this technique may be limited in many clinical contexts. Task-based functional imaging may often be impractical from the difficulties inherent in controlling such confounding task-related effects as strategy choice, motivation, attention, perception acuity and performance. Techniques with the capacity to measure baseline states may in general have more straightforward clinical utility, especially since some patient groups may experience a reduced ability to comply with complex instructions. Another limitation to clinical utility is that BOLD signal changes to complex cognitive tasks are generally small and can rarely be quantified on an individualized basis (Glover 2011). Since evoked  $CMRO_2$  changes are derived from task-evoked BOLD and ASL measurements, they suffer from the same limitation. Furthermore, though the relative  $CMRO_2$  changes obtained using calibrated fMRI can be compared across groups, these may reflect different absolute  $O_2$  consumptions if the baseline  $CMRO_2$  differs between the groups. For example, there are indications that older adults may show changes in baseline

CMRO<sub>2</sub> (Yamaguchi et al. 1986; Leenders et al. 1990; Marchal et al. 1992; Lu et al. 2011) and neurodegenerative diseases are likely associated with a large decrease in baseline CMRO<sub>2</sub> (Frackowiak et al. 1981; Nagata et al. 2000). Therefore, a method to measure baseline CMRO<sub>2</sub> would not only allow better interpretation of task-evoked changes, but also be a pertinent clinical measure on its own.

Several groups have developed MR techniques to image baseline oxidative metabolism in the last few years. Some of these techniques yield single vessel values (An et al. 2000; He et al. 2007; He et al. 2008; Xu et al. 2009; Fan et al. 2011) and are therefore limited in that they can only detect global changes in oxygenation. The method presented by Fan and colleagues (Fan et al. 2011) can be used to estimate oxidative metabolism in a cortical vein, but can so far only be used in a single large vein parallel to the main magnetic field axis. So while these methods have some potential for clinical applications, they are severely limited in cases of regional heterogeneity of metabolic changes.

Two methods allow quantification of regional CMRO<sub>2</sub>. The method presented by Bolar and colleagues (Bolar et al. 2011b) uses velocity encoding to isolate blood in venules, then quantifies T<sub>2</sub> in this compartment to obtain venous saturation. Venous saturation can then be converted to CMRO<sub>2</sub> knowing arterial saturation, hematocrit and baseline CBF. This technique is very promising in that it is a direct measurement of CMRO<sub>2</sub> and yields a voxel-wise estimate. However, this method may be difficult to use in the context of aging or disease since some populations may have different venular and capillary blood flow velocity. The second method for determining regional values of CMRO<sub>2</sub> was presented by Bulte et al. (Bulte et al. 2011) and is in fact conceptually related to the method presented in Chapter 3 of this thesis. However, the use of two models (the hypercapnia model to derive  $M$  and the hyperoxia calibration model to obtain OEF) with different sets of assumptions to derive  $M$  and resting OEF makes this model less correct than the one presented in Chapter 3.

### **6.3.1. QUO2 technique**

The QUO2 technique presented in Chapter 3 allows estimation of three baseline parameters:  $M$ , OEF and CMRO<sub>2</sub>. The value for  $M$  obtained using this technique

may be validated against the value of  $M$  derived using carbogen-10 (Appendix A). While the value of  $6.0 \pm 0.7\%$  from QUO2 over all grey matter is somewhat lower than the value of  $7.5 \pm 1.0\%$  found in the study presented in Appendix A, this may reflect the fact that the value of  $7.5\%$  was measured in visual cortex rather than in complete grey matter. There are some indications that values of  $M$  may be higher in visual areas than in some other part of the brain (Mark et al. 2011) (Chapter 2, Figure 2).

The use of this technique has also been demonstrated in functionally-defined ROIs. This data is presented in Appendix B. While the reduced averaging inherent to the smaller functional ROIs resulted in reduced convergence of the lines for each breathing manipulations in the intersection plots (Figure 3, Appendix B), the values obtained for all parameters were nevertheless within the expected physiological range. The values of  $M$  obtained within the functionally-defined ROIs presented in Appendix B are also somewhat lower than the direct measures observed in the study presented in Appendix A. This may reflect some additional changes in ROI-drawing techniques. In the data presented in Appendix B, gray matter probability for each voxel was used to reduce the contribution of other tissue types to the estimates of  $M$ , OEF and  $CMRO_2$ . This was done mainly to account for the presence of white matter and CBF within voxels, but may also have reduced the contribution of large veins in the ROIs. An indication that this may be the case is that a more stringent removal of non-grey matter voxels from the ROIs used in Appendix A resulted in a lower directly measured  $M$  value of  $5.27 \pm 0.5\%$  (data not shown). The reduced convergence of lines in the intersection plots shown in this experiment highlights, however, the fact that for these techniques to be applicable to the small signal changes observed during cognitive tasks, large groups of subjects are necessary to obtain sufficient SNR.

Validation of the accuracy of estimates of OEF and  $CMRO_2$  is not as straightforward as for  $M$ . Though PET measures exist for these quantities, the precision of these estimates is also difficult to guarantee. PET methods require administration of three compounds ( $^{15}O_2$ ,  $H^{15}O_2$  and  $C^{15}O$ ) and complex modeling to yield an estimate which cannot be compared to a 'gold standard' (Buxton 2010). The PET values may furthermore be subject to different biases than the MRI-based

method, since the modeling aspects are based on different principles. Therefore, though the values for these parameters is compared, both in Chapter 3 and in Appendix B, to the PET literature, some differences in values do not invalidate the present methods. Despite this qualification, some work is needed to improve the precision of the QUO2 method to make it applicable in lower SNR settings and in single subjects. Results from Chapter 3 in grey matter and Appendix B in visual cortex show, however, that the current implementation of the QUO2 method does perform adequately in small groups of subjects given enough averaging (grey matter averages in Chapter 3) or the readily detectable large signal changes of primary sensory areas (Appendix B).

### **6.3.2. Future improvements**

As discussed in Chapter 3 and Appendix B, ASL is a low SNR measurement and a more stable implementation of the technique would no doubt improve the precision and robustness of OEF and CMRO<sub>2</sub> estimates at the single subject level and in small, functionally-defined ROIs. Strategies to improve ASL quality could include using multiple delay times to capture the temporal profile of tag delivery at each voxel (Buxton et al., 1998) and the implementation of background suppression techniques to reduce the physiological or instrumental modulation of the background "static" tissue signal that is unrelated to flow (Dixon et al., 1991; Maleki et al., 2011). Also, since the group of participants included in the studies presented in Chapter 3 and Appendix B is fairly small, some of the decreased convergence seen with the smaller ROIs of Appendix B may stem from insufficient averaging. Furthermore, the stability of the data could be improved by using a metronome during the breathing manipulations. Preliminary data in our group suggests that the use of a metronome, by making breathing more constant across all conditions and participants, results in improved quality of the MRI time series. Therefore, future implementations of this technique will seek to improve the results on three fronts: improving the quality of the ASL data, acquisition of data in a larger cohort to allow greater averaging and will include the use of a metronome.

While ideally the QUO2 method would have been applied in the studies of aging presented in Chapters 4 and 5 of this thesis, the method was developed after

commencing the data acquisition phase on the older cohort. When the aging studies were designed, neither the GCM or the QUO2 methods existed. Therefore, the experiment was designed based on the Davis model in the context of a hypercapnia manipulation. While later results make this choice non-ideal, future studies will benefit from these new developments.

#### **6.4. Calibrated fMRI of aging**

While the research community that uses fMRI to study cognitive aging is aware that there may be vascular and metabolic confounds to the use of the BOLD technique in age comparisons (Cabeza et al. 2005; Samanez-Larkin et al. 2008), authors tend to minimize this contribution by saying that other mechanisms than the simply vascular must be at play (DiGirolamo et al. 2001; Cabeza 2002; Milham et al. 2002; Samanez-Larkin et al. 2008; Cappell et al. 2010; Reuter-Lorenz et al. 2010). While there is little doubt that this is the case, the field would benefit from a better understanding of the patterns of vascular and metabolic changes that occur with aging, and of their impact on hemodynamic measurements of brain activity. The study presented in Chapter 4 of this thesis sought to shed light on these questions and identified important biases that may undermine the conclusions drawn from BOLD signal comparisons between younger and older populations.

Calibrated fMRI was originally devised and is generally used to extract a measure of the fractional change in  $CMRO_2$  evoked by a given task. This quantity allows direct comparisons between groups and may be more representative of the amount of synaptic activity expended during performance of the task, since metabolism in the brain is now understood to be predominantly oxidative (Ishii et al. 1996; Mintun et al. 2002; Yamauchi et al. 2002; Hattori et al. 2004; Ito et al. 2005; Ibaraki et al. 2008; Ibaraki et al. 2010). However, beyond the estimation of  $CMRO_2$  changes, the calibrated fMRI framework provides a series of other physiologically-relevant parameters that can contribute to our understanding of the aging process. Calibrated fMRI techniques that include a hypercapnia manipulation may be particularly interesting since they provide measures of cerebrovascular reactivity. CVR has been shown to be affected in a variety of contexts, including aging, stroke and dementia (Nagata et al. 2002; Cantin et al. 2011; Carrera et al.

2011; Lu et al. 2011). Furthermore, the ASL data acquired in the context of the calibrated fMRI experiment can be used to quantify baseline blood flow, a measure also altered in aging (Chen et al. 2011). Finally, the parameter  $M$  is estimated as an intermediate step in the procedure. While the  $M$  parameter preserves the same ambiguity as the BOLD signal (since it is the maximal possible BOLD signal change from baseline), it is nevertheless informative in that it determines the dynamic range of the BOLD signal. The dynamic range is one of the properties that determine the amplitude of the BOLD response mounted for a given amount of metabolism. Also, since it arises from the magnetic properties of baseline deoxyhemoglobin, it is an indirect measure of its concentration in the resting brain (Hoge et al. 1999a).

The data presented in Chapter 4 show that direct comparisons of BOLD measurements between younger and older adults may lead to an underestimation of the metabolic response in the elderly. This is because decreased BOLD reactivity and to a lesser extent in CBF reactivity may result in a reduced BOLD dynamic range. Equivalent BOLD signals measured between younger and older adults in response to a task may in the older adults reflect a larger proportion of the maximal possible dynamic range and thereby be associated with a larger metabolic contribution (Chapter 4, Figure 10).

#### **6.4.1. Calibrated fMRI of aging literature**

Two other calibrated fMRI studies of aging can be found in the literature (Ances et al. 2009; Mohtasib et al. 2012). The results from these studies differ in some respects from those presented here. While one study was also based on a hypercapnia manipulation, the other was however based on hyperoxia calibration, so it does not include BOLD and CBF reactivity. BOLD and CBF reactivity were not found to differ between the two groups in the study presented by Ances et al. However, the number of subjects included in that study was smaller (10 adults in each group) and the participants included in the older group were fairly young (45-60 years). In that study as in the one presented here, baseline CBF was found to differ between groups. This is also in agreement with other ASL data in the literature (Chen et al. 2011; Lu et al. 2011). While  $M$  values were here, as in the

study by Ances et al., found to differ between the groups, the  $M$  values themselves were more similar between the two groups in our study. This may reflect however differences in ROI-drawing techniques and possible regional differences.

The study by Mohtasib et al. (Mohtasib et al. 2012) shows a different picture, with similar baseline CBF and  $M$  between the two groups. The absence of a difference in baseline CBF may reflect poor ASL data quality however, since both PET and MRI literature agree in showing age-related decreased baseline flow (Marchal et al. 1992; Ances et al. 2009; Chen et al. 2011; Lu et al. 2011). The older group showed a shallow decrease in  $M$  values. This may reflect the fact that these changes are difficult to detect in small functionally-defined ROIs. Furthermore, because the authors assumed an a priori value for the flow decrease with hyperoxia based on literature values for young adults (Bulte et al. 2007), this may have masked differences due to altered vascular reactivity in the elderly subjects.

The amplitude of the difference in  $M$  between younger and older cohorts may also be dependent on the health status of the older participants enrolled in the study. While the results from Chapter 5 should be confirmed within a larger cohort of older adults, they do indicate that there may be a link between central vascular health and the value of the  $M$  parameter. If  $M$  is related to vascular health (as seen in the association between augmentation index and  $M$  in Chapter 5), then it may be that healthier older cohorts would be closer to younger subjects in terms of aortic elasticity and  $M$  parameter than the participants included in a study with laxer inclusion criteria. Inclusion criteria should therefore be considered when comparing the value of the  $M$  parameter between different aging studies.

#### **6.4.2. Future improvements**

While the study presented in Chapter 4 of this thesis demonstrates some interesting changes with aging, both in terms of physiology of aging and in terms of identifying the possible biases inherent to direct comparisons of BOLD signal changes between age groups, future studies could incorporate some improvements. The inclusion of an additional hyperoxia manipulation, in conjunction with the improvements in ASL methods described above, would allow the estimation of baseline OEF and  $CMRO_2$  using  $QUO_2$ . This would make it

possible, not only to compare these baseline parameters between the two groups, but also to calculate the change in  $CMRO_2$  during a task in terms of absolute micromolar units. This would remove the confound present in current calibrated fMRI studies that compare relative changes from an unknown baseline.

As mentioned throughout this thesis, the quality of the ASL data is an important limiting factor for all these techniques. While ASL is in general a low SNR technique, global challenges such as hypercapnia may pose particular problems to most ASL implementations (Bolar et al. 2012; Tancredi et al. 2012). Improvements in the ASL techniques mentioned above would be beneficial also within the context of calibrated fMRI studies of aging. Aging studies suffer in fact not only from these other sources of bias, but may also be subject to other confounds if declining vascular health in the older adults results in important decreases in blood velocity. In that case, the standard set of tagging parameters and imaging delays may result in underestimation of blood flow (Campbell et al. 2006), though pseudo-continuous implementations may not be as sensitive to these effects. Future studies could therefore benefit from an investigation into the validity and optimization of the parameter set used for ASL measurements in older adults.

Future functional studies would benefit from additional repetitions of the task in each participant. This would improve the power to detect task-related significant signal changes, and might, depending on the challenge, allow individualized mapping. This is usually possible for primary sensory challenges and, in our experience, greatly improves the quality of estimates of vascular parameters, since the ROI drawn is uniquely adapted to the anatomy and physiology of each participant. Furthermore, tasks known to yield regional BOLD signal differences between young and old could be investigated. While the modified Stroop task used here is known to show behavioral differences between younger and older subjects (Figure 1, Chapter 4), the results presented here and elsewhere (DiGirolamo et al. 2001) for switching tasks indicate that this difference in behavior may not be reflected in the hemodynamic response to the task (Figure 2, Chapter 4).

Therefore, the use of a task well-characterized using fMRI and known to show differences in BOLD signal patterns and amplitude across age groups may

contribute to a better understanding of the biases and differences in cerebral physiology reported in Chapter 4.

## **6.5. Vascular changes with aging**

While Chapter 4 addressed the changes in cerebral physiology seen with aging, it did not address questions on the origin and consequences of these changes in terms of vascular and cognitive health. In Chapter 5, by investigating the link between cerebral hemodynamic changes and changes in general vascular and metabolic health, as well as cognitive performance, some more general hypotheses can start to emerge.

The studies presented in Chapters 4 and 5 confirmed within a single group of younger and older adults some important vascular, metabolic and cognitive changes known to occur with aging. Within our cohort of sixty-two younger and older adults, we were able to show differences in several cerebral hemodynamic properties, including baseline CBF, BOLD and CBF vascular reactivity to CO<sub>2</sub> and changes in the baseline BOLD signal  $M$  (Ances et al. 2009; Chen et al. 2011; Lu et al. 2011; Mohtasib et al. 2012) (Figure 7 and 8A, Chapter 4 and Figure 3, Chapter 5). In addition to these changes in cerebral hemodynamics, older adults were shown to perform more poorly on an executive function task (Figure 1, Chapter 4 and Figure 2, Chapter 5). The brain does not however act in isolation and declining vascular health in the brain is likely preceded by central arterial stiffening (O'Rourke et al. 2007; Redheuil et al. 2010). This was ascertained here and older adults were shown to have decreased aortic elasticity, as measured by aortic pulse-wave velocity and augmentation index (Figure 1A and B, Chapter 5). Finally, older adults were shown to have a reduced capacity to use oxygen during a maximal effort exercise test (VO<sub>2</sub>max) (Figure 1C, Chapter 5).

A set of hypotheses on the mechanisms of vascular aging is starting to emerge from current literature whereby aortic health may, by determining the amplitude of the pressure wave throughout the vascular tree, determine the health of vessels elsewhere in the body (Laurent et al. 2007; O'Rourke et al. 2007; Redheuil et al. 2010; Brown et al. 2011). Because the brain is not protected against the pulsatile nature of blood flow, arteries in the brain may suffer mechanical damage leading to

stiffer arteries and a decreased ability to regulate vascular tone, leading eventually to metabolic deficits, lesions and cognitive decline (Wallace 2005; Girouard et al. 2006; O'Rourke et al. 2007; Iadecola 2010; Brown et al. 2011; Gorelick et al. 2011; Mitchell et al. 2011). Some of these aging effects may however be partly mitigated by the effects of regular exercise. Regular exercise which may help reduce metabolic deficits and lead to neurogenesis and angiogenesis, thereby improving vascular health and cognition (Rogers et al. 1990; Churchill et al. 2002; Colcombe et al. 2003; Swain et al. 2003; Vaynman et al. 2004; Binder et al. 2006; Colcombe et al. 2006; Larson et al. 2006; Arena et al. 2009; Hagner et al. 2009; Kadoglou et al. 2009; Brown et al. 2010; Hopkins et al. 2010; Lazarus et al. 2010; Voss et al. 2010; Davenport et al. 2012; Hopkins et al. 2012). The correlations between the physiological parameters presented in Chapter 5 support these hypotheses, with links between augmentation index and  $M$  parameter,  $VO_2\max$  and, to a lesser extent, cognitive performance. A link between  $VO_2\max$  and cognitive performance further supports this hypothesis framework (Table 1, Chapter 5).

As mentioned in Chapter 5 however, a larger cohort would likely be needed to explore these effects in greater depth, given the fact that the cohort used here is fairly homogeneous and most correlations only marginally significant. We have in fact acquired data on an additional twenty-five participants and will combine these two cohorts for the final published version of this study. Furthermore, some data acquired in this cohort was not used in the studies presented in Chapters 4 and 5. Fasting blood draws were performed on the morning of the MRI session and all participants underwent a neuropsychological battery of tests, as well as optical imaging of baseline hemoglobin (oxygenated and deoxygenated) concentrations and task-evoked oxy- and deoxyhemoglobin changes. This data has not so far been incorporated with the aortic and brain imaging data. However, once integrated, other interesting relationships may emerge with parameters known to be associated with cognitive performance and vascular health such as glucose levels, C-reactive protein levels and lipid profile (Yaffe et al. 2003; Wallace 2005; Kadoglou et al. 2009; Wolf 2012). Furthermore, though performance on one task was examined here in relation to vascular and metabolic health, other cognitive skills could be examined in the future to explore the possibility that some aspects

of cognition may be more sensitive to declining vascular health than others. Other technical improvements could be considered for future studies.

### **6.5.1. Future improvements**

The aorta may be an early marker of arterial damage (Redheuil et al. 2010), but it may not always be the most sensitive means of assessing vascular health in adults over the age of fifty. Several markers of aortic health exist and some, such as ascending aorta distensibility may reach a plateau around middle age and provide little information on declining vascular health in later life (Redheuil et al. 2010). Valuable information may nevertheless be obtained from the aorta, since while the study by Redheuil *et al.* shows that this is true for distensibility measures, pulse-wave velocity and augmentation index may continue to change into later decades. However, other vessels may also provide valuable information, especially in the context of possible relationships with cerebrovascular health. The carotids are the main vessels that carry blood to the brain and carotid stenosis is an important factor in determining CBF and the likelihood of stroke (Bokkers et al. 2011; Tomura et al. 2011; Davies et al. 2012; Momjian-Mayor et al. 2012). Imaging of the carotids could, in future studies, help provide missing information on intermediate steps on the relationship between aortic vascular health and cerebrovascular health.

More permissive selection criteria could also be considered. While inclusion of older adults with additional vascular risk factors increases the number of potential confounding effects, it also ensures a greater variance within the sample, which may be informative for detection of correlations between various vascular parameters. Tabulation of risk factors and their inclusion as covariates in statistical models could help to better understand the physiological correlates of vascular aging.

Finally, as mentioned in the discussion relating to Chapter 4, improvements in ASL methodology and inclusion of a baseline CMRO<sub>2</sub> measure using the QUO2 technique (as presented in Chapter 3) would allow to draw a more complete picture of the vascular and metabolic changes in the brain. Improvements in ASL would allow more robust measurement of CBF on an individualized basis and yield improved composite measures arising from ratio calculations (such as  $M$  and

CMRO<sub>2</sub>). Baseline CMRO<sub>2</sub> on the other hand would permit the exploration of hypotheses on the mitochondrial nature of aging and disease (Wallace 2005).

## **6.6. Future studies**

The studies presented in this thesis are all in their own way proof-of-concept studies. An ambitious research program was used as a starting point for this thesis and various avenues for quantification of physiological properties using functional MRI were explored to yield new metrics, improve on existing ones and to investigate the vascular and metabolic changes of the aging process. Future studies will no doubt improve on these techniques to make them more robust and precise, and the lessons learned in the work presented here will allow the design of better experiments for the study of aging.

Future work on vascular aging would benefit from the use of the QUO2 technique. This technique would allow to retain all the information included in the present aging studies, while providing new physiologically-specific metrics (OEF and resting CMRO<sub>2</sub>). Measurements during breathing manipulation would benefit from the use of a metronome to regulate breathing rate. Furthermore, imaging of the carotids could replace imaging of the aorta, while retaining central aortic stiffening information with applanation tonometry (augmentation index). This would allow a more complete understanding of the state of vascular health and blood delivery to the brain. Further improvements could include quantification of white matter hyperintensities (Brickman et al. 2011). While only a three-point rating scale was used in the studies presented, quantification could provide important additional vascular information, since white matter lesion burden has been shown to be an important factor in determining cerebral hemodynamic properties and cognition (Sierra et al. 2004; Au et al. 2006). Finally, future studies could dispense with the inclusion of a task. While regional heterogeneity of vascular parameters in the brain is of interest for the interpretation of cognitive fMRI findings, this could be addressed using atlas-based region of interest. The scan time freed by removal of fMRI acquisition during a task could be used to perform the additional gas manipulations necessary for the QUO2 method. Finally, the link between cognitive performance and vascular and metabolic physiology could be addressed using

behavioral measures. This protocol would allow the in-depth investigation of vascular and metabolic physiology in the brain, as well as the exploration of the link between these properties and cognition, cardiovascular fitness and elasticity of large arteries in both health and disease.

## Conclusion

In summary, the work included in this thesis presents some new quantitative approaches to estimate resting and task-evoked oxidative metabolism using magnetic resonance imaging, as well as an exploration of age-related vascular and metabolic changes and their impact on hemodynamic functional imaging techniques. First, a generalization of calibrated fMRI methods which offers some advantages in terms of accuracy and robustness was presented. Then, a new technique to measure baseline oxidative metabolism using gas manipulations and the calibrated fMRI framework was demonstrated. In the second part of this thesis, age-related changes in vascular and metabolic physiology were studied, both in terms of biases these changes create in the interpretation of BOLD signal comparisons between age groups, and in terms of the relationship between these cerebral properties and general vascular health, cardiovascular fitness and cognitive performance. The results presented in this thesis show that functional magnetic resonance imaging may be used to characterize vascular and metabolic function in the brain and that these methods may provide valuable information on the physiological processes of aging. Aging was shown to lead to decreased vascular health both centrally and in the brain. Furthermore, there may be an association between these changes and cognitive performance, which may be partly alleviated by greater cardiovascular fitness. Future work on already available data and on data acquired using the new techniques described in the first part of this thesis will explore the physiological correlates of healthy aging, and could provide much needed information for the study of diseases such as dementia and stroke.

# **A. Appendix - Elimination of visually evoked BOLD responses during carbogen inhalation: implications for calibrated MRI**

Gauthier, C.J.<sup>1,2</sup>, Madjar, C.<sup>2</sup>, Tancredi, F.B.<sup>1,2</sup>, Stefanovic, B.<sup>3</sup>, Hoge, R.D.<sup>1,2</sup>

<sup>1</sup> Physiology/Biomedical Engineering, Université de Montréal, Montreal, Quebec, Canada, <sup>2</sup> CRIUGM, Montreal, Quebec, Canada, <sup>3</sup> Medical Biophysics, University of Toronto, Toronto, Canada

NeuroImage, 54 (2011) 1001–1011

## **A.1. Abstract**

Breathing a mixture of 10% CO<sub>2</sub> with 90%O<sub>2</sub> (referred to here as carbogen-10) increases blood flow due to the vasodilatory effect of CO<sub>2</sub>, and raises blood O<sub>2</sub> saturation due to the enriched oxygen level. These effects both tend to reduce the level of deoxygenated hemoglobin in brain tissues, thereby reducing the potential for further increases in BOLD contrast. In the present study, blocks of intense visual stimulation (60s) were presented amid longer blocks (180s) during which subjects breathed various fractional concentrations (0-100%) of carbogen-10 diluted with medical air. When breathing undiluted carbogen-10, the BOLD response to visual stimulation was reduced below the level of noise against the background of the carbogen-10 response. At these concentrations, the total (visual + carbogen) BOLD response amplitude ( $7.5 \pm 1.0\%$ ,  $n = 6$ ) converged toward that seen with carbogen alone ( $7.5 \pm 1.0\%$ ,  $n = 6$ ). In spite of the almost complete elimination of the visual BOLD response, pseudo-continuous arterial spin-labeling on a separate cohort indicated a largely preserved perfusion response ( $89 \pm 34\%$ ,  $n = 5$ ) to the visual stimulus during inhalation of carbogen-10.

The above observations suggest that venous saturation can be driven to very high levels during carbogen inhalation, a finding which has significant implications for

calibrated MRI techniques. The latter methods involve estimation of the relative change in venous O<sub>2</sub> saturation by expressing activation-induced BOLD signal increases as a fraction of the maximal BOLD signal  $M$  that would be observed as venous saturation approaches 100%. While the value of  $M$  has generally been extrapolated from much smaller BOLD responses induced using hypercapnia or hyperoxia, our results suggest that these effects could be combined through carbogen inhalation to obtain estimates of  $M$  based on larger BOLD increases. Using a hybrid BOLD calibration model taking into account changes in both blood flow and arterial oxygenation, we estimated that inhalation of carbogen-10 led to an average venous saturation of 91%, allowing us to compute an estimated  $M$  value of 9.5%.

Keywords: calibrated MRI, carbogen, hypercapnia, hyperoxia, oxygen metabolism, venous saturation

## **A.2. Introduction**

During increased brain activity, BOLD contrast in functional MRI reflects a reduction in deoxygenated hemoglobin (dHb) concentration in the venous circulation local to the activated region. This reduction is caused by an increase in the local arterial blood flow, which is generally sufficient to increase the mean O<sub>2</sub> saturation along the capillary bed, supporting, according to the oxygen limitation model (Buxton et al. 1997), an increase in delivery of O<sub>2</sub> to neural tissues under diffusion limited conditions. In principle, the BOLD signal increase observed during a particular event carries information about the change in venous dHb concentration. Since virtually all dHb in the venous circulation of healthy individuals is generated as a result of metabolic O<sub>2</sub> extraction, then the relative change in venous dHb level during stimulation should depend partly on the relative change in the cerebral metabolic rate of O<sub>2</sub> consumption, or CMRO<sub>2</sub> (Buxton et al. 1997). If the changes in blood flow and volume can be factored out, then in theory it should be possible to obtain a quantitative estimate of the fractional change in CMRO<sub>2</sub> that occurred as a result of stimulation. Although the latter notion is indeed the foundation for various MRI-based methods for CMRO<sub>2</sub> estimation (Davis et al. 1998; Chiarelli et al. 2007b), the BOLD signal change observed during activation is

not itself sufficient to determine the relative change in venous dHb concentration. Such a determination requires expressing the activation-induced BOLD response as a fraction of the maximum possible BOLD signal increase that would be observed upon complete elimination of all dHb from tissues (usually denoted  $M$  in literature). For this reason, various calibration methods have been proposed in which the total attenuation of T2\*-weighted signal attributable to dHb at baseline (conversely equivalent to the maximum possible BOLD signal increase) is estimated through extrapolation of BOLD signal increases observed during mild hypercapnia (Davis et al. 1998) or hyperoxia (Chiarelli et al. 2007b). In the hypercapnia method,  $M$  is extrapolated from the BOLD and flow responses during mild hypercapnia (typically achieved by having subjects breathe 5-10% CO<sub>2</sub> in air). This is the earliest calibration method introduced by Davis *et al.* and has since been employed in numerous studies (Davis et al. 1998; Hoge et al. 1999b; Stefanovic et al. 2006; Leontiev et al. 2007b; Ances et al. 2008; Lin et al. 2008; Perthen et al. 2008; Ances et al. 2009; Bulte et al. 2009; Chen et al. 2009b). In the more recently introduced hyperoxia calibration method, a similar model is used to estimate  $M$  from the BOLD response to hyperoxia (usually induced through inhalation of 50-100% O<sub>2</sub>). This model uses end-tidal PO<sub>2</sub> (partial pressure of oxygen) values to estimate the venous deoxygenated hemoglobin fraction, with the additional assumption of an unchanged CBF in the case of mild hyperoxia or of a fixed, pre-determined CBF decrease in the case of higher inspired O<sub>2</sub> concentrations (Chiarelli et al. 2007b; Goodwin et al. 2009).

Because of the uncertainties inherent when resorting to extrapolation, as well as some speculative aspects of the BOLD signal models applied, the validity of such calibration methods has been difficult to confirm (Hoge et al. 1999a; Hoge et al. 2001; Buxton et al. 2004; Stefanovic et al. 2006; Chiarelli et al. 2007a; Ances et al. 2008; Zappe et al. 2008; Chen et al. 2010a). Previous studies using hypercapnia or hyperoxia have reported  $M$  values ranging from 3.7 to 22 percent. An important consideration when comparing such data is that the measured value is specific not only to a particular anatomic region, but also to the applicable measurement conditions, including field strength, echo time, and the degree of vascular weighting (use of diffusion crusher gradients, prevalence of veins in ROI's). Since the

parameter  $M$  is, implicitly, a linear function of the echo time used in the experiment (see Eq. 7 in Hoge *et al.* 1999), it is necessary to correct by the ratio of echo times when comparing  $M$  values from different experiments. After adjustment to an equivalent echo-time of 30 ms, percent  $M$  values measured in visual cortex at 1.5 Tesla (only hypercapnic calibration has been used at this field strength) include 3.4 (Davis *et al.* 1998), 4.6 (Stefanovic *et al.* 2006), and 13.2 (Hoge *et al.* 1999b; Hoge *et al.* 1999a). Hypercapnic-determined visual cortex  $M$  values at 3 Tesla, adjusted to a common TE of 30 ms, include 5.3 (Bulte *et al.* 2009), 5.7 (Ances *et al.* 2008), 6.5 and 7.3 (Ances *et al.* 2009), 6.7 (Chen *et al.* 2009b), 10.5 (Lin *et al.* 2008), 11.1 (Leontiev *et al.* 2007b) and 11.6 and 12.1 (Perthen *et al.* 2008) for hypercapnia. A value of 7.0 percent was measured by Chiarelli *et al.* in visual cortex at 3 Tesla (TE=30 ms) using hyperoxic calibration (Chiarelli *et al.* 2007b). While some of the variability in reported  $M$  values may reflect differences in venous weighting associated with the ROI selection or other factors, it is also clear that the majority of estimated  $M$  values represent BOLD signal increases that are considerably higher than those typically measured during even the most intense stimulation paradigms. Although this is to be expected in a value that is supposed to represent the maximum possible signal increase, the veracity of such large signal changes has been understandably questioned (Chiarelli *et al.* 2007a; Chiarelli *et al.* 2007b) given their basis in extrapolation via biophysical models which unavoidably include a certain degree of speculation. Methods in which hypercapnia is used may further suffer from the low-signal-to-noise ratio of arterial spin-labeling measures needed to measure flow changes during this type of calibration. Use of an appropriate  $M$  value is critical in calibrated MRI, as incorrect values can lead to substantial bias in estimated  $CMRO_2$  values as well as in apparent CBF- $CMRO_2$  coupling relations, as has been pointed out by Chiarelli *et al.* (Chiarelli *et al.* 2007a).

If a method could be devised to raise the venous  $O_2$  saturation close to 100%, then the maximum achievable BOLD signal could be determined more directly for a given physiological baseline state. The objective of the present study was therefore to explore the use of a breathing gas mixture consisting of 10% carbon dioxide and 90% oxygen (referred to here as carbogen-10 since the term carbogen alone is

used to describe any mixture of CO<sub>2</sub> with balance 100% O<sub>2</sub>) as a means of producing very high levels of venous O<sub>2</sub> saturation. Hypercapnia, induced using carbon dioxide concentrations of 4 to 10%, has been explored extensively in the past as a means of producing robust BOLD signals due to the vasodilatory action of CO<sub>2</sub> (Kim et al. 1999; Kemna et al. 2001a; Posse et al. 2001; Chiarelli et al. 2007a; Leontiev et al. 2007a; Leontiev et al. 2007b; Ances et al. 2008; Perthen et al. 2008; Ances et al. 2009; Bulte et al. 2009; Chen et al. 2009a; Mark et al. 2010), and carbogen has been explored to evaluate susceptibility-weighted imaging methods and in the study of tumor oxygenation (van der Sanden et al. 1999; Landuyt et al. 2001; Dunn et al. 2002; Rauscher et al. 2005a; Ashkanian et al. 2008; Sedlacik et al. 2008; Ashkanian et al. 2009). The use of a relatively high CO<sub>2</sub> content (10%) combined with enrichment of O<sub>2</sub> (90% as opposed to 21% in atmospheric composition air) should lead to very high venous O<sub>2</sub> saturations (Ogawa et al. 1990a; Rauscher et al. 2006; Sedlacik et al. 2007; Sedlacik et al. 2008; Bulte et al. 2009; Sedlacik et al. 2009). To further increase venous O<sub>2</sub> in specific cortical areas, and to assess the degree to which BOLD reactivity approaches saturation against a background of very high venous saturation, we applied intense visual stimulation during during periods of carbogen-10 inhalation. Titration studies in which subjects breathed various concentrations of carbogen-10 in air, with and without intense visual stimulation, suggested that inhalation of pure carbogen-10 results in almost complete elimination of venous dHb in visual cortex and thus allows a more direct estimation of the asymptotic BOLD signal increase *M*.

### **A.3. Methods**

Acquisitions were conducted in nine healthy subjects, seven males and two females, aged 21 to 32 years, on a Siemens TIM Trio 3T MRI system (Siemens Medical Solutions, Erlangen, Germany) using the Siemens 32-channel receive-only head coil for all acquisitions. All subjects gave informed consent and the project was approved by the Comité mixte d'éthique de la recherche du Regroupement Neuroimagerie/Québec. Two types of scanning session were performed, each on a subset of six of the nine subjects. The first type of session consisted of the BOLD

titration experiments in which varying fractions of carbogen-10 were administered either with or without simultaneous visual stimulation. The second session type focused on perfusion imaging with pseudo-continuous arterial spin-labeling (pCASL) during combined carbogen inhalation and visual stimulation.

BOLD titration sessions included an anatomical, 1mm<sup>3</sup> MPRAGE acquisition (TR/TE/alpha = 2300ms/3ms/9°, 256x240 matrix) and nine BOLD functional runs (TR/TE/alpha = 2000ms/30ms/90° with 4x4x4mm voxels, 64x64 matrix and 33 slices). During these BOLD acquisitions, subjects underwent a titration of carbogen-10 (10% CO<sub>2</sub>, 90% O<sub>2</sub>) (Vitalaire Santé, Montreal, QC, Canada). Two runs of each of the four carbogen fractions (25%, 50%, 75%, 100%) with balance air were performed (see Table 1 for gas concentrations associated with each fraction). For each fraction, one run was conducted with a single three-minute carbogen block, after an initial 90 seconds of air breathing (all percent change values in this report are expressed relative to the air-breathing baseline). A second run was performed for each carbogen/air fraction with the addition of a one-minute block of visual stimulation. The visual stimulus was a black and white radial checkerboard, annuli scaled logarithmically with eccentricity, luminance modulated in a temporal squarewave at 8 Hz (equivalent to 16 contrast reversals per second) presented using a LCD projector (EMP-8300, Epson, Toronto, ON, Canada) onto a translucent screen viewed by subjects through a mirror integrated into the Siemens head coil. This stimulation was initiated 90 seconds into the carbogen block (actual run order was randomized). An additional run was done with the visual stimulus presented without carbogen, with the stimulus starting 180 seconds into the run as in the other acquisitions.

	%CO <sub>2</sub>	%O <sub>2</sub>	%N <sub>2</sub>
<b>Medical air</b>	0	21	79
<b>25% carbogen-10</b>	2.5	38.25	59.25
<b>50% carbogen-10</b>	5	55.5	39.5
<b>75% carbogen-10</b>	7.5	72.75	19.75
<b>100% carbogen-10</b>	10	90	0

**Table 1. Gas mixture compositions**

Concentration of each component gas of the mixtures administered to the subjects in the course of this titration experiment.

Additional acquisitions were performed on some subjects. In one subject, two susceptibility-weighted images (SWI) (Reichenbach et al. 2001; Rauscher et al. 2005b) were obtained to provide a qualitative assessment of the venous oxygenation increase with carbogen. One image was acquired during medical air breathing and one during carbogen-10 inhalation. The image obtained during carbogen breathing was acquired after an initial 1-min period of carbogen breathing to allow oxygen saturation and vasodilation to reach a plateau. Parameters used for the SWI acquisition were: TR/TE/alpha = 27ms/20ms/15° with 0.9x0.9mm in-plane resolution with 56 slices of 1.5mm on a 256x192 matrix.

To determine the effect of carbogen more specifically on the visually-evoked perfusion response, a pseudo-continuous arterial spin labeling (pCASL) acquisition (Wu et al. 2007) was used to measure changes in cerebral blood flow (CBF) in six subjects during combined carbogen-10 inhalation and visual stimulation. The data from one subject could not be used due to excessive movement. The same experimental timing and visual paradigm was used to deliver carbogen-10 during this acquisition. The parameters used in the pCASL sequence were: TR/TE/alpha = 3000ms/10ms/90° with 4x4mm in-plane resolution and 16 slices of 6mm (1mm slice gap) on a 64x64 matrix (at 7/8 partial Fourier), GRAPPA acceleration factor = 2 (Griswold et al. 2002), post-labeling delay = 900ms, Hanning window-shaped RF pulse with duration/space = 500µs/920µs, flip angle of labeling pulse = 25°, slice-selective gradient = 6mT/m, tagging duration = 2s (Wu et al. 2007).

### **A.3.1. Gas manipulations**

At the beginning of the experiment, subjects were fitted with a non-rebreathing face mask (Hudson RCI, #1059, Temecula, California, USA). To avoid discomfort from outward gas leakage blowing into the subject's eyes, skin tape (Tegaderm Film, #1626W, 3M Health Care, St-Paul, MN, USA) was used to seal the top of the mask to the face. Plastic tubing (Airlife™ Oxygen tubing #001305, Cardinal Health, McGraw Park, IL, USA) and a Y-connector were used to connect pressure/flow-meters for medical air and carbogen-10 tanks (Vitalaire, Mississauga, ON, Canada) to the mask. Gas flows were adjusted manually on the pressure/flow-meters (MEGS, Ville St-Laurent, QC, Canada) to keep a total flow rate of 16L/min. Gas flow was kept at 16L/min at all times except during administration of the highest carbogen concentration. From the control room, the reservoir bag affixed to the non-rebreathing mask could be seen. For subjects found to hyperventilate beyond the gas delivery used in the other acquisitions (causing the reservoir bag to collapse fully at the end of each breath and some atmospheric air to be entrained into the mask), gas flow rates were increased to the maximal possible rate (25L/min) achievable with our pressure/flowmeters for the highest carbogen-10 concentration acquisitions. Pulse rate and arterial O<sub>2</sub> saturation were monitored in all subjects using a pulse-oximeter (InVivo Instruments, Orlando, USA) as a safety measure and to observe the effects of carbogen breathing.

End-tidal O<sub>2</sub> and CO<sub>2</sub> values were monitored in five subjects. Gases were sampled via an indwelling nasal cannula (Airlife™ Nasal Oxygen Cannula #001321, Cardinal Health, McGraw Park, IL, USA) using the CO2100C and O2100C modules of the MP150 BIOPAC physiological monitoring unit (BIOPAC Systems Inc., Goleta, CA, USA). Calibration of the unit was done by taking into account an expired partial pressure of water of 47mmHg (Severinghaus 1989). Subjects were instructed to breathe through their nose, which ensured that only expired gas was sampled by the nasal cannula.

Following acquisition, all subjects were debriefed to assess the level of discomfort associated with the manipulation. The subjects were asked to rate the air hunger and breathing discomfort associated with the maximal carbogen-10 concentration

on a French language version of the scale proposed by Banzett et al. (Banzett et al. 1996). Subjects were asked to rate the discomfort of the carbogen-breathing block in three parts: the first half of the block, the second half, and over the whole manipulation.

### **A.3.2. Data analysis**

All MRI data were analyzed using the Neurolens data analysis software package ([www.neurolens.org](http://www.neurolens.org)). BOLD data were motion corrected (Cox et al. 1999) and spatially smoothed with a 6 mm 3D Gaussian kernel. ASL data were similarly processed, and the CBF signal was isolated through surround subtraction using linear interpolation between neighboring points (Liu et al. 2005). A general linear model (GLM) assuming a hemodynamic response function (HRF) consisting of a single gamma function (Glover 1999) and a linear drift and constant offset terms was applied, to obtain effect sizes and T-maps for each condition (visual and/or carbogen). The first 60s after gas transitions were excluded from the analyses by zeroing out relevant matrix rows in the GLM computation, as the transition periods would not be accurately modeled by the HRF used in the GLM fit (as can be appreciated from Fig. 3).

Regions of interest (ROIs) were derived from thresholded ( $p \leq 0.01$  corrected) (Worsley et al. 2002) visual activation T-maps (Fig. 1). Fractional changes were then calculated by dividing effect sizes over the visual ROI by the constant DC term from the GLM averaged within the region. Group average values  $\pm$  standard error are reported here. Time courses were obtained by averaging the fractional signal change traces for five subjects at each carbogen concentration. The linear trend and DC terms from the full linear model were removed from the pre-processed ROI-average signal traces of each subject before averaging signal traces (converted to percent change) between subjects. One subject was excluded from this analysis because of a missing acquisition for one carbogen concentration. Separate visual ROIs were made for ASL acquisitions with the same statistical ( $p = 0.01$ ) threshold as for BOLD acquisitions.

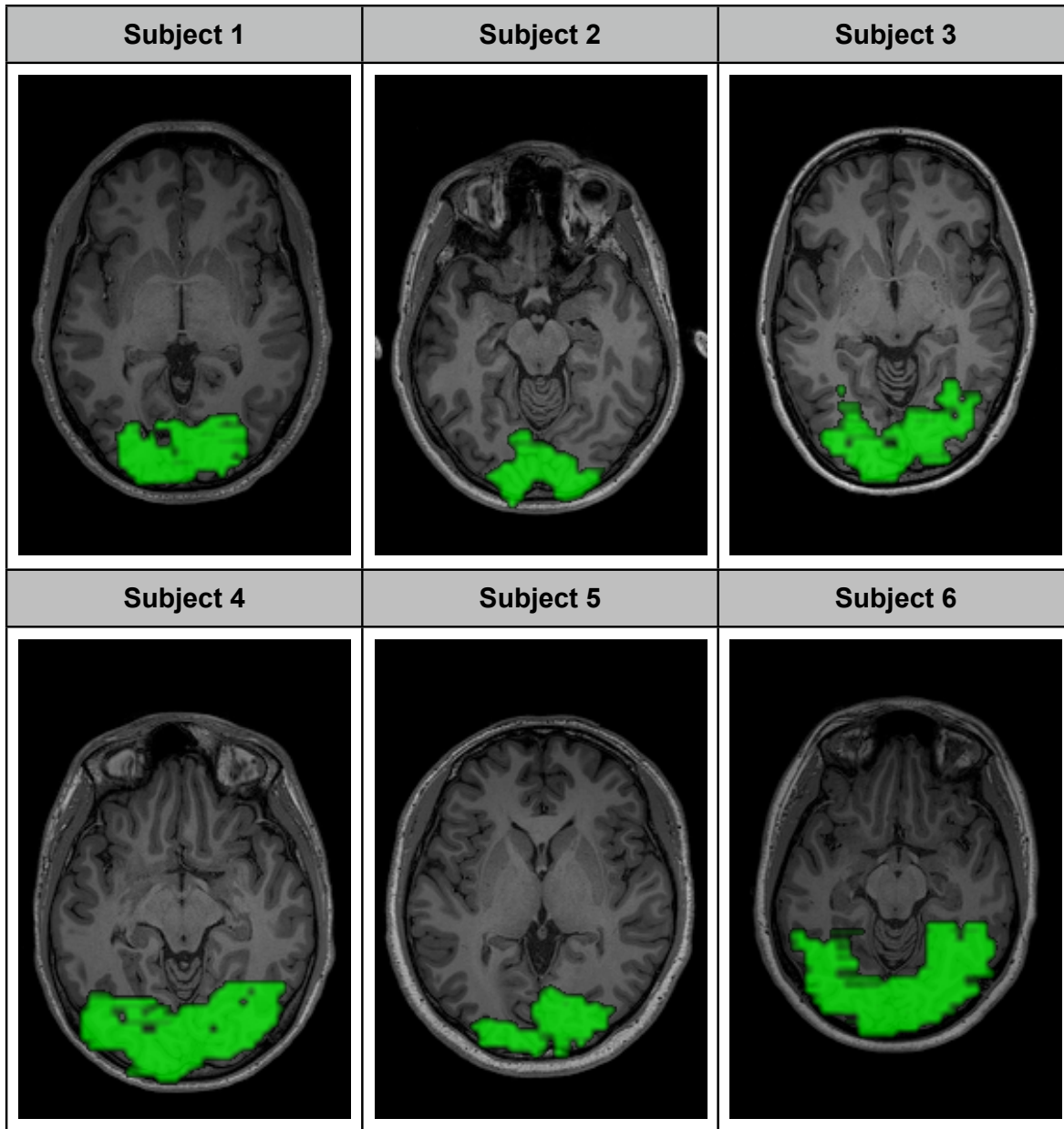


**Figure 1. Visual cortex regions of interest for each subject**

Regions of interest (ROI) for each subject, defined from significantly activated voxels ( $p \leq 0.01$ ) from the visual-only BOLD acquisition of each subject. This procedure yielded diffuse ROIs over visual areas.

To estimate the incremental response due to visual stimulation against the background of carbogen-10 breathing in BOLD and CBF signals, a linear model was fit to the group average time course for the respective signals (BOLD and ASL, expressed as percent change) for the visual stimulation + carbogen experiment. For the BOLD signal, the regressors consisted of a carbogen response term based on the group average data (after de-trending and normalization) for carbogen

alone, plus a 60 second square pulse representing the visual response term. Other GLM parameters (HRF, etc.) were as described above.

End-tidal CO<sub>2</sub> and O<sub>2</sub> values were picked manually and averaged over all subjects, for the first five breaths of the experiment, when subjects were breathing air, and for the last ten breaths of the carbogen-10 breathing block.

Arterial spin-labeling measurements acquired during carbogen inhalation were corrected for T1 changes using the approach described in (Chalela et al. 2000; Zaharchuk et al. 2008). Arterial blood T1 values of 1660 ms and 1487 ms were used, respectively, for normoxia and the hyperoxic state produced by carbogen-10 (from T1 vs. FiO<sub>2</sub> values tabulated in Bulte *et al.* (Bulte et al. 2007). Since the T1 depends specifically on the level of dissolved O<sub>2</sub> in the plasma, and since we obtained different PaO<sub>2</sub> (arterial partial pressure of O<sub>2</sub>) values at a given FiO<sub>2</sub> (fraction of inspired O<sub>2</sub>) than the latter study (their PaO<sub>2</sub> values were higher, likely due to the use of a tightly sealed face mask), the values were interpolated to account for this difference (i.e. the table from Bulte was converted to T1 vs. group average PaO<sub>2</sub>, and the T1 corresponding to our group average PaO<sub>2</sub> during inhalation of carbogen-10 was interpolated). The T1 correction factor was thus determined to be 1.07 (i.e. flow would be underestimated by 7% without correction). Values for the absolute blood flow at the air-breathing baseline were computed using Equation 1 from Wang *et al.* (Wang et al. 2003b), assuming the same constant values as in this reference.

## A.4. Results

Visual stimulation alone resulted in extensive BOLD activation throughout visual cortex, as shown in ROI masks in Fig. 1. Inhalation of carbogen-10 caused large BOLD signal increases in cortical and sub-cortical grey matter (Fig. 2), with the incremental contribution from the addition of visual stimulation becoming successively smaller at higher fractional carbogen concentrations (Fig. 3 and 5). Percent changes for both stimuli (carbogen-10 alone and carbogen-10 + visual) averaged over visually-activated areas in individual subjects show a universal tendency to converge towards a common maximal signal change (Fig. 4). Group

average response curves for carbogen-10 inhalation alone and carbogen-10 plus visual stimulation show an apparent convergence of response amplitudes at the highest carbogen fractions (Fig. 5). Unpaired two-tailed t-tests on ROI group averages for each level, comparing with and without visual stimulation, reveal a decreasing significance level of the difference with increasing carbogen fraction ( $p=0.002$  at 25% carbogen-10 to  $p = 0.96$  at 100% carbogen-10). The average percent signal change over subjects was  $7.5\% \pm 1.0$  in visual cortex for carbogen-10 inhalation alone. This was equal within measurement error to the average signal change of  $7.5\% \pm 1.0$  for carbogen-10 breathing combined with intense visual stimulation (Fig. 3 and 5). The visually-evoked BOLD signal change of  $2.0 \pm 0.1\%$  measured during visual stimulation alone (i.e. breathing air) was thus largely eliminated against the carbogen background. Pulse oximetry showed a tendency for arterial  $O_2$  saturation to rise from baseline levels (typically 98%) toward 100% in all subjects.

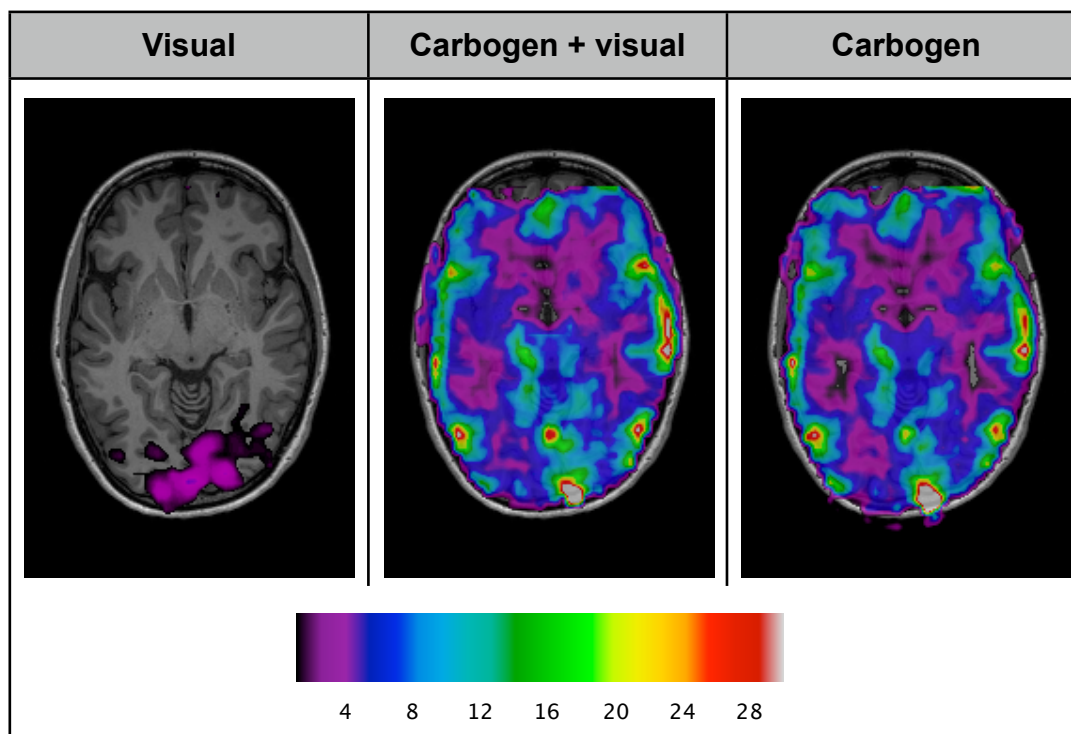


**Figure 2. Percent BOLD response maps from example subject**

Example maps of percent change in a representative subject for each stimulus paradigm: visual only (left), carbogen only (right) and superimposition of both stimuli (center). Maps show high percent BOLD signal increase throughout grey matter in response to carbogen-10 inhalation. The spatial distribution of BOLD response during the combined stimulus paradigm demonstrates

saturation of the visually evoked component, as the latter is not discernible against the background of carbogen response.

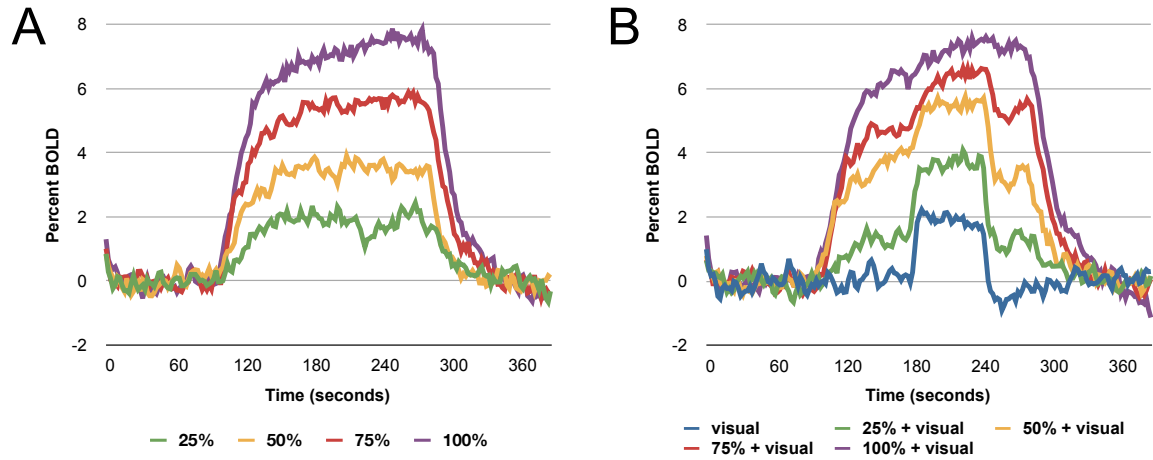


**Figure 3. BOLD Time course for carbogen inhalation and carbogen + visual stimulation**

Average over five subjects of BOLD time course in visual cortex ROI during carbogen-10 inhalation alone (A) and carbogen-10 inhalation plus visual stimulation (B). This figure shows a diminishing contribution of visually-evoked BOLD signal when combined with carbogen breathing. Maximal signal changes obtained with and without visual stimulation during carbogen-10 breathing are equal, within measurement error.

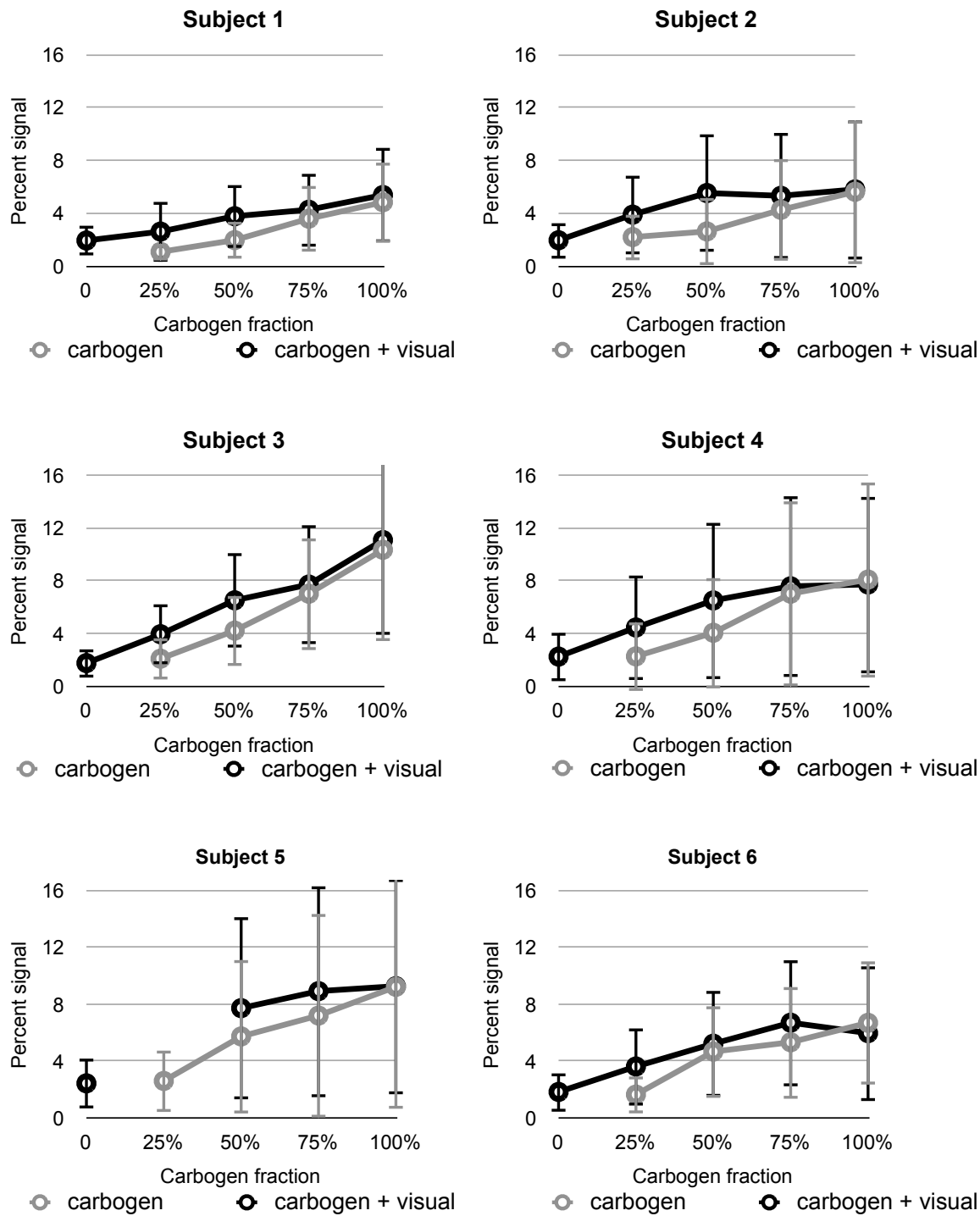


**Figure 4. Individual BOLD percent changes in visual ROI**

Visual ROI average percent changes ( $\pm$  SD) measured in each individual subject at the different fractional carbogen-10 concentrations, with and without the additional visual stimulation. All subjects demonstrated convergent responses for the two conditions. The average end-tidal gas changes for the 100% carbogen-10 condition were  $59.2 \pm 2.4$  mmHg for CO<sub>2</sub> and  $387.9 \pm 34.1$  mmHg for O<sub>2</sub>.

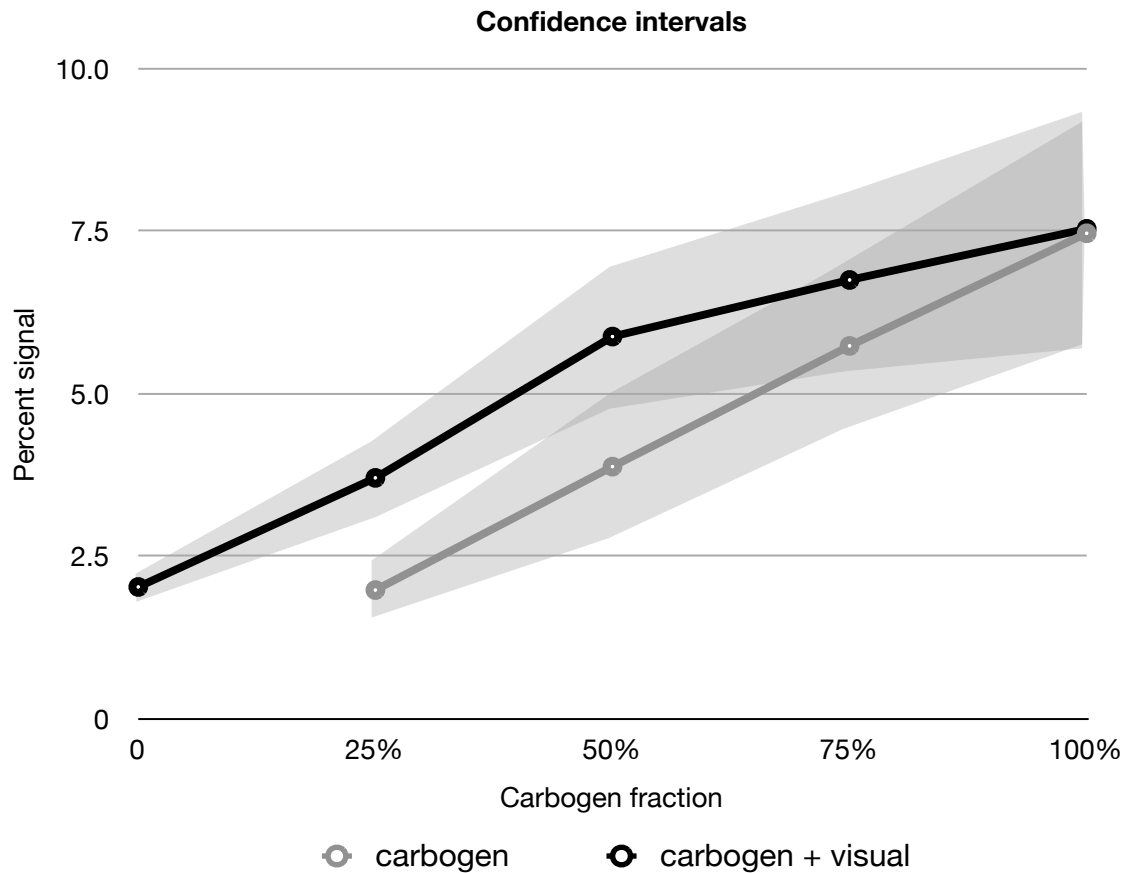


**Figure 5. Group-average BOLD response amplitudes**

Group average percent BOLD signal change over a visual ROI (solid lines) within standard error bounds (grey shading) for each stimulus paradigm. The convergence of the two curves suggests saturation of the total BOLD response at values above 7.5%.

Due to technical limitations, end-tidal  $O_2$  and  $CO_2$  values were only acquired on a subset of five subjects during carbogen-10 inhalation. Average baseline end-tidal values were  $44.4 \pm 1.1$  mmHg for  $CO_2$  and  $120.0 \pm 3.8$  mmHg for  $O_2$ . The group average end-tidal values during the last ten breaths of carbogen-10 inhalation were  $59.2 \pm 2.4$  mmHg for  $CO_2$  and  $387.9 \pm 34.1$  mmHg for  $O_2$ .

#### A.4.1. Additional tests

SWI data acquired in one subject during air and carbogen-10 breathing demonstrated an almost complete loss of venous contrast during carbogen-10 breathing (Fig. 6). Analysis of ASL data acquired in five subjects revealed a substantial visually induced flow increase ( $88.9 \pm 34.2\%$ ) against the background of carbogen inhalation, in spite of the greatly reduced visual BOLD response under

similar conditions (Fig. 7). The group average flow increase from carbogen-10 inhalation was  $104.5 \pm 24.0\%$  from an absolute baseline of  $51.4 \pm 7.0$  ml/100g/min.

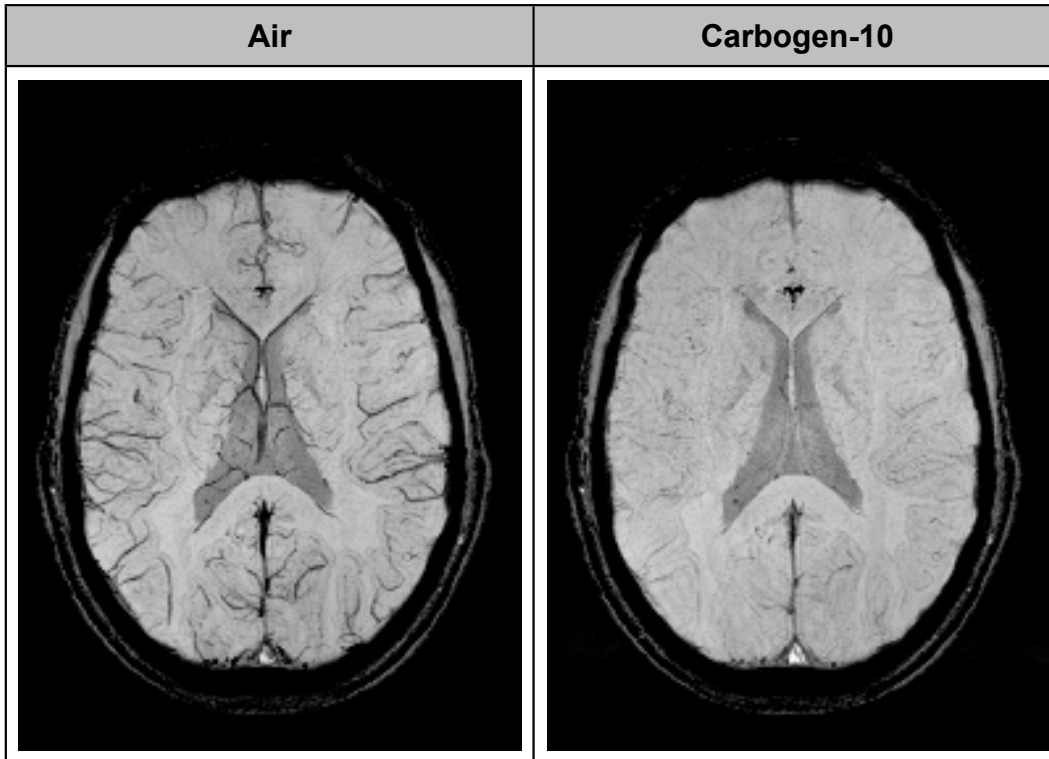


**Figure 6. Susceptibility-weighted venogram**

SWI data acquired during air and carbogen-10 inhalation in a single subject. There is an almost complete loss of venous contrast during carbogen inhalation, demonstrating the high venous oxygen saturation attained.

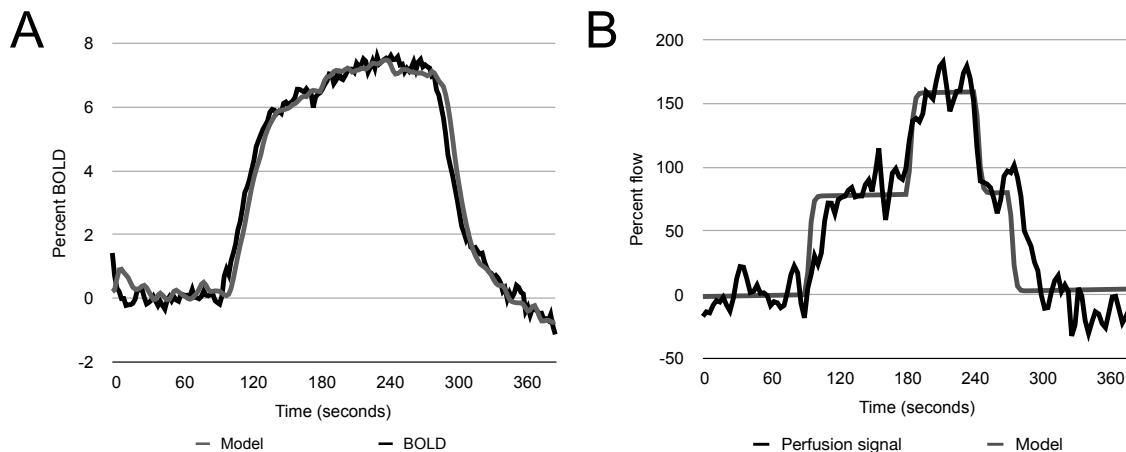


**Figure 7. BOLD and ASL time courses for visual stimulation during carbogen-10 breathing**

Visual ROI time-course averages (five subjects) for BOLD (A) and ASL (B). The average time courses are shown in black, along with the GLM fits in grey. Although the visually evoked BOLD response is barely detectable, the perfusion response to the visual stimulus is distinctly apparent

against the background perfusion increase from breathing carbogen-10. This suggests that a largely intact visual flow response may be invoked in spite of the background hyperoxia due to carbogen-10 inhalation, and even though the BOLD response component has been all but eliminated.

#### **A.4.2. Subjective discomfort rating**

Subjects reported a moderate to high degree of discomfort from carbogen-10 breathing. All subjects reported sensations of air hunger and hot flushes (a generalized feeling of warmth) during carbogen inhalation, which increased progressively over time during the carbogen block. All subjects included in this study had prior experience as MRI volunteers and most had already participated in at least one study including hypercapnia. Subjects were briefed extensively on the importance of reporting discomfort and reminded regularly that the experiment could be stopped immediately at their discretion if it became too uncomfortable. Two subjects asked to interrupt the experiment to request a higher gas flow rate during the highest carbogen concentration. Increasing the flow rate of carbogen beyond 16L/min for subjects reporting a difficulty breathing relieved much of the discomfort and allowed them to complete the experiment (illustrating the subjective nature of air hunger and complex interplay between CO<sub>2</sub> level and ventilation parameters (Lansing et al. 2009)). Average discomfort ratings were  $4.7 \pm 0.5$  out of a possible of 7 for the whole block, with all subjects reporting a discomfort rating one to two points higher for the second half of the carbogen-inhalation block, as compared to the first half.

#### **A.5. Discussion**

The diminishing incremental response from visual stimulation at high carbogen concentrations suggests that the BOLD signal obtained with this manipulation approaches the saturation plateau  $M$ . We observed a convergence of percent signal changes towards a common value of  $7.5 \pm 1.0\%$  for both carbogen-10 inhalation alone and combined with intense visual stimulation (Fig. 3 and 5). This saturation effect was found to be robust and was observed in all individual subjects data (Fig. 4). While investigation of the visually evoked BOLD component against a varying background of carbogen inhalation was the primary objective of this study,

additional measures were also performed to elucidate the mechanisms of the observed behavior. These ancillary measures are discussed below.

### **A.5.1. Arterial spin-labeling**

Analysis of pseudo-continuous arterial spin labeling data acquired in five subjects confirms that the saturation effect observed in the BOLD signal response to carbogen-10 does not arise from a reduction of the perfusion response to the visual stimulus against the carbogen background. The signal time courses averaged over the visually-activated areas of both subjects show a substantial perfusion increase in response to visual stimulation ( $88.9 \pm 34.2\%$ ) that is distinctly visible against the superimposed flow response to carbogen (Fig. 7B). This is in spite of the striking abolition of virtually any apparent visual contribution in the BOLD signal (Fig. 7A), and the profound tissue hyperoxia that must exist under this condition (further confirmation that activation-induced perfusion increases are unlikely to be triggered by decreased tissue  $pO_2$  during activation).

It should be noted that two competing effects represent potential confounds to flow quantification in the ASL acquisitions: T1 lengthening due to an increased arterial  $O_2$  saturation and T1 shortening due to increased plasma  $O_2$  concentration (Buxton et al. 1998a; Bulte et al. 2007). Because we expect T1 shortening to be the predominant effect (Bulte et al. 2007; Bulte et al. 2009), this should result in the underestimation of blood flow changes during carbogen inhalation. The effects of T1 shortening were therefore taken into account here according to the signal formulation for continuous ASL (Chalela et al. 2000; Zaharchuk et al. 2008). The values for arterial blood T1 were adjusted from literature values (Bulte et al. 2007) for the  $Pa_{O_2}$  reached in our experiments.

The perfusion increase of  $104.5 \pm 24.0\%$  measured in the present study during inhalation of carbogen-10 is similar to values found for similar end-tidal  $P_{CO_2}$  values in previous studies using radiotracer methods (Kety et al. 1948; Kemna et al. 2001b). Recent studies using pulsed ASL (PASL) have yielded smaller estimates of flow changes in response to inhalation of 10%  $CO_2$  (Stefanovic et al. 2006; Mark et al. 2010). A number of authors have discussed the difficulty of acquiring accurate PASL measures of CBF change under conditions where the arterial transit time

undergoes a large variation (such as hypercapnia) (Wong et al. 1997; Buxton et al. 1998a; Yang et al. 2000). A reduced dependence of the calibration procedure on ASL measures is indeed one of the motivations for the hyperoxia method (Chiarelli et al. 2007b; Goodwin et al. 2009). We have found (in a parallel study, manuscript in preparation) that the pseudo-continuous ASL method used in the present study may avoid downward bias on flow estimates during global challenges which may be inherent in some pulsed ASL implementations due to shifts in the timing of label delivery during such manipulations (i.e. if global blood flow increases sufficiently, then the trailing edge of the tag bolus may leave the tagging region before the time  $T_{I1}$  at which QUIPSS 2 saturation pulses are applied (Wong et al. 1997)). This may explain the higher average flow value obtained in the present study.

### **A.5.2. Susceptibility-weighted imaging**

Saturation of BOLD signal with carbogen-10 inhalation is demonstrated by the marked loss of venous contrast in SWI data acquired during carbogen-10 inhalation, when compared to data acquired during air breathing in the single subject thus studied (Fig. 6). Carbogen-5 (95% O<sub>2</sub>, 5% CO<sub>2</sub>) inhalation has been shown before to lead to an almost complete loss of susceptibility contrast in SWI (susceptibility-weighted imaging) images (Rauscher et al. 2005b; Sedlacik et al. 2007; Sedlacik et al. 2008; Sedlacik et al. 2009). Sedlacik et al., have used SWI to quantify venous oxygenation in response to carbogen breathing in both a single vessel and whole brain approach (Sedlacik et al. 2007; Sedlacik et al. 2008; Sedlacik et al. 2009). The linear relationship between the CO<sub>2</sub> content of carbogen and venous oxygenation observed by this group predicts a complete O<sub>2</sub> saturation at around 6.3% CO<sub>2</sub> content of carbogen (Sedlacik et al. 2008), well below the 10% CO<sub>2</sub> concentration used here (although the latter study used a continuous positive airway pressure system, which may be more efficient at raising saturation at a given fraction of inspired CO<sub>2</sub>).

### **A.5.3. Implications for calibrated MRI**

As noted in the introduction, existing calibrated MRI methods for estimating changes in CMRO<sub>2</sub> involve determination of the BOLD signal increase  $M$  that would correspond to complete elimination of deoxygenated hemoglobin in tissues.

This intermediate step has been performed in previous studies by measuring increases in cerebral blood flow and BOLD signal during hypercapnia (Davis et al. 1998) and also by measuring BOLD and end-tidal O<sub>2</sub> changes during hyperoxia (Chiarelli et al. 2007b). The large changes in both flow and arterial oxygenation that occur during inhalation of carbogen offer the possibility of a unified calibration method that consolidates the two approaches mentioned above. In the Appendix, we provide an example of how a modified form of the equations used in Chiarelli *et al.* (Chiarelli et al. 2007b) can be used to integrate both flow and oxygenation changes to provide an estimate of the  $M$  parameter that is extrapolated from a BOLD signal increase that is much closer to the 'true' value (and thus potentially more robust). The example calculation in the Appendix is performed using our group average values for end-tidal O<sub>2</sub> and changes in CBF and BOLD signal, since these measurements were not simultaneously acquired in all subjects (the primary focus being on saturation of visually evoked BOLD signals). Application of this modified calibration procedure to our group average data (see Appendix) indicated that venous O<sub>2</sub> saturation rose to 91% during inhalation of carbogen-10 (from a baseline value of 70%), and the 'true'  $M$  value was extrapolated to be 9.5%. If this is correct, then the BOLD signal increase measured directly during carbogen-10 breathing was 75% of the true  $M$  value, which represents a considerably closer starting point for extrapolation than the measured BOLD values used in hypercapnic methods (with typical BOLD increases of 2-3%; e.g. (Ances et al. 2008; Perthen et al. 2008; Ances et al. 2009; Bulte et al. 2009) or hyperoxia (typical BOLD increases of 4%; (Chiarelli et al. 2007b), adjusted to TE of 30 ms). The implied values for saturation and  $M$  reported above should be considered an illustrative approximation, since the input measurements were acquired at different times in cohorts which, while overlapping, were not identical. Nonetheless the calculations shown in the Appendix demonstrate a unified calibration framework that could be used to process imaging and blood gas data acquired during manipulations, such as carbogen inhalation, which change both blood flow and arterial O<sub>2</sub> content.

Regardless of the approximations involved, the BOLD signal measured in response to carbogen-10 puts a lower bound of 7.5% on the possible value of  $M$  in

visual cortex under the conditions of our experiment (TE = 30ms, 3 Tesla). This is in the middle range of literature values reported for similar populations (Table 2) and adjusted to the TE used in our experiment (Stefanovic et al. 2006; Leontiev et al. 2007a; Leontiev et al. 2007b; Ances et al. 2008; Lin et al. 2008; Perthen et al. 2008; Ances et al. 2009; Bulte et al. 2009; Chen et al. 2009b). Figure 8 shows maps of the BOLD signal change measured during inhalation of carbogen-10 for all subjects, which show clear delineation of cortical and vascular anatomy at response amplitudes are likely to be much closer to the maximum possible BOLD signal increase than was possible with other calibration methods. Calibrated MRI maps of CMRO<sub>2</sub> change based on such data may prove more robust, due to the reduced range of extrapolation involved in estimating the *M* parameter.

	<b>Calibration technique</b>	<b>M</b>
<b>Bulte 2009</b>	HC (4%)	5.3
<b>Ances 2008a</b>	HC (5%)	5.7
<b>Ances 2008b</b>	HC (5%)	6.5
<b>Chen 2009</b>	HC (5%)	6.7
<b>Chiarelli 2007</b>	HO	7.0
<b>Ances 2008b</b>	HC (5%)	7.3
<b>Current data</b>	CG (10%)	~9.5
<b>Lin 2008</b>	HC (5%)	10.5
<b>Leontiev 2007</b>	HC (5%)	11.1
<b>Perthen 2008</b>	HC (5%)	11.6
		12.1

**Table 2. Literature *M* values at 3 Tesla**

Literature *M* values for visual cortex from calibrated MR studies at 3 Tesla, adjusted to TE = 30ms (commonly used at 3 T as in the present study). HC = hypercapnia (CO<sub>2</sub>/air mixture), HO = hyperoxia, CG = carbogen (CO<sub>2</sub>/O<sub>2</sub> mixture). The *M* value of 9.5%, approximated from group average values in the current study, is in the middle range of literature values.

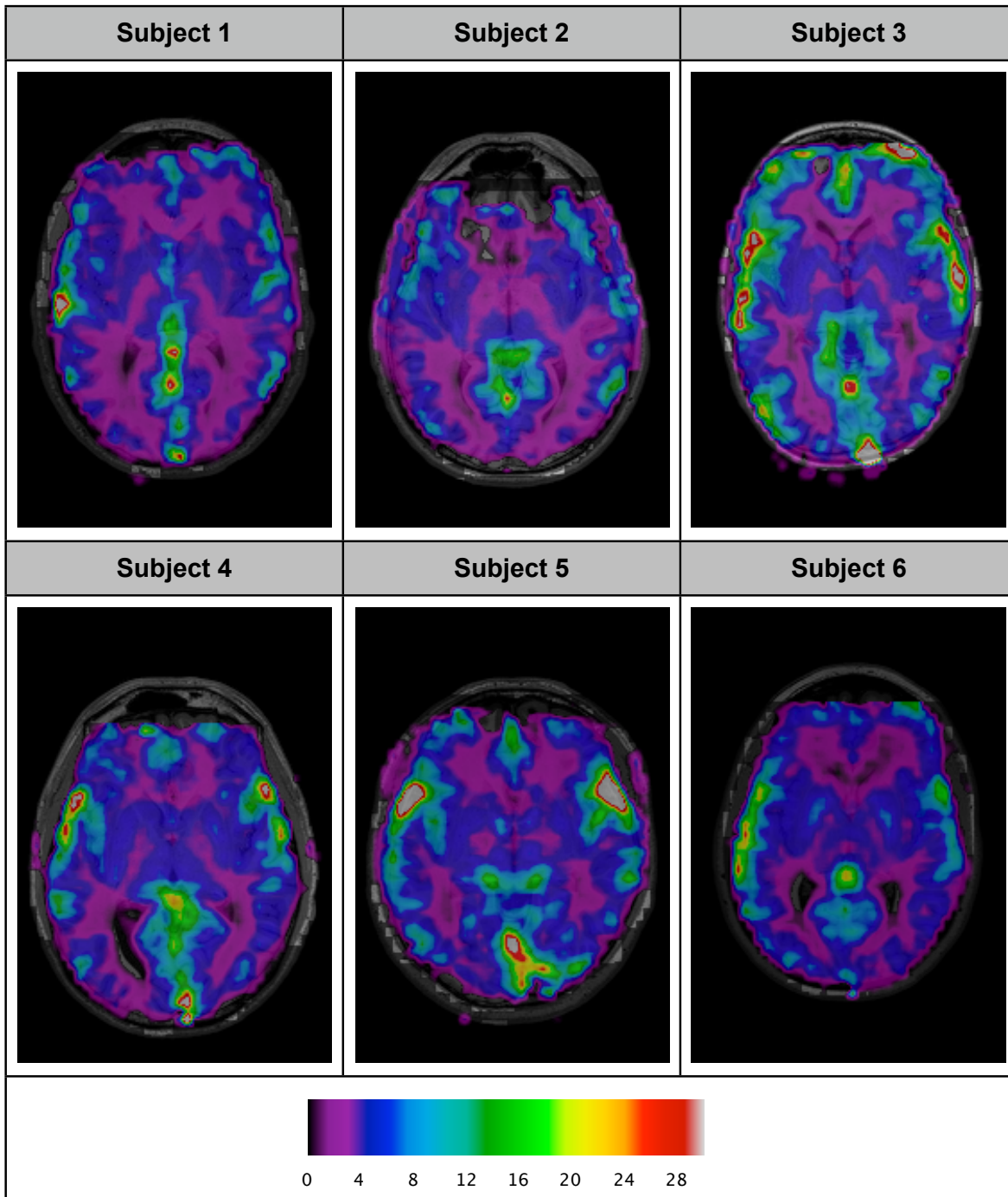


**Figure 8. Maps of percent BOLD increase during carbogen-10 breathing**

Individual percent BOLD change maps in response to carbogen-10 inhalation. The percent change values observed represent a lower bound on regional  $M$  values.

*A.5.3.1. Pitfalls and future directions*

While the potential of calibrated MRI using carbogen-10 inhalation appears promising, the discomfort associated with this high level of CO<sub>2</sub> is likely to preclude

its application in frail and aging populations. This limitation is largely a question of comfort, and the procedure was found to be safely tolerated by young healthy volunteers. This is consistent with prior studies in which the safety of hypercapnia has been demonstrated at levels comparable to those used in the present study (Kemna et al. 2001a; Kemna et al. 2001b; Posse et al. 2001; Stefanovic et al. 2006; Goode et al. 2009b; Mark et al. 2010). Higher levels of hypercapnia are routinely attained in clinical procedures such as permissive hypercapnia, during which end-tidal CO<sub>2</sub> may reach 100 mmHg without adverse effects in patients who do not have elevated intra-cranial pressure (Feihl et al. 1994).

Inhalation of 10% CO<sub>2</sub> has been used in several previous studies and these studies report only moderate degrees of discomfort from their subject. All subjects that participated in this study had previous experience as MRI subjects. Most had already taken part in hypercapnia studies and reported mild discomfort ratings on the Banzett scale to the level of hypercapnia typically used in our experiments (e.g. 5 mmHg increase from baseline). In the experiments presented here with carbogen-10, the average air hunger rating was  $4.7 \pm 0.5$  on the Banzett scale over the whole block (representing a moderate degree of discomfort) and  $5.7 \pm 0.7$  during the end of the block. All subjects reported feeling a much milder degree of discomfort during the first half of the 3-min carbogen block and the two reports of extreme discomfort occurred within 10 seconds of the end of the block. This is clearly a concern when considering adoption of the carbogen-10 manipulation as a general calibration method for fMRI. It is nonetheless possible that a lower CO<sub>2</sub> concentration (e.g. 7% CO<sub>2</sub>) could be used to achieve similar results with less discomfort.

The degree of hypercapnia and hyperoxia induced in our subjects during inhalation of carbogen-10 may have been influenced by mixing of ambient air with the inspired gases. Though the mask fit well most subjects and despite the sealing of the top portion with tape, it is possible that there was some air entrained into the mask during periods of hyperventilation. However, to minimize this effect, the volume of the reservoir bag was monitored visually and gas inflow rate was adjusted to ensure that some small residual capacity remained in the bag at all times.

Alternate approaches to determine the maximal BOLD signal could include measurement of the BOLD signal produced with a combination of hyperoxia (100% O<sub>2</sub> breathing) with acetazolamide challenge. This would circumvent the discomfort of CO<sub>2</sub> inhalation and allow a controlled investigation of the increased perfusion needed to saturate venous blood and the BOLD signal. Time domain optical measures (Gagnon et al. 2008) could also be used to investigate tissue deoxy- and oxyhemoglobin concentrations with carbogen breathing. Furthermore, animal studies in which more invasive measurements (e.g. intrinsic optical imaging on exposed cortex) and manipulations including broader blood gas manipulations using hyperbaric conditions would also allow a more thorough study of these effects.

## **A.6. Conclusion**

Carbogen-10 breathing, through direct O<sub>2</sub> enrichment combined with the vasodilatory action of CO<sub>2</sub>, can be used to saturate the BOLD fMRI signal to the point where the response to intense sensory stimulation is reduced below the level of measurement error (the same BOLD signal increase of 7.5% was found during both carbogen-10 inhalation alone and during carbogen-10 plus visual stimulation). These observations put a lower bound on  $M$  that is in the middle range of TE-adjusted values from the literature. While the discomfort associated with the high level of CO<sub>2</sub> employed here would rule out its application in frail or aging populations, lower concentrations may be more tolerable. The robustness of the BOLD signal measured with carbogen inhalation makes it attractive as a new option for calibrated MRI, and for validation of existing calibrated MRI methods in which  $M$  is extrapolated over a larger range. We are currently carrying out more in-depth studies incorporating dual-echo pCASL and different carbogen compositions to explore the interplay between the flow and oxygenation responses under the conditions explored in the present study. These studies also aim to compare  $M$  values and CMRO<sub>2</sub> response estimates obtained using carbogen, in conjunction with the hybrid calibration model shown in the appendix, with those determined using hypercapnia or hyperoxia.

## A.7. Acknowledgments

We thank Carollyn Hurst, André Cyr and Olivia Bibollet-Bahena for help with data acquisition, as well as Clarisse Mark and Joseph Fisher for helpful discussions on respiratory physiology and Daniel Bulte for helpful discussions on gas monitoring. We would also like to thank Jiongjiong Wang, who provided the pseudo-continuous arterial spin-labeling sequence used. This work was supported by the Canadian Institutes for Health Research (MOP 84378, Banting and Best Scholarship held by CJG), the Canadian Foundation for Innovation (Leaders Opportunity Fund 17380), and the Quebec Bio-Imaging Network (Pilot Grant 5886). We would also like to thank Jean-Marc Lina and the Fonds de la Recherche sur la Nature et les Technologies for salary support provided to FBT.

## A.8. Appendix

The hyperoxia calibration method introduced by Chiarelli *et al.*, was derived for conditions where cerebral blood flow would be expected to undergo a small decrease during hyperoxia. Equation 12 in Chiarelli can be modified to be valid under an arbitrary change in cerebral blood flow:

$$CBF \cdot C_{V_{O_2}} = CBF \cdot Ca_{O_2} - CBF_0 \cdot \left( Ca_{O_2} \Big|_0 \cdot OEF_0 \right) \quad [1]$$

where, as in Chiarelli, CBF is the cerebral blood flow in milliliters per second,  $C_{V_{O_2}}$  is the venous oxygen content in milliliters of  $O_2$  per deciliter of blood,  $Ca_{O_2}$  is the arterial oxygen content (also in ml  $O_2$ /dl blood), and OEF is the oxygen extraction fraction (dimensionless, and assumed here to be 0.3 as in Chiarelli *et al.*). The subscript '0' is used to denote resting values for  $Ca_{O_2}$ , OEF, and CBF (note that only the *resting* OEF value, which has been shown to be remarkably constant throughout the brain and across individuals (Frackowiak et al. 1980; Ito et al. 2004; Ashkanian et al. 2008; Bremmer et al. 2010; Sedlacik et al. 2010), is required). The above expression can be easily solved for the venous  $O_2$  content during an arbitrary change in blood flow and oxygenation:

$$Cv_{O_2} = Ca_{O_2} - \frac{\left( Ca_{O_2} \Big|_0 \cdot OEF_0 \right)}{\left( \frac{CBF}{CBF_0} \right)} \quad [2]$$

With the above expression for  $Cv_{O_2}$ , the CBF correction term ‘C’ in Equation 8 of Chiarelli et al. can be dropped, resulting in a more explicit modeling of cerebral blood flow effects.

We can approximate the effect of increased arterial  $O_2$  content and CBF increase from carbogen using our group average end-tidal  $O_2$  value of  $387 \pm 34$  mmHg, which can be used as a surrogate for  $Pa_{O_2}$ , the arterial partial pressure of  $O_2$ . We can then calculate the total arterial  $O_2$  content during carbogen-10 breathing as in Equation 11 of Chiarelli:

$$\begin{aligned} Ca_{O_2} &= (\phi \cdot [Hb] \cdot Sa_{O_2}) + (Pa_{O_2} \cdot \varepsilon) \\ &= \left( 1.34 \left[ \frac{ml_{O_2}}{g_{Hb}} \right] \cdot 15 \left[ \frac{g_{Hb}}{dl_{blood}} \right] \cdot 0.9996 \right) + \left( 387 [mmHg] \cdot 0.0031 \left[ \frac{ml_{O_2}}{dl_{blood} \cdot mmHg} \right] \right) \\ &= 20.09 \left[ \frac{ml_{O_2}}{dl_{blood}} \right]_{Hb} + 1.20 \left[ \frac{ml_{O_2}}{dl_{blood}} \right]_{plasma} \\ &= 21.29 \left[ \frac{ml_{O_2}}{dl_{blood}} \right] \end{aligned} \quad [3]$$

where  $\phi$  is the  $O_2$  carrying capacity of hemoglobin,  $[Hb]$  is the concentration of hemoglobin in blood,  $Sa_{O_2}$  is the hemoglobin saturation (estimated from our group average  $Pa_{O_2}$  value using the Severinghaus equation as in Equation 10 in Chiarelli et al.), and  $\varepsilon$  represents the solubility of  $O_2$  in plasma. The values used are the same as those in Chiarelli et al., except for  $Sa_{O_2}$  and  $Pa_{O_2}$  which are based on our group average end-tidal  $O_2$  values. Units for the different quantities are indicated in square brackets. The second last line shows the relative contributions of  $O_2$  bound to Hb and  $O_2$  dissolved in plasma, indicating that the plasma holds approximately six percent of the total arterial  $O_2$  content during carbogen-10 inhalation. At

normoxia the group average arterial O<sub>2</sub> content of hemoglobin was similar (19.83 ml O<sub>2</sub>/dl blood) but, as expected, the arterial plasma O<sub>2</sub> content was substantially lower (0.37 ml O<sub>2</sub>/dl blood, or 2% of the total arterial O<sub>2</sub> content) than the value obtained during inhalation of carbogen-10.

We can then proceed to estimate the venous O<sub>2</sub> content, C<sub>vO<sub>2</sub></sub>, during carbogen-10 breathing, using Equation 2:

$$\begin{aligned}
 C_{vO_2} &= C_{aO_2} - \frac{\left( C_{aO_2}|_0 \cdot OEF_0 \right)}{\left( \frac{CBF}{CBF_0} \right)} \\
 &= 21.29 \left[ \frac{ml_{O_2}}{dl_{blood}} \right] - \frac{\left( 20.21 \left[ \frac{ml_{O_2}}{dl_{blood}} \right] \cdot 0.3 \right)}{2.04} \\
 &= 18.33 \left[ \frac{ml_{O_2}}{dl_{blood}} \right]
 \end{aligned} \tag{4}$$

where the value for C<sub>aO<sub>2</sub></sub>|<sub>0</sub> is determined using the group average P<sub>aO<sub>2</sub></sub> value at normoxia (120 ± 4 mmHg), the OEF<sub>0</sub> value of 0.3 is assumed from literature, and the baseline-normalized CBF value of 2.04 is the group average over five subjects who underwent carbogen-10 breathing during pCASL imaging. As expected, the venous O<sub>2</sub> content was lower during normoxia, with a value of 14.14 ml O<sub>2</sub>/dl blood.

As a penultimate step, we can estimate the venous O<sub>2</sub> saturation during breathing of carbogen-10 using Equation 14 from Chiarelli (setting the negligible venous plasma O<sub>2</sub> content to zero) and the C<sub>vO<sub>2</sub></sub> value computed above:

$$\begin{aligned}
 S_{vO_2} &= \frac{C_{vO_2} - \left( P_{vO_2} \cdot \epsilon \right)}{\varphi \cdot [Hb]} \\
 &= \frac{18.33 \left[ \frac{ml_{O_2}}{dl_{blood}} \right]}{1.34 \left[ \frac{ml_{O_2}}{g_{Hb}} \right] \cdot 15 \left[ \frac{g_{Hb}}{dl_{blood}} \right]} \\
 &= 0.91
 \end{aligned} \tag{5}$$

from which it is seen that, based on group average results, the venous O<sub>2</sub> saturation has been driven to 91% during inhalation of carbogen-10.

We can now estimate an *M* value based on our group average values for Sv<sub>O<sub>2</sub></sub>, BOLD signal increase, and CBF increase during inhalation of carbogen-10. With variable CBF incorporated explicitly in our revised expression for Cv<sub>O<sub>2</sub></sub>, we can drop the CBF correction term 'C' from Equation 8 in Chiarelli, yielding:

$$\begin{aligned} \frac{\Delta BOLD}{BOLD_0} &= M \left( 1 - \left( \frac{CBF}{CBF_0} \right)^\alpha \left( \frac{[dHb]}{[dHb]_0} \right)^\beta \right) \\ &= M \left( 1 - \left( \frac{CBF}{CBF_0} \right)^\alpha \left( \frac{(1 - Sv_{O_2})}{(1 - Sv_{O_2}|_0)} \right)^\beta \right) \end{aligned} \quad [6]$$

where the term (CBF/CBF<sub>0</sub>)<sup>α</sup> is used to model cerebral blood volume, assuming α = 0.38 (Grubb et al., 1974), and β = 1.5 is used to model the influence of deoxygenated hemoglobin on transverse relaxation (Boxerman et al. 1995). The above expression can be readily solved for *M*:

$$\begin{aligned} M &= \frac{\frac{\Delta BOLD}{BOLD_0}}{1 - \left( \frac{CBF}{CBF_0} \right)^\alpha \left( \frac{(1 - Sv_{O_2})}{(1 - Sv_{O_2}|_0)} \right)^\beta} \\ &= \frac{0.075}{1 - (2.04)^{0.38} \left( \frac{(1 - 0.91)}{(1 - 0.70)} \right)^{1.5}} \\ &= 0.095 \end{aligned} \quad [7]$$

which indicates a true maximal BOLD signal increase of 9.5%.

## **B. Appendix - Absolute quantification of resting oxygen metabolism and metabolic reactivity during functional activation using QUO2 MRI**

Gauthier, C.J.<sup>1,2</sup> Desjardins-Crépeau, L.<sup>2,3</sup>, Madjar, C.<sup>2</sup>, Bherer, L.<sup>2,3</sup>, Hoge, R.D.<sup>1,2</sup>

<sup>1</sup> Physiology/Biomedical Engineering, Université de Montréal, Montreal, Quebec, Canada, <sup>2</sup> CRIUGM, Montreal, Quebec, Canada, <sup>3</sup>UQAM, Psychology Department,

Accepted in Neuroimage, July 24, 2012

### **B.1. Abstract**

We have recently described an extension of calibrated MRI, which we term QUO2 (for QUAntitative O<sub>2</sub> imaging), providing absolute quantification of resting oxidative metabolism (CMRO<sub>2</sub>) and oxygen extraction fraction (OEF<sub>0</sub>). By combining BOLD, arterial spin labeling (ASL) and end-tidal O<sub>2</sub> measurements in response to hypercapnia, hyperoxia and combined hyperoxia/hypercapnia manipulations, and the same MRI measurements during a task, a comprehensive set of vascular and metabolic measurements can be obtained using a generalized calibration model (GCM). These include the baseline absolute CBF in units of ml/100g/min, cerebrovascular reactivity (CVR) in units of %Δ CBF/mmHg,  $M$  in units of percent, OEF<sub>0</sub> and CMRO<sub>2</sub> at rest in units of μmol/100g/min, percent evoked CMRO<sub>2</sub> during the task and  $n$ , the value for flow-metabolic coupling associated with the task. The  $M$  parameter is a calibration constant corresponding to the maximal BOLD signal that would occur upon removal of all deoxyhemoglobin. We have previously shown that the GCM provides estimates of the above resting parameters in grey matter that are in excellent agreement with literature. Here we demonstrate the method using functionally-defined regions-of-interest in the context of an activation study. We applied the method under high and low signal-to-noise conditions, corresponding respectively to a robust visual stimulus and a modified Stroop task.

The estimates fall within the physiological range of literature values, showing the general validity of the GCM approach to yield non-invasively an extensive array of relevant vascular and metabolic parameters.

Keywords: calibrated fMRI, baseline oxygen use, evoked oxidative metabolism, Stroop task, hypercapnia, hyperoxia.

## **B.2. Introduction**

Blood oxygen-level dependent (BOLD) fMRI has been used extensively since its discovery to investigate non-invasively the brain activity associated with a large variety of tasks. Though BOLD contrast is a sensitive measure of activity, it is unfortunately also an ambiguous one, as it arises from a combination of changes in oxidative metabolism, blood flow and blood volume. Calibrated fMRI techniques were developed to isolate the oxidative metabolic component of the BOLD signal, a quantity thought to better reflect the underlying synaptic activity of neurons. These techniques use gas manipulations such as hypercapnia (Davis et al. 1998; Hoge et al. 1999a), hyperoxia (Chiarelli et al. 2007b) or a combination of both (Gauthier et al. 2012b) to estimate the purely vascular component of the BOLD response and remove it from the BOLD signal measured during a task. The resulting estimate of percent cerebral metabolic rate of O<sub>2</sub> (CMRO<sub>2</sub>) change evoked by that specific task can then be directly compared between groups, even if these groups are known to differ in their hemodynamic function.

The importance of the baseline state in understanding the meaning of vascular and metabolic dynamic changes is becoming more and more appreciated. Task-induced BOLD signal changes cannot, in standard fMRI protocols, be related to a known baseline state. This reduces the strength of inferences that can be made about the signal changes measured, since not only are these BOLD changes ambiguous physiologically, but they are expressed as a function of an unknown baseline with an unknown inter-subject and inter-group variability. Until recently, calibrated fMRI studies have suffered from a related weakness in that even though the actual percent changes in CMRO<sub>2</sub> have a physiological meaning that allows direct group comparisons, these percent changes arise from an unknown baseline,

thereby limiting the conclusions that may be drawn from the observation of group differences.

Efforts to characterize the resting state of the brain have led to the development of a number of new imaging and analysis techniques for the measurement of baseline metabolism (He et al. 2007; He et al. 2008; Bolar et al. 2011a; Bulte et al. 2011; Fan et al. 2011). We have recently proposed an extension of our Generalized calibration model (GCM) technique (Gauthier et al. 2012b) that takes advantage of the common and orthogonal information contained in the MRI and end-tidal partial pressure of expired  $O_2$  ( $ETO_2$ ) measured in response to different combinations of hypercapnia and hyperoxia to get an estimate of baseline properties including  $M$ , the oxygen extraction fraction at rest ( $OE_{F_0}$ ) and oxidative metabolism at rest ( $CMRO_2$ ) in micromolar units (Gauthier et al. 2012c). The parameter  $M$  corresponds to the BOLD signal attenuation at rest from baseline deoxyhemoglobin content and is used in calibrated fMRI experiments to calibrate task-evoked BOLD signal changes. It is estimated using a BOLD biophysical model by extrapolation from the signal changes observed during gas manipulations to the maximal possible BOLD signal increase that would theoretically occur upon complete removal of deoxyhemoglobin. The technique to measure baseline properties (Gauthier et al. 2012c), combined with the established calibrated fMRI of task-evoked metabolism, provides a rich array of vascular and metabolic parameters including measures of oxygen delivery, resting cerebral blood flow,  $CO_2$ -mediated cerebrovascular reactivity, the resting BOLD signal  $M$ , flow-metabolic coupling, as well as both absolute measures of baseline and task-evoked oxidative metabolism. This approach, which we have dubbed QUO2 MRI (for QUantitative  $O_2$ ), could be of great value in the interpretation of basic neuroscience research results, but also in the investigation of complex diseases that include functional and hemodynamic deficits.

Here we present the framework by which these different aspects of the model can be combined to characterize the brain vasculature and metabolism using two widely used paradigms: intense stimulation of primary visual areas using a flashing checkerboard and a modified version of the Stroop task, producing much more subtle brain responses. New functional imaging techniques are often tested using

simple visual paradigms, since these tasks represent a best case scenario for functional imaging, giving rise to well characterized, very large signal changes readily observable even with low signal-to-noise ratio (SNR) techniques. While this provides a good proof-of-concept framework for testing new techniques, cognitive tasks used in basic neuropsychology and clinical settings typically produce much smaller responses and are thus more challenging to image than primary sensory stimulation. The modified Stroop task (Bohnen et al. 1992) used here includes both an inhibition and a task switching component. This makes this task interesting for an in-depth study of local physiology since these executive functions have been shown to be specifically affected by aging and some diseases (Milham et al. 2002; Wasylyshyn et al. 2011; Yun et al. 2011). It is therefore possible that the regions implicated in these tasks show signs of a more fragile underlying physiology that would explain their vulnerability to age and disease.

### **B.3. Methods**

Acquisitions were conducted in seven healthy male subjects (aged 21 to 38 years) on a Siemens TIM Trio 3T MRI system (Siemens Medical Solutions, Erlangen, Germany) using the vendor-supplied 32-channel receive-only head coil for all acquisitions. All subjects gave informed consent and the project was approved by the Comité mixte d'éthique de la recherche du Regroupement Neuroimagerie/Québec.

#### **B.3.1. Image acquisition**

Sessions included an anatomical, 1mm<sup>3</sup> MPRAGE acquisition with TR/TE/alpha = 2300ms/3ms/9°, 256x240 matrix and a GRAPPA acceleration factor of 2 (Griswold et al. 2002).

Functional image series were acquired using a dual-echo pseudo-continuous arterial spin labeling (pCASL) acquisition (Wu et al. 2007) to measure changes in cerebral blood flow (CBF). The parameters used include: TR/TE1/TE2/alpha = 3000ms/10ms/30ms/90° with 4x4mm in-plane resolution and 11 slices of 7mm (1mm slice gap) on a 64x64 matrix (at 7/8 partial Fourier), GRAPPA acceleration factor = 2, post-labeling delay = 900ms, label offset = 100mm, Hanning window-

shaped RF pulse with duration/space = 500 $\mu$ s/360 $\mu$ s, flip angle of labeling pulse = 25°, slice-selective gradient = 6mT/m, tagging duration = 1.5s (Wu et al. 2007).

### **B.3.2. Gas manipulations**

Each session included three functional runs each including a different gas manipulation. During each gas manipulation run, a single three-minute block of gas inhalation was preceded with one minute and followed by two minutes of medical air breathing. The three gas manipulations used were: 100% O<sub>2</sub> (hyperoxia), 7% CO<sub>2</sub>/21%O<sub>2</sub>/72%N<sub>2</sub> (hypercapnia) and 7% CO<sub>2</sub>/93% O<sub>2</sub> (simultaneous hyperoxia/hypercapnia). The latter gas is a specific formulation of carbogen, which in general may contain different O<sub>2</sub>/CO<sub>2</sub> ratios.

At the beginning of the experiment, subjects were fitted with a non-rebreathing face mask (Hudson RCI, #1059, Temecula, California, USA). To avoid discomfort from outward gas leakage blowing into the subject's eyes, skin tape (Tegaderm Film, #1626W, 3M Health Care, St-Paul, MN, USA) was used to seal the top of the mask to the face. Plastic tubing (Airlife™ Oxygen tubing #001305, Cardinal Health, McGraw Park, IL, USA) and a series of two Y-connectors were used to connect pressure/flow-meters for medical air, 100% O<sub>2</sub> (hyperoxia), 7% CO<sub>2</sub>/93% air (hypercapnia) and 7% CO<sub>2</sub>/93% O<sub>2</sub> (simultaneous hyperoxia/hypercapnia) tanks (Vitalaire, Mississauga, ON, Canada) to the mask. Gas flows were adjusted manually on the pressure/flow-meters (MEGS, Ville St-Laurent, QC, Canada) to keep a total flow rate of 16L/min. Gas flow was kept at 16L/min at all times except during administration of the hyperoxia/hypercapnia and the hypercapnia gas mixtures. To accommodate the elevated minute ventilation caused by CO<sub>2</sub> breathing, gas flow rates were increased to the maximal possible rate (25L/min) achievable with our pressure/flowmeters. Pulse rate and arterial O<sub>2</sub> saturation were monitored in all subjects using a pulse-oximeter (InVivo Instruments, Orlando, USA) as a safety measure and to observe the effects of the different gas manipulations.

End-tidal O<sub>2</sub> and CO<sub>2</sub> values were monitored during all acquisitions. Gases were sampled via an indwelling (15 mm) nasal cannula (Airlife™ Nasal Oxygen Cannula #001321, Cardinal Health, McGraw Park, IL, USA) using the CO2100C

and O2100C modules of the MP150 BIOPAC physiological monitoring unit (BIOPAC Systems Inc., Goleta, CA, USA). Calibration of the unit was done by taking into account an expired partial pressure of water of 47mmHg (Severinghaus 1989). Subjects were instructed to breathe through their nose, which ensured that only expired gas was sampled by the nasal cannula. End-tidal PCO<sub>2</sub> and PO<sub>2</sub> values were selected manually from continuous respiratory traces sampled at 200 Hz. The first 10 breaths of the first baseline period and the last 10 breaths of the gas-inhalation block were averaged to give baseline values and gas manipulation values respectively.

After the experiment, all subjects were debriefed to assess the level of discomfort associated with the breathing manipulations. The subjects were asked to rate the air hunger and breathing discomfort associated with the hypercapnia and carbogen mixtures on a French language version of the scale proposed in (Banzett et al. 1996).

### **B.3.3. Visual stimulus**

The visual stimulus used was a black and white radial checkerboard, with annuli scaled logarithmically with eccentricity, luminance modulated in a temporal squarewave at 8 Hz (equivalent to 16 contrast reversals per second) presented using an LCD projector (EMP-8300, Epson, Toronto, ON, Canada) onto a translucent screen viewed by subjects through a mirror integrated into the Siemens head coil. This stimulation was initiated one minute into the acquisition and lasted three minutes, followed by two minutes of rest.

### **B.3.4. Stroop task**

The Stroop task consisted of two 60-second blocks each of control and Stroop conditions, interspersed with 60-second rest blocks. In total, there were therefore four task and five resting blocks, for an acquisition of nine minutes. During task blocks, control or Stroop events always lasted two seconds, preceded by two seconds with a fixation cross to maintain focus. In all cases, subjects had only two possible answers (blue or green), selected using an MRI-compatible button box (FIU-005 interface with 8 buttons bimanual response pads, Current Designs). All subjects were native French speakers and the color words were written in French

(‘BLEU’ and ‘VERT’). The task was presented to the participant using the same setup as for the visual task.

During the Stroop/switching condition blocks, two different types of events were given in random order. In all cases, letter color and word semantic were non-congruent. In ten of fifteen cases, when the color word appeared, the correct answer was letter color. In five cases out of fifteen, a large white rectangle appeared around the word for the whole event, starting during the two seconds with the fixation cross. This rectangle indicated to the subject that the rule had changed and that the right answer now corresponded to word semantic rather than letter color. During the control task blocks (color naming), a series of four X’s were written either in blue or green and the participant was asked to give the color of the letters.

### **B.3.5. Data analysis**

All analyses except for Stroop ROIs definition were done using the NeuroLens data analysis software package ([www.neurolens.org](http://www.neurolens.org)). The raw EPI series were preprocessed by motion correction (Cox et al. 1999) and spatial smoothing with a 3D Gaussian kernel (6 mm FWHM). The CBF signal was isolated from the series of first echoes using linear surround subtraction (Liu et al. 2005), while the BOLD signal was extracted using linear surround addition of the second echo series.

Fractional changes in BOLD and CBF signals were then determined for each gas manipulation by fitting a GLM to the respective signals and dividing the estimated effect size by the estimated constant term. Model fits used a single-gamma hemodynamic response function (HRF) with parameters described by Glover et al. (Glover, 1999) and included a first order polynomial to represent baseline signal and linear drift (higher order polynomial fits were deemed unsuitable due to the single long block during the gas runs). Because the canonical HRF cited above actually bears little resemblance to the impulse response describing transitions between respiratory states, the first 60 seconds after each transition in gas composition were excluded from the analyses by zeroing out relevant rows in the GLM computational matrices, to select responses at steady-state. CBF and BOLD data for the visual and Stroop tasks were treated similarly, but no frames were

excluded. For the Stroop task, a third order drift polynomial was used in the GLM and a contrast was used to isolate the signal changes during the Stroop/switching blocks.

Because the flow changes produced by hyperoxia were considerably smaller than the noise level in our ASL acquisitions, a constant fixed value of -3.11% was assumed for this CBF change (only for hyperoxia). This value was the average flow change determined by first averaging the O<sub>2</sub>-induced change in ASL signal (after correction for T1 changes as described below) over all cortical and sub-cortical grey matter in each subject, and then pooling average values from the seven subjects. The use of a fixed value for the O<sub>2</sub>-induced flow response is also advocated in the Chiarelli method (Chiarelli et al. 2007b), as these changes are generally agreed to be too small for reliable measurement at the single voxel level with current ASL methods.

As noted above, it was necessary to correct values of the fractional CBF change during hyperoxic manipulations to account for changes in the T1 of blood known to occur during changes in the plasma concentration of O<sub>2</sub> (which is paramagnetic). This was carried out using the approach described in (Chalela et al. 2000; Zaharchuk et al. 2008). We estimated arterial blood T1 values based on the end-tidal O<sub>2</sub> (ETO<sub>2</sub>) measurements obtained in each subject, along with T1 vs. FiO<sub>2</sub> values tabulated in Bulte *et al.* (Bulte et al. 2007) and PaO<sub>2</sub> vs FiO<sub>2</sub> values tabulated by Chiarelli *et al.* (Chiarelli et al. 2007b). Since the exact T1 depends on the level of dissolved O<sub>2</sub> in plasma, and because we obtained slightly different ETO<sub>2</sub> values at a given fraction of inspired O<sub>2</sub> than in these studies because of differences in gas delivery techniques, the values were linearly interpolated to account for this difference.

Following determination of average end-tidal O<sub>2</sub> values as described above, the latter were converted to arterial O<sub>2</sub> content in ml O<sub>2</sub>/ml blood as described in Chiarelli *et al.* (Chiarelli et al. 2007b). The following parameters were assumed for all subjects in the latter conversion:  $\phi = 1.34$  mlO<sub>2</sub>/gHb, [Hb] = 15 gHb/dl blood, and  $\varepsilon = 0.0031$  mlO<sub>2</sub>/dl blood/mmHg (the solubility of O<sub>2</sub> in plasma) (Chiarelli et al. 2007b; Rhoades et al. 2009). While hemoglobin concentration was assumed here

to be 15 gHb/dl blood, this value can be determined more accurately through a blood draw for each subject. Two of our participants underwent this test as part of another study and their blood hemoglobin concentrations were 14.5 and 15.2 gHb/dl blood, close to the assumed value of 15 gHb/dl blood.

For the three gas manipulations, the corresponding fractional changes in BOLD and CBF along with arterial O<sub>2</sub> content values were substituted into the generalized calibration model to determine the  $M$  vs. OEF<sub>0</sub> curve for each gas (the averaging performed on the measured MRI and respiratory values is described below). The intersection point of the two curves was then determined numerically using the bisection method (Press et al. 1992), starting from an OEF<sub>0</sub> value of 1. The midpoint between the intersection between the hypercapnia (HC) and hyperoxia (HO) curves and the intersection point between the combined hyperoxia/hypercapnia (HO-HC) and hyperoxia (HO) curves was used to determine the  $M$  vs. OEF<sub>0</sub> solution coordinates used in further analyses.

Computation of resting CMRO<sub>2</sub> required the absolute resting CBF, which was determined from the pCASL data using the approach described by Wang *et al.* (Wang et al. 2003a) assuming blood brain partition coefficient = 0.9, labeling efficiency = 0.80, blood T1 = 1.49 s, and grey matter T1 = 1.4 s. For this computation, the baseline ASL difference signal estimated in the GLM fit for each gas manipulation was divided by an estimate of the baseline (raw) EPI signal computed in a similar GLM fit. The resultant ratio converted to absolute CBF units based on the parameters above.

Evoked percent CMRO<sub>2</sub> changes during the visual and modified Stroop tasks were determined using the GCM as in Gauthier *et al.* (Gauthier et al. 2012b) and the  $M$  values estimated using the procedure described above over each task-specific ROI (Gauthier et al. 2012c).

Other than the coordinates for intersection of group average  $M$  vs. OEF<sub>0</sub> curves, for which the range of intersection coordinates was used, all uncertainties are provided as  $\pm$  standard error. Uncertainties on evoked CMRO<sub>2</sub> were computed from uncertainties on  $M$ , CBF and BOLD as described in Davis *et al.* (Davis et al. 1998).

### **B.3.6. Visual ROI**

Because responses to the flashing checkerboard are large enough to be detectable at the single subject level, regions of interest (ROIs) were derived from the intersection of the flow and BOLD thresholded ( $p \leq 0.01$  corrected) (Worsley et al. 2002) visual activation T-maps for each individual subject from the NeuroLens analysis. One subject (subject 1) fell asleep during the visual task and was therefore excluded from all analyses requiring a visual ROI. The ROIs for the visual task are the same as presented in a previous report (Gauthier et al. 2012b). The  $M$  parameter and evoked  $CMRO_2$  data were included in that publication and are reproduced here to facilitate comparison with the other ROIs. Baseline  $OEF_0$  and  $CMRO_2$  measures over this ROI represent however a novel result.

### **B.3.7. Stroop ROIs definition**

Because the modified Stroop task yields smaller signal changes not readily detectable at the single subject level for a single run, individual subject ROIs for the Stroop task were defined from the significant BOLD signal changes during the inhibition/switching blocks for the seven participants included in this study. Two regions of interest were drawn for this task, one over bilateral frontal areas and one over parietal areas.

This analysis was done using FSL. All functional data were motion corrected with MCFLIRT (Jenkinson et al. 2002) and the brain was extracted using BET (Brain Extraction Tool, version 2.1) (Smith 2002). A  $6\text{mm}^3$  FWHM 3D Gaussian smoothing kernel, high-pass filter (100s cutoff) and pre-whitening (FILM) (Woolrich et al. 2001) were applied to the time series. Spatial normalization to standard space (MNI152 template) (Jenkinson et al. 2001; Jenkinson et al. 2002) was performed (12 degrees of freedom) on the 30ms echo time series. The BOLD time series was extracted from the second echo time series ( $TE = 30\text{ms}$ ) by isolating the control images from the original time series. A GLM was performed with the main experimental paradigm convolved with a dual gamma function. Temporal derivatives were included in the model. Fixed effect group analysis was performed using FLAME1 (Beckmann et al. 2003; Woolrich et al. 2004; Woolrich 2008) to generate group average statistical maps for the contrast representing the

subtraction of the control blocks from the Stroop blocks (isolating the areas specifically involved in inhibition/switching). The group average map thresholded at  $Z = 2.3$  for the 30ms echo was used to derive the individual ROIs. The transformations for spatial normalization of the seven subjects were inverted to project the group ROIs into individual subject space (Figure 1) to perform ROI quantifications in native space.

In order to account for the fact that our large EPI voxels inevitably contained a mixture of grey matter, white matter, and CSF, average BOLD and ASL responses were determined by computing weighted-averages within ROIs, with the weighting provided by the estimated grey matter volume fraction in each voxel. The grey matter volume fraction was determined using automatic tissue segmentation of anatomical images using the FAST module of FSL (Zhang et al. 2001). Grey matter probability maps generated by FAST were projected into native EPI space using linear interpolation. Binarized individual ROI maps (both visual and Stroop task-derived) were multiplied by grey matter probability. This approach assumes that the responses in white matter and CSF are negligible compared with the grey matter response, which is supported by our observations in these tissue compartments (data not shown).

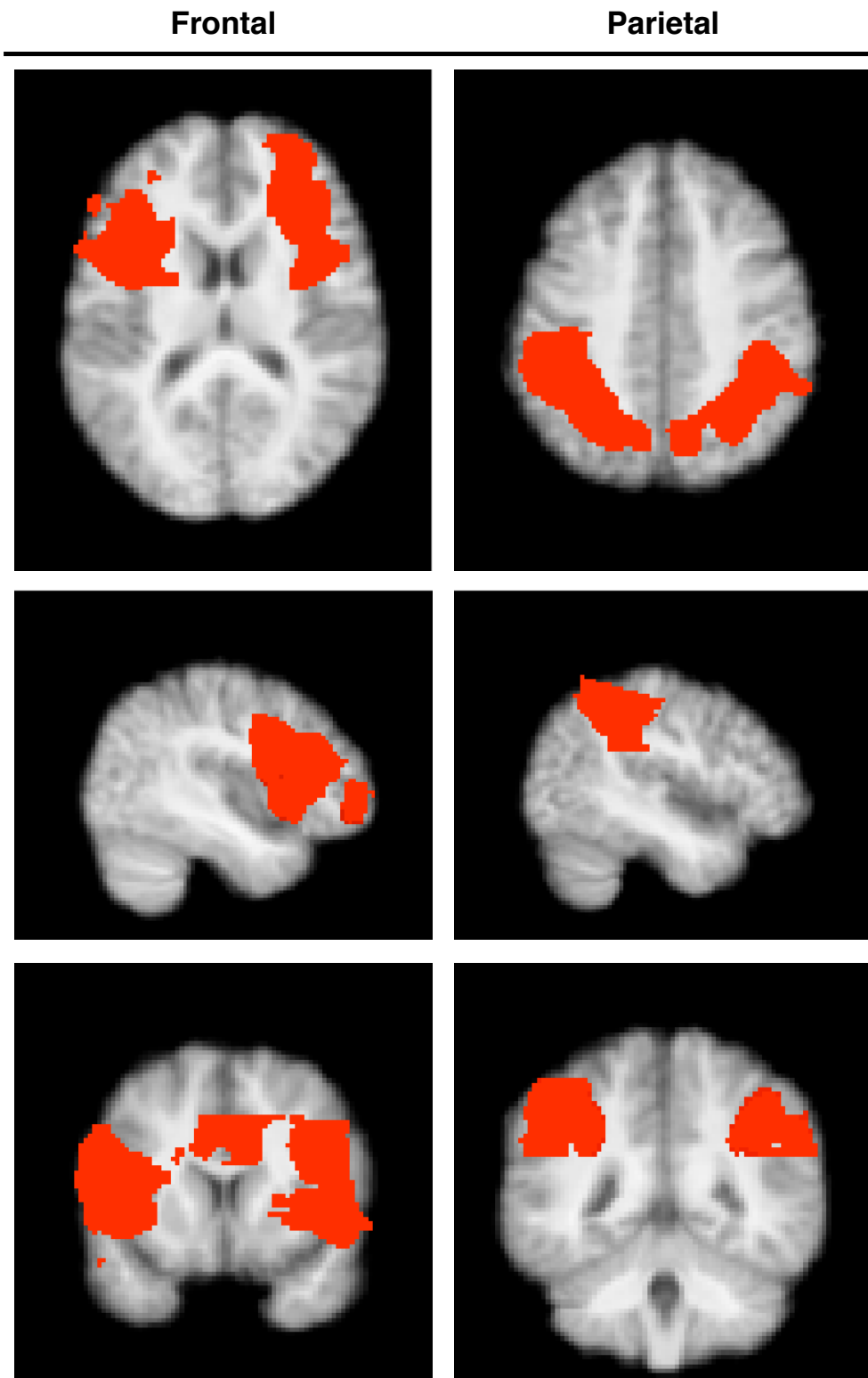


**Figure 1. ROI for Stroop task**

ROIs for the modified Stroop task determined using the significant ( $Z \geq 2.3$ ) signal increases in BOLD group maps. Two regions were drawn to reflect the bilateral frontal and parietal components to the task.

## B.4. Results

### B.4.1. Gas manipulations

All gas manipulations lead to the expected changes in end-tidal gas partial pressures (Table 1). Breathing of 100% O<sub>2</sub> lead to an increase in ETO<sub>2</sub> of 425.83 ± 31.28 mmHg during the hyperoxia block. A slight hypocapnia was induced by the manipulation with a decrease in ETCO<sub>2</sub> of 3.21 ± 0.37 mmHg. Breathing the 7% CO<sub>2</sub> in air mixture lead to an average increase ETCO<sub>2</sub> of 9.04 ± 1.31 mmHg, with a concomitant increase in ETO<sub>2</sub> from hyperventilation during the CO<sub>2</sub> block of 14.22 ± 2.08 mmHg. Both ETO<sub>2</sub> and ETCO<sub>2</sub> were successfully elevated during breathing of 7% CO<sub>2</sub> in 93% O<sub>2</sub>, with an ETCO<sub>2</sub> increase of 7.41 ± 0.65 mmHg and an ETO<sub>2</sub> increase of 304.26 ± 26.85 mmHg. The ETCO<sub>2</sub> and ETO<sub>2</sub> values during each breathing manipulations are given in Table 1.

	Hyperoxia	Hypercapnia	Combined
<b>Baseline ETCO<sub>2</sub> (mmHg)</b>	40.11 ± 0.95	40.21 ± 0.68	40.63 ± 0.61
<b>Manipulated ETCO<sub>2</sub> (mmHg)</b>	36.90 ± 0.88	49.26 ± 0.94	48.04 ± 0.82
<b>Baseline ETO<sub>2</sub> (mmHg)</b>	117.54 ± 5.49	121.63 ± 6.68	116.92 ± 5.08
<b>Manipulated ETO<sub>2</sub> (mmHg)</b>	543.37 ± 30.00	135.84 ± 5.29	421.18 ± 23.44

**Table 1. Respiratory parameters**

End-tidal CO<sub>2</sub> and O<sub>2</sub> values (mmHg) for each breathing manipulations (hypercapnia, hyperoxia and combined hyperoxia/hypercapnia). These values are used in the GCM as a surrogate for arterial concentrations of gases.

The percent BOLD and CBF changes evoked by the three breathing manipulations are shown in Figure 2. Percent CBF changes (Figure 2A) are shown only for the hypercapnia (HC) and combined hyperoxia/hypercapnia (HO-HC) manipulations, since a fixed flow decrease was assumed for hyperoxia (see Methods). Similar average percent CBF changes were obtained for HC and HO-HC over all ROIs. Percent BOLD signal changes (Figure 2B) are shown in response to all breathing manipulations. In general, as shown before (Gauthier et al. 2012c; Gauthier et al.

2012b), the amplitude of percent BOLD changes in response to hyperoxia and hypercapnia are approximately half of that found for combined hyperoxia/hypercapnia. Both percent CBF and BOLD changes show a trend towards lower amplitude signals in more frontal areas.

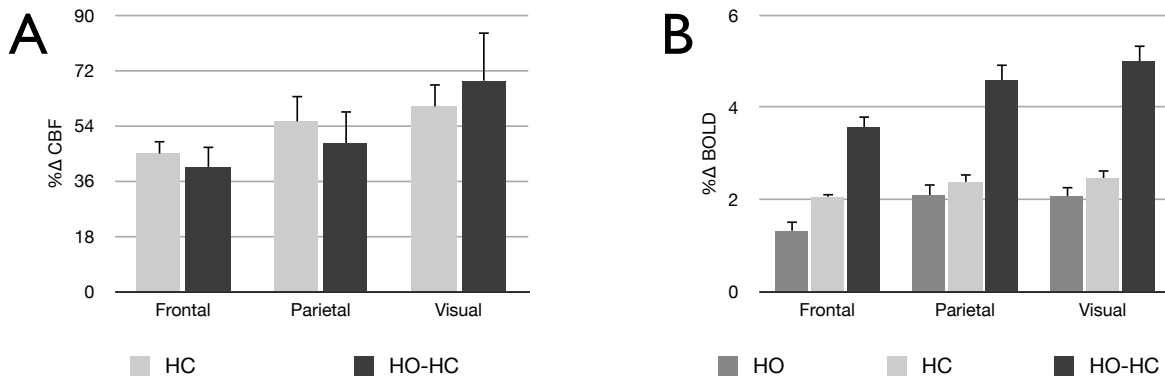


**Figure 2. Percent CBF and BOLD changes during breathing manipulations**

Percent CBF (A) and BOLD (B) changes in response to hyperoxia (HO), hypercapnia (HC) and combined hyperoxia/hypercapnia (HO-HC) over the different functionally-determined ROIs. CBF changes to the hyperoxia manipulation are not given as they are too small to be measured reliably in small ROIs. Error bars represent the inter-subject standard error.

#### B.4.2. $M$ , $OEF_0$ and resting $CMRO_2$

Percent changes in BOLD and CBF, as well as end-tidal  $PO_2$  values at baseline and during the breathing manipulations were input into the GCM to construct the  $M$  vs.  $OEF_0$  curves and solve for a unique value of  $M$  and  $OEF_0$ . Figure 3 shows the graphs for each ROI, with a star representing the value used in subsequent analyses. The value for grey matter was taken from a previous study for visual comparison (Gauthier et al. 2012c). It can be seen from these graphs that, while the three lines intersect at a common point for grey matter, they form a small triangle of intersection points around physiological values for the functionally-determined ROIs. The resulting  $M$ ,  $OEF_0$  and  $CMRO_2$  estimates over the functional ROIs are shown in Figure 4 and Table 2.  $M$  values were found to be similar over all areas, with values of  $6.09 \pm 1.11\%$ ,  $6.11 \pm 1.20\%$  and  $5.94 \pm 1.08\%$  for the frontal, parietal and visual ROIs respectively.  $OEF_0$  values were found to be close to literature values, with values of  $0.45 \pm 0.07$ ,  $0.29 \pm 0.06$  and  $0.29 \pm 0.05$  for the frontal, parietal and visual ROIs respectively. Baseline  $CMRO_2$  values of  $173.62 \pm$

27.74  $\mu\text{mol}/100\text{g}/\text{min}$ ,  $99.59 \pm 18.83 \mu\text{mol}/100\text{g}/\text{min}$  and  $125.09 \pm 21.82 \mu\text{mol}/100\text{g}/\text{min}$  were measured for the frontal, parietal and visual ROIs respectively.

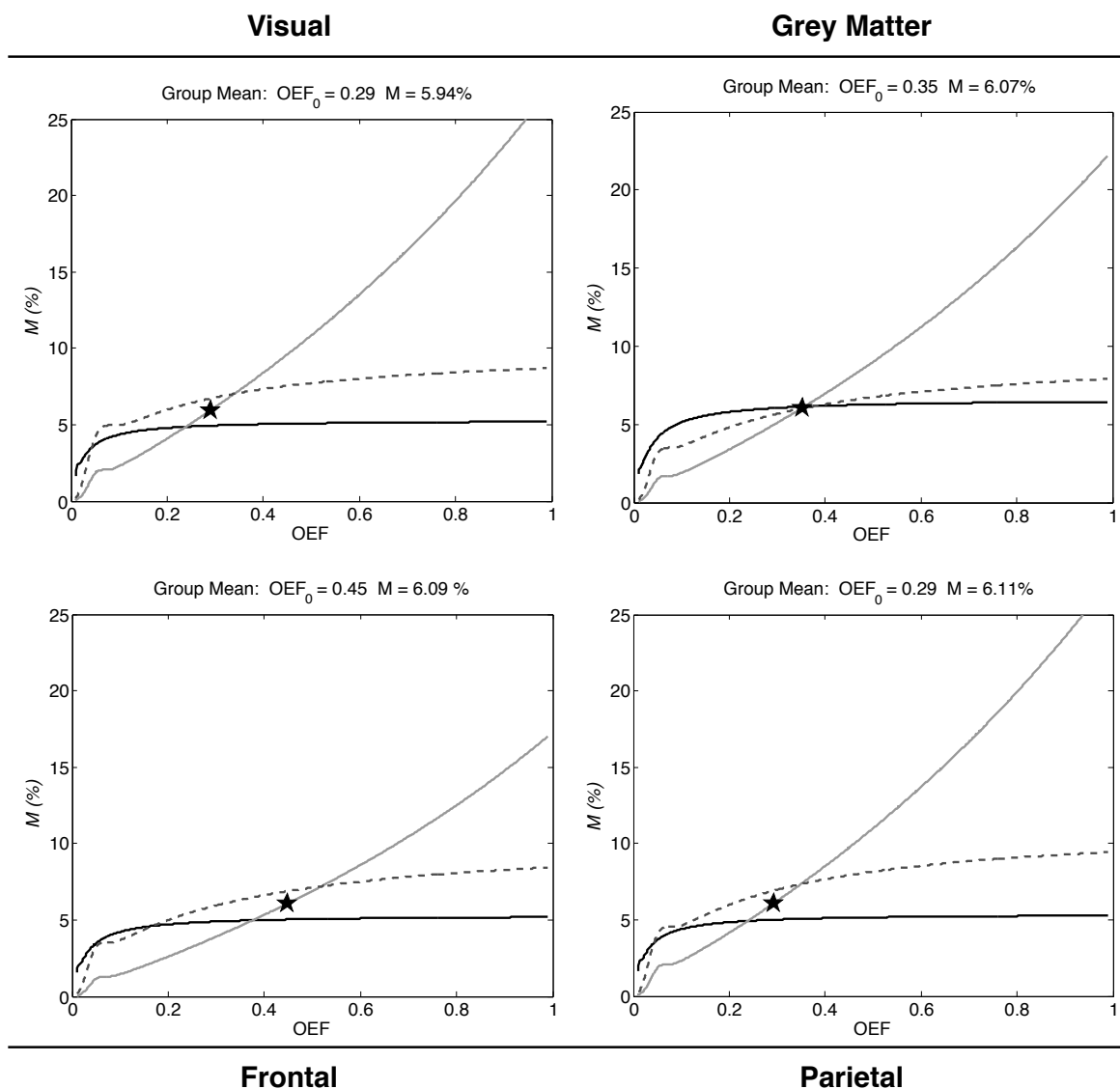


**Figure 3. Intersection plots for all ROIs.**

Plots of the  $M$  vs.  $\text{OEF}_0$  curves estimated using the three gas manipulations over all ROIs. The star represents the solution for  $M$  and  $\text{OEF}_0$ . Solid grey lines show the curve for hyperoxia, solid black lines for hypercapnia and dashed black lines for combined hyperoxia/hypercapnia. The plot for grey matter (GM) group average values for the same group is taken from another study and included for comparison.

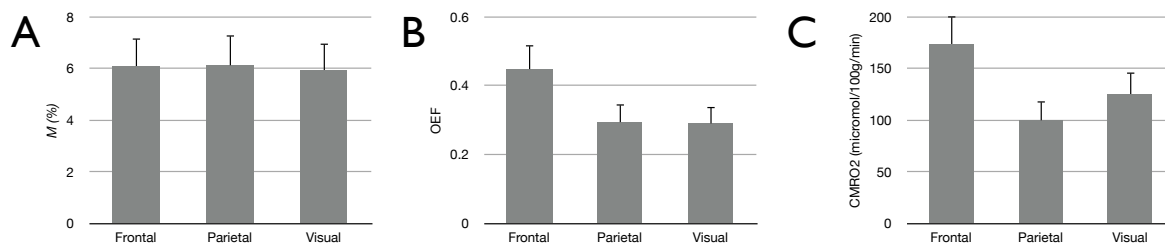


**Figure 4.  $M$ ,  $OEF_0$  and resting  $CMRO_2$  values over all ROIs**

Graphs of the  $M$  (A),  $OEF_0$  (B) and resting  $CMRO_2$  (C) values obtained over all ROIs. Error bars show the range of values used and represent the intersection point of the hypercapnia and hyperoxia curves and the intersection point of the combined hyperoxia/hypercapnia (carbogen) and hyperoxia curves.

### B.4.3. Task-evoked $CMRO_2$

The  $M$  value used for evoked  $CMRO_2$  calculations was taken as the average of the intersection point for the hypercapnia and hyperoxia curves and the intersection point for the combined hyperoxia/hypercapnia (carbogen) and the hyperoxia curves (represented by a star in each subplot within Figure 3). Percent CBF (A) and BOLD (B) changes in response to the visual and Stroop tasks over their specific ROI (frontal and parietal ROIs for the Stroop task and the visual ROI for the flashing checkerboard stimulus) are shown in Figure 5. CBF and BOLD percent changes in response to the visual task ( $68.54 \pm 8.95\%$  and  $1.31 \pm 0.11\%$  for CBF and BOLD respectively) were much larger than the percent changes in response to the modified Stroop task. The percent CBF changes during the Stroop task were  $8.98 \pm 1.36\%$  and  $14.47 \pm 1.84\%$  for frontal and parietal ROIs respectively. Percent BOLD signal changes during the Stroop task were  $0.33 \pm 0.04\%$  and  $0.43 \pm 0.07\%$  for frontal and parietal ROIs respectively. Percent  $CMRO_2$  change evoked by the task were  $3.87 \pm 1.20\%$  and  $7.33 \pm 1.62\%$  over the frontal and parietal ROIs during performance of the modified Stroop task. The visual task evoked a larger  $34.02 \pm 7.43\%$  increase in metabolism over the visual ROI. The percent increase in oxidative metabolism evoked by the tasks over the ROIs in units of  $\mu\text{mol}/100\text{g}/\text{min}$  units are shown in Figure 6.

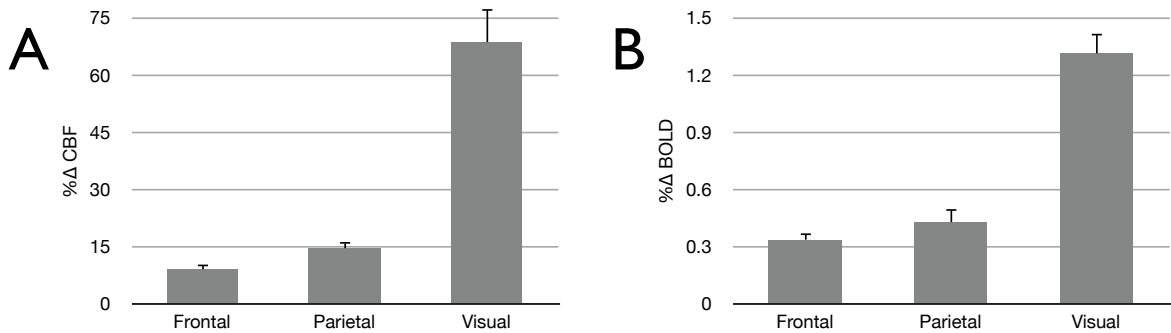


**Figure 5. Task-evoked percent CBF and BOLD changes**

Average percent CBF (A) and BOLD (B) changes evoked by the modified Stroop (in Frontal and Parietal ROIs) and the visual (Visual) tasks. Error bars represent the inter-subject standard error.

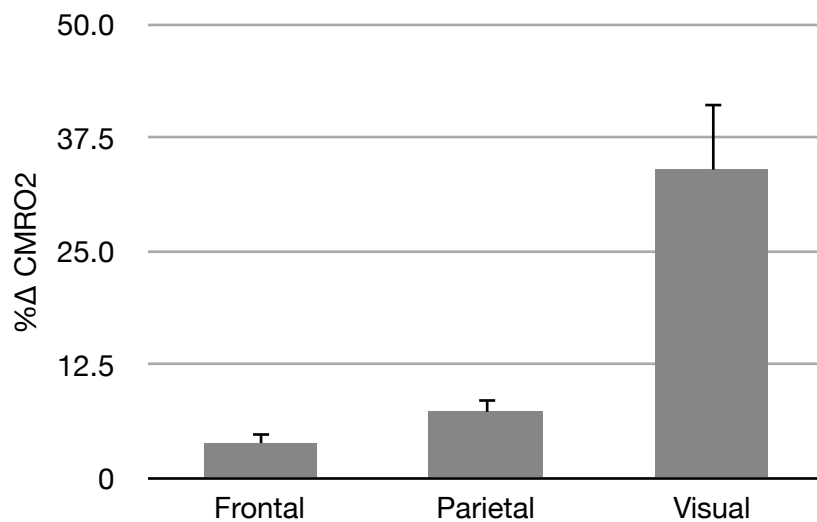


**Figure 6. Task-evoked percent CMRO<sub>2</sub> change**

Percent task-evoked CMRO<sub>2</sub> change for the modified Stroop (in Frontal and Parietal ROIs) and the visual (Visual) tasks. Error bars represent the standard error obtained using the error analysis presented by Davis *et al.* (Davis *et al.* 1998).

#### **B.4.4. Vascular and metabolic profile**

Table 2 summarizes the vascular and metabolic information to be obtained from our technique. It includes the baseline absolute CBF in units of ml/100g/min, cerebrovascular reactivity (CVR) in units of %Δ CBF/mmHg, *M* in units of percent, OEF<sub>0</sub> and CMRO<sub>2</sub> at rest in units of μmol/100g/min, percent evoked CMRO<sub>2</sub> during the two tasks and *n*, the value for flow-metabolic coupling. CVR corresponds to the increase in CBF per unit increase in ETCO<sub>2</sub> during the hypercapnia manipulation.

The flow-metabolic coupling parameter  $n$  represents the percent flow increase during a task divided by the  $\text{CMRO}_2$  increase during that same task.

	Frontal	Parietal	Visual
<b>Baseline CBF</b> (ml/100g/min)	48.88 ± 0.92	42.75 ± 3.00	54.45 ± 3.10
<b>CVR</b> (% $\Delta$ CBF/mmHg)	5.44 ± 0.70	6.57 ± 0.94	7.48 ± 0.53
<b><math>M</math></b> (%)	6.09 ± 1.11	6.11 ± 1.20	5.94 ± 1.08
<b>OEF<sub>0</sub></b>	0.45 ± 0.07	0.29 ± 0.06	0.29 ± 0.05
<b>CMRO<sub>2</sub></b> ( $\mu\text{mol}/100\text{g}/\text{min}$ )	173.62 ± 27.74	99.59 ± 18.83	125.09 ± 21.82
<b>%<math>\Delta</math> CMRO<sub>2</sub></b>	3.87 ± 1.20	7.33 ± 1.62	34.02 ± 7.43
<b><math>n</math></b>	3.32 ± 1.18	1.98 ± 0.80	2.01 ± 0.78

**Table 2. Vascular and metabolic profile**

Values obtained from the different elements of our procedure to provide an overview of the vascular and metabolic properties of the different ROIs. It includes the baseline absolute CBF in units of ml/100g/min, cerebrovascular reactivity (CVR) in units of % $\Delta$  CBF/mmHg,  $M$  in units of percent, OEF<sub>0</sub> and CMRO<sub>2</sub> at rest in units of  $\mu\text{mol}/100\text{g}/\text{min}$ , percent evoked CMRO<sub>2</sub> during the two tasks and  $n$ , the value for flow-metabolic coupling. CVR corresponds to the increase in CBF per unit increase in ETCO<sub>2</sub> during the hypercapnia manipulation.  $n$  represents the percent flow increase during a task divided by the CMRO<sub>2</sub> increase during that same task.

## B.5. Discussion

We have shown that our GCM framework allows absolute quantification of CMRO<sub>2</sub> and other physiological parameters both at rest and during task activation. In a previous report (Gauthier et al. 2012c), we demonstrated the possibility of using the GCM with different combinations of hypercapnia and hyperoxia to estimate resting values of  $M$  and OEF<sub>0</sub> throughout grey matter. We have shown here that this approach can also be applied in the context of a task activation study. The  $M$  and OEF<sub>0</sub> values determined at rest can subsequently be combined with BOLD and CBF changes measured in response to a functional challenge, to yield task-evoked changes in CMRO<sub>2</sub> and flow-metabolism coupling. In all ROIs, a

physiological value was estimated for the absolute resting CBF, cerebrovascular reactivity, the calibration factor  $M$ ,  $OEF_0$ ,  $CMRO_2$  at rest, percent evoked  $CMRO_2$  during both a visual and a modified Stroop task and  $n$ , the value for flow-metabolism coupling.

### **B.5.1. Accuracy of estimates**

The values for  $M$ ,  $OEF_0$ , baseline  $CMRO_2$  and task-evoked  $CMRO_2$  estimated using the method described here fall within the physiological range. While other MRI methods exist to obtain an estimate of these parameters (Davis et al. 1998; Chiarelli et al. 2007b; He et al. 2007; Xu et al. 2009; Jain et al. 2010; Bolar et al. 2011b; Bulte et al. 2011; Fan et al. 2011), all methods rely on complex modeling and a certain number of assumptions. The  $M$  parameter is specific to MRI, since it represents the magnetic properties of baseline deoxyhemoglobin content, but nuclear medicine techniques can be used to assess oxidative metabolism. PET measurements of  $CMRO_2$  and  $OEF$  rely on three separate acquisitions with injection of  $^{15}O$  labeled  $O_2$ ,  $H_2O$  and  $CO$ . These three measurements are necessary to model the combined contribution of  $O_2$  diffusion into tissue, its conversion to water during oxidative metabolism, as well as the dependence on blood volume, assessed with  $C^{15}O$  (Mintun et al. 1984; Buxton 2010). While these PET measures of oxygen utilization are also indirect, and subject to their own sets of confounds, they can be used as a benchmark measure to assess qualitatively the accuracy of the estimates obtained using our technique.

#### *B.5.1.1. Visual*

Stimulation of primary visual cortex is commonly used to test new imaging techniques as it yields very large and reliably detectable signal changes. The  $M$  value detected here for visual cortex of  $5.94 \pm 1.08$  was at the lower end of the range of values found in literature. In a previous survey of 3T  $M$  values in visual cortex (in which  $M$  values were adjusted to reflect values at a TE of 30ms) (Gauthier et al. 2012b), we found values ranging from 5.3 (Bulte et al. 2009) to 12.1 (Perthen et al. 2008). Our own values, derived from simultaneous hypercapnia and hyperoxia manipulations (carbogen breathing) have in the past been typically slightly higher (Gauthier et al. 2011b; Gauthier et al. 2012c; Gauthier

et al. 2012b). This may however reflect the contribution in this case from all three gas manipulations in the determination of  $M$  and  $OEF_0$ , since hypercapnia and hyperoxia are associated with lower estimates for these parameters (Figure 3) (Gauthier et al. 2012b). Also, it is possible that the current estimate is a more accurate representation of grey matter values. The ROIs presented here include a reduced contribution from veins and other tissue types since we have corrected for grey matter probability when averaging over the ROIs.

The robust CBF and BOLD signal changes evoked by a flashing checkerboard led to a  $34.02 \pm 7.43\%$  increase in oxidative metabolism from the value of  $125.09 \pm 21.82 \mu\text{mol}/100\text{g}/\text{min}$  determined at rest. The values for percent evoked metabolism and flow metabolism coupling ratio ( $n = 2.01 \pm 0.78$ ) found here were both consistent with previous reports using similar visual stimuli at 3T (Leontiev et al. 2007b; Ances et al. 2008; Lin et al. 2008; Ances et al. 2009). The value for visual resting  $CMRO_2$  determined here ( $125.09 \pm 21.82 \mu\text{mol}/100\text{g}/\text{min}$ ) is somewhat lower than values obtained using  $^{15}\text{O}$ -PET techniques in visual cortex, with values ranging from  $169.2 \pm 31.5 \mu\text{mol}/100\text{g}/\text{min}$  to  $206.5 \pm 22.8 \mu\text{mol}/100\text{g}/\text{min}$  (Ishii et al. 1996; Mintun et al. 2002; Yamauchi et al. 2002; Ibaraki et al. 2008). However, this may be due to the fact that the techniques use very different approaches to estimate metabolism, with different biases. Furthermore, since visual information is still present at rest, the value for baseline visual cortex metabolism must depend on the particular implementation of “rest”. In this case, subjects had their eyes open, with gaze fixed on a white dot in the center of a uniform grey screen, with lights turned off in the scanner bore.

Literature MRI estimates of baseline OEF and  $CMRO_2$  are not available for the visual cortex, but the value we observe for occipital cortex is well within the range observed for grey matter or whole brain, with values of  $132 \pm 20 \mu\text{mol}/100\text{g}/\text{min}$  (Xu et al. 2009),  $125 \pm 15 \mu\text{mol}/100\text{g}/\text{min}$  (Bolar et al. 2011a),  $127 \pm 6$  (Jain et al. 2010),  $151 \pm 15 \mu\text{mol}/100\text{g}/\text{min}$  (Fan et al. 2011) and  $155 \pm 39 \mu\text{mol}/100\text{g}/\text{min}$  (Bulte et al. 2011) for MRI-derived estimates. This is also true of PET-derived grey-matter values, as indicated by a survey of literature PET values in Xu *et al.* (Xu et al. 2009) showing values in young subjects spanning the range from  $110.2 \pm 19.6 \mu\text{mol}/100\text{g}/\text{min}$  to  $149.5 \pm 27.5 \mu\text{mol}/100\text{g}/\text{min}$  (Ishii et al. 1996; Hattori et al. 2004;

Ito et al. 2004; Ito et al. 2005; Coles et al. 2006; Ibaraki et al. 2008; Ibaraki et al. 2010). The conversion from ml/100g/min to  $\mu\text{mol}/100\text{g}/\text{min}$  was done using Equation 5 from Gauthier *et al.* (Gauthier et al. 2012c) starting with the values in the original papers rather than the values reported by Xu *et al.*, which explains the slight discrepancies in the reported values.

Our  $\text{OEF}_0$  estimate over visual cortex of  $0.29 \pm 0.05$  is within the physiological range. Though this value is somewhat lower than values reported in the PET literature, going from  $0.36 \pm 0.03$  to  $0.59 \pm 0.06$  (Mintun et al. 2002; Yamauchi et al. 2002; Ito et al. 2005; Ibaraki et al. 2008), it is similar to the value for grey matter ( $0.26 \pm 0.02$ ) and whole brain ( $0.36 \pm 0.02$  and  $0.38 \pm 0.14$ ) found using three other MRI techniques (Bolar et al. 2011a; Bulte et al. 2011). PET values over all grey matter from the literature range from  $0.36 \pm 0.06$  to  $0.44 \pm 0.06$ . The fact that these are systematically higher than all MR-based estimates may indicate that the assumptions or noise biases for these two modalities pull estimates in opposite directions (Yamaguchi et al. 1986; Ito et al. 2004; Ibaraki et al. 2008). Further exploration is clearly warranted to assess the accuracy of these values.

#### *B.5.1.2. Stroop*

Cognitive tasks give rise to much more subtle signal changes than primary sensory stimuli and are generally used to assess neurological correlates of specific cognitive subcomponents. To reproduce this situation with the modified Stroop task used here, blocks of a more complex version of the task, that included components of inhibition and switching, were interspersed with blocks of a simpler version of the task that only required color-naming (no inhibition or switching). Though the signal changes to each version of the task were readily detectable, the difference between them was not. This is most likely due to both the small number of subjects included in this proof-of-concept study, but also to the fact that a single acquisition with the modified Stroop task was obtained for each subject. Because of this, we elected to use only the signal changes obtained during the inhibition/switching blocks, without subtracting from them the signal changes obtained in the control, simpler version of the task. It is to be noted that the lack of a significant difference in the fMRI signal changes obtained during the inhibition/switching and control

blocks in the small cohort of subjects presented here is not due to an absence of behavioral effect of the task. This is indicated by the fact that participants performed significantly better both in terms of reaction time ( $p = 0.003$ ) and accuracy ( $p = 0.004$ ) during the control blocks as compared to the inhibition/switching blocks.

Testing the accuracy of values associated with the modified Stroop task is made more difficult by the fact that there are many versions of this task. The extent and exact localization of the significant signal changes will depend on the exact implementation of the task, but also on the SNR of the imaging technique used to detect the changes. Lower SNR techniques, such as ASL, may not be as efficient for the detection of small signal changes, especially in areas known to be more affected by distortions and signal losses due to susceptibility effects. Even with these potential confounds, the modified Stroop task has the advantage of having been extensively characterized using a variety of imaging techniques and some robust and conserved signal changes exist across modalities. Two main positive signal change foci were found here: an extensive bilateral frontal component covering parts of Brodmann areas 6, 9, 45 and 46, with partial extension into cingulate cortex around Brodmann area 32 and into part of the frontal pole. The second focus encompassed regions in parietal areas, covering mainly parts of bilateral Brodmann areas 7, 39 and 40. The frontal component corresponds well to the literature on the localization of activation during the inhibition component of Stroop and during task switching (Leung et al. 2000; MacDonald et al. 2000; Brass et al. 2002; Milham et al. 2002; Derrfuss et al. 2005; Zysset et al. 2007), while parietal activation has been observed during task switching (Dove et al. 2000; Kimberg et al. 2000; MacDonald et al. 2000; Brass et al. 2002; Yeung et al. 2006). A contribution from anterior cingulate cortex (Brodmann 32) was also detected, as expected in this type of task (Leung et al. 2000; MacDonald et al. 2000; Brass et al. 2002; Milham et al. 2002; Derrfuss et al. 2005; Zysset et al. 2007). We also detected a frontal pole component, thought to reflect the flexibility required to inhibit automatic responses in the context of changing stimulus contingencies (Nobre et al. 1999).

Only three calibrated fMRI studies have so far looked at cognitive tasks (Restom et al. 2008; Goodwin et al. 2009; Mohtasib et al. 2012), two of them using the Stroop task with the hyperoxia calibration method (Goodwin et al. 2009; Mohtasib et al. 2012). In Goodwin *et al.* (Goodwin et al. 2009),  $M$  values were found to be higher than in the present study both in frontal ( $9.0 \pm 5.8$  and  $7.4 \pm 4.0$  for left and right middle frontal gyri respectively) and parietal ( $10.2 \pm 4.9$  and  $7.7 \pm 4.4$  for left and right parietal lobules respectively) regions, though the value found here is within the standard deviation of that study. The  $M$  values obtained using the same task in a slightly larger cohort in Mohtasib *et al.* (Mohtasib et al. 2012) of  $5.6 \pm 0.7$  and  $6.0 \pm 0.6$  for left and right middle frontal gyri respectively agrees closely with the value of  $6.09 \pm 1.11$  found here for bilateral frontal areas. Values for the flow-metabolism coupling parameter  $n$  in medial frontal areas in Mohtasib *et al.* (Mohtasib et al. 2012) were in good agreement with the value for frontal areas found here. Literature flow metabolism coupling values are not available for the regions corresponding to our other ROIs, but these fall within the physiological expected range with values close to two (Table 2).

OEF<sub>0</sub> values for medial frontal areas fell within the expected range with a value of  $0.45 \pm 0.07$ . This estimate is consistent with the literature estimates in frontal areas of  $0.41 \pm 0.07$  and  $0.35 \pm 0.06$  (Ishii et al. 1996; Ibaraki et al. 2008). Our parietal estimate was however below literature estimates with a value of  $0.29 \pm 0.06$  as compared to the literature values of  $0.41 \pm 0.07$  and  $0.40 \pm 0.05$  for that region (Ishii et al. 1996; Ibaraki et al. 2008). The accuracy of CMRO<sub>2</sub> estimates shows a similar pattern as OEF values. Our frontal values of  $173.62 \pm 27.74$   $\mu\text{mol}/100\text{g}/\text{min}$  for the frontal ROI is somewhat higher than literature estimates of  $133.8 \pm 23.6$  and  $137.7 \pm 25.2$   $\mu\text{mol}/100\text{g}/\text{min}$  for frontal lobes (Ishii et al. 1996; Ibaraki et al. 2008). Our parietal estimate of  $99.59 \pm 18.83$   $\mu\text{mol}/100\text{g}/\text{min}$  is however lower than literature values of  $153.4 \pm 31.4$  and  $141.6 \pm 23.6$   $\mu\text{mol}/100\text{g}/\text{min}$  (Ishii et al. 1996; Ibaraki et al. 2008). The discrepancy between the values presented here and the PET literature values may reflect the fact that more subjects are required for robust characterization of a cognitive task, since signal changes in the areas involved are more subtle.

A recent paper by Bulte *et al.* (Bulte et al. 2011) uses a technique similar to ours to measure the same set of physiological parameters. In brief, this study uses a hypercapnia manipulation to derive  $M$  using the Davis model (Davis et al. 1998), then uses this  $M$  value in the context of a hyperoxia manipulation to calculate  $OEF_0$  using the Chiarelli model (Chiarelli et al. 2007b). Conceptually very close to the method proposed here, we would expect the values obtained by both methods to be quite similar. Though the method proposed by Bulte and colleagues has so far only been applied to complete grey matter, the values agree very well with our own grey matter values published in a previous report (Gauthier et al. 2012c). Though values are not available for smaller ROIs, the close agreement in the values obtained through both methods in different subjects is an encouraging sign that these techniques may provide valid estimates of baseline OEF and  $CMRO_2$ .

### **B.5.2. Implementation biases and confounds**

All baseline measures were found to be in the physiological range, but somewhat different from PET-derived estimates. This could be due to inherent biases associated with each method and their underlying assumptions, especially since all methods include a substantial component of modeling. While we feel that the current results support the general validity of the GCM framework, the ultimate precision of the method will clearly benefit from further optimization. Moreover, the small number of subjects included in this proof-of-concept study highlights the increased challenge of quantifying cognitive responses compared with the much more robust responses to primary sensory stimulation. While the intersection plots obtained in grey matter are generally robust and adequate for quantification, data obtained in smaller ROIs show a reduced precision and robustness to errors in measurement. While visual estimates may be somewhat spared given the large signal changes obtained in visual cortical areas, it is clear that a much larger cohort would be required for robust characterization of cognitive effects.

The precision of this method is dependent on the coincidence of intersection points between the curves generated from the three breathing manipulations. Inspection of the three curve plots from Figure 3 shows that since the three intersection points are not coincident in these ROIs, the value of the final estimate depends on the

relative position of the curves. In all cases, the curve for the combined hyperoxia/hypercapnia (HO-HC) breathing manipulation intersects the  $O_2$  manipulation (HO) curve at a higher point (for both  $M$  and  $OEF_0$ ) than the hypercapnia manipulation (HC) curve. Since the estimate reported here corresponds to the average between these two intersection points, a systematic downward bias in the HC curve (or upward bias in the combined HO-HC curve) will result in a similar bias in the final estimate.

While we cannot rule out conclusively the possibility that this relationship between the curves is due to a systematic error introduced by our model, the fact that with enough averaging (as in the case of complete grey matter ROIs) we obtain tight convergence suggests that this divergence may instead be due to systematic bias arising from the lower SNR obtained with small ROIs. The model includes ratio estimates and non-linear terms, which are prone to bias under low SNR conditions. Since the quality of the ultimate measurements is mainly limited by the quality of the ASL data, and since accurate CBF measurements of the changes associated with breathing manipulations are known to be difficult to obtain (Tancredi et al. 2012), it is possible that this systematic bias may arise from suboptimal measurement of flow changes during gas manipulations. To rule this out, future studies will use ASL methods yielding improved measurements of gas manipulations. Strategies to improve ASL quality could include using multiple delay times to capture the temporal profile of tag delivery at each voxel, which can then be fit with a kinetic model (Buxton et al. 1998a) to provide a more accurate estimate of flow (Bulte et al. 2011). Another possibility would be to implement background suppression techniques to reduce the physiological or instrumental modulation of the background "static" tissue signal that is unrelated to flow (Dixon et al. 1991; Maleki et al. 2011).

Alternatively, this effect could arise from errors in the BOLD signal change measurement. The BOLD response to hypercapnia has a lower amplitude than the BOLD response to combined HO-HC. This smaller response means that the contrast-to-noise ratio (CNR) of the hypercapnia BOLD experiment is lower than that of combined HO-HC, given a similar level of noise in both measurements. This reduced CNR could lead to an underestimation of the BOLD response to

hypercapnia, thereby leading to an underestimation of the  $M$  value associated with a given OEF. This underestimation would be reduced for combined HO-HC, since the measured BOLD changes are larger and therefore easier to measure against a similar level of noise.

The values for all parameters were estimated over functionally-defined ROIs using fairly large voxels. It is likely therefore that the measurements suffer from biases due to some inclusion of cerebro-spinal fluid (CSF) and white matter through partial volume effects. ASL is a low SNR technique and large voxels are therefore necessary to obtain meaningful measurement values. For the same reason, good quality single voxel and small ROI estimates are difficult to obtain. However, by weighting each voxel within the ROI by the grey matter volume, estimated for that voxel using automatic tissue segmentation, this is unlikely to be the major factor at play to explain divergence of the curves.

The technique chosen to administer the gases, by delivering gases of fixed mixture concentrations through an unsealed face mask gives rise to somewhat variable end-tidal gas concentrations. While other techniques exist to more accurately control and target specific end-tidal values of  $\text{CO}_2$  and  $\text{O}_2$  (Slessarev et al. 2007; Mark et al. 2010), fluctuations over a moderate range are of no significant consequence for the method described here, as long as end-tidal measurements are performed. The variability in end-tidal values could furthermore be reduced by using a mask with a larger inflow bag and a regulator allowing higher flow rates. This would allow the mask to be sealed to the face and prevent room air from being entrained into the mask during periods of hyperventilation. Also, the use of a metronome to control breathing rate could help reduce inter-subject and inter-run variability. Finally, inhalation of  $\text{CO}_2$  may be uncomfortable in high concentrations and lead to important changes in breathing pattern and attentional state that could potentially affect the results obtained using this approach. In this case however, subjects in general found the inhalation of 7%  $\text{CO}_2$  to be quite tolerable with this specific setup, as indicated by the range of responses given on our subjective rating questionnaire. Average rating was  $2.1 \pm 0.6$  over all subject, indicating a very low level of breathing discomfort.

One of the most debated assumptions of calibrated fMRI is that gas manipulations do not affect oxidative metabolism. Short periods of hyperoxia are not usually assumed to change metabolism, though some groups report a suppressive effect of O<sub>2</sub> on oxidative metabolism (Xu et al. 2011a). Furthermore, there is no consensus about the effects of hypercapnia with some studies reporting increases in metabolism (Horvath et al. 1994; Jones et al. 2005), decreases (Zappe et al. 2008; Xu et al. 2011b), and no detectable change (McPherson et al. 1991; Hino et al. 2000; Chen et al. 2010a). In a previous report (Gauthier et al. 2012c), we have modeled the effects of both decreased and increased CMRO<sub>2</sub> on our model. Modeling the effects of decreases or increases in CMRO<sub>2</sub> during hypercapnia manipulations resulted in reduced convergence towards a unique solution for the intersection of the HC, HO and combined HO-HC curves. Because this intersection point corresponds to a baseline physiological property of the brain, a single point is expected. While the latter observations were not compatible with a significant CO<sub>2</sub>-induced change in CMRO<sub>2</sub>, results of other studies (Zappe et al. 2008; Xu et al. 2011b) have suggested there may be such an effect. It is clear that further exploration of the impact of CO<sub>2</sub> on CMRO<sub>2</sub> in different brain systems and under different conditions is required.

The selection of values for model parameters  $\alpha$  and  $\beta$  has also been the subject of some contention. We used here values of  $\alpha = 0.18$  and  $\beta = 1.5$ . This value for  $\alpha$  is taken from experimental measurements of venous blood volume change (Chen et al. 2009a; Chen et al. 2010c). Though  $\beta$  was originally taken to reflect the field-specific effects of deoxyhemoglobin on R<sub>2</sub><sup>\*</sup>, it can instead be viewed as a lumped constant encompassing additional physiological and physical factors. Numerical simulations published by Griffeth et al. suggested that, in an application of the original Davis model, consistency with an alternate multi-compartment model was maximized using a value of  $\beta = 0.91$  (Griffeth et al. 2011). Although we have chosen to adhere to the original definitions and currently "standard" values of  $\alpha$  and  $\beta$  for the present study, alternate values such as those proposed by Griffeth could readily be inserted in the method presented here.

## **B.6. Conclusion**

We have demonstrated that QUO2 MRI allows absolute quantification of  $CMRO_2$  both at rest and in the context of a functional challenge. Additional quantitative information on resting physiology is also furnished, including resting CBF, CVR,  $M$  and  $OEF_0$ . The sensitivity of the method is limited mainly by the low SNR inherent in currently available ASL techniques, so while reliable quantification was achieved for visual stimulation, a substantially larger cohort would be required for precise characterization of a cognitive process like the inhibition and switching components of the modified Stroop task. The lower SNR conditions prevailing in the functionally defined ROIs highlight the possibility of systematic error related either to noise bias or regional differences that are not captured in the model, motivating further experimental and theoretical exploration. Significant improvements in ASL performance will be required for application of this method in individual patients or subjects.

## **B.7. Acknowledgments**

We thank Carolyn Hurst, André Cyr and Tarik Hafyane for help with data acquisition, Felipe Tancredi and Maude Laguë-Bauvais for helpful discussions. We would also like to thank Jiongjong Wang, who provided the pseudo-continuous arterial spin-labeling sequence used. This work was supported by the Canadian Institutes for Health Research (MOP 84378, Banting and Best Scholarship held by CJG), the Canadian Foundation for Innovation (Leaders Opportunity Fund 17380), and the Ministère du développement économique, de l'innovation et de l'exportation (PSR-SIIRI-239).

## Bibliography

- Abounader, R. and Hamel, E., 1997. Associations between neuropeptide Y nerve terminals and intraparenchymal microvessels in rat and human cerebral cortex. J Comp Neurol 388: 444-453.
- Aleardi, A. M., Benard, G., Augereau, O., Malgat, M., Talbot, J. C., Mazat, J. P., Letellier, T., Dachary-Prigent, J., Solaini, G. C. and Rossignol, R., 2005. Gradual alteration of mitochondrial structure and function by beta-amyloids: importance of membrane viscosity changes, energy deprivation, reactive oxygen species production, and cytochrome c release. J Bioenerg Biomembr 37: 207-225.
- Amar, J., Ruidavets, J. B., Peyrieux, J. C., Mallion, J. M., Ferrieres, J., Safar, M. E. and Chamontin, B., 2005. C-reactive protein elevation predicts pulse pressure reduction in hypertensive subjects. Hypertension 46: 151-155.
- An, H. and Lin, W., 2000. Quantitative measurements of cerebral blood oxygen saturation using magnetic resonance imaging. J Cereb Blood Flow Metab 20: 1225-1236.
- Anantharaman, M., Tangpong, J., Keller, J. N., Murphy, M. P., Markesbery, W. R., Kinningham, K. K. and St Clair, D. K., 2006. Beta-amyloid mediated nitration of manganese superoxide dismutase: implication for oxidative stress in a APPNLH/NLH X PS-1P264L/P264L double knock-in mouse model of Alzheimer's disease. Am J Pathol 168: 1608-1618.
- Ances, B. M., Leontiev, O., Perthen, J. E., Liang, C., Lansing, A. E. and Buxton, R. B., 2008. Regional differences in the coupling of cerebral blood flow and oxygen metabolism changes in response to activation: implications for BOLD-fMRI. Neuroimage 39: 1510-1521.
- Ances, B. M., Liang, C. L., Leontiev, O., Perthen, J. E., Fleisher, A. S., Lansing, A. E. and Buxton, R. B., 2009. Effects of aging on cerebral blood flow, oxygen metabolism, and blood oxygenation level dependent responses to visual stimulation. Hum Brain Mapp 30: 1120-1132.

- Andersson, E. A., Lundahl, G., Wecke, L., Lindblom, I. and Nilsson, J., 2011. Maximal aerobic power versus performance in two aerobic endurance tests among young and old adults. Gerontology 57: 502-512.
- Andreasson, K., 2010. Emerging roles of PGE2 receptors in models of neurological disease. Prostaglandins Other Lipid Mediat 91: 104-112.
- Arena, R., Arrowood, J. A., Fei, D. Y., Helm, S. and Kraft, K. A., 2009. Maximal aerobic capacity and the oxygen uptake efficiency slope as predictors of large artery stiffness in apparently healthy subjects. J Cardiopulm Rehabil Prev 29: 248-254.
- Ashkanian, M., Borghammer, P., Gjedde, A., Ostergaard, L. and Vafaee, M., 2008. Improvement of brain tissue oxygenation by inhalation of carbogen. Neuroscience 156: 932-938.
- Ashkanian, M., Gjedde, A., Mouridsen, K., Vafaee, M., Hansen, K. V., Ostergaard, L. and Andersen, G., 2009. Carbogen inhalation increases oxygen transport to hypoperfused brain tissue in patients with occlusive carotid artery disease: increased oxygen transport to hypoperfused brain. Brain Res 1304: 90-95.
- Au, R., Massaro, J. M., Wolf, P. A., Young, M. E., Beiser, A., Seshadri, S., D'Agostino, R. B. and DeCarli, C., 2006. Association of white matter hyperintensity volume with decreased cognitive functioning: the Framingham Heart Study. Arch Neurol 63: 246-250.
- Baltes, P. B. and Lindenberger, U., 1997. Emergence of a powerful connection between sensory and cognitive functions across the adult life span: a new window to the study of cognitive aging? Psychol Aging 12: 12-21.
- Banzett, R. B., Lansing, R. W., Evans, K. C. and Shea, S. A., 1996. Stimulus-response characteristics of CO<sub>2</sub>-induced air hunger in normal subjects. Respir Physiol 103: 19-31.
- Bartley, M. G., Marquardt, K., Kirchhof, D., Wilkins, H. M., Patterson, D. and Linseman, D. A., 2012. Overexpression of amyloid-beta protein precursor induces mitochondrial oxidative stress and activates the intrinsic apoptotic cascade. J Alzheimers Dis 28: 855-868.

- Beckmann, C. F., Jenkinson, M. and Smith, S. M., 2003. General multilevel linear modeling for group analysis in FMRI. Neuroimage 20: 1052-1063.
- Bhardwaj, A., Northington, F. J., Carhuapoma, J. R., Falck, J. R., Harder, D. R., Traystman, R. J. and Koehler, R. C., 2000. P-450 epoxygenase and NO synthase inhibitors reduce cerebral blood flow response to N-methyl-D-aspartate. Am J Physiol Heart Circ Physiol 279: H1616-1624.
- Binder, J., Bailey, K. R., Seward, J. B., Squires, R. W., Kunihiro, T., Hensrud, D. D. and Kullo, I. J., 2006. Aortic augmentation index is inversely associated with cardiorespiratory fitness in men without known coronary heart disease. Am J Hypertens 19: 1019-1024.
- Blockley, N. P., Griffeth, V. E. and Buxton, R. B. (2011a). Can the calibrated BOLD scaling factor M be estimated just from R2' in the baseline state without administering gases? International Society for Magnetic Resonance in Medicine, Montreal, Canada.
- Blockley, N. P., Griffeth, V. E. and Buxton, R. B., 2011b. A general analysis of calibrated BOLD methodology for measuring CMRO(2) responses: Comparison of a new approach with existing methods. Neuroimage.
- Bohnen, N., Jolles, J. and Twijnstra, A., 1992. Modification of the Stroop Color Word Test improves differentiation between patients with mild head injury and matched controls. Clinical Neuropsychologist 6: 178-184.
- Bokkers, R. P., van Osch, M. J., Klijn, C. J., Kappelle, L. J. and Hendrikse, J., 2011. Cerebrovascular reactivity within perfusion territories in patients with an internal carotid artery occlusion. J Neurol Neurosurg Psychiatry 82: 1011-1016.
- Bolar, D. S., Rosen, B. R., Sorensen, A. G. and Adalsteinsson, E., 2011a. QUantitative Imaging of eXtraction of oxygen and Tissue consumption (QUIXOTIC) using venular-targeted velocity-selective spin labeling. Magn Reson Med.
- Bolar, D. S., Rosen, B. R., Sorensen, A. G. and Adalsteinsson, E., 2011b. QUantitative Imaging of eXtraction of oxygen and Tissue consumption (QUIXOTIC) using venular-targeted velocity-selective spin labeling. Magn Reson Med 66: 1550-1562.

- Bolar, D. S., Tancredi, F. B., Lajoie, I., Benner, T., Adalsteinsson, E., Mandeville, J. B., Sorensen, A. G. and Hoge, R. D., 2012. Pulsed arterial spin-labeling MRI of hypercapnic challenge in brain: Tag width and timing effects. PLoS One In review.
- Bonda, D. J., Lee, H. P., Lee, H. G., Friedlich, A. L., Perry, G., Zhu, X. and Smith, M. A., 2010. Novel therapeutics for Alzheimer's disease: an update. Curr Opin Drug Discov Devel 13: 235-246.
- Bonnefond, A., Doignon-Camus, N., Hoeft, A. and Dufour, A., 2011. Impact of motivation on cognitive control in the context of vigilance lowering: an ERP study. Brain Cogn 77: 464-471.
- Boutouyrie, P., Tropeano, A. I., Asmar, R., Gautier, I., Benetos, A., Lacolley, P. and Laurent, S., 2002. Aortic stiffness is an independent predictor of primary coronary events in hypertensive patients: a longitudinal study. Hypertension 39: 10-15.
- Boxerman, J. L., Hamberg, L. M., Rosen, B. R. and Weisskoff, R. M., 1995. MR contrast due to intravascular magnetic susceptibility perturbations. Magn Reson Med 34: 555-566.
- Brass, M. and von Cramon, D. Y., 2002. The role of the frontal cortex in task preparation. Cereb Cortex 12: 908-914.
- Bremmer, J. P., van Berckel, B. N., Persoon, S., Kappelle, L. J., Lammertsma, A. A., Kloet, R., Luurtsema, G., Rijbroek, A., Klijn, C. J. and Boellaard, R., 2010. Day-to-Day Test-Retest Variability of CBF, CMRO(2), and OEF Measurements Using Dynamic (15)O PET Studies. Mol Imaging Biol.
- Brickman, A. M., Sneed, J. R., Provenzano, F. A., Garcon, E., Johnert, L., Muraskin, J., Yeung, L. K., Zimmerman, M. E. and Roose, S. P., 2011. Quantitative approaches for assessment of white matter hyperintensities in elderly populations. Psychiatry Res 193: 101-106.
- Brown, A. D., McMorris, C. A., Longman, R. S., Leigh, R., Hill, M. D., Friedenreich, C. M. and Poulin, M. J., 2010. Effects of cardiorespiratory fitness and cerebral blood flow on cognitive outcomes in older women. Neurobiol Aging 31: 2047-2057.

- Brown, W. R. and Thore, C. R., 2011. Review: cerebral microvascular pathology in ageing and neurodegeneration. Neuropathol Appl Neurobiol 37: 56-74.
- Bulte, D. P., Chiarelli, P. A., Wise, R. G. and Jezzard, P., 2007. Cerebral perfusion response to hyperoxia. J Cereb Blood Flow Metab 27: 69-75.
- Bulte, D. P., Drescher, K. and Jezzard, P., 2009. Comparison of hypercapnia-based calibration techniques for measurement of cerebral oxygen metabolism with MRI. Magn Reson Med 61: 391-398.
- Bulte, D. P., Kelly, M., Germuska, M., Xie, J., Chappell, M. A., Okell, T. W., Bright, M. G. and Jezzard, P., 2011. Quantitative measurement of cerebral physiology using respiratory-calibrated MRI. Neuroimage.
- Buxton, R. B., 2010. Interpreting oxygenation-based neuroimaging signals: the importance and the challenge of understanding brain oxygen metabolism. Front Neuroenergetics 2: 8.
- Buxton, R. B. and Frank, L. R., 1997. A model for the coupling between cerebral blood flow and oxygen metabolism during neural stimulation. J Cereb Blood Flow Metab 17: 64-72.
- Buxton, R. B., Frank, L. R., Wong, E. C., Siewert, B., Warach, S. and Edelman, R. R., 1998a. A general kinetic model for quantitative perfusion imaging with arterial spin labeling. Magn Reson Med 40: 383-396.
- Buxton, R. B., Uludag, K., Dubowitz, D. J. and Liu, T. T., 2004. Modeling the hemodynamic response to brain activation. Neuroimage 23 Suppl 1: S220-233.
- Buxton, R. B., Wong, E. C. and Frank, L. R., 1998b. Dynamics of blood flow and oxygenation changes during brain activation: the balloon model. Magn Reson Med 39: 855-864.
- Cabeza, R., 2002. Hemispheric asymmetry reduction in older adults: the HAROLD model. Psychol Aging 17: 85-100.
- Cabeza, R., McIntosh, A. R., Tulving, E., Nyberg, L. and Grady, C. L., 1997. Age-related differences in effective neural connectivity during encoding and recall. Neuroreport 8: 3479-3483.
- Cabeza, R., Nyberg, L. and Park, D. C. (2005). Cognitive neuroscience of aging: Linking cognitive and cerebral aging. Oxford, Oxford University Press.

- Campbell, A. M. and Beaulieu, C., 2006. Pulsed arterial spin labeling parameter optimization for an elderly population. J Magn Reson Imaging 23: 398-403.
- Canevari, L., Clark, J. B. and Bates, T. E., 1999. beta-Amyloid fragment 25-35 selectively decreases complex IV activity in isolated mitochondria. FEBS Lett 457: 131-134.
- Cantin, S., Villien, M., Moreaud, O., Tropres, I., Keignart, S., Chipon, E., Le Bas, J. F., Warnking, J. and Krainik, A., 2011. Impaired cerebral vasoreactivity to CO<sub>2</sub> in Alzheimer's disease using BOLD fMRI. Neuroimage 58: 579-587.
- Cappell, K. A., Gmeindl, L. and Reuter-Lorenz, P. A., 2010. Age differences in prefrontal recruitment during verbal working memory maintenance depend on memory load. Cortex 46: 462-473.
- Carrera, E., Kim, D. J., Castellani, G., Zweifel, C., Smielewski, P., Pickard, J. D., Kirkpatrick, P. J. and Czosnyka, M., 2011. Cerebral arterial compliance in patients with internal carotid artery disease. Eur J Neurol 18: 711-718.
- Chalela, J. A., Alsop, D. C., Gonzalez-Atavales, J. B., Maldjian, J. A., Kasner, S. E. and Detre, J. A., 2000. Magnetic resonance perfusion imaging in acute ischemic stroke using continuous arterial spin labeling. Stroke 31: 680-687.
- Chen, J. J. and Pike, G. B., 2009a. BOLD-specific cerebral blood volume and blood flow changes during neuronal activation in humans. NMR Biomed 22: 1054-1062.
- Chen, J. J. and Pike, G. B., 2010a. Global cerebral oxidative metabolism during hypercapnia and hypocapnia in humans: implications for BOLD fMRI. J Cereb Blood Flow Metab 30: 1094-1099.
- Chen, J. J. and Pike, G. B., 2010b. Global cerebral oxidative metabolism during hypercapnia and hypocapnia in humans: implications for BOLD fMRI. J Cereb Blood Flow Metab.
- Chen, J. J. and Pike, G. B., 2010c. MRI measurement of the BOLD-specific flow-volume relationship during hypercapnia and hypocapnia in humans. Neuroimage 53: 383-391.
- Chen, J. J., Rosas, H. D. and Salat, D. H., 2011. Age-associated reductions in cerebral blood flow are independent from regional atrophy. Neuroimage 55: 468-478.

- Chen, Y. and Parrish, T. B., 2009b. Caffeine dose effect on activation-induced BOLD and CBF responses. Neuroimage 46: 577-583.
- Chiarelli, P. A., Bulte, D. P., Piechnik, S. and Jezzard, P., 2007a. Sources of systematic bias in hypercapnia-calibrated functional MRI estimation of oxygen metabolism. Neuroimage 34: 35-43.
- Chiarelli, P. A., Bulte, D. P., Wise, R., Gallichan, D. and Jezzard, P., 2007b. A calibration method for quantitative BOLD fMRI based on hyperoxia. Neuroimage 37: 808-820.
- Churchill, J. D., Galvez, R., Colcombe, S., Swain, R. A., Kramer, A. F. and Greenough, W. T., 2002. Exercise, experience and the aging brain. Neurobiol Aging 23: 941-955.
- Colcombe, S. and Kramer, A. F., 2003. Fitness effects on the cognitive function of older adults: a meta-analytic study. Psychol Sci 14: 125-130.
- Colcombe, S. J., Erickson, K. I., Scalf, P. E., Kim, J. S., Prakash, R., McAuley, E., Elavsky, S., Marquez, D. X., Hu, L. and Kramer, A. F., 2006. Aerobic exercise training increases brain volume in aging humans. J Gerontol A Biol Sci Med Sci 61: 1166-1170.
- Coles, J. P., Fryer, T. D., Bradley, P. G., Nortje, J., Smielewski, P., Rice, K., Clark, J. C., Pickard, J. D. and Menon, D. K., 2006. Intersubject variability and reproducibility of 15O PET studies. J Cereb Blood Flow Metab 26: 48-57.
- Coskun, P., Wyrembak, J., Schriener, S., Chen, H. W., Marciniack, C., Laferla, F. and Wallace, D. C., 2011. A mitochondrial etiology of Alzheimer and Parkinson disease. Biochim Biophys Acta.
- Cotman, C. W., Berchtold, N. C. and Christie, L. A., 2007. Exercise builds brain health: key roles of growth factor cascades and inflammation. Trends Neurosci 30: 464-472.
- Cox, R. W. and Jesmanowicz, A., 1999. Real-time 3D image registration for functional MRI. Magn Reson Med 42: 1014-1018.
- Dai, W., Garcia, D., de Bazelaire, C. and Alsop, D. C., 2008. Continuous flow-driven inversion for arterial spin labeling using pulsed radio frequency and gradient fields. Magn Reson Med 60: 1488-1497.

- Dash, R. K. and Bassingthwaite, J. B., 2004. Blood HbO<sub>2</sub> and HbCO<sub>2</sub> dissociation curves at varied O<sub>2</sub>, CO<sub>2</sub>, pH, 2,3-DPG and temperature levels. Ann Biomed Eng 32: 1676-1693.
- Dash, R. K. and Bassingthwaite, J. B., 2010. Erratum to: Blood HbO<sub>2</sub> and HbCO<sub>2</sub> dissociation curves at varied O<sub>2</sub>, CO<sub>2</sub>, pH, 2,3-DPG and temperature levels. Ann Biomed Eng 38: 1683-1701.
- Davenport, M. H., Hogan, D. B., Eskes, G. A., Longman, R. S. and Poulin, M. J., 2012. Cerebrovascular reserve: the link between fitness and cognitive function? Exerc Sport Sci Rev.
- Davies, K. J., Thapar, A., Kasivisvanathan, V., Shalhoub, J. and Davies, A. H., 2012. Review of Trans-Atlantic Cardiovascular Best Medical Therapy Guidelines Recommendations for Asymptomatic Carotid Atherosclerosis. Curr Vasc Pharmacol.
- Davis, S. W., Dennis, N. A., Daselaar, S. M., Fleck, M. S. and Cabeza, R., 2008. Que PASA? The posterior-anterior shift in aging. Cereb Cortex 18: 1201-1209.
- Davis, T. L., Kwong, K. K., Weisskoff, R. M. and Rosen, B. R., 1998. Calibrated functional MRI: mapping the dynamics of oxidative metabolism. Proc Natl Acad Sci U S A 95: 1834-1839.
- Delis, D. C., Kaplan, E., & Kramer, J. H. (2001). Delis-Kaplan Executive Function System (D-KEFS), The Psychological Corporation.
- Derrfuss, J., Brass, M., Neumann, J. and von Cramon, D. Y., 2005. Involvement of the inferior frontal junction in cognitive control: meta-analyses of switching and Stroop studies. Hum Brain Mapp 25: 22-34.
- Detre, J. A., Rao, H., Wang, D. J., Chen, Y. F. and Wang, Z., 2012. Applications of arterial spin labeled MRI in the brain. J Magn Reson Imaging 35: 1026-1037.
- Devaraj, S., Kumaresan, P. R. and Jialal, I., 2011. C-reactive protein induces release of both endothelial microparticles and circulating endothelial cells in vitro and in vivo: further evidence of endothelial dysfunction. Clin Chem 57: 1757-1761.

- Devor, A., Sakadzic, S., Saisan, P. A., Yaseen, M. A., Roussakis, E., Srinivasan, V. J., Vinogradov, S. A., Rosen, B. R., Buxton, R. B., Dale, A. M. and Boas, D. A., 2011. "Overshoot" of O is required to maintain baseline tissue oxygenation at locations distal to blood vessels. J Neurosci 31: 13676-13681.
- DiGirolamo, G. J., Kramer, A. F., Barad, V., Cepeda, N. J., Weissman, D. H., Milham, M. P., Wszalek, T. M., Cohen, N. J., Banich, M. T., Webb, A., Belopolsky, A. V. and McAuley, E., 2001. General and task-specific frontal lobe recruitment in older adults during executive processes: a fMRI investigation of task-switching. Neuroreport 12: 2065-2071.
- Dirnagl, U., Lindauer, U. and Villringer, A., 1993. Role of nitric oxide in the coupling of cerebral blood flow to neuronal activation in rats. Neurosci Lett 149: 43-46.
- Dixon, W. T., Sardashti, M., Castillo, M. and Stomp, G. P., 1991. Multiple inversion recovery reduces static tissue signal in angiograms. Magn Reson Med 18: 257-268.
- Dogui, A., Redheuil, A., Lefort, M., DeCesare, A., Kachenoura, N., Herment, A. and Mousseaux, E., 2011. Measurement of aortic arch pulse wave velocity in cardiovascular MR: comparison of transit time estimators and description of a new approach. J Magn Reson Imaging 33: 1321-1329.
- Donahue, M. J., Lu, H., Jones, C. K., Edden, R. A., Pekar, J. J. and van Zijl, P. C., 2006. Theoretical and experimental investigation of the VASO contrast mechanism. Magn Reson Med 56: 1261-1273.
- Dove, A., Pollmann, S., Schubert, T., Wiggins, C. J. and von Cramon, D. Y., 2000. Prefrontal cortex activation in task switching: an event-related fMRI study. Brain Res Cogn Brain Res 9: 103-109.
- Dunn, J. F., O'Hara, J. A., Zaim-Wadghiri, Y., Lei, H., Meyerand, M. E., Grinberg, O. Y., Hou, H., Hoopes, P. J., Demidenko, E. and Swartz, H. M., 2002. Changes in oxygenation of intracranial tumors with carbogen: a BOLD MRI and EPR oximetry study. J Magn Reson Imaging 16: 511-521.
- Edelman, R. R., Siewert, B., Darby, D. G., Thangaraj, V., Nobre, A. C., Mesulam, M. M. and Warach, S., 1994. Qualitative mapping of cerebral blood flow and

- functional localization with echo-planar MR imaging and signal targeting with alternating radio frequency. Radiology 192: 513-520.
- Elias, M. F., Robbins, M. A., Budge, M. M., Abhayaratna, W. P., Dore, G. A. and Elias, P. K., 2009. Arterial pulse wave velocity and cognition with advancing age. Hypertension 53: 668-673.
- Erecinska, M. and Dagani, F., 1990. Relationships between the neuronal sodium/potassium pump and energy metabolism. Effects of K<sup>+</sup>, Na<sup>+</sup>, and adenosine triphosphate in isolated brain synaptosomes. J Gen Physiol 95: 591-616.
- Erickson, K. I., Voss, M. W., Prakash, R. S., Basak, C., Szabo, A., Chaddock, L., Kim, J. S., Heo, S., Alves, H., White, S. M., Wojcicki, T. R., Mailey, E., Vieira, V. J., Martin, S. A., Pence, B. D., Woods, J. A., McAuley, E. and Kramer, A. F., 2011. Exercise training increases size of hippocampus and improves memory. Proc Natl Acad Sci U S A 108: 3017-3022.
- Etnier, J. L., Nowell, P. M., Landers, D. M. and Sibley, B. A., 2006. A meta-regression to examine the relationship between aerobic fitness and cognitive performance. Brain Res Rev 52: 119-130.
- Fan, A. P., Benner, T., Bolar, D. S., Rosen, B. R. and Adalsteinsson, E., 2011. Phase-based regional oxygen metabolism (PROM) using MRI. Magn Reson Med.
- Feihl, F. and Perret, C., 1994. Permissive hypercapnia. How permissive should we be? Am J Respir Crit Care Med 150: 1722-1737.
- Fiat, D., Hankiewicz, J., Liu, S., Trbovic, S. and Brint, S., 2004. 17O magnetic resonance imaging of the human brain. Neurol Res 26: 803-808.
- Fiat, D. and Kang, S., 1992. Determination of the rate of cerebral oxygen consumption and regional cerebral blood flow by non-invasive 17O in vivo NMR spectroscopy and magnetic resonance imaging: Part 1. Theory and data analysis methods. Neurol Res 14: 303-311.
- Fiat, D. and Kang, S., 1993. Determination of the rate of cerebral oxygen consumption and regional cerebral blood flow by non-invasive 17O in vivo NMR spectroscopy and magnetic resonance imaging. Part 2. Determination of CMRO<sub>2</sub> for the rat by 17O NMR, and CMRO<sub>2</sub>, rCBF and the partition coefficient for the cat by 17O MRI. Neurol Res 15: 7-22.

- Folstein, M. F., Folstein, S. E. and McHugh, P. R., 1975. "Mini-mental state". A practical method for grading the cognitive state of patients for the clinician. J Psychiatr Res 12: 189-198.
- Forbes, M. L., Hendrich, K. S., Kochanek, P. M., Williams, D. S., Schiding, J. K., Wisniewski, S. R., Kelsey, S. F., DeKosky, S. T., Graham, S. H., Marion, D. W. and Ho, C., 1997. Assessment of cerebral blood flow and CO<sub>2</sub> reactivity after controlled cortical impact by perfusion magnetic resonance imaging using arterial spin-labeling in rats. J Cereb Blood Flow Metab 17: 865-874.
- Fox, M. D., Snyder, A. Z., Vincent, J. L., Corbetta, M., Van Essen, D. C. and Raichle, M. E., 2005. The human brain is intrinsically organized into dynamic, anticorrelated functional networks. Proc Natl Acad Sci U S A 102: 9673-9678.
- Fox, P. T. and Raichle, M. E., 1986. Focal physiological uncoupling of cerebral blood flow and oxidative metabolism during somatosensory stimulation in human subjects. Proc Natl Acad Sci U S A 83: 1140-1144.
- Frackowiak, R. S., Lenzi, G. L., Jones, T. and Heather, J. D., 1980. Quantitative measurement of regional cerebral blood flow and oxygen metabolism in man using <sup>15</sup>O and positron emission tomography: theory, procedure, and normal values. J Comput Assist Tomogr 4: 727-736.
- Frackowiak, R. S., Pozzilli, C., Legg, N. J., Du Boulay, G. H., Marshall, J., Lenzi, G. L. and Jones, T., 1981. Regional cerebral oxygen supply and utilization in dementia. A clinical and physiological study with oxygen-15 and positron tomography. Brain 104: 753-778.
- Fritze, O., Romero, B., Schleicher, M., Jacob, M. P., Oh, D. Y., Starcher, B., Schenke-Layland, K., Bujan, J. and Stock, U. A., 2012. Age-related changes in the elastic tissue of the human aorta. J Vasc Res 49: 77-86.
- Gagnon, L., Gauthier, C., Hoge, R. D., Lesage, F., Selb, J. and Boas, D. A., 2008. Double-layer estimation of intra- and extracerebral hemoglobin concentration with a time-resolved system. J Biomed Opt 13: 054019.
- Garcia, D. M., Duhamel, G. and Alsop, D. C., 2005. Efficiency of inversion pulses for background suppressed arterial spin labeling. Magn Reson Med 54: 366-372.

- Gauthier, C. J., Desjardins-Crépeau, L., Madjar, C., Bherer, L. and Hoge, R. D., 2012a. Absolute quantification of resting oxygen metabolism and metabolic reactivity during functional activation using QUO2 MRI. Neuroimage In press.
- Gauthier, C. J. and Hoge, R. D., 2011a. A generalized procedure for calibrated MRI incorporating hyperoxia and hypercapnia. Hum Brain Mapp In press.
- Gauthier, C. J. and Hoge, R. D., 2012b. A generalized procedure for calibrated MRI incorporating hyperoxia and hypercapnia. Hum Brain Mapp In press.
- Gauthier, C. J. and Hoge, R. D., 2012c. Magnetic resonance imaging of resting OEF and CMRO2 using a generalized calibration model for hypercapnia and hyperoxia. Neuroimage In press.
- Gauthier, C. J., Madjar, C., Tancredi, F. B., Stefanovic, B. and Hoge, R. D., 2011b. Elimination of visually evoked BOLD responses during carbogen inhalation: Implications for calibrated MRI. Neuroimage 54: 1001-1011.
- Girouard, H. and Iadecola, C., 2006. Neurovascular coupling in the normal brain and in hypertension, stroke, and Alzheimer disease. J Appl Physiol 100: 328-335.
- Glover, G. H., 1999. Deconvolution of impulse response in event-related BOLD fMRI. Neuroimage 9: 416-429.
- Glover, G. H., 2011. Overview of functional magnetic resonance imaging. Neurosurg Clin N Am 22: 133-139, vii.
- Glover, G. H., Li, T. Q. and Ress, D., 2000. Image-based method for retrospective correction of physiological motion effects in fMRI: RETROICOR. Magn Reson Med 44: 162-167.
- Golay, X., Silvennoinen, M. J., Zhou, J., Clingman, C. S., Kauppinen, R. A., Pekar, J. J. and van Zij, P. C., 2001. Measurement of tissue oxygen extraction ratios from venous blood T(2): increased precision and validation of principle. Magn Reson Med 46: 282-291.
- Gold, B. T., Powell, D. K., Xuan, L., Jicha, G. A. and Smith, C. D., 2010. Age-related slowing of task switching is associated with decreased integrity of frontoparietal white matter. Neurobiol Aging 31: 512-522.

- Goode, S. D., Altaf, N., Auer, D. P. and MacSweeney, S. T., 2009a. Carotid endarterectomy improves cerebrovascular reserve capacity preferentially in patients with preoperative impairment as indicated by asymmetric BOLD response to hypercapnia. Eur J Vasc Endovasc Surg 38: 546-551.
- Goode, S. D., Krishan, S., Alexakis, C., Mahajan, R. and Auer, D. P., 2009b. Precision of cerebrovascular reactivity assessment with use of different quantification methods for hypercapnia functional MR imaging. AJNR Am J Neuroradiol 30: 972-977.
- Goodwin, J. A., Vidyasagar, R., Balanos, G. M., Bulte, D. and Parkes, L. M., 2009. Quantitative fMRI using hyperoxia calibration: reproducibility during a cognitive Stroop task. Neuroimage 47: 573-580.
- Gorelick, P. B., Scuteri, A., Black, S. E., Decarli, C., Greenberg, S. M., Iadecola, C., Launer, L. J., Laurent, S., Lopez, O. L., Nyenhuis, D., Petersen, R. C., Schneider, J. A., Tzourio, C., Arnett, D. K., Bennett, D. A., Chui, H. C., Higashida, R. T., Lindquist, R., Nilsson, P. M., Roman, G. C., Sellke, F. W. and Seshadri, S., 2011. Vascular contributions to cognitive impairment and dementia: a statement for healthcare professionals from the american heart association/american stroke association. Stroke 42: 2672-2713.
- Grady, C. L., Maisog, J. M., Horwitz, B., Ungerleider, L. G., Mentis, M. J., Salerno, J. A., Pietrini, P., Wagner, E. and Haxby, J. V., 1994. Age-related changes in cortical blood flow activation during visual processing of faces and location. J Neurosci 14: 1450-1462.
- Graham, G. D., Zhong, J., Petroff, O. A., Constable, R. T., Prichard, J. W. and Gore, J. C., 1994. BOLD MRI monitoring of changes in cerebral perfusion induced by acetazolamide and hypercarbia in the rat. Magn Reson Med 31: 557-560.
- Griffeth, V. E. and Buxton, R. B., 2011. A theoretical framework for estimating cerebral oxygen metabolism changes using the calibrated-BOLD method: modeling the effects of blood volume distribution, hematocrit, oxygen extraction fraction, and tissue signal properties on the BOLD signal. Neuroimage 58: 198-212.

- Griswold, M. A., Jakob, P. M., Heidemann, R. M., Nittka, M., Jellus, V., Wang, J., Kiefer, B. and Haase, A., 2002. Generalized autocalibrating partially parallel acquisitions (GRAPPA). Magn Reson Med 47: 1202-1210.
- Grubb, R. L., Jr., Raichle, M. E., Eichling, J. O. and Ter-Pogossian, M. M., 1974. The effects of changes in PaCO<sub>2</sub> on cerebral blood volume, blood flow, and vascular mean transit time. Stroke 5: 630-639.
- Gsell, W., Burke, M., Wiedermann, D., Bonvento, G., Silva, A. C., Dauphin, F., Buhle, C., Hoehn, M. and Schwindt, W., 2006. Differential effects of NMDA and AMPA glutamate receptors on functional magnetic resonance imaging signals and evoked neuronal activity during forepaw stimulation of the rat. J Neurosci 26: 8409-8416.
- Hagner, W., Hagner-Derengowska, M., Wiacek, M. and Zubrzycki, I. Z., 2009. Changes in level of VO<sub>2</sub>max, blood lipids, and waist circumference in the response to moderate endurance training as a function of ovarian aging. Menopause 16: 1009-1013.
- Hajnal, J. V., Saeed, N., Oatridge, A., Williams, E. J., Young, I. R. and Bydder, G. M., 1995. Detection of subtle brain changes using subvoxel registration and subtraction of serial MR images. J Comput Assist Tomogr 19: 677-691.
- Hattori, N., Bergsneider, M., Wu, H. M., Glenn, T. C., Vespa, P. M., Hovda, D. A., Phelps, M. E. and Huang, S. C., 2004. Accuracy of a method using short inhalation of (15)O-O<sub>2</sub> for measuring cerebral oxygen extraction fraction with PET in healthy humans. J Nucl Med 45: 765-770.
- He, X. and Yablonskiy, D. A., 2007. Quantitative BOLD: mapping of human cerebral deoxygenated blood volume and oxygen extraction fraction: default state. Magn Reson Med 57: 115-126.
- He, X., Zhu, M. and Yablonskiy, D. A., 2008. Validation of oxygen extraction fraction measurement by qBOLD technique. Magn Reson Med 60: 882-888.
- Herholz, K., Carter, S. F. and Jones, M., 2007. Positron emission tomography imaging in dementia. Br J Radiol 80 Spec No 2: S160-167.
- Herment, A., Kachenoura, N., Lefort, M., Bensalah, M., Dogui, A., Frouin, F., Mousseaux, E. and De Cesare, A., 2010. Automated segmentation of the aorta from phase contrast MR images: validation against expert tracing in

- healthy volunteers and in patients with a dilated aorta. J Magn Reson Imaging 31: 881-888.
- Hino, J. K., Short, B. L., Rais-Bahrami, K. and Seale, W. R., 2000. Cerebral blood flow and metabolism during and after prolonged hypercapnia in newborn lambs. Crit Care Med 28: 3505-3510.
- Hirano, S., Eckert, T., Flanagan, T. and Eidelberg, D., 2009. Metabolic networks for assessment of therapy and diagnosis in Parkinson's disease. Mov Disord 24 Suppl 2: S725-731.
- Hoge, R. D., Atkinson, J., Gill, B., Crelier, G. R., Marrett, S. and Pike, G. B., 1999a. Investigation of BOLD signal dependence on cerebral blood flow and oxygen consumption: the deoxyhemoglobin dilution model. Magn Reson Med 42: 849-863.
- Hoge, R. D., Atkinson, J., Gill, B., Crelier, G. R., Marrett, S. and Pike, G. B., 1999b. Linear coupling between cerebral blood flow and oxygen consumption in activated human cortex. Proc Natl Acad Sci U S A 96: 9403-9408.
- Hoge, R. D. and Pike, G. B., 2001. Oxidative metabolism and the detection of neuronal activation via imaging. J Chem Neuroanat 22: 43-52.
- Hopkins, M. E. and Bucci, D. J., 2010. BDNF expression in perirhinal cortex is associated with exercise-induced improvement in object recognition memory. Neurobiol Learn Mem 94: 278-284.
- Hopkins, M. E., Davis, F. C., Vantieghem, M. R., Whalen, P. J. and Bucci, D. J., 2012. Differential effects of acute and regular physical exercise on cognition and affect. Neuroscience.
- Horvath, I., Sandor, N. T., Ruttner, Z. and McLaughlin, A. C., 1994. Role of nitric oxide in regulating cerebrocortical oxygen consumption and blood flow during hypercapnia. J Cereb Blood Flow Metab 14: 503-509.
- Iadecola, C., 2010. The overlap between neurodegenerative and vascular factors in the pathogenesis of dementia. Acta Neuropathol 120: 287-296.
- Ibaraki, M., Miura, S., Shimosegawa, E., Sugawara, S., Mizuta, T., Ishikawa, A. and Amano, M., 2008. Quantification of cerebral blood flow and oxygen metabolism with 3-dimensional PET and  $^{15}\text{O}$ : validation by comparison with 2-dimensional PET. J Nucl Med 49: 50-59.

- Ibaraki, M., Shinohara, Y., Nakamura, K., Miura, S., Kinoshita, F. and Kinoshita, T., 2010. Interindividual variations of cerebral blood flow, oxygen delivery, and metabolism in relation to hemoglobin concentration measured by positron emission tomography in humans. J Cereb Blood Flow Metab 30: 1296-1305.
- Ishii, K., Sasaki, M., Kitagaki, H., Sakamoto, S., Yamaji, S. and Maeda, K., 1996. Regional difference in cerebral blood flow and oxidative metabolism in human cortex. J Nucl Med 37: 1086-1088.
- Isozaki, M., Arai, Y., Kudo, T., Kiyono, Y., Kobayashi, M., Kubota, T., Kikuta, K. and Okazawa, H., 2010. Clinical implication and prognosis of normal baseline cerebral blood flow with impaired vascular reserve in patients with major cerebral artery occlusive disease. Ann Nucl Med 24: 371-377.
- Ito, H., Ibaraki, M., Kanno, I., Fukuda, H. and Miura, S., 2005. Changes in cerebral blood flow and cerebral oxygen metabolism during neural activation measured by positron emission tomography: comparison with blood oxygenation level-dependent contrast measured by functional magnetic resonance imaging. J Cereb Blood Flow Metab 25: 371-377.
- Ito, H., Kanno, I., Ibaraki, M., Suhara, T. and Miura, S., 2008. Relationship between baseline cerebral blood flow and vascular responses to changes in PaCO<sub>2</sub> measured by positron emission tomography in humans: implication of inter-individual variations of cerebral vascular tone. Acta Physiol (Oxf) 193: 325-330.
- Ito, H., Kanno, I., Kato, C., Sasaki, T., Ishii, K., Ouchi, Y., Iida, A., Okazawa, H., Hayashida, K., Tsuyuguchi, N., Kuwabara, Y. and Senda, M., 2004. Database of normal human cerebral blood flow, cerebral blood volume, cerebral oxygen extraction fraction and cerebral metabolic rate of oxygen measured by positron emission tomography with <sup>15</sup>O-labelled carbon dioxide or water, carbon monoxide and oxygen: a multicentre study in Japan. Eur J Nucl Med Mol Imaging 31: 635-643.
- Jain, V., Langham, M. C. and Wehrli, F. W., 2010. MRI estimation of global brain oxygen consumption rate. J Cereb Blood Flow Metab 30: 1598-1607.
- Janssens, J. P., Pache, J. C. and Nicod, L. P., 1999. Physiological changes in respiratory function associated with ageing. Eur Respir J 13: 197-205.

- Jenkinson, M., Bannister, P., Brady, M. and Smith, S., 2002. Improved optimization for the robust and accurate linear registration and motion correction of brain images. Neuroimage 17: 825-841.
- Jenkinson, M. and Smith, S., 2001. A global optimisation method for robust affine registration of brain images. Med Image Anal 5: 143-156.
- Jimura, K. and Braver, T. S., 2010. Age-related shifts in brain activity dynamics during task switching. Cereb Cortex 20: 1420-1431.
- Jones, M., Berwick, J., Hewson-Stoate, N., Gias, C. and Mayhew, J., 2005. The effect of hypercapnia on the neural and hemodynamic responses to somatosensory stimulation. Neuroimage 27: 609-623.
- Kadoglou, N. P., Iliadis, F., Angelopoulou, N., Sailer, N., Fotiadis, G., Voliotis, K., Vitta, I., Liapis, C. D. and Alevizos, M., 2009. Cardiorespiratory capacity is associated with favourable cardiovascular risk profile in patients with Type 2 diabetes. J Diabetes Complications 23: 160-166.
- Kemna, L. J. and Posse, S., 2001a. Effect of respiratory CO(2) changes on the temporal dynamics of the hemodynamic response in functional MR imaging. Neuroimage 14: 642-649.
- Kemna, L. J., Posse, S., Tellmann, L., Schmitz, T. and Herzog, H., 2001b. Interdependence of regional and global cerebral blood flow during visual stimulation: an O-15-butanol positron emission tomography study. J Cereb Blood Flow Metab 21: 664-670.
- Kety, S. S. and Schmidt, C. F., 1948. The nitrous oxide method for the quantitative determination of cerebral blood flow in man; theory, procedure and normal values. J Clin Invest 27: 476-483.
- Kilner, J. M., Mattout, J., Henson, R. and Friston, K. J., 2005. Hemodynamic correlates of EEG: a heuristic. Neuroimage 28: 280-286.
- Kim, S. G. and Ogawa, S., 2012. Biophysical and physiological origins of blood oxygenation level-dependent fMRI signals. J Cereb Blood Flow Metab.
- Kim, S. G., Rostrup, E., Larsson, H. B., Ogawa, S. and Paulson, O. B., 1999. Determination of relative CMRO<sub>2</sub> from CBF and BOLD changes: significant increase of oxygen consumption rate during visual stimulation. Magn Reson Med 41: 1152-1161.

- Kimberg, D. Y., Aguirre, G. K. and D'Esposito, M., 2000. Modulation of task-related neural activity in task-switching: an fMRI study. Brain Res Cogn Brain Res 10: 189-196.
- Kocharyan, A., Fernandes, P., Tong, X. K., Vaucher, E. and Hamel, E., 2008. Specific subtypes of cortical GABA interneurons contribute to the neurovascular coupling response to basal forebrain stimulation. J Cereb Blood Flow Metab 28: 221-231.
- Kontush, A., Berndt, C., Weber, W., Akopyan, V., Arlt, S., Schippling, S. and Beisiegel, U., 2001. Amyloid-beta is an antioxidant for lipoproteins in cerebrospinal fluid and plasma. Free Radic Biol Med 30: 119-128.
- Kramer, A. F., Erickson, K. I. and Colcombe, S. J., 2006. Exercise, cognition, and the aging brain. J Appl Physiol 101: 1237-1242.
- Kruger, G. and Glover, G. H., 2001. Physiological noise in oxygenation-sensitive magnetic resonance imaging. Magn Reson Med 46: 631-637.
- Kubota, Y., Hattori, R. and Yui, Y., 1994. Three distinct subpopulations of GABAergic neurons in rat frontal agranular cortex. Brain Res 649: 159-173.
- Kuschinsky, W., Wahl, M., Bosse, O. and Thureau, K., 1972. Perivascular potassium and pH as determinants of local pial arterial diameter in cats. A microapplication study. Circ Res 31: 240-247.
- Kwong, K. K., Belliveau, J. W., Chesler, D. A., Goldberg, I. E., Weisskoff, R. M., Poncelet, B. P., Kennedy, D. N., Hoppel, B. E., Cohen, M. S., Turner, R. and et al., 1992. Dynamic magnetic resonance imaging of human brain activity during primary sensory stimulation. Proc Natl Acad Sci U S A 89: 5675-5679.
- Landuyt, W., Hermans, R., Bosmans, H., Sunaert, S., Beatse, E., Farina, D., Meijerink, M., Zhang, H., Van Den Bogaert, W., Lambin, P. and Marchal, G., 2001. BOLD contrast fMRI of whole rodent tumour during air or carbogen breathing using echo-planar imaging at 1.5 T. Eur Radiol 11: 2332-2340.
- Langenecker, S. A., Nielson, K. A. and Rao, S. M., 2004. fMRI of healthy older adults during Stroop interference. Neuroimage 21: 192-200.
- Lansing, R. W., Gracely, R. H. and Banzett, R. B., 2009. The multiple dimensions of dyspnea: review and hypotheses. Respir Physiol Neurobiol 167: 53-60.

- Larson, E. B., Wang, L., Bowen, J. D., McCormick, W. C., Teri, L., Crane, P. and Kukull, W., 2006. Exercise is associated with reduced risk for incident dementia among persons 65 years of age and older. Ann Intern Med 144: 73-81.
- Laurent, S. and Boutouyrie, P., 2007. Recent advances in arterial stiffness and wave reflection in human hypertension. Hypertension 49: 1202-1206.
- Laurent, S., Cockcroft, J., Van Bortel, L., Boutouyrie, P., Giannattasio, C., Hayoz, D., Pannier, B., Vlachopoulos, C., Wilkinson, I. and Struijker-Boudier, H., 2006. Expert consensus document on arterial stiffness: methodological issues and clinical applications. Eur Heart J 27: 2588-2605.
- Laurent, S., Katsahian, S., Fassot, C., Tropeano, A. I., Gautier, I., Laloux, B. and Boutouyrie, P., 2003. Aortic stiffness is an independent predictor of fatal stroke in essential hypertension. Stroke 34: 1203-1206.
- Lauritzen, M. and Gold, L., 2003. Brain function and neurophysiological correlates of signals used in functional neuroimaging. J Neurosci 23: 3972-3980.
- Lazarus, N. R. and Harridge, S. D., 2010. Exercise, physiological function, and the selection of participants for aging research. J Gerontol A Biol Sci Med Sci 65: 854-857.
- Lecrux, C. and Hamel, E., 2011. The neurovascular unit in brain function and disease. Acta Physiol (Oxf) 203: 47-59.
- Leenders, K. L., Perani, D., Lammertsma, A. A., Heather, J. D., Buckingham, P., Healy, M. J., Gibbs, J. M., Wise, R. J., Hatazawa, J., Herold, S. and et al., 1990. Cerebral blood flow, blood volume and oxygen utilization. Normal values and effect of age. Brain 113 ( Pt 1): 27-47.
- Leontiev, O. and Buxton, R. B., 2007a. Reproducibility of BOLD, perfusion, and CMRO<sub>2</sub> measurements with calibrated-BOLD fMRI. Neuroimage 35: 175-184.
- Leontiev, O., Dubowitz, D. J. and Buxton, R. B., 2007b. CBF/CMRO<sub>2</sub> coupling measured with calibrated BOLD fMRI: sources of bias. Neuroimage 36: 1110-1122.

- Leung, H. C., Skudlarski, P., Gatenby, J. C., Peterson, B. S. and Gore, J. C., 2000. An event-related functional MRI study of the stroop color word interference task. Cereb Cortex 10: 552-560.
- Levy, D. E., Brierley, J. B., Silverman, D. G. and Plum, F., 1975. Brief hypoxia-ischemia initially damages cerebral neurons. Arch Neurol 32: 450-456.
- Li, S. C. and Sikstrom, S., 2002. Integrative neurocomputational perspectives on cognitive aging, neuromodulation, and representation. Neurosci Biobehav Rev 26: 795-808.
- Lin, A. L., Fox, P. T., Yang, Y., Lu, H., Tan, L. H. and Gao, J. H., 2008. Evaluation of MRI models in the measurement of CMRO<sub>2</sub> and its relationship with CBF. Magn Reson Med 60: 380-389.
- Lindauer, U., Megow, D., Matsuda, H. and Dirnagl, U., 1999. Nitric oxide: a modulator, but not a mediator, of neurovascular coupling in rat somatosensory cortex. Am J Physiol 277: H799-811.
- Liu, P., Xu, F. and Lu, H., 2012. Test-retest reproducibility of a rapid method to measure brain oxygen metabolism. Magn Reson Med.
- Liu, T. T. and Wong, E. C., 2005. A signal processing model for arterial spin labeling functional MRI. Neuroimage 24: 207-215.
- Lo, R. Y., Hubbard, A. E., Shaw, L. M., Trojanowski, J. Q., Petersen, R. C., Aisen, P. S., Weiner, M. W. and Jagust, W. J., 2011. Longitudinal Change of Biomarkers in Cognitive Decline. Arch Neurol.
- Logothetis, N. K., Pauls, J., Augath, M., Trinath, T. and Oeltermann, A., 2001. Neurophysiological investigation of the basis of the fMRI signal. Nature 412: 150-157.
- Logothetis, N. K. and Wandell, B. A., 2004. Interpreting the BOLD signal. Annu Rev Physiol 66: 735-769.
- Lu, H. and Ge, Y., 2008. Quantitative evaluation of oxygenation in venous vessels using T2-Relaxation-Under-Spin-Tagging MRI. Magn Reson Med 60: 357-363.
- Lu, H., Golay, X., Pekar, J. J. and Van Zijl, P. C., 2003. Functional magnetic resonance imaging based on changes in vascular space occupancy. Magn Reson Med 50: 263-274.

- Lu, H. and van Zijl, P. C., 2012a. A review of the development of Vascular-Space-Occupancy (VASO) fMRI. Neuroimage.
- Lu, H., Xu, F., Grgac, K., Liu, P., Qin, Q. and van Zijl, P., 2012b. Calibration and validation of TRUST MRI for the estimation of cerebral blood oxygenation. Magn Reson Med 67: 42-49.
- Lu, H., Xu, F., Rodrigue, K. M., Kennedy, K. M., Cheng, Y., Flicker, B., Hebrank, A. C., Uh, J. and Park, D. C., 2011. Alterations in cerebral metabolic rate and blood supply across the adult lifespan. Cereb Cortex 21: 1426-1434.
- MacDonald, A. W., 3rd, Cohen, J. D., Stenger, V. A. and Carter, C. S., 2000. Dissociating the role of the dorsolateral prefrontal and anterior cingulate cortex in cognitive control. Science 288: 1835-1838.
- Magri, C., Schridde, U., Murayama, Y., Panzeri, S. and Logothetis, N. K., 2012. The amplitude and timing of the BOLD signal reflects the relationship between local field potential power at different frequencies. J Neurosci 32: 1395-1407.
- Maleki, N., Dai, W. and Alsop, D. C., 2011. Optimization of background suppression for arterial spin labeling perfusion imaging. MAGMA.
- Mandell, D. M., Han, J. S., Poublanc, J., Crawley, A. P., Stainsby, J. A., Fisher, J. A. and Mikulis, D. J., 2008. Mapping cerebrovascular reactivity using blood oxygen level-dependent MRI in Patients with arterial steno-occlusive disease: comparison with arterial spin labeling MRI. Stroke 39: 2021-2028.
- Marchal, G., Rioux, P., Petit-Taboue, M. C., Sette, G., Travere, J. M., Le Poec, C., Courtheoux, P., Derlon, J. M. and Baron, J. C., 1992. Regional cerebral oxygen consumption, blood flow, and blood volume in healthy human aging. Arch Neurol 49: 1013-1020.
- Mark, C. I., Fisher, J. A. and Pike, G. B., 2011. Improved fMRI calibration: Precisely controlled hyperoxic versus hypercapnic stimuli. Neuroimage 54: 1102-1111.
- Mark, C. I., Slessarev, M., Ito, S., Han, J., Fisher, J. A. and Pike, G. B., 2010. Precise control of end-tidal carbon dioxide and oxygen improves BOLD and ASL cerebrovascular reactivity measures. Magn Reson Med.
- Mattay, V. S., Fera, F., Tessitore, A., Hariri, A. R., Berman, K. F., Das, S., Meyer-Lindenberg, A., Goldberg, T. E., Callicott, J. H. and Weinberger, D. R., 2006.

- Neurophysiological correlates of age-related changes in working memory capacity. Neurosci Lett 392: 32-37.
- McPherson, R. W., Derrer, S. A. and Traystman, R. J., 1991. Changes in cerebral CO<sub>2</sub> responsivity over time during isoflurane anesthesia in the dog. J Neurosurg Anesthesiol 3: 12-19.
- Milham, M. P., Erickson, K. I., Banich, M. T., Kramer, A. F., Webb, A., Wszalek, T. and Cohen, N. J., 2002. Attentional control in the aging brain: insights from an fMRI study of the stroop task. Brain Cogn 49: 277-296.
- Miller, P. W., Long, N. J., Vilar, R. and Gee, A. D., 2008. Synthesis of <sup>11</sup>C, <sup>18</sup>F, <sup>15</sup>O, and <sup>13</sup>N radiolabels for positron emission tomography. Angew Chem Int Ed Engl 47: 8998-9033.
- Mintun, M. A., Raichle, M. E., Martin, W. R. and Herscovitch, P., 1984. Brain oxygen utilization measured with O-15 radiotracers and positron emission tomography. J Nucl Med 25: 177-187.
- Mintun, M. A., Vlassenko, A. G., Shulman, G. L. and Snyder, A. Z., 2002. Time-related increase of oxygen utilization in continuously activated human visual cortex. Neuroimage 16: 531-537.
- Mitchell, G. F., van Buchem, M. A., Sigurdsson, S., Gotlib, J. D., Jonsdottir, M. K., Kjartansson, O., Garcia, M., Aspelund, T., Harris, T. B., Gudnason, V. and Launer, L. J., 2011. Arterial stiffness, pressure and flow pulsatility and brain structure and function: the Age, Gene/Environment Susceptibility--Reykjavik study. Brain 134: 3398-3407.
- Mohtasib, R. S., Lumley, G., Goodwin, J. A., Emsley, H. C., Sluming, V. and Parkes, L. M., 2012. Calibrated fMRI during a cognitive Stroop task reveals reduced metabolic response with increasing age. Neuroimage 59: 1143-1151.
- Momjian-Mayor, I., Burkhard, P., Murith, N., Mugnai, D., Yilmaz, H., Narata, A. P., Lovblad, K., Pereira, V., Righini, M., Bounameaux, H. and Sztajzel, R. F., 2012. Diagnosis of and treatment for symptomatic carotid stenosis: an updated review. Acta Neurol Scand.
- Nagata, K., Maruya, H., Yuya, H., Terashi, H., Mito, Y., Kato, H., Sato, M., Satoh, Y., Watahiki, Y., Hirata, Y., Yokoyama, E. and Hatazawa, J., 2000. Can PET

- data differentiate Alzheimer's disease from vascular dementia? Ann N Y Acad Sci 903: 252-261.
- Nagata, K., Sato, M., Satoh, Y., Watahiki, Y., Kondoh, Y., Sugawara, M., Box, G., Wright, D., Leung, S., Yuya, H. and Shimosegawa, E., 2002. Hemodynamic aspects of Alzheimer's disease. Ann N Y Acad Sci 977: 391-402.
- Ngai, A. C., Coyne, E. F., Meno, J. R., West, G. A. and Winn, H. R., 2001. Receptor subtypes mediating adenosine-induced dilation of cerebral arterioles. Am J Physiol Heart Circ Physiol 280: H2329-2335.
- Niwa, K., Araki, E., Morham, S. G., Ross, M. E. and Iadecola, C., 2000. Cyclooxygenase-2 contributes to functional hyperemia in whisker-barrel cortex. J Neurosci 20: 763-770.
- Nobre, A. C., Coull, J. T., Frith, C. D. and Mesulam, M. M., 1999. Orbitofrontal cortex is activated during breaches of expectation in tasks of visual attention. Nat Neurosci 2: 11-12.
- Nolde, S. F., Johnson, M. K. and Raye, C. L., 1998. The role of prefrontal cortex during tests of episodic memory. Trends Cogn Sci 2: 399-406.
- O'Rourke, M. F. and Hashimoto, J., 2007. Mechanical factors in arterial aging: a clinical perspective. J Am Coll Cardiol 50: 1-13.
- Ogawa, S., Lee, T. M., Kay, A. R. and Tank, D. W., 1990a. Brain magnetic resonance imaging with contrast dependent on blood oxygenation. Proc Natl Acad Sci U S A 87: 9868-9872.
- Ogawa, S., Lee, T. M., Nayak, A. S. and Glynn, P., 1990b. Oxygenation-sensitive contrast in magnetic resonance image of rodent brain at high magnetic fields. Magn Reson Med 14: 68-78.
- Ogawa, S., Tank, D. W., Menon, R., Ellermann, J. M., Kim, S. G., Merkle, H. and Ugurbil, K., 1992. Intrinsic signal changes accompanying sensory stimulation: functional brain mapping with magnetic resonance imaging. Proc Natl Acad Sci U S A 89: 5951-5955.
- Park, D. C. and Reuter-Lorenz, P., 2009. The adaptive brain: aging and neurocognitive scaffolding. Annu Rev Psychol 60: 173-196.

- Parkes, L. M., Rashid, W., Chard, D. T. and Tofts, P. S., 2004. Normal cerebral perfusion measurements using arterial spin labeling: reproducibility, stability, and age and gender effects. Magn Reson Med 51: 736-743.
- Pase, M. P., Pipingas, A., Kras, M., Nolidin, K., Gibbs, A. L., Wesnes, K. A., Scholey, A. B. and Stough, C., 2010. Healthy middle-aged individuals are vulnerable to cognitive deficits as a result of increased arterial stiffness. J Hypertens 28: 1724-1729.
- Perlmutter, J. S., Herscovitch, P., Powers, W. J., Fox, P. T. and Raichle, M. E., 1985. Standardized mean regional method for calculating global positron emission tomographic measurements. J Cereb Blood Flow Metab 5: 476-480.
- Perthen, J. E., Lansing, A. E., Liao, J., Liu, T. T. and Buxton, R. B., 2008. Caffeine-induced uncoupling of cerebral blood flow and oxygen metabolism: a calibrated BOLD fMRI study. Neuroimage 40: 237-247.
- Petrides, M., 2005. Lateral prefrontal cortex: architectonic and functional organization. Philos Trans R Soc Lond B Biol Sci 360: 781-795.
- Pialoux, V., Brown, A. D., Leigh, R., Friedenreich, C. M. and Poulin, M. J., 2009. Effect of cardiorespiratory fitness on vascular regulation and oxidative stress in postmenopausal women. Hypertension 54: 1014-1020.
- Podewils, L. J., Guallar, E., Kuller, L. H., Fried, L. P., Lopez, O. L., Carlson, M. and Lyketsos, C. G., 2005. Physical activity, APOE genotype, and dementia risk: findings from the Cardiovascular Health Cognition Study. Am J Epidemiol 161: 639-651.
- Posse, S., Kemna, L. J., Elghahwagi, B., Wiese, S. and Kiselev, V. G., 2001. Effect of graded hypo- and hypercapnia on fMRI contrast in visual cortex: quantification of  $T^*(2)$  changes by multiecho EPI. Magn Reson Med 46: 264-271.
- Poston, K. L. and Eidelberg, D., 2010. FDG PET in the Evaluation of Parkinson's Disease. PET Clin 5: 55-64.
- Prakash, R. S., Voss, M. W., Erickson, K. I., Lewis, J. M., Chaddock, L., Malkowski, E., Alves, H., Kim, J., Szabo, A., White, S. M., Wojcicki, T. R., Klamm, E. L.,

- McAuley, E. and Kramer, A. F., 2011. Cardiorespiratory fitness and attentional control in the aging brain. Front Hum Neurosci 4: 229.
- Press, W. H., Flannery, B. P., Teukolsky, S. A. and Vetterling, W. T. (1992). Numerical Recipes in C: The Art of Scientific Computing, Cambridge University Press.
- Quaglino, D., Jr., Bergamini, G., Boraldi, F. and Pasquali Ronchetti, I., 1996. Ultrastructural and morphometrical evaluations on normal human dermal connective tissue--the influence of age, sex and body region. Br J Dermatol 134: 1013-1022.
- Rauscher, A., Sedlacik, J., Barth, M., Haacke, E. M. and Reichenbach, J. R., 2005a. Noninvasive assessment of vascular architecture and function during modulated blood oxygenation using susceptibility weighted magnetic resonance imaging. Magn Reson Med 54: 87-95.
- Rauscher, A., Sedlacik, J., Deistung, A., Mentzel, H. J. and Reichenbach, J. R., 2006. Susceptibility weighted imaging: data acquisition, image reconstruction and clinical applications. Z Med Phys 16: 240-250.
- Rauscher, A., Sedlacik, J., Fitzek, C., Walter, B., Hochstetter, A., Kalff, R., Kaiser, W. A. and Reichenbach, J. R., 2005b. High resolution susceptibility weighted MR-imaging of brain tumors during the application of a gaseous agent. Rofu 177: 1065-1069.
- Raz, N., Ghisletta, P., Rodrigue, K. M., Kennedy, K. M. and Lindenberger, U., 2010. Trajectories of brain aging in middle-aged and older adults: regional and individual differences. Neuroimage 51: 501-511.
- Redheuil, A., Yu, W. C., Wu, C. O., Mousseaux, E., de Cesare, A., Yan, R., Kachenoura, N., Bluemke, D. and Lima, J. A., 2010. Reduced ascending aortic strain and distensibility: earliest manifestations of vascular aging in humans. Hypertension 55: 319-326.
- Reichenbach, J. R. and Haacke, E. M., 2001. High-resolution BOLD venographic imaging: a window into brain function. NMR Biomed 14: 453-467.
- Reitan, R. M., 1958. Validity of the Trail Making Test as an indicator of organic brain damage. Perceptual and Motor Skills 8: 271-276.

- Restom, K., Behzadi, Y. and Liu, T. T., 2006. Physiological noise reduction for arterial spin labeling functional MRI. Neuroimage 31: 1104-1115.
- Restom, K., Perthen, J. E. and Liu, T. T., 2008. Calibrated fMRI in the medial temporal lobe during a memory-encoding task. Neuroimage 40: 1495-1502.
- Reuter-Lorenz, P. A. and Cappell, K. A., 2008. Neurocognitive aging and the compensation hypothesis. Curr Dir in Psych Sc 17: 177-182.
- Reuter-Lorenz, P. A., Jonides, J., Smith, E. E., Hartley, A., Miller, A., Marshuetz, C. and Koeppel, R. A., 2000. Age differences in the frontal lateralization of verbal and spatial working memory revealed by PET. J Cogn Neurosci 12: 174-187.
- Reuter-Lorenz, P. A. and Park, D. C., 2010. Human neuroscience and the aging mind: a new look at old problems. J Gerontol B Psychol Sci Soc Sci 65: 405-415.
- Reuter-Lorez, P. A. and Cappell, K. A., 2008. Neurocognitive aging and the compensation hypothesis. Curr Dir in Psych Sc 17: 177-182.
- Rhoades, R. and Bell, D. R. (2009). Medical physiology : principles for clinical medicine. Philadelphia, Pa. ; London, Lippincott Williams & Wilkins.
- Rigby, B. J., 1964. Effect of Cyclic Extension on the Physical Properties of Tendon Collagen and Its Possible Relation to Biological Ageing of Collagen. Nature 202: 1072-1074.
- Robbins, M. A., Elias, M. F., Elias, P. K. and Budge, M. M., 2005. Blood pressure and cognitive function in an African-American and a Caucasian-American sample: the Maine-Syracuse Study. Psychosom Med 67: 707-714.
- Rodriguez, G., Arnaldi, D. and Picco, A., 2011. Brain functional network in Alzheimer's disease: diagnostic markers for diagnosis and monitoring. Int J Alzheimers Dis 2011: 481903.
- Rogers, R. L., Meyer, J. S. and Mortel, K. F., 1990. After reaching retirement age physical activity sustains cerebral perfusion and cognition. J Am Geriatr Soc 38: 123-128.
- Sahathevan, R., Brodtmann, A. and Donnan, G. A., 2012. Dementia, stroke, and vascular risk factors; a review. Int J Stroke 7: 61-73.

- Salat, D. H., Buckner, R. L., Snyder, A. Z., Greve, D. N., Desikan, R. S., Busa, E., Morris, J. C., Dale, A. M. and Fischl, B., 2004. Thinning of the cerebral cortex in aging. Cereb Cortex 14: 721-730.
- Salat, D. H., Williams, V. J., Leritz, E. C., Schnyer, D. M., Rudolph, J. L., Lipsitz, L. A., McGlinchey, R. E. and Milberg, W. P., 2012. Inter-individual variation in blood pressure is associated with regional white matter integrity in generally healthy older adults. Neuroimage 59: 181-192.
- Samanez-Larkin, G. R. and D'Esposito, M., 2008. Group comparisons: imaging the aging brain. Soc Cogn Affect Neurosci 3: 290-297.
- Satterthwaite, T. D., Ruparel, K., Loughhead, J., Elliott, M. A., Gerraty, R. T., Calkins, M. E., Hakonarson, H., Gur, R. C., Gur, R. E. and Wolf, D. H., 2012. Being right is its own reward: load and performance related ventral striatum activation to correct responses during a working memory task in youth. Neuroimage 61: 723-729.
- Schneider-Garces, N. J., Gordon, B. A., Brumback-Peltz, C. R., Shin, E., Lee, Y., Sutton, B. P., Maclin, E. L., Gratton, G. and Fabiani, M., 2010. Span, CRUNCH, and beyond: working memory capacity and the aging brain. J Cogn Neurosci 22: 655-669.
- Schwarzbauer, C. and Deichmann, R., 2011. Vascular component analysis of hyperoxic and hypercapnic BOLD contrast. Neuroimage.
- Sedlacik, J., Kutschbach, C., Rauscher, A., Deistung, A. and Reichenbach, J. R., 2008. Investigation of the influence of carbon dioxide concentrations on cerebral physiology by susceptibility-weighted magnetic resonance imaging (SWI). Neuroimage 43: 36-43.
- Sedlacik, J., Rauscher, A. and Reichenbach, J. R., 2007. Obtaining blood oxygenation levels from MR signal behavior in the presence of single venous vessels. Magn Reson Med 58: 1035-1044.
- Sedlacik, J., Rauscher, A. and Reichenbach, J. R., 2009. Quantification of modulated blood oxygenation levels in single cerebral veins by investigating their MR signal decay. Z Med Phys 19: 48-57.
- Sedlacik, J. and Reichenbach, J. R., 2010. Validation of quantitative estimation of tissue oxygen extraction fraction and deoxygenated blood volume fraction in

- phantom and in vivo experiments by using MRI. Magn Reson Med 63: 910-921.
- Sergi, G., Coin, A., Sarti, S., Perissinotto, E., Peloso, M., Mulone, S., Trolese, M., Inelmen, E. M., Enzi, G. and Manzato, E., 2010. Resting VO<sub>2</sub>, maximal VO<sub>2</sub> and metabolic equivalents in free-living healthy elderly women. Clin Nutr 29: 84-88.
- Severinghaus, J. W., 1979. Simple, accurate equations for human blood O<sub>2</sub> dissociation computations. J Appl Physiol 46: 599-602.
- Severinghaus, J. W., 1989. Water vapor calibration errors in some capnometers: respiratory conventions misunderstood by manufacturers? Anesthesiology 70: 996-998.
- Sharma, G. and Goodwin, J., 2006. Effect of aging on respiratory system physiology and immunology. Clin Interv Aging 1: 253-260.
- Shmuel, A., Yacoub, E., Pfeuffer, J., Van de Moortele, P. F., Adriany, G., Hu, X. and Ugurbil, K., 2002. Sustained negative BOLD, blood flow and oxygen consumption response and its coupling to the positive response in the human brain. Neuron 36: 1195-1210.
- Sierra, C., De La Sierra, A., Salamero, M., Sobrino, J., Gomez-Angelats, E. and Coca, A., 2004. Silent cerebral white matter lesions and cognitive function in middle-aged essential hypertensive patients. Am J Hypertens 17: 529-534.
- Slessarev, M., Han, J., Mardimae, A., Prisman, E., Preiss, D., Volgyesi, G., Ansel, C., Duffin, J. and Fisher, J. A., 2007. Prospective targeting and control of end-tidal CO<sub>2</sub> and O<sub>2</sub> concentrations. J Physiol 581: 1207-1219.
- Smith, S. M., 2002. Fast robust automated brain extraction. Hum Brain Mapp 17: 143-155.
- Sonntag, W. E., Lynch, C. D., Cooney, P. T. and Hutchins, P. M., 1997. Decreases in cerebral microvasculature with age are associated with the decline in growth hormone and insulin-like growth factor 1. Endocrinology 138: 3515-3520.
- Spoelgen, R., Meyer, A., Moraru, A., Kirsch, F., Vogt-Eisele, A., Plaas, C., Pitzer, C. and Schneider, A., 2011. A novel flow cytometry-based technique to measure adult neurogenesis in the brain. J Neurochem 119: 165-175.

- Spreng, R. N., Wojtowicz, M. and Grady, C. L., 2010. Reliable differences in brain activity between young and old adults: a quantitative meta-analysis across multiple cognitive domains. Neurosci Biobehav Rev 34: 1178-1194.
- Stefanovic, B. and Pike, G. B., 2005. Venous refocusing for volume estimation: VERVE functional magnetic resonance imaging. Magn Reson Med 53: 339-347.
- Stefanovic, B., Warnking, J. M., Rylander, K. M. and Pike, G. B., 2006. The effect of global cerebral vasodilation on focal activation hemodynamics. Neuroimage 30: 726-734.
- Stella, N., Tence, M., Glowinski, J. and Premont, J., 1994. Glutamate-evoked release of arachidonic acid from mouse brain astrocytes. J Neurosci 14: 568-575.
- Swain, R. A., Harris, A. B., Wiener, E. C., Dutka, M. V., Morris, H. D., Theien, B. E., Konda, S., Engberg, K., Lauterbur, P. C. and Greenough, W. T., 2003. Prolonged exercise induces angiogenesis and increases cerebral blood volume in primary motor cortex of the rat. Neuroscience 117: 1037-1046.
- Tancredi, F. B., Gauthier, C. J., Madjar, C., Bolar, D. S., Fisher, J. A., Wang, D. J. and Hoge, R. D., 2012. Comparison of pulsed and pseudocontinuous arterial spin-labeling for measuring CO<sub>2</sub>-induced cerebrovascular reactivity. J Magn Reson Imaging.
- Tohka, J., Zijdenbos, A. and Evans, A., 2004. Fast and robust parameter estimation for statistical partial volume models in brain MRI. Neuroimage 23: 84-97.
- Tomura, N., Otani, T., Koga, M. and Ishiyama, K., 2011. Correlation Between Severity of Carotid Stenosis and Vascular Reserve Measured by Acetazolamide Brain Perfusion Single Photon Emission Computed Tomography. J Stroke Cerebrovasc Dis.
- Toro, R., Fox, P. T. and Paus, T., 2008. Functional coactivation map of the human brain. Cereb Cortex 18: 2553-2559.
- Triantafyllou, C., Hoge, R. D., Krueger, G., Wiggins, C. J., Potthast, A., Wiggins, G. C. and Wald, L. L., 2005. Comparison of physiological noise at 1.5 T, 3 T and 7 T and optimization of fMRI acquisition parameters. Neuroimage 26: 243-250.

- Valtschanoff, J. G., Weinberg, R. J., Kharazia, V. N., Schmidt, H. H., Nakane, M. and Rustioni, A., 1993. Neurons in rat cerebral cortex that synthesize nitric oxide: NADPH diaphorase histochemistry, NOS immunocytochemistry, and colocalization with GABA. Neurosci Lett 157: 157-161.
- van der Sanden, B. P., Heerschap, A., Hoofd, L., Simonetti, A. W., Nicolay, K., van der Toorn, A., Colier, W. N. and van der Kogel, A. J., 1999. Effect of carbogen breathing on the physiological profile of human glioma xenografts. Magn Reson Med 42: 490-499.
- van Zijl, P. C., Eleff, S. M., Ulatowski, J. A., Oja, J. M., Ulug, A. M., Traystman, R. J. and Kauppinen, R. A., 1998. Quantitative assessment of blood flow, blood volume and blood oxygenation effects in functional magnetic resonance imaging. Nat Med 4: 159-167.
- Vaynman, S., Ying, Z. and Gomez-Pinilla, F., 2004. Hippocampal BDNF mediates the efficacy of exercise on synaptic plasticity and cognition. Eur J Neurosci 20: 2580-2590.
- Voss, M. W., Prakash, R. S., Erickson, K. I., Basak, C., Chaddock, L., Kim, J. S., Alves, H., Heo, S., Szabo, A. N., White, S. M., Wojcicki, T. R., Mailey, E. L., Gothe, N., Olson, E. A., McAuley, E. and Kramer, A. F., 2010. Plasticity of brain networks in a randomized intervention trial of exercise training in older adults. Front Aging Neurosci 2.
- Wahlund, L. O., Barkhof, F., Fazekas, F., Bronge, L., Augustin, M., Sjogren, M., Wallin, A., Ader, H., Leys, D., Pantoni, L., Pasquier, F., Erkinjuntti, T. and Scheltens, P., 2001. A new rating scale for age-related white matter changes applicable to MRI and CT. Stroke 32: 1318-1322.
- Waldstein, S. R., Rice, S. C., Thayer, J. F., Najjar, S. S., Scuteri, A. and Zonderman, A. B., 2008. Pulse pressure and pulse wave velocity are related to cognitive decline in the Baltimore Longitudinal Study of Aging. Hypertension 51: 99-104.
- Wallace, D. C., 2005. A mitochondrial paradigm of metabolic and degenerative diseases, aging, and cancer: a dawn for evolutionary medicine. Annu Rev Genet 39: 359-407.

- Wallace, D. C., 2011. Bioenergetic Origins of Complexity and Disease. Cold Spring Harb Symp Quant Biol.
- Wang, J., Aguirre, G. K., Kimberg, D. Y., Roc, A. C., Li, L. and Detre, J. A., 2003a. Arterial spin labeling perfusion fMRI with very low task frequency. Magn Reson Med 49: 796-802.
- Wang, J., Alsop, D. C., Song, H. K., Maldjian, J. A., Tang, K., Salvucci, A. E. and Detre, J. A., 2003b. Arterial transit time imaging with flow encoding arterial spin tagging (FEAST). Magn Reson Med 50: 599-607.
- Wang, J. M., Huang, Y. J., Wang, Y., Xu, M. G., Wang, L. C., Wang, S. M. and Tao, J., 2007. Increased circulating CD31+/CD42- microparticles are associated with impaired systemic artery elasticity in healthy subjects. Am J Hypertens 20: 957-964.
- Wang, J. M., Su, C., Wang, Y., Huang, Y. J., Yang, Z., Chen, L., Wu, F., Xu, S. Y. and Tao, J., 2009. Elevated circulating endothelial microparticles and brachial-ankle pulse wave velocity in well-controlled hypertensive patients. J Hum Hypertens 23: 307-315.
- Wasylyshyn, C., Verhaeghen, P. and Sliwinski, M. J., 2011. Aging and task switching: a meta-analysis. Psychol Aging 26: 15-20.
- Wechsler, D. (1997). WAIS-III administration and scoring manual, The Psychological Corporation.
- Williams, D. S., Detre, J. A., Leigh, J. S. and Koretsky, A. P., 1992. Magnetic resonance imaging of perfusion using spin inversion of arterial water. Proc Natl Acad Sci U S A 89: 212-216.
- Wolf, P. A., 2012. Contributions of the Framingham Heart Study to Stroke and Dementia Epidemiologic Research at 60 Years. Arch Neurol.
- Wong, E. C., Buxton, R. B. and Frank, L. R., 1997. Implementation of quantitative perfusion imaging techniques for functional brain mapping using pulsed arterial spin labeling. NMR Biomed 10: 237-249.
- Wong, E. C., Buxton, R. B. and Frank, L. R., 1998. Quantitative imaging of perfusion using a single subtraction (QUIPSS and QUIPSS II). Magn Reson Med 39: 702-708.

- Woolrich, M., 2008. Robust group analysis using outlier inference. Neuroimage 41: 286-301.
- Woolrich, M. W., Behrens, T. E., Beckmann, C. F., Jenkinson, M. and Smith, S. M., 2004. Multilevel linear modelling for fMRI group analysis using Bayesian inference. Neuroimage 21: 1732-1747.
- Woolrich, M. W., Ripley, B. D., Brady, M. and Smith, S. M., 2001. Temporal autocorrelation in univariate linear modeling of FMRI data. Neuroimage 14: 1370-1386.
- Worsley, K. J., Liao, C. H., Aston, J., Petre, V., Duncan, G. H., Morales, F. and Evans, A. C., 2002. A general statistical analysis for fMRI data. Neuroimage 15: 1-15.
- Worthy, D. A. and Maddox, W. T., 2012. Age-based differences in strategy use in choice tasks. Front Neurosci 5: 145.
- Wu, W. C., Fernandez-Seara, M., Detre, J. A., Wehrli, F. W. and Wang, J., 2007. A theoretical and experimental investigation of the tagging efficiency of pseudocontinuous arterial spin labeling. Magn Reson Med 58: 1020-1027.
- Xu, F., Ge, Y. and Lu, H., 2009. Noninvasive quantification of whole-brain cerebral metabolic rate of oxygen (CMRO<sub>2</sub>) by MRI. Magn Reson Med 62: 141-148.
- Xu, F., Liu, P. and Lu, H., 2011a. Effect of graded O<sub>2</sub> challenge on vascular and metabolic parameters. Proc. Intl. Soc. Mag. Reson. Med. 19th annual meeting: 765.
- Xu, F., Uh, J., Brier, M. R., Hart, J., Jr., Yezhuvath, U. S., Gu, H., Yang, Y. and Lu, H., 2011b. The influence of carbon dioxide on brain activity and metabolism in conscious humans. J Cereb Blood Flow Metab 31: 58-67.
- Xu, F., Uh, J., Liu, P. and Lu, H., 2011c. On improving the speed and reliability of T(2) -relaxation-under-spin-tagging (TRUST) MRI. Magn Reson Med.
- Yablonskiy, D. A. and Haacke, E. M., 1994. Theory of NMR signal behavior in magnetically inhomogeneous tissues: the static dephasing regime. Magn Reson Med 32: 749-763.
- Yaffe, K., Barnes, D., Nevitt, M., Lui, L. Y. and Covinsky, K., 2001. A prospective study of physical activity and cognitive decline in elderly women: women who walk. Arch Intern Med 161: 1703-1708.

- Yaffe, K., Lindquist, K., Penninx, B. W., Simonsick, E. M., Pahor, M., Kritchevsky, S., Launer, L., Kuller, L., Rubin, S. and Harris, T., 2003. Inflammatory markers and cognition in well-functioning African-American and white elders. Neurology 61: 76-80.
- Yamaguchi, T., Kanno, I., Uemura, K., Shishido, F., Inugami, A., Ogawa, T., Murakami, M. and Suzuki, K., 1986. Reduction in regional cerebral metabolic rate of oxygen during human aging. Stroke 17: 1220-1228.
- Yamauchi, H., Fukuyama, H., Nagahama, Y., Nabatame, H., Ueno, M., Nishizawa, S., Konishi, J. and Shio, H., 1999. Significance of increased oxygen extraction fraction in five-year prognosis of major cerebral arterial occlusive diseases. J Nucl Med 40: 1992-1998.
- Yamauchi, H., Nishii, R., Higashi, T., Kagawa, S. and Fukuyama, H., 2009. Hemodynamic compromise as a cause of internal border-zone infarction and cortical neuronal damage in atherosclerotic middle cerebral artery disease. Stroke 40: 3730-3735.
- Yamauchi, H., Okazawa, H., Kishibe, Y., Sugimoto, K. and Takahashi, M., 2002. Changes in blood flow and oxygen metabolism during visual stimulation in carotid artery disease: effect of baseline perfusion and oxygen metabolism. Stroke 33: 1294-1300.
- Yang, G. and Iadecola, C., 1996. Glutamate microinjections in cerebellar cortex reproduce cerebrovascular effects of parallel fiber stimulation. Am J Physiol 271: R1568-1575.
- Yang, Y., Engelen, W., Xu, S., Gu, H., Silbersweig, D. A. and Stern, E., 2000. Transit time, trailing time, and cerebral blood flow during brain activation: measurement using multislice, pulsed spin-labeling perfusion imaging. Magn Reson Med 44: 680-685.
- Yeung, N., Nystrom, L. E., Aronson, J. A. and Cohen, J. D., 2006. Between-task competition and cognitive control in task switching. J Neurosci 26: 1429-1438.
- Yun, J. Y., Lee, D. Y., Seo, E. H., Choo, I. H., Park, S. Y., Kim, S. G. and Woo, J. I., 2011. Neural Correlates of Stroop Performance in Alzheimer's Disease: A FDG-PET Study. Dement Geriatr Cogn Dis Extra 1: 190-201.

- Zaharchuk, G., Martin, A. J. and Dillon, W. P., 2008. Noninvasive imaging of quantitative cerebral blood flow changes during 100% oxygen inhalation using arterial spin-labeling MR imaging. AJNR Am J Neuroradiol 29: 663-667.
- Zappe, A. C., Uludag, K., Oeltermann, A., Ugurbil, K. and Logothetis, N. K., 2008. The influence of moderate hypercapnia on neural activity in the anesthetized nonhuman primate. Cereb Cortex 18: 2666-2673.
- Zhang, Y., Brady, M. and Smith, S., 2001. Segmentation of brain MR images through a hidden Markov random field model and the expectation-maximization algorithm. IEEE Trans Med Imaging 20: 45-57.
- Zhou, R. H., Vendrov, A. E., Tchivilev, I., Niu, X. L., Molnar, K. C., Rojas, M., Carter, J. D., Tong, H., Stouffer, G. A., Madamanchi, N. R. and Runge, M. S., 2012. Mitochondrial oxidative stress in aortic stiffening with age: the role of smooth muscle cell function. Arterioscler Thromb Vasc Biol 32: 745-755.
- Zipfel, G. J., Sagar, J., Miller, J. P., Videen, T. O., Grubb, R. L., Jr., Dacey, R. G., Jr. and Derdeyn, C. P., 2009. Cerebral hemodynamics as a predictor of stroke in adult patients with moyamoya disease: a prospective observational study. Neurosurg Focus 26: E6.
- Zonta, M., Angulo, M. C., Gobbo, S., Rosengarten, B., Hossmann, K. A., Pozzan, T. and Carmignoto, G., 2003. Neuron-to-astrocyte signaling is central to the dynamic control of brain microcirculation. Nat Neurosci 6: 43-50.
- Zysset, S., Schroeter, M. L., Neumann, J. and von Cramon, D. Y., 2007. Stroop interference, hemodynamic response and aging: an event-related fMRI study. Neurobiol Aging 28: 937-946.